LUND UNIVERSITY

Control Strategies for Physical Human—Robot Collaboration

Salt Ducaju, Julian

2024

Document Version:
Publisher's PDF, also known as Version of record

Link to publication

Citation for published version (APA):
Salt Ducaju, J. (2024). *Control Strategies for Physical Human—Robot Collaboration*. [Doctoral Thesis (compilation), Department of Automatic Control]. Department of Automatic Control, Lund Institute of Technology, Lund University.

Total number of authors:
1

General rights
Unless other specific re-use rights are stated the following general rights apply:
Copyright and moral rights for the publications made accessible in the public portal are retained by the authors and/or other copyright owners and it is a condition of accessing publications that users recognise and abide by the legal requirements associated with these rights.
• Users may download and print one copy of any publication from the public portal for the purpose of private study or research.
• You may not further distribute the material or use it for any profit-making activity or commercial gain
• You may freely distribute the URL identifying the publication in the public portal

Read more about Creative commons licenses: https://creativecommons.org/licenses/

Take down policy
If you believe that this document breaches copyright please contact us providing details, and we will remove access to the work immediately and investigate your claim.

LUND UNIVERSITY

PO Box 117
221 00 Lund
+46 46-222 00 00

Control Strategies for Physical Human–Robot Collaboration

JULIAN M. SALT DUCAJU
DEPARTMENT OF AUTOMATIC CONTROL | LUND UNIVERSITY

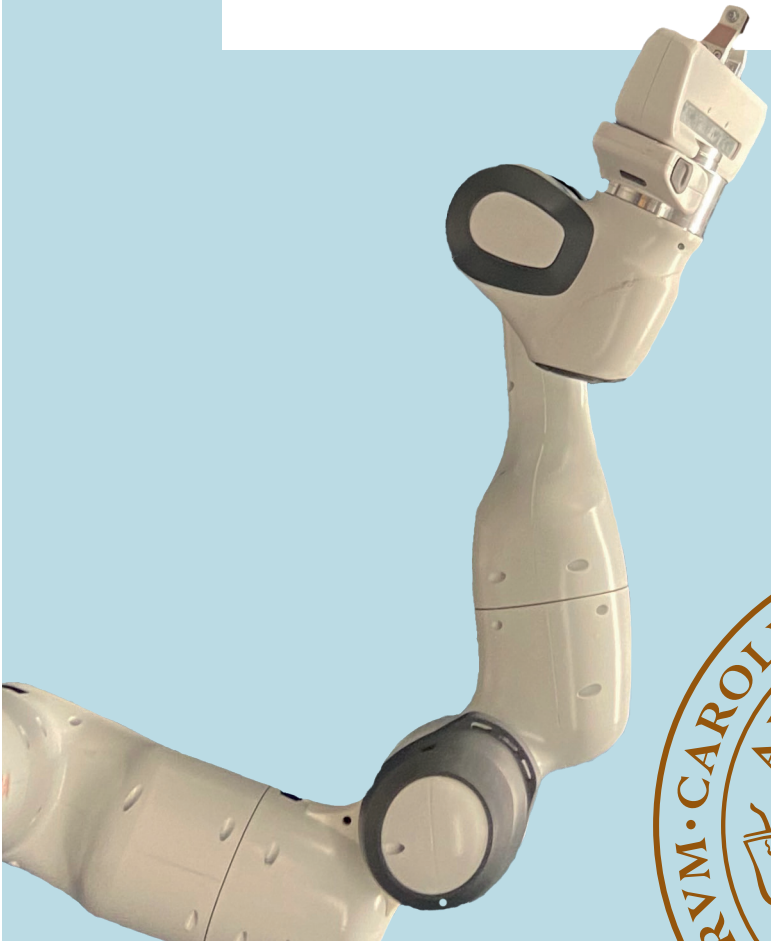

Control Strategies for Physical Human–Robot Collaboration

Julian M. Salt Ducaju

LUND
UNIVERSITY

Department of Automatic Control

PhD Thesis TFRT-1144
ISBN 978-91-8104-024-1 (print)
ISBN 978-91-8104-023-4 (web)
ISSN 0280-5316

Department of Automatic Control
Lund University
Box 118
SE-221 00 LUND
Sweden

© 2024 by Julian M. Salt Ducaju. All rights reserved.
Printed in Sweden by Media-Tryck.
Lund 2024

Abstract

Recent industrial interest in producing smaller volumes of products in shorter time frames, in contrast to mass production in previous decades, motivated the introduction of human–robot collaboration (HRC) in industrial settings, to increase flexibility in manufacturing applications. As a consequence, industrial environments would lose their fixed structure, thus increasing the uncertainties present in this workspace shared between humans and robots. This thesis presents robot control methods to mitigate such uncertainties and to improve the involvement of human operators in industrial settings where robots are present, with a particular focus on manual robot guidance, or kinesthetic teaching.

First, the accuracy of manual robot guidance was increased by reducing the joint static friction without altering the robotic task execution, using additional degrees of freedom (DOFs) available in collaborative robots. Additionally, previous methods for a fast identification of the source of robot–environment physical contact in partially-unknown industrial environments were evaluated, extended, and modified to perform effective manual corrections of the robot motion. Then, an iterative learning method was proposed to achieve a more accurate use of manually-defined trajectories, while allowing a safe physical robot–environment interaction.

Moreover, safety is a major concern in uncertain scenarios where humans and robots collaborate. Regulating the robot–environment interaction forces, *e.g.*, using impedance control, would improve safety, yet undesired parts of the collaborative workspace might need to be entirely avoided. To this purpose, a stable online variation of robot impedance during the manual guidance of the robot was proposed. This proposal was later extended to further improve safety by considering a prediction of human guidance with coordinated robot control. Furthermore, the additional DOFs in collaborative robots were used to develop a stable online impedance variation method for robot obstacle avoidance without requiring modification of the main robot task.

All methods presented were tested experimentally on a real collaborative robot.

Acknowledgments

First, I would like to honor the memory of Prof. Anders Robertsson, my early supervisor, whose unbreakable enthusiasm and encouragement continues to inspire me. Though Anders is no longer with us, his impact endures in my work and life.

I would also like to thank my supervisors Dr. Björn Olofsson and Prof. Rolf Johansson, for sharing your knowledge and experience with me. I am very fortunate to have received your advice and guidance throughout these years.

I would like to extend my gratitude to Dr. Yiannis Karayiannidis for our valuable discussions.

I am also grateful to the administrative staff: Dr. Eva Westin, Mika Nishimura, Cecilia Edelborg Christensen, and Monika Rasmusson. Thanks for ensuring that our department runs smoothly, and especially, thanks for making my life so much easier. On this behalf, I cannot forget about all the people that have helped me on technical problems: Dr. Anders Nilsson, Anders Blomdell, Pontus Andersson, Alexander Pisarevskiy, Dr. Marcus Klang, Oskar Stenberg and Anton Tetov Johansson. Thanks for your great patience.

Thanks to my colleagues at the Department of Automatic Control for creating such a wonderful environment to work in, and to all the guests that have visited the department during my time here. Thanks for the interesting seminars and events, for our conversations during lunch and fika, and for being such great travel companions and friends. Moreover, I would like to acknowledge my colleagues from the RobotLab, and especially to Alexander Dürr and Matthias Mayr. Thanks for the interesting discussions.

And last but not least, I am thankful to my parents, to Angelica, and to my friends, for bringing comfort and joy to my life, and for your endless support.

Financial Support

Financial support is gratefully acknowledged from the ELLIIT Strategic Research Area at Lund University and the Wallenberg AI, Autonomous Systems and Software Program (WASP), funded by the Knut and Alice Wallenberg Foundation (KAW).

Contents

1

Introduction

Robot manipulators were largely adopted in industry during the second half of the twentieth century, as they were deemed as the machinery needed to automate mass production. These industrial robots could reproduce repetitive tasks with high speed and accuracy, thus increasing the productivity of an industry whose goal at the time was to manufacture large amounts of identical products in their assembly lines [Kurfess, 2005, Ch. 1]. Human workers were then displaced out of such industrial environments, characterized by being rigid and structured to facilitate mass production.

However, recent trends in the manufacturing industry indicate a shift from mass production to mass customization [Schou *et al.*, 2013], where smaller volumes of products are manufactured during shorter time frames. The intelligence and dexterity of human operators can be useful to increase the manufacturing flexibility required in this novel scenario [Cencen *et al.*, 2018]. Thereby, the robots that were once used to replace human labor are currently starting to be seen as direct collaborators to humans in an industrial working structure that can best exploit the different and complementary aptitudes of humans and robots [IFR, 2018b]. Moreover, the robot manufacturing industry has addressed this trend by developing collaborative robots, also known as cobots [Colgate *et al.*, 1996; El Zaatari *et al.*, 2019], in recent years. The lightweight and compliant design of collaborative robots makes them better suited to share their workspace with human operators than traditional industrial robots [IFR, 2020]. There is an increasing interest in the use of collaborative robots, especially by Small and Medium-sized Enterprises (SMEs), since these robots are economically more viable than traditional industrial robots [Cencen *et al.*, 2018; Suomalainen *et al.*, 2022], thus providing an economically-viable entry-point to robotic automation [IFR, 2020], which historically has been restricted to large companies, since they could finance its high capital cost [IFR, 2018a].

An interesting way that humans and robots can collaborate in a manufacturing task is through physical Human–Robot Interaction (pHRI), *i.e.*, by manually guiding the robot [Hirzinger, 1986]. This method is known as kinesthetic teaching [Argall *et al.*, 2009; Akgun *et al.*, 2012; Wrede *et al.*, 2013; Karayiannidis *et al.*, 2014] and consists in leading-through the robot to program a robot trajectory, or to reprogram a segment of a pre-existing trajectory, allowing a human operator

to easily modify the robot's motion online to adapt it to a manufacturing process, whose requirements have changed. Kinesthetic teaching is the most common approach for introducing human demonstrations in manufacturing applications, since it facilitates non-expert robot programming [Ravichandar *et al*., 2020] by assuming that a human can perform the manufacturing task efficiently [Suomalainen *et al*., 2022]. However, the effective and efficient integration of humans and robots in a shared workspace still represents a significant challenge [Cencen *et al*., 2018], which hinders the advantages that the adoption of collaborative robots by industry can provide to meet the current demand for flexibility in industrial manufacturing processes.

From a robot control perspective, this challenge is primarily because of the inherent complexity of robot physical interaction with its surroundings, particularly in collaborative scenarios due to the dynamic nature of human behavior, and as a result of the need for robots to adapt to varying tasks and scenarios with minimal downtime [Vicentini, 2021]. Existing robot control solutions might lack the necessary versatility to handle robot physical interaction in collaborative environments, not fully utilize the capabilities of collaborative robots, and/or require significant time or additional resources to reconfigure collaborative robot tasks, thus increasing downtime and reducing overall efficiency [Ajoudani *et al*., 2018].

1.1 Problem Formulation

The previously described circumstances have motivated the research presented in this thesis, whose objective is to improve the involvement of human operators in industrial environments where robots are present through kinesthetic teaching applications (an application example is shown in Fig. 1.1), to increase the flexibility of the manufacturing industry. Two main research questions have arisen from this research problem:

1. How to improve the use of human manual guidance of a robot for an effective robot adaptation to changing conditions in collaborative industrial environments?

2. How to improve robot control strategies to increase functional safety in collaborative industrial environments without compromising efficiency?

The first research question has been addressed in this thesis by

- Decreasing the uncertainty of the necessary force that a human should apply to the robot, to improve the accuracy of kinesthetic teaching (*Paper I*).

- Quickly detecting robot–environment contacts and distinguishing their source (*Paper II*).

- Improving robot tracking of a human manual demonstration without altering the robot–environment interaction (*Paper III*).

and the second research question has been addressed by

- Adapting the behavior of the robot with respect to the external forces/torques applied from its environment, including human manual guidance, to avoid undesired collisions (*Papers IV* and *VI*).

- Avoid perturbing the main robot task if it is not necessary to avoid undesired collisions (*Paper V*).

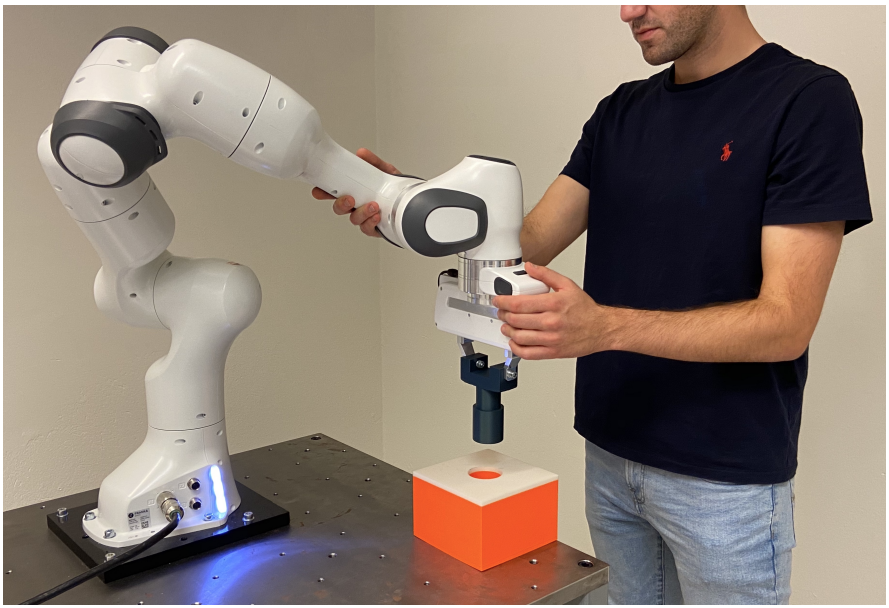

Figure 1.1 Example of the use of kinesthetic teaching for a collaborative assembly task. The image shows a human operator manually guiding a Franka Emika Panda robot [Franka Emika, 2019] mounted on a table to demonstrate a cylinder insertion (peg-in-hole) task.

1.2 Thesis Outline

This thesis is structured as four chapters followed by a collection of papers, and has the following outline:

Chapter I – Introduction

The introduction chapter presents the motivation and problem formulation of the thesis. Also, the publications included in the thesis and their main contributions are introduced in this chapter.

Chapter II – Background

The background chapter presents concepts in the fields of robotics and automatic control that are relevant for the thesis. The contents of this chapter are based on previous knowledge, and their use in this thesis is highlighted when appropriate.

Chapter III – Physical Human–Robot Interaction (pHRI)

This chapter contextualizes the problems that have been studied throughout this thesis and provides a comparative analysis of the previous solutions available in the literature with respect to the proposals included in this thesis.

Chapter IV – Conclusion and Future Research

The final chapter provides a conclusion for this thesis and discusses future research topics.

1.3 Publications

In this section, the publications that have been included in the thesis are presented. Preliminary versions of parts of the research presented in this thesis have been published in the Licentiate Thesis by the author:

Salt Ducaju, J. M. (2023). *Human-Robot Collaboration for Kinesthetic Teaching*. Licentiate Thesis TRFT-3278. Department of Automatic Control, Lund University, Lund, Sweden.

The publications included in this thesis are:

Paper I

Salt Ducaju, J. M., B. Olofsson, A. Robertsson, and R. Johansson (2021). "Joint stiction avoidance with null-space motion in real-time model predictive control for redundant collaborative robots". In: *IEEE International Conference on Robot and Human Interactive Communication (RO-MAN)*. Aug. 8–12. Vancouver, Canada (Virtual), pp. 307–314.

Null-space motion was used to reduce the friction-torque dispersion at the joints of a redundant collaborative robot to aid a human collaborator in applying the force/torque necessary to guide the robot, thus facilitating kinesthetic teaching. An experimental evaluation of the proposed method for a trajectory generated online

using model predictive control [Ghazaei Ardakani *et al*., 2019] was included in this paper.

Paper II

Salt Ducaju, J. M., B. Olofsson, A. Robertsson, and R. Johansson (2022). "Fast contact detection and classification for kinesthetic teaching in robots using only embedded sensors". In: *IEEE International Conference on Robot and Human Interactive Communication (RO-MAN)*. Aug. 29–Sep. 2. Naples, Italy, pp. 1138–1145.

Fast contact detection and classification methods based on the frequency-response analysis of the estimated external force [Kouris *et al*., 2016; Kouris *et al*., 2018] were experimentally evaluated in this paper, and necessary modifications and extensions were proposed for kinesthetic teaching applications in an assembly task when only using sensors conventionally embedded in commercial collaborative robots and using robot impedance control[1].

Paper III

Salt Ducaju, J. M., B. Olofsson, and R. Johansson (2024). "Iterative reference learning for Cartesian impedance control of robot manipulators". Submitted to review for presentation at IEEE/RSJ International Conference on Intelligent Robots and Systems (IROS) 2024.

An iterative learning strategy has been used to improve the trajectory tracking of robot manipulators in collaborative scenarios by updating the Cartesian reference of a robot impedance controller. The impedance dynamics of the robot were considered when analyzing the convergence of the proposed method. An experimental evaluation of the proposal for different robot tasks and scenarios was included in this paper.

Paper IV

Salt Ducaju, J. M., B. Olofsson, A. Robertsson, and R. Johansson (2022). "Robot Cartesian compliance variation for safe kinesthetic teaching using safety control barrier functions". In: *IEEE International Conference on Automation Science and Engineering (CASE)*. Aug. 20–24. Mexico City, pp. 2259–2266.

Safety control barrier functions [Ames *et al*., 2019] have been used in this paper to online modify the Cartesian impedance behavior of a robot to avoid that an operator could guide the end-effector of the robot to an unsafe position, in the context of

[1] A video that includes the most relevant aspects of the experiments performed for Paper II is available in the Lund University Research Portal: `https://lucris.lub.lu.se/ws/portalfiles/portal/173495591/PaperII.mp4`.

safe kinesthetic teaching. A passivity-based energy-storage formulation [Ferraguti *et al*., 2013] has been modified to include a strict Lyapunov function, which subsequently was used to ensure stability of the proposed method.

Paper V

Salt Ducaju, J. M., B. Olofsson, A. Robertsson, and R. Johansson (2023). "Null-space compliance variation for safe human-robot collaboration in redundant manipulators using safety control barrier functions". In: *IEEE/RSJ International Conference on Intelligent Robots and Systems (IROS)*. October 1–5. Detroit, MI, USA, pp. 5903–5909.

In this paper, the null-space compliant behavior of a robot has been modified online using safety control barrier functions [Ames *et al*., 2019] for collaborative scenarios that do not require to alter the main robot task to achieve robot obstacle avoidance. Conditions that guarantee the stability of the proposed method were included when formulating the variation of the null-space compliance of the robot[2].

Paper VI

Salt Ducaju, J. M., B. Olofsson, and R. Johansson (2024). "Model-based predictive impedance variation for robot obstacle avoidance in safe human-robot collaboration". Submitted to review for publication in IEEE Transactions on Automation Science and Engineering.

A model predictive control strategy that included linearized control barrier functions [Ames *et al*., 2019] was proposed in this paper to improve physical safety during human guidance of a robot by considering a prediction of the robot motion and the human behavior. Stability of the resulting online modification of the Cartesian impedance behavior of the robot was proven using Lyapunov theory[3].

Moreover, an overview of the notation used in each of the publications included in this thesis is presented in Appendix A.

Contributions to Publications by the Author

These publications were developed by J. M. Salt Ducaju as the main contributor. J.M. Salt Ducaju proposed the initial ideas, conducted the experiments, and drafted the first version of the manuscripts. B. Olofsson, A. Robertsson, and R. Johansson provided constructive comments on the research and assisted in structuring the manuscripts.

[2] A video that includes the most relevant aspects of the experiments performed for Paper V is available in the Lund University Research Portal: `https://lucris.lub.lu.se/ws/portalfiles/portal/173495629/PaperV.mp4`.

[3] A video that includes the most relevant aspects of the experiments performed for Paper VI is available at YouTube: `https://youtu.be/020LBMCWKAY`.

Additional Publications

The following publications, where the author has made contributions, were decided not to be part of the present thesis:

Mayr, M. and J. M. Salt Ducaju (2024). "A C++ implementation of a Cartesian impedance controller for robotic manipulators". *Journal of Open Source Software (JOSS)* **9**:93, p. 5194.

Salt Ducaju, J. M., J. J. Salt Llobregat, Á. Cuenca, and M. Tomizuka (2021). "Autonomous ground vehicle lane-keeping LPV model-based control: Dual-rate state estimation and comparison of different real-time control strategies". *Sensors* **21**:4, p. 1531.

Salt Ducaju, J. M., C. Tang, M. Tomizuka, and C.-Y. Chan (2020). "Application specific system identification for model-based control in self-driving cars". In: *IEEE Intelligent Vehicles Symposium (IV)*. Oct. 19–Nov. 13. Las Vegas, NV, USA (Virtual), pp. 384–390.

1.4 Contributions

The main contributions of this thesis are:

- The formulation of a method to facilitate kinesthetic teaching in redundant robots by the use of null-space motion, complemented by an experimental analysis.

- The empirical evaluation of fast contact detection and classification methods for impedance-controlled robots using data only from embedded sensors, and the proposal of necessary modifications and extensions to use these methods for kinesthetic teaching applications in an assembly task.

- The development of an iterative learning method to improve trajectory tracking for impedance-controlled robots in collaborative scenarios, evaluated in experimental assembly scenarios.

- The proposal and experimental evaluation of a method to modify the Cartesian impedance behavior of a robot (while ensuring strict stability at the controller) to avoid unsafe situations during kinesthetic teaching using safety control barrier functions.

- The extension of the previous contribution to further improve functional safety during human guidance by considering prediction of human behavior with coordinated robot control using model predictive control with linearized control barrier functions, supported by an experimental evaluation.

- The proposal of a method, which was evaluated through experiments, to modify the null-space compliant behavior of a robot to avoid collisions without altering the main robot task, in a stable manner, using safety control barrier functions.

2

Background

The most relevant concepts for this thesis in the fields of robotics and automatic control have been summarized in this chapter.

2.1 Robot Manipulators

Stationary robot manipulators have immobile bases and limited workspaces, as opposed to mobile robots that are able to modify their entire position with respect to a world frame [Corke, 2013]. Robot manipulators are defined by two key elements: joints and links. Joints, which can be rotational or translational, are the actuated elements of the robot, *i.e.*, their degrees of freedom (DOFs); whereas links are the unactuated elements of the robot that connect the joints.

Moreover, there are several types of robot manipulators such as serial-link, parallel-link, Selective Compliance Assembly Robot Arms (SCARA), gantry robots, and humanoids. In this thesis, the focus is on serial-link robot manipulators, which are composed of a chain of rigid links and rotational joints, and where one end of the chain is fixed to a static base and the other end is free to move and has an end-effector attached.

Robot Kinematics

Robot kinematics study the geometric relationship between the position of the joints of a robot manipulator, and the pose (*i.e.*, position and orientation) of its end-effector, without considering the masses or the forces and torques acting on it,

$$\xi = \mathscr{K}(q) \tag{2.1}$$

where $\xi \in \mathbb{R}^m$ represents the m coordinates of the robot end-effector pose in operational space [Khatib, 1987], and $q \in \mathbb{R}^n$ represents the n coordinates of the joint space of the robot. Cartesian space coordinates have been used to represent the operational space of the robot throughout this thesis, although different operational

space coordinates could be chosen depending on the particular robot tasks to be performed. Additionally, the manipulator Jacobian $J(q) \in \mathbb{R}^{m \times n}$ relates the end-effector velocity $\dot{\xi}$ to the joint angular velocity $\dot{q}$ by the differential kinematics

$$\dot{\xi} = J(q)\dot{q} \tag{2.2}$$

with

$$J(q) = \frac{\partial \mathscr{K}(q)}{\partial q} \tag{2.3}$$

Robot Dynamics

Robot dynamics study the motion of robots considering the forces and torques that cause it [Lynch and Park, 2017]. The rigid-body dynamics of robot manipulators can be described, in the joint space of the robot, $q \in \mathbb{R}^n$, [Bejczy, 1974]

$$M(q)\ddot{q} + C(q,\dot{q})\dot{q} + G(q) = \tau + \tau^{\text{ext}} \tag{2.4}$$

where $M(q) \in \mathbb{R}^{n \times n}$ is the inertia matrix, $C(q,\dot{q}) \in \mathbb{R}^{n \times n}$ describes the Coriolis and centripetal forces effects, and $G(q) \in \mathbb{R}^n$ captures the gravity-induced torques. Finally, $\tau \in \mathbb{R}^n$ represents the joints input torques, and $\tau^{\text{ext}} \in \mathbb{R}^n$ are the external torques.

Moreover, since the main robot task is usually represented in terms of its end-effector pose ξ, it might be relevant to express the rigid-body dynamics description of the robot in these coordinates,

$$M_\xi(q)\ddot{\xi} + C_\xi(q,\dot{q})\dot{\xi} + G_\xi(q) = F + F^{\text{ext}} \tag{2.5}$$

where $F \in \mathbb{R}^m$ is the input force, and, for a fully-actuated nonredundant robot ($n = m$), $M_\xi \in \mathbb{R}^{m \times m}$, $C_\xi \in \mathbb{R}^{m \times m}$, and $G_\xi \in \mathbb{R}^m$ are equal to

$$M_\xi = J^{-\mathrm{T}}(q)M(q)J^{-1}(q) \tag{2.6}$$

$$C_\xi = J^{-\mathrm{T}}(q)(C(q,\dot{q}) - M(q)J^{-1}(q)\dot{J}(q))J^{-1}(q) \tag{2.7}$$

$$G_\xi = J^{-\mathrm{T}}(q)G(q) \tag{2.8}$$

assuming that the Jacobian relative to the base frame of the robot, $J(q) \in \mathbb{R}^{m \times m}$, to have full rank [Khatib, 1987]; see [Chiaverini *et al.*, 1994] for a review of Jacobian inversion techniques in the neighborhood of singular joint configurations.

Furthermore, two relevant properties of the robot dynamics should be highlighted, since they were relevant for some of the controllers synthesized in the papers included in this thesis (*Papers III–VI*). First, the inertia matrix is a positive definite matrix,

$$x^{\mathrm{T}}Mx > 0, \ \ \forall x \neq 0 \tag{2.9}$$

Second, the matrix $\dot{M} - 2C$ is skew-symmetric,

$$x^{\mathrm{T}}\Big(\dot{M} - 2C\Big)x = 0, \ \ \forall x \neq 0 \tag{2.10}$$

It is noted that, even though (contrary to joint coordinates) a Cartesian representation does not necessarily have the properties of canonical coordinates, it was shown in [Ott, 2008, Ch. 3] that these two properties are valid both in joint space and in Cartesian space.

Joint Redundancy

A robot manipulator is kinematically redundant if it has a greater number n of joints than the m coordinates used to define its main task, which are usually the Cartesian coordinates that represent its end-effector pose ξ. Joint redundancy has been used in this thesis (*Papers I* and *V)* to perform additional robot tasks complementary to the main robot task to augment the collaborative abilities of the robot.

For redundant manipulators, a possible solution for the inverse of the kinematic relationship presented in Eq. (2.2) is [Corke, 2013]

$$\dot{q} = J_W^{\dagger}(q)\dot{\xi} + P(q)\dot{q}_0 \tag{2.11}$$

where $\dot{q}_0 \in \mathbb{R}^n$ is an arbitrary vector in the joint space of the robot, $P(q) \in \mathbb{R}^{n\times n}$ is a matrix that projects $\dot{q}_0$ into the null-space of the main task,

$$P(q) = I_n - J_W^{\dagger}(q)J(q) \tag{2.12}$$

with $I_n \in \mathbb{R}^{n\times n}$ representing an identity matrix, and $J_W^{\dagger}(q)$ being the weighted generalized inverse

$$J_W^{\dagger}(q) = W^{-1}(q)J^{\mathrm{T}}(q)(J(q)W^{-1}(q)J^{\mathrm{T}}(q))^{-1} \tag{2.13}$$

with $W \in \mathbb{R}^{n\times n}$ being a symmetric positive definite matrix, $W \in S_{++}^n$.

Moreover, a kinematic relationship analogous to Eq. (2.2) but for the null-space of the main task was proposed by [Park, 2000] by defining null-space velocities, v_N,

$$v_N = J_N(q)\dot{q} \tag{2.14}$$

with a null-space Jacobian $J_N(q) \in \mathbb{R}^{r\times n}$,

$$J_N(q) = (ZWZ^{\mathrm{T}})^{-1}ZW \tag{2.15}$$

where $Z(q) \in \mathbb{R}^{r\times n}$ is composed by linearly independent vectors in the null-space of the main task, $J(q)Z^{\mathrm{T}}(q) = 0$, with $r = n - m$ being the degrees of redundancy, and where the velocity in the null-space of the main task can be rewritten as [Park, 2000]

$$\dot{q}_{\mathrm{NS}} = P(q)\dot{q}_0 = Z^{\mathrm{T}}(q)v_N \tag{2.16}$$

Furthermore, for a kinematically redundant robot, the input torques in Eq. (2.4) can also be decoupled into the torques involved in the Cartesian space, τ_ξ, and the torques in the null-space of the Cartesian space, τ_{ns},

$$\tau = \tau_\xi + \tau_{\mathrm{ns}} \tag{2.17}$$

where

$$\tau_\xi = J^{\mathrm{T}}(q) F_\xi \tag{2.18}$$

$$\tau_{\mathrm{ns}} = J_N^{\mathrm{T}}(q) F_N \tag{2.19}$$

with F_ξ being the forces that are involved in the robot's main task and F_N being the forces acting in the null-space of the main task. Then, it has been shown in [Khatib, 1995] that if the inertia matrix M of Eq. (2.4) is chosen as the weighting matrix W of the generalized inverse in Eq. (2.13), $W = M$, the null-space torque, τ_{ns} in Eq. (2.17), would not cause an acceleration in the Cartesian coordinates of the robot end-effector ξ. Therefore, the dynamics of each space can be considered separately,

$$M_\xi(q)\ddot{\xi} + C_\xi(q,\dot{q})\dot{\xi} + G_\xi(q) = F_\xi + F_\xi^{\mathrm{ext}} \tag{2.20}$$

$$M_N(q)\dot{v}_N + C_N(q,\dot{q})v_N + G_N(q) = F_N + F_N^{\mathrm{ext}} \tag{2.21}$$

However, to obtain fully decoupled dynamics as in Eqs. (2.20) and (2.21), a power-preserving feedback compensation on the centrifugal and Coriolis cross-terms should be included [Ott *et al.*, 2008].

Additional Robot Hardware: Sensing and Actuation

Links and joints are not the only components of robot manipulators. Electric motors are often used for the actuation of rotational joints (alternatively, pneumatic or hydraulic cylinders would be used for translational joints), and a transmission mechanically connects these two components. Also, this transmission is used to amplify the torque transferred to the joints at the expense of reducing the angular velocity [Lynch and Park, 2017], and incorporates additional rotational parts that contribute to detrimental frictional effects that were discussed in *Paper I*. Moreover, brakes can be used to stop the robot fast, usually in combination with a prior active braking from the motors, or to keep a stationary posture. Additionally, the end-effector of a robot could be chosen depending on the requirements of the task performed by the robot and range in complexity, although task-specific end-effectors might reduce the versatility of a robot manipulator. Examples of possible robot end-effectors are 2-finger grippers, suction cups, or fully-actuated robot hands, but also more dedicated tools, such as welding guns or drills. Additionally, tool changers [Voellmer, 1991] could be used to allow interchanging different end-effectors for a single robot.

Furthermore, a number of sensors are often embedded in a robot manipulator and provide useful data regarding the state of the robot (called *proprioceptive sensors*, as opposed to *exteroceptive sensors* that provide data related to the surroundings of the robot [Christensen and Hager, 2008]). First, encoders, potentiometers, or resolvers are utilized to measure the joint angular displacement. Second, to measure forces and torques, either torque sensors are placed at each joint or wrist-mounted

(*i.e.*, placed between the last robot joint and the robot end-effector) six-axis force-torque sensors can be used. Strain gauges are often used inside these two components. Also, other equipment can be mounted on the robot, such as cameras (both able to record color and depth), as shown in the application scenario of *Paper IV*, or capacitive proximity sensors [Ergun *et al*., 2021]. However, maximizing the use of sensors that are conventionally embedded in robots for proprioception allows to increase the adaptability of collaborative robots by reducing the need for task-specific work setups, as discussed in *Paper II*.

Collaborative Robots

Collaborative robots, also known as *cobots*, are robots that have been designed to share their workspace with humans [Colgate *et al*., 1996; El Zaatari *et al*., 2019], as mentioned in Ch. 1. Before collaborative robots were introduced in industrial settings, robots were placed in cages that separated them from human operators. This precaution was necessary to prevent any physical injuries to the operators from the motion of the robots. Nevertheless, safety is still a central concern in industrial applications where collaborative robots and operators share their workspace. To regulate these collaborative workspaces, international standard rules and specifications have been developed, such as ISO/TS 15066 [ISO, 2016]. This international standard is focused on safety when using collaborative robots and it was created as an addition to previous international standards on industrial robots, ISO 10218-1 [ISO, 2011a] and ISO 10218-2 [ISO, 2011b].

2.2 Robot Control

The aim of robot control is for a robotic manipulator to achieve a desired behavior, which might be focused on either the motion of the robot (*motion control*) or on the forces and torques that the robot applies to its environment (*force control*, discussed in Sec. 2.3). Additionally, the desired robot behavior might be defined in the robot joint space, but it is also possible to define it in the Cartesian space of its end-effector for a higher correspondence with the robot task design. The kinematic expressions that relate these two spaces were presented in Sec. 2.1.

Moreover, direct actuation of the motors that drive the joints of commercial collaborative robots is usually not possible from a robot operator standpoint. Instead, a robot operator might design a controller that inputs position references q_r, velocity references $\dot{q}_r$ (as in *Paper I*), and/or torque references τ_r (as in *Papers I–VI*) through a robot control interface designed by the manufacturer of the robot. Then, the error signals (e_q, $e_{\dot{q}}$, and e_τ) resulting from comparing these inputs to the position q, velocity $\dot{q}$, and/or torque τ feedback data obtained from the robot sensors [Åström and Murray, 2021], would be handled by an internal robot controller to determine, for example, the electrical current, i, commanded to each joint motor that would achieve a torque τ at its driven joint. A schematic view of a possible joint internal

controller is provided in Fig. 2.1 (see [Johansson *et al.*, 2014] or [Chung *et al.*, 2008] for similar proposals for robot internal joint controllers). It should be noted that the block *Joint* of Fig. 2.1 represents the dynamics behavior of the joint as expressed in Eq. (2.4), but joint acceleration $\ddot{q}$ is rarely measured by the robot proprioceptive sensors. Instead, as commented in Sec. 2.1 and represented in Fig. 2.1, joint position q is often measured and then differentiated to obtain joint velocity $\dot{q}$.

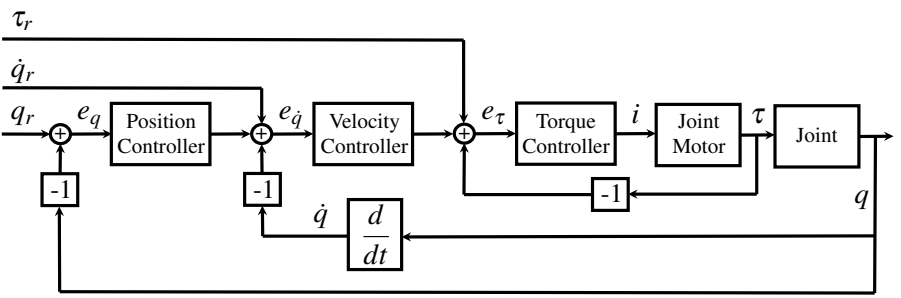

Figure 2.1 Schematic view of a possible robot joint internal controller.

Furthermore, robots are physical systems with continuous-time input and output signals, whereas robot controllers are implemented using digital systems, which work at discrete-time instants; see [Åström and Wittenmark, 2013] for an extensive explanation of the implications regarding the communication between these two entities.

Optimization-Based Control

Optimization-based control can be used to determine the input u commanded to a robot, with state x and dynamics described by $\dot{x} = f(x,u)$, by minimizing a cost function

$$J(x,u) = \int_0^T L(x,u)dt + V(x(T)) \tag{2.22}$$

where $\int_0^T L(x,u)dt$ is called integral cost and $V(x(T))$ is the terminal cost [Murray, 2023], with T being the time horizon of the control problem.

In optimization-based control, equality and inequality constraints are often useful to define the optimization problem. First, equality constraints (2.24) allow to adhere the robot to its model $\dot{x} = f(x,u)$ and to define initial and final conditions. Second, inequality constraints (2.25) allow to set up bounds on the robot input and/or

states. An overview of the optimization-based control problem is

$$\underset{u(\cdot)}{\text{minimize}}\ J(x,u) = \int_0^T L(x,u)dt + V(x(T)) \tag{2.23}$$

$$\text{s.t. } g_1(x,u) = 0 \tag{2.24}$$

$$g_2(x,u) \leq 0 \tag{2.25}$$

Moreover, a distinction can be made between infinite horizon optimal control problems ($T = +\infty$) and finite horizon optimal control problems ($T < +\infty$), the latter being more common in robotic manipulators, since usually robots are required to complete a task with defined time requirements rather than to reach a stationary, or time-invariant, robot state. Additionally, the optimal control signal u could be computed at time k over a finite time horizon T, used for a short period of time $\delta < T$, and then recomputed at time $k+\delta$, in a receding horizon fashion, which is called Model Predictive Control (MPC) [Garcia *et al.*, 1989]. This control strategy has been used in *Papers I* and *VI* of this thesis.

Furthermore, the computational time that a controller would need to numerically solve the optimal control problem (2.23)–(2.25) would depend on its formulation, which in its general form is NP-hard [Lewis, 1996]. Then, to be able to compute an input at every sampling time k, it can be advantageous that the cost function to be minimized (2.23) is chosen as (convex) quadratic and the constraint functions (2.24) and (2.25) are affine. By this choice of cost function and constraints, a special type of optimization problem, called Quadratic Program (QP) [Boyd and Vandenberghe, 2004], which can be solved in polynomial time [Kozlov *et al.*, 1979], can be obtained.

Control Barrier Functions (CBFs)

It is possible to make a robot avoid obstacles in the previously introduced optimization-based formulation (2.23)–(2.25), *e.g.*, by including an inequality constraint in (2.25) that bounds the robot behavior within some safe limits. To this purpose, Control Barrier Functions (CBFs) have gained popularity in recent years. To use CBFs, first, a safe set $\mathscr{C}$ of robot states x, with boundary $\partial\mathscr{C}$ and interior $\text{Int}(\mathscr{C})$, is defined as [Ames *et al.*, 2019]

$$\mathscr{C} = \{x \in \mathbb{R}^n \mid h(x) \geq 0\} \tag{2.26}$$

$$\partial\mathscr{C} = \{x \in \mathbb{R}^n \mid h(x) = 0\} \tag{2.27}$$

$$\text{Int}(\mathscr{C}) = \{x \in \mathbb{R}^n \mid h(x) > 0\} \tag{2.28}$$

Then, the sufficient and necessary forward-invariance condition of the safe set $\mathscr{C}$, *i.e.*, the condition that, if guaranteed, ensures that the robot states would stay in $\mathscr{C}$ for $t \in [0, +\infty]$, is [Ames *et al.*, 2019]

$$\sup_{u \in \mathscr{U}} [L_f h(x) + L_g h(x) u] \geq -\kappa(h(x)) \tag{2.29}$$

for all $x \in \mathscr{D}$, h being the barrier function, $h : \mathscr{D} \to \mathbb{R}$ with $\mathscr{C} \subseteq \mathscr{D} \subset \mathbb{R}^n$, κ an extended class-$\mathscr{K}_\infty$ function (strictly monotonically increasing), and $L_f h(x) = (\partial h/\partial x) f(x)$ and $L_g h(x) = (\partial h/\partial x) g(x)$, with robot dynamics described by $\dot{x} = f(x) + g(x)u$. Therefore, collision avoidance can be achieved using CBFs by including the forward-invariance condition (2.29) of the safe set $\mathscr{C}$ (2.26) as an inequality constraint in (2.25). This strategy for robot safety was used in *Papers IV–VI* of this thesis.

Moreover, alternative methods such as Artificial Potential Fields (APFs) [Khatib, 1985] have been used extensively. This method aims to achieve robot obstacle avoidance by positioning virtual repulsive fields centered around obstacles. After adequate tuning, APFs might provide similar results to CBFs for certain scenarios, and a broad class of APFs could even be used to construct CBFs [Singletary *et al.*, 2021a]. However, compared to CBFs, APFs would not encode the dynamics behavior of the robot in its formulation, leading to reduced formal safety guarantees and to possible overcompensation for collision avoidance [Rauscher *et al.*, 2016], which would be worsen if APFs disregarded the directionality of robot motion in its formulation. Additionally, for reasons of high-gain feedback, APFs may induce instability [Johansson *et al.*, 2009], and restrictions to stable cases may impose serious application restraints. Also, it should be noted that APFs might induce local minima problems that could prevent robot task completion [Koren *et al.*, 1991]. This issue does not seem to be inherently solved by the CBFs formulation and these methods would require further considerations in this regard [Stavridis *et al.*, 2017].

Furthermore, robot obstacle avoidance remains an open problem and might not be limited to robot behavior-constraining methods that use inequality constraints as in (2.29). Indeed, equality-constraint based methods such as virtual holonomic constraints (used for robot stabilization [Shiriaev *et al.*, 2007] and haptic robot interfacing [Ardakani *et al.*, 2018], among other applications), could also be used to improve robot physical safety. However, the application of virtual holonomic constraints in the context of robot collision avoidance might overrestrict the robot motion depending on the definition of safe paths to be followed by robot manipulators.

Iterative Learning Control

The controllers introduced previously in this chapter were intended to be applied in an online feedback fashion, *i.e.*, an input signal commanded to the robot was being computed based on the error between the robot output signal and the reference signal occurring at the moment of the robot task execution. However, for repetitive tasks, such as the ones that robotic manipulators often perform, this reference error can be reduced for the entire robot task by *learning* an improved input signal from previous trials, or iterations, as was done in *Paper III* of this thesis. This is shown in Fig. 2.2, where the entire input sequence for iteration $j+1$ is calculated based on the entire input and output sequences (U_j and Y_j, respectively) of the previous

iteration, j.

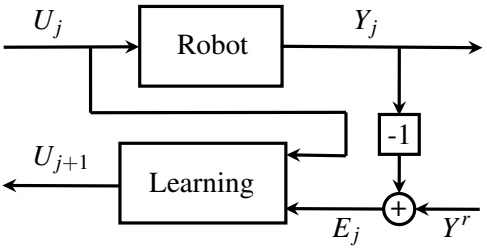

Figure 2.2 Schematic view of an iterative learning robot control loop.

Moreover, a common update law for robot controller iterative learning is

$$U_{j+1} = Q\big(U_j + LE_j\big) \tag{2.30}$$

where L is the learning filter, and Q is often chosen as a low-pass filter for robustness purposes [Arimoto *et al*., 1984]. Note that these filters may use forward-looking anticipative learning action, since the entire input and error sequences of iteration j (U_j and E_j, respectively) are available at the time of the computation of U_{j+1}. A general framework for the convergence analysis of these learning algorithms was provided in [Norrlöf and Gunnarsson, 2002].

2.3 Robot Interaction with its Environment

Robot tasks could be classified in terms of the need for interaction between the robot and its environment. On the one side, *free motion tasks* [Villani and De Schutter, 2008] do not imply a physical interaction of the robot with its surroundings. These robot tasks require the displacement of the robot end-effector from an initial pose to a number of target poses, and often include a notion of time associated with the completion of a robot task. Examples of these tasks in industrial settings are spray painting [Egeland, 1987], visual inspection/quality control [Zhu *et al*., 2021], or pick-and-place operations [Lozano-Pérez *et al*., 1989]. On the other side, *contact-rich tasks* intrinsically consider a physical interaction between the robot and its environment for the completion of the task, which increases their complexity. Assembly tasks (*e.g.*, peg-in-hole insertion [Abu-Dakka *et al*., 2014] or snap-fit assembly [Stolt *et al*., 2011]) or machining tasks (*e.g.*, drilling [Olsson *et al*., 2010], milling [Sörnmo *et al*., 2012; Schneider *et al*., 2014], deburring [Robertsson *et al*., 2006], or friction stir welding [Karlsson *et al*., 2023]) are examples of robot *contact-rich tasks*.

However, examining only interaction scenarios that require physical contact between the robot and its environment to complete a robot task would limit the applicability of robot manipulators, especially taking into consideration the latest trends

of industrial manufacturing introduced in Ch. 1 that aim at allowing robot operation in less structured layouts. Indeed, accidental contacts, or *collisions*, between a robot manipulator and its environment might occur during nominal robot operation, and therefore, should also be taken into consideration when programming robot tasks.

Moreover, the involvement of human operators during robot tasks should not be disregarded. Human–robot interaction can be included in the previously introduced robot task classification: some contact-rich robot tasks would be expected to involve a physical cooperation between a robot manipulator and a human operator, *i.e.*, the robot and the operator work toward the same goal by physically interacting. Nevertheless, human–robot cooperation might not imply physical human–robot interaction (pHRI), *e.g.*, a cooperative assembly task that is divided in subtasks performed either by a robot or by an operator would not necessarily involve pHRI, as discussed in *Paper V* [Salt Ducaju *et al*., 2023], whereas a cooperative pick-and-place task of a workpiece where a robot and an operator grasp different ends of this workpiece would involve pHRI [Caliskan *et al*., 2022].

Furthermore, this may not be the only situation in pHRI, and antagonist relationships between robot and the operator might occur instead, where the robot-operator contact (already taking place or about to take place in the near future) is not desired from the current robot task-completion standpoint. It should be mentioned that, in this perspective, an antagonistic relationship might be caused by an accidental collision, but might also serve the role of robot trajectory definition or modification by means of human guidance, *e.g.*, using *kinesthetic teaching* [Schou *et al*., 2013].

Robot Control Strategies for Physical Interaction

As introduced in Sec. 2.1, *force control* is used to handle physical interaction between the robot and its surroundings. In the literature, robot force controllers are often classified based on whether the behavior of the robot with respect to its external forces is regulated by the robot hardware [González Rodríguez *et al*., 2009] (called *passive force control*) or its software (called *active force control*) [Villani and De Schutter, 2008].

Most industrial robot manipulators that perform force control use *active force controllers*, since they offer a more versatile implementation compared to *passive force controllers*, which are often designed for a particular task. Within *active force controllers*, a further categorization can be made into *direct force control* and *indirect force control* [Villani and De Schutter, 2008]:

- *Direct force control*: Direct force control implements a force feedback loop to control the external force applied by the robot. For its effective implementation, it requires a model of the interaction of the robot environment [Villani and De Schutter, 2016].

- *Indirect force control*: Indirect force control addresses the direct force-control limitations caused by the difficulty to obtain an accurate description of the

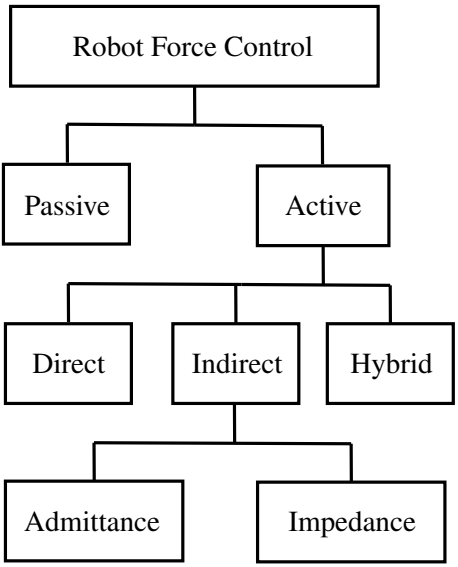

Figure 2.3 Schematic view of a classification for robot force control strategies.

robot environment. It aims to control the relationship between the robot-environment interaction forces and the robot motion. Widely used implementations of indirect force control include *impedance control* and *admittance control* [Hogan, 1985]. A mass-spring-damper relationship between the motion deviation from a reference and the interaction force is established in both of these implementations. In robotics, the difference between them is that in *impedance control* (used in *Papers II–VI*), the robot applies a force to its environment (response) because of a motion deviation (input), whereas in *admittance control* (used in *Paper I*), a force applied to the robot by its environment (input) causes a motion deviation (response).

- *Hybrid force/motion control*: Hybrid force/motion control implements force control along the desired directions of the robot task frame and implements motion control along the remaining directions [Raibert and Craig, 1981].

A schematic view of the different robot control strategies discussed for physical interaction with its environment is shown in Fig. 2.3.

Moreover, the aforementioned capacity of indirect force controllers to be deployed into partially-unknown robot environments makes this type of force controllers attractive for pHRI scenarios. Also, force controllers can be formulated in a Cartesian frame of reference that often corresponds to the robot task being performed, which eases the robot task planning for tasks involving pHRI. Thus, a Cartesian impedance controller formulation (used in *Papers II–VI*) [Hogan, 1985]

[Ott, 2008, Ch. 3] would allow to define the robot desired trajectory by choosing appropriate Cartesian reference poses for its end-effector, $\xi_d(t)$:

$$F = K\Delta\xi + D\Delta\dot{\xi} + G_{\xi}(q) \tag{2.31}$$

with F being the input force commanded to the robot (2.5), the Cartesian pose and velocity variations from their reference being $\Delta\xi = \xi_d - \xi$ and $\Delta\dot{\xi} = \dot{\xi}_d - \dot{\xi}$, respectively, and where $G_{\xi}(q)$ handles gravity compensation. Also, $K \in S^m_{++}$ and $D \in S^m_{++}$ are diagonal matrices that represent the control-induced, *i.e.*, virtual, stiffness and damping, respectively. As mentioned earlier, an impedance controller input would shape the rigid-body dynamics of the robot as a mass-spring-damper system:

$$F^{\text{ext}} = M_{\xi}(q)\ddot{\xi} + C_{\xi}(q,\dot{q})\dot{\xi} - D\Delta\dot{\xi} - K\Delta\xi \tag{2.32}$$

Furthermore, the Cartesian space is not the only frame of reference that these indirect force control methods can be formulated in. Indeed, for redundant manipulators (see Sec. 2.1), it might be advantageous to formulate an impedance controller in the null-space of the Cartesian, or task, frame (2.21) (used in *Paper V*) [Ott *et al.*, 2008]. A null-space component of the commanded input force equal to

$$F_N = k_n Z(q)\Delta q - d_n v_N \tag{2.33}$$

would achieve an impedance behavior in the null-space of the Cartesian space:

$$F_N^{\text{ext}} = M_N(q)\dot{v}_N + (d_n + C_N(q,\dot{q}))v_N - k_n Z(q)\Delta q \tag{2.34}$$

with F_N^{ext} being the external forces acting on the null-space of the Cartesian frame, k_n being a virtual spring stiffness term with respect to the joint position variation from its reference, $\Delta q = q_d - q$, and d_n being a virtual damping term for the null-space velocities, v_N (2.14).

Finally, it is important that robot force-control methods are designed so that robot end-effector overshoots are minimized in contact operations, as studied in the rendezvous problem [Book *et al.*, 1985], which considers the relative robot position and velocity with respect to the manipulated object at the time of collision when establishing contacts.

3

Physical Human–Robot Interaction (pHRI)

As introduced in Ch. 1, in previous decades, industrial manufacturing environments were designed for mass production of identical products, which hinders their capacity to adapt to the increasingly changing requirements from industrial production tasks. To address these adaptation issues, a new generation of industrial manufacturing environments should be designed. Collaborative industrial scenarios are a promising strategy to progress toward this goal. In these collaborative scenarios, human operators and robot manipulators share a common workspace and are allowed to physically interact among themselves to benefit from the aforementioned inherent intelligence and dexterity of humans.

Nevertheless, transitioning from a situation where robots in industrial environments were isolated in safety cells to one where robot manipulators occupy the same workspace as their human counterparts, introduces its own set of challenges. The goal of this chapter is to provide an overview of the most relevant challenges regarding pHRI in industrial environments from a robot-control perspective. Additionally, it is detailed in this chapter how the contributions presented in this thesis can improve the use of pHRI in industrial environments, including a comparison between the research presented in this thesis and previously proposed solutions.

3.1 Uncertainty in pHRI

From a robot-control perspective, the challenges presented by pHRI, and in general with less-structured industrial work environments with robots, are caused by the increase of uncertainty in different elements involved in robot tasks. A categorization of these uncertainties with respect to their relationship with robots is presented in this section. Additionally, this section includes a description of the limitations, in the context of pHRI, presented by solutions that have been proposed in literature to address these uncertainties.

Uncertainties in the Robot Dynamics

An incomplete knowledge of the robot behavior would lead to uncertainty regarding the relationship between the input commanded to the robot, and both the position of each of the different components of the robot manipulator and the force interaction by the robot with its surroundings. It should be noted that uncertainties in the robot dynamics are not exclusively found in pHRI and have been extensively addressed in the past, because of their long-standing presence in robot industrial scenarios. Therefore, this section provides an overview of uncertainties in the robot dynamics with a focus on the issues that manifest in pHRI.

Unmodeled Robot Dynamics

The robot dynamics description presented in Eq. (2.4),

$$M(q)\ddot{q} + C(q,\dot{q})\dot{q} + G(q) = \tau + \tau^{\text{ext}} \tag{3.1}$$

implies the availability of accurate and complete sensor data regarding the angular position and velocity of the robot joints, and regarding the external force applied to the robot by the environment to be able to map the torque input commanded to the robot to the motion of the robot. Also, this expression assumes a correct mapping of the angular position and velocity of the robot joints to the inertia, Coriolis, centripetal and gravitational forces that the robot would experience throughout its motion.

Additionally, several physical phenomena were omitted in Eq. (3.1) for the sake of simplicity, such as joint friction. Joint friction has extensively been studied, and several friction models have been formulated, *e.g.*, the Dahl model [Dahl, 1968], the Armstrong model [Armstrong-Hélouvry *et al*., 1994], or the LuGre model [Canudas de Wit *et al*., 1995]. In robotics, friction models have been used to compensate joint friction effects [Freidovich *et al*., 2009; Shiriaev *et al*., 2003] so that a torque input $\tau' \in \mathbb{R}^n$,

$$\tau' = \tau + \tau_{\text{f}} \tag{3.2}$$

where $\tau_{\text{f}} \in \mathbb{R}^n$ is the input torque commanded to the robot to compensate its joint friction, can be implemented to achieve the robot dynamics behavior in Eq. (3.1).

Compensating the modeled joint friction is a strategy used to deal with most of friction-related effects, since joint friction modeling can effectively create a map between joint friction and the velocity, load, and temperature of the robot joints. However, as shown in Fig. 3.1, in the vicinity of zero-crossings of the joint velocity, the magnitude of joint friction would not be repeatable, in the sense that under the same measurable conditions, the magnitude of joint friction might change. This phenomenon is known as joint static friction, or *stiction* [Haug *et al*., 1986] and it is caused by the interactions between the asperities of the surfaces (such as gears, bearings, and shafts) in contact inside the joints of robot manipulators [Bittencourt and Gunnarsson, 2012; Bagge Carlson *et al*., 2015]. A common strategy to mitigate joint static friction is the use of a high-frequency oscillatory signal as torque feedforward, which is known as *dithering* [Ipri and Asada, 1995]. Nevertheless, a high

amplitude of the feedforward torque signal used in the dithering method may cause structural vibrations in the robot. In the context of pHRI, the manual guidance of a vibrating robot could cause, at least, discomfort in the guiding human operator and reduce the effectiveness of the manual guidance, hence the appeal for an alternative approach to mitigate joint stiction.

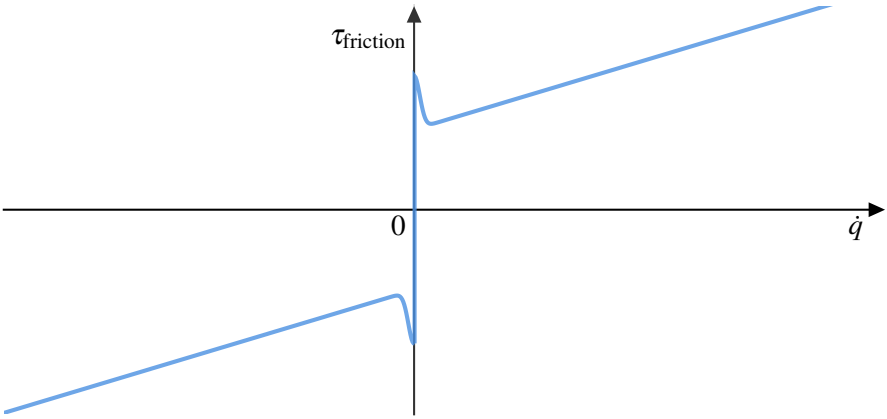

Figure 3.1 Simplified plot of the relationship between joint friction torque, τ_{friction}, and joint angular velocity, $\dot{q}$.

Control-Induced Uncertainties

Indirect force controllers used in robot tasks where pHRI is often present, such as the Cartesian impedance controller formulation discussed in Sec. 2.3, would allow the end-effector pose of the robot to reach a user-defined Cartesian reference, $\xi_d(t)$, while also allowing the robot to behave as a mass-spring-damper system, Eq. (2.32), at its end-effector, which is beneficial in an unknown robot-environment interaction scenario. However, as a trade-off, these force controllers might be responsible for a series of uncertainties. Contrary to stiffer position controllers, as presented in Sec. 2.2, impedance controllers would introduce a robot tracking error with respect to a user-defined reference that might cause a robot task to not be completed.

Moreover, feedback-control strategies, which have been extensively used to improve robot trajectory tracking, are not catered for these force controllers since their implementation would increase the robot stiffness when interacting with its surroundings, to the point of being able to cause unforeseeable damages. Also, alternative tracking strategies that involve time-scaling of the trajectory along a desired robot end-effector path [Dahl, 1992; Olofsson and Nielsen, 2017; Dahlin and Karayiannidis, 2021] would inherently disregard the temporal characteristics of the

desired robot trajectory and might not ensure the robot task completion for not fully-modeled robot dynamics.

Therefore, robot trajectory following should be improved in these controllers to achieve robot task completion, while minimally modifying the possible force exchange between the robot and its surroundings. Additionally, obtaining, or learning, robot controller improvements should not require time-consuming learning processes, such as the ones that can be seen when applying *reinforcement learning* to robot task-learning [Ibarz *et al*., 2021], since the new industrial manufacturing trends that motivate the use of pHRI also require flexibility to adapt to rapidly-changing industrial settings.

Uncertainty Sources External to the Robot

Collaborative industrial scenarios would also be populated by human operators and other agents, which might interact with the robot, thus increasing the complexity of robot control.

Human Behavior

Human operators that share their workspace with robot manipulators might behave in different ways with respect to the robot tasks. An overview of the different HRC scenarios was presented in Sec. 2.3: physical human–robot interaction might occur or not, and might be voluntary (from the human operator standpoint) or accidental; also, it might be cooperative (from the robot-task design standpoint, *e.g.*, a collaborative pick-and-place operation [Sadrfaridpour and Wang, 2018]) or antagonistic. Depending on the scenario, a proper robot reaction could be to anticipate and avoid the involuntary contact by using a robot collision-avoidance strategy (if the collision should be avoided and the available sensor data contain enough information to achieve a successful avoidance), or to allow the collision and handle it using one of the force control strategies discussed in Sec. 2.3.

Moreover, robot collision-avoidance strategies could be used to avoid that human guidance leads a robot to unsafe situations in the collaborative industrial environment. Control Barrier Functions (CBFs) [Ames *et al*., 2019] have been used for robot collision avoidance in recent years [Landi *et al*., 2019; Ferraguti *et al*., 2020; Rauscher *et al*., 2016; Singletary *et al*., 2021b] (a comparison of CBFs with respect to alternative robot collision-avoidance strategies can be found in Sec. 2.2). Barrier functions incorporate a model of the robot to minimally modify its behavior while achieving robot safety, thus addressing the industry interest in not compromising task efficiency [El Zaatari *et al*., 2019]. However, the simplified models (both kinematics and dynamics models) that have been used so far to formulate CBFs with robot manipulators might lead to safety violations [Singletary *et al*., 2021b; Rauscher *et al*., 2016]. Additionally, CBFs have often been used to command position or velocity references to the robot, which would disregard the ability of the

internal controller at the robot joints (see Fig. 2.1) to accurately track such position or velocity references.

Furthermore, robot joint redundancy, as presented in Sec. 2.1, could be used for robot collision avoidance without modifying the main (Cartesian) robot task. This would further decrease the cost, in terms of task-efficiency reduction, of achieving robot safety. Nevertheless, previous contributions in this regard have used APFs (see Sec. 2.2) that did not consider the dynamics behavior of the robot [Flacco *et al*., 2012; Lin *et al*., 2016; Liu *et al*., 2022], which, as mentioned earlier, might lead to robot safety violations.

Finally, a longer-time prediction of the behaviors of human operators and robots would allow anticipatory robot control action for collision avoidance, which might be useful to increase robot safety. For safety purposes, MPC strategies (see Sec. 2.2) have been combined with the aforementioned barrier functions formulation, so far, in other types of robotic systems, such as legged robots ([González Rodríguez *et al*., 2011]) [Grandia *et al*., 2021] and ground vehicles [Zeng *et al*., 2021]. However, these contributions proposed nonlinear MPC formulations, which cannot ensure achieving optimal solutions, and, more critically, have been shown to require long computational times that would invalidate their use in the context of robot safety during human–robot collaboration [Mukherjee *et al*., 2022].

Other Agents in Workspace

It should not be disregarded that additional agents, possibly with time-changing position and geometry, would also occupy the workspace shared by robot manipulators and human operators. Therefore, one of the main challenges that comes from the desire in the manufacturing industry to increase its flexibility is having to deal with partially unknown industrial environments, where humans and robots can effectively cooperate [Jaberzadeh Ansari and Karayiannidis, 2017], but where unexpected collisions with the environment may also occur. In such partially unknown environments, it is necessary to detect in a quick and accurate manner if a contact has occurred between the robot and its environment, and also to distinguish if this contact has been caused by voluntary human cooperation or by an accidental collision with an obstacle to identify the source of robot–environment contact.

External force/torque measurements or estimates [Haddadin *et al*., 2017] are often used for this purpose, and there are two main sets of methods, namely analyzing the frequency response of these signals or using machine learning (ML) [Cioffi *et al*., 2020], where the faster detection and classification provided by frequency response analysis can be advantageous compared to ML proposals to allow an online adaptation of the robot behavior. However, methods based on analyzing the frequency response require tuning numerous threshold parameters (*e.g.*, six per robot joint in [Geravand *et al*., 2013]), thus reducing the efficiency of these methods, and are yet to be tested alongside indirect robot force control methods used for pHRI (see Sec. 2.3) and without the use of sensors that are not embedded in collaborative robots [Kouris *et al*., 2016; Kouris *et al*., 2018].

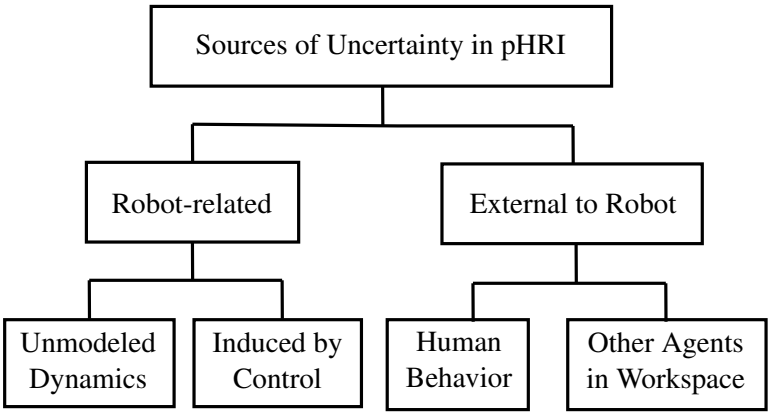

Figure 3.2 Schematic view of possible sources of uncertainty in pHRI.

Consequences of Uncertainty in pHRI

The aforementioned uncertainties that are present in collaborative scenarios alter the robot perception of its surroundings, including the robot awareness regarding the intentions and actions of human collaborators, and hinder the ability to achieve intuitive robot programming by human operators [Hägele *et al.*, 2016]. Therefore, these uncertainties have detrimental effects in both the functional safety of all the agents present in the shared workspace, and in a successful use of human manual guidance to modify the behavior of a robot. The remaining sections of this chapter have been dedicated to explaining how the contributions presented in this thesis have addressed the challenges motivated by these uncertainties, and also to compare the presented contributions to solutions available in the literature.

3.2 Safety in pHRI

As instructed in the international standards for collaborative robots [ISO, 2016] introduced in Sec. 2.1, safety related to robot operation (*i.e.*, *functional safety* [IEC, 2021]), requires to identify and eliminate hazards for the sake of risk reduction in human–robot collaborative operation. Hazards related to safety in pHRI would be caused by uncertainties in the relative position and motion of human operators and robots, and in terms of the force exchange between these two actors and between the robot manipulator and the rest of their workspace, as discussed in Sec. 3.1.

Methods suggested in [ISO, 2016, Sec. 5.5] to eliminate safety hazards could be summarized in two strategies, as shown in Fig. 3.3. The first strategy would be some form of obstacle avoidance, which could range from a complete stop of the robot before the operator enters the collaborative workspace, to maintaining at all times a protective separation distance between robot and operator (including, or not, speed

monitoring based on this distance). Second, the other strategy would be to assume that in the case of physical contact between robot and operator, the power and force exchange should be limited. These limits on the force exchange would also depend on the human body part involved, the head being the most sensitive part of operators bodies [ISO, 2016, Annex A.2].

Furthermore, within the force/power-limitation strategy, a categorization between active and passive safety-design methods, analogous to the one found for robot force controllers in Sec. 2.3 can be found in the international standards on collaborative robots [ISO, 2016, Sec. 5.5.5.4]. Indeed, the force controllers presented in Sec. 2.3 would fall into their corresponding category. Additionally, [ISO, 2016, Sec. 5.5.5.4] covers other non-functional aspects such as design strategies currently used in the production of collaborative robots [Franka Emika, 2019; Bischoff *et al.*, 2010] as passive safety methods (*e.g.*, rounded edges and corners, smooth surfaces, padding and cushioning), or software (computed-controlled) limitations of robot characteristics (*e.g.*, forces, torques, and velocities) as active safety methods.

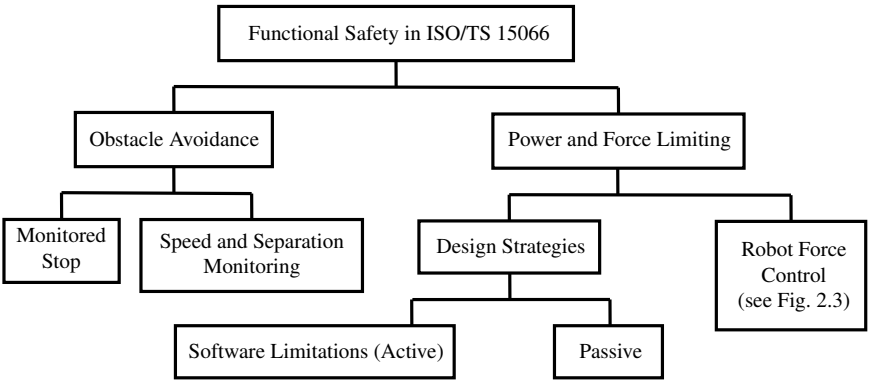

Figure 3.3 Schematic view of strategies for functional safety proposed in the international standards for collaborative robots [ISO, 2016].

As mentioned in [ISO, 2016, Sec. 5.5], the two strategies for eliminating functional safety hazards (obstacle avoidance and force/power limitation) can be combined. A proposal that would achieve this desirable combination from a robot control perspective could be to modulate the impedance behavior of a robot depending on a particular need for obstacle avoidance, *e.g.*, using CBFs (see Ch. 2.2), as presented in *Paper IV* [Salt Ducaju *et al.*, 2022b] (included in the Licentiate Thesis by the author [Salt Ducaju, 2023]), and then further developed in *Papers V* and *VI* [Salt Ducaju *et al.*, 2023; Salt Ducaju *et al.*, 2024b]. This proposal would allow pHRI, including manual guidance of a robot operator, while establishing prohibited robot behaviors, *i.e.*, scenarios where a safety hazard would need to be addressed by a robot collision-avoidance strategy, such as speed or separation monitoring.

A suitable indirect force-control implementation should be able to ensure safe robot operation for most of the collisions (*i.e.*, involuntary contacts) with operators. However, it is known that further protection should be considered for the operators heads [ISO, 2016, Annex A.2], thus the appeal of impedance control implementations that incorporate certain obstacle-avoidance strategies, as presented in *Paper V* [Salt Ducaju *et al*., 2023]. Additionally, most of the international standards on robot safety focus on the health of human operators. However, a truly flexible workspace would also protect other actors (*e.g.*, other equipment) present in the robot workspace that might take the role of obstacles during pHRI, and would also avoid that this other equipment could harm robots (which might also be a limitation of the current international standards that advise against the presence of objects with sharp, pointed, or cutting edges in the collaborative environment [ISO, 2016, Subclause 5.5.5.3]). Therefore, to maximize the capabilities of collaborative environments, robot impedance modulation should allow these scenarios, but directly translate into an arduous manual guidance of the robot that would first discourage, and then disallow, a collision with any of these obstacles, as proposed in *Papers IV* and *VI* [Salt Ducaju *et al*., 2022b; Salt Ducaju *et al*., 2024b].

As a common trait of these collaborative scenarios, the capacity of the functional safety strategies to address possible hazards would rely on the knowledge of the scenario and the capacity to react to changes in it. First, in *Paper IV* [Salt Ducaju *et al*., 2022b], CBFs (see Sec. 2.2) were used for a minimal variation of the nominal Cartesian impedance behavior of a robot in a collaborative scenario to avoid human guidance of this robot toward an unsafe situation. A model of rigid-body dynamics was used to achieve a more accurate description of the robot behavior than in previous contributions [Landi *et al*., 2019; Ferraguti *et al*., 2020; Rauscher *et al*., 2016; Singletary *et al*., 2021b], thus increasing robot safety guarantees. Not only was the model used to describe the robot behavior more accurately, but also, global stability guarantees, valid for passive environments [Lozano *et al*., 2013, Ch. 7], and novel in the context of modifying the behavior of robotic manipulators using CBFs, were provided.

Nevertheless, these functional safety strategies would modify the main (Cartesian) robot task. However, as mentioned in Sec. 2.1, a redundant robot would be allowed to perform additional subtasks, such as collision avoidance, without modifying its main task, by executing these subtasks in the null-space of the main task. Compared to previous contributions found in literature [Flacco *et al*., 2012; Lin *et al*., 2016; Liu *et al*., 2022], the novel use of CBFs presented in *Paper V* [Salt Ducaju *et al*., 2023] allowed to improve safety in collaborative scenarios by considering robot dynamics to control the null-space motion of the robot. In *Paper V* [Salt Ducaju *et al*., 2023], the null-space impedance behavior of Eq. (2.34) of the robot was modulated (using CBFs), which had the additional benefit of allowing the execution of other robot subtasks beneficial to HRC, such as improving the joint range available [Egeland *et al*., 1988] for manual guidance of the robot, in a single shared null-space DOF of the main robot task. Also, analogous to the formulation

in *Paper IV* [Salt Ducaju *et al*., 2022b], novel stability guarantees were provided for null-space impedance modulation. Moreover, it must be noted that the scenarios where null-space impedance modulation would improve functional safety, often would not achieve obstacle avoidance with respect to the robot end-effector, but only with respect to the rest of the body of the robot, as discussed in *Paper V* [Salt Ducaju *et al*., 2023]. However, null-space modulation could be combined with the previously presented Cartesian impedance formulation in *Paper IV* [Salt Ducaju *et al*., 2022b] to achieve more complete safety characteristics together with minimal perturbation of the robot main task that would avoid unnecessarily compromising robot task execution.

Furthermore, another shortcoming of the aforementioned robot collision-avoidance strategies [Landi *et al*., 2019; Ferraguti *et al*., 2020; Rauscher *et al*., 2016; Singletary *et al*., 2021b], which is also present in the contributions found in *Paper IV* [Salt Ducaju *et al*., 2022b] and *Paper V* [Salt Ducaju *et al*., 2023] is the lack of a longer time prediction of the robot behavior to anticipate possible undesired collisions and further decrease risks in human–robot collaboration. *Paper VI* [Salt Ducaju *et al*., 2024b] addressed this by using MPC (see Sec. 2.2) to include a longer time-frame prediction of both the behavior of the robot and of the human operator guiding it. Additionally, as an advantage compared to previous contributions [Grandia *et al*., 2021; Zeng *et al*., 2021] that also combined MPC with barrier functions for robot collision avoidance, the formulation in *Paper VI* could guarantee optimality in its computed solutions and allowed a fast computation of the MPC optimization problem, thus being able to ensure a fast robot reaction to changes in the collaborative environment.

3.3 Physical Human–Robot Collaboration (pHRC) for Kinesthetic Teaching

As discussed in Ch. 1, during *kinesthetic teaching*, which is also known as *Programming by Demonstration* (*PbD*) [Billard *et al*., 2008], a human operator manually guides a robot manipulator to define or modify its trajectory. This robot programming strategy aspires to reduce the need for specialized human operators (*i.e.*, operators with technical knowledge in robotics) in industrial environments, who would be complemented by unspecialized operators, by capitalizing skills inherent to human operators of any level of technical knowledge, such as their intelligence, dexterity, and responsiveness. The relevance of kinesthetic teaching becomes apparent when addressing the rapidly-changing modern industrial environments and their need for flexibility. Also, kinesthetic teaching is the quickest method for capturing a human demonstration and is often preferred by users to similar strategies, such as teleoperation [Fischer *et al*., 2016].

However, before the widespread adoption of kinesthetic teaching in industrial scenarios, it is necessary to first address current technical limitations on the use

of physical Human–Robot Collaboration (pHRC) from a robot control standpoint, some of which emerge from the uncertainties described in Sec. 3.1. Not only do these uncertainties have an effect on the functional safety of robot manipulators (and the other actors in their shared workspace), as discussed in Sec. 3.2, but they also have an influence on different aspects that condition the implementation success of kinesthetic teaching.

Figure 3.4 A human–robot collaborative scenario where an operator was guiding a Franka Emika Panda robot mounted on a table (figure included in *Paper VI* [Salt Ducaju *et al.*, 2024b]).

Facilitating Manual Guidance for Kinesthetic Teaching

A human operator whose role is to define or modify a robot trajectory via kinesthetic teaching, *i.e.*, by manually guiding the robot manipulator, has to be comfortable with the physical interaction with the robot [Hägele *et al.*, 2016]. Contributions

to improve operator ergonomics [Busch *et al*., 2017] and to reduce muscle fatigue [Peternel *et al*., 2016] have been proposed in this regard. However, not repeatable robot dynamics phenomena might also hinder manual robot guidance since they cannot be learnt and/or compensated, thus varying the necessary force that operators should exert to the robot in each interaction.

As described in Ch 3.1 and shown in Fig. 3.1, joint *stiction*, is not a repeatable component of joint friction that manifests in the proximity of zero joint-velocities, which might be mitigated at the risk of causing structural vibrations in the robot (see *dithering* [Stolt *et al*., 2011]). In addition, the problem of stiction becomes apparent for collaborative robots, since their often redundant joint configuration (*i.e.*, collaborative robots are often equipped with more than 6 rotational joints), designed to achieve a greater robot dexterity [Crowe, 2022], also causes that, if the robot is not at a singular joint configuration, not all of the robot DOFs need to be used during a robot Cartesian trajectory execution.

Therefore, to avoid the possible structural vibrations that might appear if dithering [Stolt *et al*., 2011] were used to reduce joint friction-torque dispersion, an alternative method for redundant collaborative robots was proposed in *Paper I* [Salt Ducaju *et al*., 2021] to facilitate the teaching process. The method proposed exploited joint redundancy and consisted in adding joint motion in the null-space of the task frame, *i.e.*, a linear combination of joint angular velocities that causes no change in the velocity of the end-effector of the robot [Sadeghian *et al*., 2013], to ensure that no joint remains still during the trajectory execution, thus suppressing stiction.

Moreover, in the formulation presented in *Paper I* [Salt Ducaju *et al*., 2021], null-space joint velocity references were added to a velocity-based robot controller (see Fig. 2.1) that used MPC for trajectory tracking. Then, it was suggested in *Paper I* that pHRI could be used by implementing a dual-mode robot controller that would allow to switch between a trajectory-tracking mode and an admittance (see Sec. 2.3) mode. Nevertheless, applying the joint-stiction suppression proposal in *Paper I* would not be limited to this robot control architecture, and it might be used together with any other strategy that controls robot motion in its task frame, such as Cartesian impedance control.

Distinguishing Kinesthetic Teaching from other Physical Interaction Sources

As mentioned in Sec. 3.1, in modern industrial environments, robot manipulators should be able to share their workspace with human operators and with other actors, such as equipment and tools. These other actors present in the robot workspace might obstruct the motion of the robot and cause an involuntary collision with the robot, thus taking the role of obstacles from the robot task perspective. Then, to benefit from human operator guidance, it is necessary to detect fast if the robot is experiencing a contact with respect to its environment, and to distinguish the

source of this contact, which could be an involuntary collision with an obstacle or a voluntary human guidance event.

Two are the main uses of fast contact detection and classification in the context of kinesthetic teaching: First, if human guidance occurred during the robot trajectory execution, physical interaction of the robot with its surroundings might be modified online to ease human guidance. Second, after a robot trajectory execution, a contact event accurately classified as human guidance can be used for trajectory correction, whereas possible accidental collisions could be, if determined as persistent, avoided in future trajectory executions.

In *Paper II* [Salt Ducaju *et al*., 2022a], a contact detection and classification strategy compatible with a force controller that allows safe physical interaction between the robot and its surroundings (see Sec. 2.3) was proposed. The method proposed in *Paper II* included necessary modifications and extensions to overcome the limitations observed in previous frequency-based proposals [Kouris *et al*., 2016; Kouris *et al*., 2018] to quickly detect and classify contacts in any direction for a collaborative assembly task relying only on embedded sensors of an impedance-controlled robot. Advantageously, removing the need for additional sensors to detect and classify robot collisions would reduce the total hardware costs that would be derived from purchasing extra components in a robot setup [Hägele *et al*., 2016].

Moreover, the proposal in *Paper II* [Salt Ducaju *et al*., 2022a] required tuning only of two parameters, and presented novel benefits for its use in HRC compared to previous contributions in literature [Kouris *et al*., 2016; Kouris *et al*., 2018; Geravand *et al*., 2013; Golz *et al*., 2015; Popov *et al*., 2017; Briquet-Kerestedjian *et al*., 2019; Cioffi *et al*., 2020]: it was able to detect and classify human interaction that occurred while the robot was collided (beneficial for corrective trajectory demonstrations), and also, it was robust to different levels of skill of human operators (reducing the necessity for specialized human operators for robot guidance). As a limitation, the proposal in *Paper II* was only demonstrated for stiff and static obstacles.

Using Kinesthetic Teaching for Robot Trajectory Correction

Once a human operator has manually guided a robot to define or modify its trajectory, and the human guidance has been properly detected and classified as such, the use of this acquired information (in terms of data provided by the sensors embedded in the robot) to correct the robot trajectory in future task executions remains an open problem. It is possible to use these data to modify the reference used in a robot indirect force controller. In the case of a Cartesian impedance controller, it would be straightforward to use the Cartesian trajectory recorded during the previous human guidance as the new reference Cartesian pose, ξ_d. However, as mentioned in Sec. 3.1, impedance controllers would introduce a slight trajectory-tracking error that might cause non-completion of the robot task.

In *Paper III* [Salt Ducaju *et al*., 2024a], a strategy to improve robot trajectory

tracking while using an impedance controller by slightly modifying its Cartesian reference was proposed. Compared to stiff position-feedback controllers used to improve robot trajectory tracking, the proposal in *Paper III* allowed a reasonable physical interaction between the robot and its surroundings that would not damage any of the actors involved in this interaction; and also, would not modify the temporal characteristics of the robot trajectory, as opposed to time-scaling alternatives [Dahl, 1992; Olofsson and Nielsen, 2017; Dahlin and Karayiannidis, 2021].

Additionally, the proposal in *Paper III* [Salt Ducaju *et al*., 2024a] provided a strategy more suitable for learning robot impedance-controller references than previous learning formulations. First, iterative learning control (ILC) [Arimoto *et al*., 1984], in its linear formulation [Norrlöf and Gunnarsson, 2001; Cano Marchal *et al*., 2014], might not fully consider the robot dynamics when defining convergence guarantees [Norrlöf and Gunnarsson, 2020]. As a consequence, a linear ILC strategy [Norrlöf and Gunnarsson, 2001] allowed, as shown in the experiments presented in *Paper III*, an aggressive reference correction, which translated in an, undesirable, large impedance force variation. In comparison, the proposal in *Paper III* [Salt Ducaju *et al*., 2024a] considered the nonlinearities of robot dynamics in its convergence analysis, and provided a smoother, more conservative, reference correction, that lead to a faster (*i.e.*, in less iterations) convergence to robot task completion.

Moreover, adaptive learning strategies, such as AILC [Park *et al*., 1996; Lee *et al*., 2019], considered nonlinearities in robot dynamics. However, these strategies would online modify the impedance behavior of the robot, hence could not be used for learning impedance-reference corrections. Furthermore, as discussed in Sec. 3.1, reinforcement learning (RL) strategies [Ibarz *et al*., 2021], although capable of allowing to learn complex robot behaviors, often required a high number of learning iterations, which would negatively affect the flexibility to adapt to the rapidly-changing industrial settings that motivated human corrective guidance of the robot.

4

Conclusions and Future Research

The research presented in this thesis aimed to improve the involvement of human operators in workspaces shared with robot manipulators by addressing the two research questions that arose from this research problem, namely improving the effectiveness of kinesthetic teaching and increasing safety in collaborative industrial environments. Different methods were proposed to achieve this goal from a robot control perspective.

First, the addition of null-space motion to robot trajectories showed to reduce uncertainty in the force needed for human guidance caused by joint static friction, thus facilitating kinesthetic teaching. The structural vibrations and possible wear of the robot components caused using alternative state-of-the-art methods, such as dithering, was avoided in the proposed method, although the application scope of the proposed method might be limited to redundant manipulators.

Second, necessary modifications and extensions were proposed in this thesis to state-of-the-art methods to achieve fast contact detection and classification in any contact direction for kinesthetic teaching applications. The proposed method provided an accurate distinction between voluntary human cooperation and accidental collisions with stiff and static obstacles in a collaborative assembly task with collaborative robots.

Third, an iterative reference-learning strategy was proposed to improve the robot trajectory tracking of human manual demonstrations for impedance-controlled robots, while allowing the physical interaction of the robot with its surroundings. The impedance dynamics of the robot were included in its convergence analysis.

Forth, using CBFs to online modify the Cartesian impedance behavior of a robot provided a stable and effective method for improving safety in kinesthetic teaching applications. The method proposed was able to avoid that a human operator could guide a robotic manipulator to an undesired part of the workspace of the robot. Additionally, this online Cartesian impedance variation method was included in the Licentiate Thesis by the author [Salt Ducaju, 2023] and later extended including

linearized CBFs in a linear MPC strategy to consider a prediction of human behavior with coordinated robot control that further improved physical safety in collaborative applications.

Fifth, the null-space impedance behavior of a redundant robot was modulated online using CBFs to achieve robot obstacle avoidance for scenarios that did not involve the end-effector of the robot, thus avoiding unnecessary modifications of the main robot task while increasing the robot functional safety.

4.1 Future Research

Different contributions have been presented in this thesis to improve the involvement of human operators in industrial environments by the use of kinesthetic teaching and while considering functional safety aspects in these collaborative scenarios. Nevertheless, the robot control questions addressed throughout this thesis can be further studied toward a desirable enhanced integration of humans and robots in industrial collaborative environments in certain research directions.

First, to further improve the use of human guidance for robot task adaptation, the concept presented in *Paper I* of using null-space motion to avoid stiction by ensuring the motion of all robot joints during robot trajectory execution could be included alongside other tasks performed in shared null-space DOFs, as shown in *Paper IV* for robot obstacle avoidance together with manipulability maximization. Moreover, the method for fast collision detection and classification presented in *Paper II* could be tested and, if needed, additional extensions might be suggested to enable its application for soft and/or non-static obstacles. Furthermore, the impedance-controlled robot dynamics used in *Paper III* to show the convergence of the learning proposal might be incorporated in the selection of a learning gain that further improved iterative learning for bettering robot tracking of human manual demonstrations.

Second, to further increase functional safety in collaborative environments without compromising efficiency, stability conditions for the implementation of the Cartesian impedance-modulation method presented in *Paper IV* in non-passive robot environments [Müller *et al.*, 2019] could be developed. Moreover, experiments could be proposed to evaluate the behavior of the robot collision-avoidance method presented in *Papers IV* and *VI* in multi-obstacle collaborative scenarios, and possible extensions might be proposed to deal with the possible appearance of problems related to local minima. Furthermore, the prediction capabilities of the impedance-variation method proposed in *Paper VI* could be further improved by including more complex strategies to anticipate the intention and future motion of the human operator [Bandi and Thomas, 2021]. These strategies might involve considering the neurological ability of human operators to estimate the behavior of collaborative robots [Wolpert and Ghahramani, 2000].

Bibliography

Abu-Dakka, F. J., B. Nemec, A. Kramberger, A. G. Buch, N. Krüger, and A. Ude (2014). "Solving peg-in-hole tasks by human demonstration and exception strategies". *Industrial Robot* **41**:6, pp. 575–584.

Ajoudani, A., A. M. Zanchettin, S. Ivaldi, A. Albu-Schäffer, K. Kosuge, and O. Khatib (2018). "Progress and prospects of the human–robot collaboration". *Autonomous Robots* **42**, pp. 957–975.

Akgun, B., M. Cakmak, J. W. Yoo, and A. L. Thomaz (2012). "Trajectories and keyframes for kinesthetic teaching: A human-robot interaction perspective". In: *ACM/IEEE International Conference on Human-Robot Interaction*. Mar. 5–8. Boston, MA, USA, pp. 391–398.

Ames, A. D., S. Coogan, M. Egerstedt, G. Notomista, K. Sreenath, and P. Tabuada (2019). "Control barrier functions: Theory and applications". In: *European Control Conference (ECC)*. Jun. 25–28. Naples, Italy, pp. 3420–3431.

Ardakani, M. M. G., M. Karlsson, K. Nilsson, A. Robertsson, and R. Johansson (2018). "Master-slave coordination using virtual constraints for a redundant dual-arm haptic interface". In: *IEEE/RSJ International Conference on Intelligent Robots and Systems (IROS)*. Oct. 1–5. Madrid, Spain, pp. 8751–8757.

Argall, B. D., S. Chernova, M. Veloso, and B. Browning (2009). "A survey of robot learning from demonstration". *Robotics and Autonomous Systems* **57**:5, pp. 469–483.

Arimoto, S., S. Kawamura, and F. Miyazaki (1984). "Bettering operation of robots by learning". *Journal of Robotic systems* **1**:2, pp. 123–140.

Armstrong-Hélouvry, B., P. Dupont, and C. Canudas de Wit (1994). "A survey of models, analysis tools and compensation methods for the control of machines with friction". *Automatica* **30**:7, pp. 1083–1138.

Åström, K. J. and B. Wittenmark (2013). *Computer-Controlled Systems: Theory and Design*. Courier Corporation, Chelmsford, MA, USA.

Åström, K. J. and R. M. Murray (2021). *Feedback systems: An introduction for scientists and engineers*. Princeton Univ. Press, Princeton, NJ, USA.

Bagge Carlson, F., A. Robertsson, and R. Johansson (2015). "Modeling and identification of position and temperature dependent friction phenomena without temperature sensing". In: *IEEE/RSJ International Conference on Intelligent Robots and Systems (IROS)*. Sep. 28–Oct. 2. Hamburg, Germany, pp. 3045–3051.

Bandi, C. and U. Thomas (2021). "Skeleton-based action recognition for human-robot interaction using self-attention mechanism". In: *IEEE International Conference on Automatic Face and Gesture Recognition (FG)*. Dec. 15–18. Jodhpur, India, pp. 1–8.

Bejczy, A. K. (1974). *Robot arm dynamics and control*. Tech. rep. NASA-CR-136935. Jet Propulsion Laboratory, California Institute of Technology, Pasadena, CA, USA.

Billard, A. G., S. Calinon, and R. Dillmann (2008). "Learning from human". In: Siciliano, B. *et al*. (Eds.). *Springer Handbook of Robotics*. 2nd. Vol. 200. Springer, Berlin, Germany. Chap. 74, pp. 1995–2014.

Bischoff, R., J. Kurth, G. Schreiber, R. Koeppe, A. Albu-Schäffer, A. Beyer, O. Eiberger, S. Haddadin, A. Stemmer, G. Grunwald, and G. Hirzinger (2010). "The KUKA-DLR lightweight robot arm—A new reference platform for robotics research and manufacturing". In: *International Symposium on Robotics (ISR)*. Jun. 7–9. Munich, Germany, pp. 1–8.

Bittencourt, A. C. and S. Gunnarsson (2012). "Static friction in a robot joint—Modeling and identification of load and temperature effects". *Journal of Dynamic Systems, Measurement, and Control* **134**:5, pp. 1–10.

Book, W. J., S. Le, and V. Sangveraphunsiri (1985). "Bracing strategy for robot operation". In: *Theory and Practice of Robots and Manipulators: Proceedings of RoManSy'84: The Fifth CISM—IFToMM Symposium*. Springer, pp. 179–185.

Boyd, S. P. and L. Vandenberghe (2004). *Convex Optimization*. Cambridge Univ. Press, Cambridge, UK.

Briquet-Kerestedjian, N., A. Wahrburg, M. Grossard, M. Makarov, and P. Rodriguez-Ayerbe (2019). "Using neural networks for classifying human-robot contact situations". In: *18th European Control Conference (ECC)*. Jul. 25–28. Naples, Italy, pp. 3279–3285.

Busch, B., G. Maeda, Y. Mollard, M. Demangeat, and M. Lopes (2017). "Postural optimization for an ergonomic human-robot interaction". In: *IEEE/RSJ International Conference on Intelligent Robots and Systems (IROS)*. Sep. 24–28. Vancouver, Canada, pp. 2778–2785.

Caliskan, U., F. Ulloa Rios, W. Decré, and E. Aertbeliën (2022). "Dual constraint-based controllers for wheeled mobile manipulators". In: *IEEE International Conference on Automation Science and Engineering (CASE)*. Aug. 20–24. Mexico City, pp. 1002–1008.

Cano Marchal, P., O. Sörnmo, B. Olofsson, A. Robertsson, J. Gómez Ortega, and R. Johansson (2014). "Iterative learning control for machining with industrial robots". *IFAC Proceedings Volumes* **47**:3, pp. 9327–9333.

Canudas de Wit, C., H. Olsson, K. J. Åström, and P. Lischinsky (1995). "A new model for control of systems with friction". *IEEE Transactions on Automatic Control* **40**:3, pp. 419–425.

Cencen, A., J. C. Verlinden, and J. Geraedts (2018). "Design methodology to improve human-robot coproduction in small-and-medium-sized enterprises". *IEEE/ASME Transactions on Mechatronics* **23**:3, pp. 1092–1102.

Chiaverini, S., B. Siciliano, and O. Egeland (1994). "Review of the damped least-squares inverse kinematics with experiments on an industrial robot manipulator". *IEEE Transactions on Control Systems Technology* **2**:2, pp. 123–134.

Christensen, H. I. and G. D. Hager (2008). "Sensing and estimation". In: Siciliano, B. *et al*. (Eds.). *Springer Handbook of Robotics*. 2nd. Vol. 200. Springer, Berlin, Germany. Chap. 5, pp. 91–112.

Chung, W. K., L.-C. Fu, and T. Kröger (2008). "Motion control". In: Siciliano, B. *et al*. (Eds.). *Springer Handbook of Robotics*. 2nd. Vol. 200. Springer, Berlin, Germany. Chap. 8, pp. 163–194.

Cioffi, G., S. Klose, and A. Wahrburg (2020). "Data-efficient online classification of human-robot contact situations". In: *European Control Conference (ECC)*. May 12–15. Saint Petersburg, Russia, pp. 608–614.

Colgate, J. E., J. Edward, M. A. Peshkin, and W. Wannasuphoprasit (1996). "Cobots: Robots for collaboration with human operators". In: *Proceedings of the ASME Dynamic Systems and Control Division: ASME International Mechanical Engineering Congress and Exposition*. Nov. 17–22. Atlanta, GA, USA, pp. 433–439.

Corke, P. (2013). *Robotics, Vision and Control: Fundamental Algorithms in MATLAB*. Springer, Berlin, Germany.

Crowe, S. (2022). *Collaborative robots comparison tool*. URL: `https://www.cobottrends.com/cobot-comparison-tool/` (visited on 2022-10-25).

Dahl, O. (1992). *Path Constrained Robot Control*. Thesis No. TFRT-1038. Doctoral Thesis. Department of Automatic Control, Faculty of Engineering LTH, Lund University, Lund, Sweden.

Dahl, P. R. (1968). *A solid friction model*. Tech. rep. TOR-01 58(3 107-1 8)- 1. The Aerospace Corporation, El Segundo, CA, USA, pp. 1–24.

Dahlin, A. and Y. Karayiannidis (2021). "Temporal coupling of dynamical movement primitives for constrained velocities and accelerations". *IEEE Robotics and Automation Letters* **6**:2, pp. 2233–2239.

Egeland, O., J. Sagli, and B. Jansen (1988). "Optimal continuous-path control for manipulators with redundant degrees of freedom". In: *Robot Control (Syroco'88)*. Oct. 5–7. Karlsruhe, Germany, pp. 237–242.

Egeland, O. (1987). "Task-space tracking with redundant manipulators". *IEEE Journal on Robotics and Automation* **3**:5, pp. 471–475.

El Zaatari, S., M. Marei, W. Li, and Z. Usman (2019). "Cobot programming for collaborative industrial tasks: An overview". *Robotics and Autonomous Systems* **116**, pp. 162–180.

Ergun, S., Y. Ding, H. Alagi, C. Schöffmann, B. Ubezio, G. Soti, M. Rathmair, S. Mühlbacher-Karrer, U. Thomas, B. Hein, *et al.* (2021). "A unified perception benchmark for capacitive proximity sensing towards safe human-robot collaboration (HRC)". In: *IEEE International Conference on Robotics and Automation (ICRA)*. May 31–Jun. 4. Xi'an, China, pp. 3634–3640.

Ferraguti, F., M. Bertuletti, C. T. Landi, M. Bonfè, C. Fantuzzi, and C. Secchi (2020). "A control barrier function approach for maximizing performance while fulfilling to ISO/TS 15066 regulations". *IEEE Robotics and Automation Letters* **5**:4, pp. 5921–5928.

Ferraguti, F., C. Secchi, and C. Fantuzzi (2013). "A tank-based approach to impedance control with variable stiffness". In: *IEEE International Conference on Robotics and Automation (ICRA)*. May 6–10. Karlsruhe, Germany, pp. 4948–4953.

Fischer, K., F. Kirstein, L. C. Jensen, N. Krüger, K. Kukliński, M. V. aus der Wieschen, and T. R. Savarimuthu (2016). "A comparison of types of robot control for programming by demonstration". In: *ACM/IEEE International Conference on Human-Robot Interaction (HRI)*. Mar. 7–10. Christchurch, New Zealand, pp. 213–220.

Flacco, F., T. Kröger, A. De Luca, and O. Khatib (2012). "A depth space approach to human-robot collision avoidance". In: *IEEE International Conference on Robotics and Automation (ICRA)*. May. 14–19. St. Paul, MN, USA, pp. 338–345.

Franka Emika (2019). *Franka Emika Panda – Data Sheet*. `https://www.generationrobots.com/media/panda-franka-emika-datasheet.pdf`. (Visited on 2022-09-13).

Freidovich, L., A. Robertsson, A. Shiriaev, and R. Johansson (2009). "LuGre-model-based friction compensation". *IEEE Transactions on Control Systems Technology* **18**:1, pp. 194–200.

Garcia, C. E., D. M. Prett, and M. Morari (1989). "Model predictive control: Theory and practice—A survey". *Automatica* **25**:3, pp. 335–348.

Geravand, M., F. Flacco, and A. De Luca (2013). "Human-robot physical interaction and collaboration using an industrial robot with a closed control architecture". In: *IEEE International Conference on Robotics and Automation (ICRA)*. May 6–10. Karlsruhe, Germany, pp. 4000–4007.

Ghazaei Ardakani, M., B. Olofsson, A. Robertsson, and R. Johansson (2019). "Model predictive control for real-time point-to-point trajectory generation". *IEEE Transactions on Automation Science and Engineering* **16**:2, pp. 972–983.

Golz, S., C. Osendorfer, and S. Haddadin (2015). "Using tactile sensation for learning contact knowledge: Discriminate collision from physical interaction". In: *IEEE International Conference on Robotics and Automation (ICRA)*. May 26–30. Seattle, USA, pp. 3788–3794.

González Rodríguez, A., N. Eduardo Nava Rodriguez, and Á. G. González Rodríguez (2009). "Design and validation of a novel actuator with adaptable compliance for application in human-like robotics". *Industrial Robot: An International Journal* **36**:1, pp. 84–90.

González Rodríguez, A., Á. G. González Rodríguez, and P. Rea (2011). "A new articulated leg for mobile robots". *Industrial Robot: An International Journal* **38**:5, pp. 521–532.

Grandia, R., A. J. Taylor, A. D. Ames, and M. Hutter (2021). "Multi-layered safety for legged robots via control barrier functions and model predictive control". In: *IEEE International Conference on Robotics and Automation (ICRA)*. May 31–Jun. 4. Xi'an, China, pp. 8352–8358.

Haddadin, S., A. De Luca, and A. Albu-Schäffer (2017). "Robot collisions: A survey on detection, isolation, and identification". *IEEE Transactions on Robotics* **33**:6, pp. 1292–1312.

Hägele, M., K. Nilsson, J. Norberto Pires, and R. Bischoff (2016). "Industrial robotics". In: Siciliano, B. *et al.* (Eds.). *Springer Handbook of Robotics*. Springer, Berlin, Germany. Chap. 54, pp. 1385–1421.

Haug, E. J., S. C. Wu, and S. M. Yang (1986). "Dynamics of mechanical systems with Coulomb friction, stiction, impact and constraint addition-deletion—I Theory". *Mechanism and Machine Theory* **21**:5, pp. 401–406.

Hirzinger, G. (1986). "Robot systems completely based on sensory feedback". *IEEE Transactions on Industrial Electronics* **IE-33**:2, pp. 105–109.

Hogan, N. (1985). "Impedance control: An approach to manipulation: Parts I–III". *Journal of Dynamic Systems, Measurement, and Control* **107**:1, pp. 1–24.

Ibarz, J., J. Tan, C. Finn, M. Kalakrishnan, P. Pastor, and S. Levine (2021). "How to train your robot with deep reinforcement learning: Lessons we have learned". *The International Journal of Robotics Research* **40**:4-5, pp. 698–721.

IEC (2021). *IEC 62061:2021*. Safety of machinery — Functional safety of safety-related control systems. International Electrotechnical Commission.

IFR (2018a). *Robots and the workplace of the future*. https://ifr.org/downloads/hidden/IFR_Robots_and_the_Workplace_of_the_Future_Positioning_Paper_V01.pdf. A positioning paper by the International Federation of Robotics (Visited on 2022-11-10).

IFR (2018b). *The impact of robots on productivity, employment and jobs*. https://ifr.org/downloads/hidden/IFR_The_Impact_of_Robots_on_Employment_Positioning_Paper_updated_V02.pdf. A positioning paper by the International Federation of Robotics (Visited on 2022-11-10).

IFR (2020). *Demystifying collaborative industrial robots*. https://ifr.org/downloads/hidden/IFR_Demystifying_Collaborative_Robots_Update_v03.pdf. A positioning paper by the International Federation of Robotics (Visited on 2022-11-10).

Ipri, S. L. and H. Asada (1995). "Tuned dither for friction suppression during force-guided robotic assembly". In: *IEEE/RSJ International Conference on Intelligent Robots and Systems. Human Robot Interaction and Cooperative Robots*. Vol. 1. Aug. 5–9. Pittsburgh, PA, USA, pp. 310–315.

ISO (2011a). *ISO 10218-1:2011(E)*. Robots and robotic devices — Safety requirements for industrial robots — Part 1: Robots. International Organization for Standardization.

ISO (2011b). *ISO 10218-2:2011(E)*. Robots and robotic devices — Safety requirements for industrial robots — Part 2: Robot systems and integration. International Organization for Standardization.

ISO (2016). *ISO/TS 15066:2016(E)*. Robots and robotic devices — Collaborative robots. International Organization for Standardization.

Jaberzadeh Ansari, R. and Y. Karayiannidis (2017). "Reducing the human effort for human-robot cooperative object manipulation via control design". *IFAC-PapersOnLine* **50**:1, pp. 14922–14927.

Johansson, R., K. Nilsson, and A. Robertsson (2014). "Force control". In: Nee, A. Y. C. (Ed.). *Handbook of Manufacturing Engineering and Technology*. Springer, London, UK. Chap. 54, pp. 1933–1965.

Johansson, R., M. Annerstedt, and A. Robertsson (2009). "Stability of haptic obstacle avoidance and force interaction". In: *2009 IEEE/RSJ International Conference on Intelligent Robots and Systems*. Oct. 11–15. St. Louis, USA, pp. 3238–3243.

Karayiannidis, Y., C. Smith, and D. Kragic (2014). "Mapping human intentions to robot motions via physical interaction through a jointly-held object". In: *IEEE International Symposium on Robot and Human Interactive Communication (RO-MAN)*. Aug. 25–29. Edinburgh, Scotland, UK, pp. 391–397.

Karlsson, M., F. Bagge Carlson, M. Holmstrand, A. Robertsson, J. De Backer, L. Quintino, E. Assuncao, and R. Johansson (2023). "Robotic friction stir welding–seam-tracking control, force control and process supervision". *Industrial Robot – The International Journal of Robotics Research and Application (IR)* **50**:5, pp. 722–730.

Khatib, O. (1985). "Real-time obstacle avoidance for manipulators and mobile robots". In: *IEEE International Conference on Robotics and Automation (ICRA)*. Vol. 2. Mar. 25–28. St. Louis, MO, USA, pp. 500–505.

Khatib, O. (1987). "A unified approach for motion and force control of robot manipulators: The operational space formulation". *IEEE Journal on Robotics and Automation* **3**:1, pp. 43–53.

Khatib, O. (1995). "Inertial properties in robotic manipulation: An object-level framework". *The International Journal of Robotics Research* **14**:1, pp. 19–36.

Koren, Y. *et al*. (1991). "Potential field methods and their inherent limitations for mobile robot navigation." In: *IEEE International Conference on Robotics and Automation (ICRA)*. Vol. 2. Apr. 7–12. Sacramento, CA, USA, pp. 1398–1404.

Kouris, A., F. Dimeas, and N. Aspragathos (2016). "Contact distinction in human-robot cooperation with admittance control". In: *IEEE International Conference on Systems, Man, and Cybernetics (SMC)*. Oct. 9–12. Budapest, Hungary, pp. 1951–1956.

Kouris, A., F. Dimeas, and N. Aspragathos (2018). "A frequency domain approach for contact type distinction in human–robot collaboration". *IEEE Robotics and Automation Letters* **3**:2, pp. 720–727.

Kozlov, M. K., S. P. Tarasov, and L. G. Khachiyan (1979). "Polynomial solvability of convex quadratic programming". In: *Doklady Akademii Nauk*. Vol. 248. 5. Russian Academy of Sciences. Moscow, pp. 1049–1051.

Kurfess, T. R. (2005). *Robotics and Automation Handbook*. Vol. 414. Boca Raton, FL, USA.

Landi, C. T., F. Ferraguti, S. Costi, M. Bonfè, and C. Secchi (2019). "Safety barrier functions for human-robot interaction with industrial manipulators". In: *European Control Conference (ECC)*. Jun. 25–28. Naples, Italy, pp. 2565–2570.

Lee, R., L. Sun, Z. Wang, and M. Tomizuka (2019). "Adaptive iterative learning control of robot manipulators for friction compensation". *IFAC-PapersOnLine* **52**:15, pp. 175–180.

Lewis, F. (1996). "Essentials of theoretical computer science". *Dept. Computer Science, University of Kentucky, Lexington, KY, USA*.

Lin, H.-C., Y. Fan, T. Tang, and M. Tomizuka (2016). "Human guidance programming on a 6-DOF robot with collision avoidance". In: *IEEE/RSJ International Conference on Intelligent Robots and Systems (IROS)*. Oct. 9–14. Daejeon, Korea, pp. 2676–2681.

Liu, H., D. Qu, F. Xu, Z. Du, K. Jia, J. Song, and M. Liu (2022). "Real-time and efficient collision avoidance planning approach for safe human-robot interaction". *Journal of Intelligent & Robotic Systems* **105**:4, p. 93.

Lozano, R., B. Brogliato, O. Egeland, and B. Maschke (2013). *Dissipative systems analysis and control: Theory and applications*. Springer-Verlag, London, UK.

Lozano-Pérez, T., J. L. Jones, E. Mazer, and P. A. O'Donnell (1989). "Task-level planning of pick-and-place robot motions". *Computer* **22**:3, pp. 21–29.

Lynch, K. M. and F. C. Park (2017). *Modern Robotics*. Cambridge Univ. Press, Cambridge, UK.

Mukherjee, D., K. Gupta, L. H. Chang, and H. Najjaran (2022). "A survey of robot learning strategies for human-robot collaboration in industrial settings". *Robotics and Computer-Integrated Manufacturing* **73**, p. 102231.

Müller, F., J. Jäkel, J. Suchỳ, and U. Thomas (2019). "Stability of nonlinear time-delay systems describing human–robot interaction". *IEEE/ASME Transactions on Mechatronics* **24**:6, pp. 2696–2705.

Murray, R. M. (2023). "Optimization-based control". *Div. Biology and Biological Eng., California Institute of Technology, Pasadena, CA, USA*, pp. 1–159.

Norrlöf, M. and S. Gunnarsson (2001). "Disturbance aspects of iterative learning control". *Engineering Applications of Artificial Intelligence* **14**:1, pp. 87–94.

Norrlöf, M. and S. Gunnarsson (2002). "Time and frequency domain convergence properties in iterative learning control". *International Journal of Control* **75**:14, pp. 1114–1126.

Norrlöf, M. and S. Gunnarsson (2020). "An ILC approach to feed-forward friction compensation". *IFAC-PapersOnLine* **53**:2, pp. 1409–1414.

Olofsson, B. and L. Nielsen (2017). "Path-tracking velocity control for robot manipulators with actuator constraints". *Mechatronics* **45**, pp. 82–99.

Olsson, T., M. Haage, H. Kihlman, R. Johansson, K. Nilsson, A. Robertsson, M. Björkman, R. Isaksson, G. Ossbahr, and T. Brogårdh (2010). "Cost-efficient drilling using industrial robots with high-bandwidth force feedback". *Robotics and Computer-Integrated Manufacturing* **26**:1, pp. 24–38.

Ott, C. (2008). *Cartesian impedance control of redundant and flexible-joint robots*. Springer, Berlin, Germany.

Ott, C., A. Kugi, and Y. Nakamura (2008). "Resolving the problem of non-integrability of nullspace velocities for compliance control of redundant manipulators by using semi-definite Lyapunov functions". In: *IEEE International Conference on Robotics and Automation (ICRA)*. May 19–23. Pasadena, CA, USA, pp. 1999–2004.

Park, B., T.-Y. Kuc, and J. S. Lee (1996). "Adaptive learning control of uncertain robotic systems". *International Journal of Control* **65**:5, pp. 725–744.

Park, J. (2000). *Analysis and control of kinematically redundant manipulators: An approach based on kinematically decoupled joint space decomposition*. Doc. No. 991000372949703286. PhD thesis. Dept. Mech. Eng., Pohang University of Science and Technology, Pohang, South Korea.

Peternel, L., N. Tsagarakis, D. Caldwell, and A. Ajoudani (2016). "Adaptation of robot physical behaviour to human fatigue in human-robot co-manipulation". In: *IEEE-RAS International Conference on Humanoid Robots (Humanoids)*. Nov. 15–17. Cancun, Mexico, pp. 489–494.

Popov, D., A. Klimchik, and N. Mavridis (2017). "Collision detection, localization & classification for industrial robots with joint torque sensors". In: *26th IEEE International Symposium on Robot and Human Interactive Communication (RO-MAN)*. Aug. 28–31. Lisbon, Portugal, pp. 838–843.

Raibert, M. H. and J. J. Craig (1981). "Hybrid position/force control of manipulators". *Journal of Dynamic Systems, Measurement, and Control* **103**:2, pp. 126–133.

Rauscher, M., M. Kimmel, and S. Hirche (2016). "Constrained robot control using control barrier functions". In: *IEEE/RSJ International Conference on Intelligent Robots and Systems (IROS)*. Oct. 9–14. Daejeon, Korea, pp. 279–285.

Ravichandar, H., A. S. Polydoros, S. Chernova, and A. Billard (2020). "Recent advances in robot learning from demonstration". *Annual Review of Control, Robotics, and Autonomous Systems* **3**, pp. 297–330.

Robertsson, A., T. Olsson, R. Johansson, A. Blomdell, K. Nilsson, M. Haage, B. Lauwers, H. De Baerdemaeker, T. Brogårdh, and H. Brantmark (2006). "Implementation of industrial robot force control case study: High power stub grinding and deburring". In: *IEEE/RSJ International Conference on Intelligent Robots and Systems (IROS)*. Oct. 9–15. Beijing, China, pp. 2743–2748.

Sadeghian, H., L. Villani, M. Keshmiri, and B. Siciliano (2013). "Task-space control of robot manipulators with null-space compliance". *IEEE Transactions on Robotics* **30**:2, pp. 493–506.

Sadrfaridpour, B. and Y. Wang (2018). "Collaborative assembly in hybrid manufacturing cells: An integrated framework for human–robot interaction". *IEEE Transactions on Automation Science and Engineering* **15**:3, pp. 1178–1192.

Salt Ducaju, J. M. (2023). *Human-Robot Collaboration for Kinesthetic Teaching*. Licentiate Thesis TRFT-3278. Department of Automatic Control, Lund University, Lund, Sweden.

Salt Ducaju, J. M., B. Olofsson, and R. Johansson (2024a). "Iterative reference learning for Cartesian impedance control of robot manipulators". Submitted to review for presentation at IEEE/RSJ International Conference on Intelligent Robots and Systems (IROS) 2024.

Salt Ducaju, J. M., B. Olofsson, and R. Johansson (2024b). "Model-based predictive impedance variation for robot obstacle avoidance in safe human-robot collaboration". Submitted to review for publication in IEEE Transactions on Automation Science and Engineering.

Salt Ducaju, J. M., B. Olofsson, A. Robertsson, and R. Johansson (2021). "Joint stiction avoidance with null-space motion in real-time model predictive control for redundant collaborative robots". In: *IEEE International Conference on Robot and Human Interactive Communication (RO-MAN)*. Aug. 8–12. Vancouver, Canada (Virtual), pp. 307–314.

Salt Ducaju, J. M., B. Olofsson, A. Robertsson, and R. Johansson (2022a). "Fast contact detection and classification for kinesthetic teaching in robots using only embedded sensors". In: *IEEE International Conference on Robot and Human Interactive Communication (RO-MAN)*. Aug. 29–Sep. 2. Naples, Italy, pp. 1138–1145.

Salt Ducaju, J. M., B. Olofsson, A. Robertsson, and R. Johansson (2022b). "Robot Cartesian compliance variation for safe kinesthetic teaching using safety control barrier functions". In: *IEEE International Conference on Automation Science and Engineering (CASE)*. Aug. 20–24. Mexico City, pp. 2259–2266.

Salt Ducaju, J. M., B. Olofsson, A. Robertsson, and R. Johansson (2023). "Null-space compliance variation for safe human-robot collaboration in redundant manipulators using safety control barrier functions". In: *IEEE/RSJ International Conference on Intelligent Robots and Systems (IROS)*. October 1–5. Detroit, MI, USA, pp. 5903–5909.

Schneider, U., B. Olofsson, O. Sörnmo, M. Drust, A. Robertsson, M. Hägele, and R. Johansson (2014). "Integrated approach to robotic machining with macro/micro-actuation". *Robotics and Computer-Integrated Manufacturing* **30**:6, pp. 636–647.

Schou, C., J. Damgaard, S. Bøgh, and O. Madsen (2013). "Human-robot interface for instructing industrial tasks using kinesthetic teaching". In: *44th IEEE International Symposium on Robotics (ISR)*. Oct. 19–27. Seoul, Korea, pp. 1–6.

Shiriaev, A., A. Robertsson, and R. Johansson (2003). "Friction compensation for passive systems based on the LuGre model". In: *2nd IFAC Workshop on Lagrangian and Hamiltonian Methods for Nonlinear Control*. Apr. 3–5. Seville, Spain, pp. 183–188.

Shiriaev, A. S., L. B. Freidovich, A. Robertsson, R. Johansson, and A. Sandberg (2007). "Virtual-holonomic-constraints-based design of stable oscillations of furuta pendulum: Theory and experiments". *IEEE Transactions on Robotics* **23**:4, pp. 827–832.

Singletary, A., K. Klingebiel, J. Bourne, A. Browning, P. Tokumaru, and A. Ames (2021a). "Comparative analysis of control barrier functions and artificial potential fields for obstacle avoidance". In: *IEEE/RSJ International Conference on*

Intelligent Robots and Systems (IROS). Sep. 27–Oct. 1. Prague, Czech Republic, pp. 8129–8136.

Singletary, A., S. Kolathaya, and A. D. Ames (2021b). "Safety-critical kinematic control of robotic systems". *IEEE Control Systems Letters* **6**, pp. 139–144.

Sörnmo, O., B. Olofsson, U. Schneider, A. Robertsson, and R. Johansson (2012). "Increasing the milling accuracy for industrial robots using a piezo-actuated high-dynamic micro manipulator". In: *IEEE/ASME International Conference on Advanced Intelligent Mechatronics (AIM)*. Jul. 11–14. Kaohsiung, Taiwan, pp. 104–110.

Stavridis, S., D. Papageorgiou, and Z. Doulgeri (2017). "Dynamical system based robotic motion generation with obstacle avoidance". *IEEE Robotics and Automation Letters* **2**:2, pp. 712–718.

Stolt, A., M. Linderoth, A. Robertsson, and R. Johansson (2011). "Force controlled assembly of emergency stop button". In: *IEEE International Conference on Robotics and Automation (ICRA)*. May 9–13. Shanghai, China, pp. 3751–3756.

Suomalainen, M., Y. Karayiannidis, and V. Kyrki (2022). "A survey of robot manipulation in contact". *Robotics and Autonomous Systems* **156**, p. 104224.

Vicentini, F. (2021). "Collaborative robotics: A survey". *Journal of Mechanical Design* **143**:4, p. 040802.

Villani, L. and J. De Schutter (2008). "Force control". In: Siciliano, B. *et al*. (Eds.). *Springer Handbook of Robotics*. 2nd. Vol. 200. Springer, Berlin, Germany. Chap. 9, pp. 195–219.

Villani, L. and J. De Schutter (2016). "Force control". In: Siciliano, B. *et al*. (Eds.). *Springer Handbook of Robotics*. Springer, Berlin. Chap. 9, pp. 195–217.

Voellmer, G. M. (1991). *Robotic tool change mechanism*. US Patent 5,044,063. URL: `https://ntrs.nasa.gov/api/citations/19910022342/downloads/19910022342.pdf` (visited on 2024-03-20).

Wolpert, D. M. and Z. Ghahramani (2000). "Computational principles of movement neuroscience". *Nature neuroscience* **3**:11, pp. 1212–1217.

Wrede, S., C. Emmerich, R. Grünberg, A. Nordmann, A. Swadzba, and J. Steil (2013). "A user study on kinesthetic teaching of redundant robots in task and configuration space". *Journal of Human-Robot Interaction* **2**:1, pp. 56–81.

Zeng, J., B. Zhang, and K. Sreenath (2021). "Safety-critical model predictive control with discrete-time control barrier function". In: *American Control Conference (ACC)*. May 25–28. New Orleans, LA, USA, pp. 3882–3889.

Zhu, L., P. Spachos, E. Pensini, and K. N. Plataniotis (2021). "Deep learning and machine vision for food processing: A survey". *Current Research in Food Science* **4**, pp. 233–249.

A

Notation Overview

Some symbols have been used with different meanings in each of the papers included in this thesis. This section shows the symbols that have been used differently, and also their meaning for each of the papers.

Table A.1 Lowercase Latin letters used differently in each of the papers included in this thesis.

Symbol	Meaning					
	Paper I	**Paper II**	**Paper III**	**Paper IV**	**Paper V**	**Paper VI**
f	Auxiliary function	-	-	Auxiliary function		Force variable
g	Auxiliary function	-	-	Auxiliary function		-
	Gravity-induced torques	-	-	-	-	-
h	Sampling period			Barrier function		
k	-	-	-	State-feedback controller		Discrete time-step
r	-	-	-	-	Degree of redundancy	Rate of change
s	-	-	Complex-valued frequency variable	-	Null-space variable	-
x	X-coordinate				-	-
	State variable		Auxiliary variable	State variable		
y	Y-coordinate				-	-
	Output variable	-	Output variable		-	-
z	Z-coordinate				-	-
	-	-	-	Reservoir state	Auxiliary variable	Auxiliary variable

Table A.2 Uppercase Latin letters used differently in each of the papers included in this thesis.

Symbol	Meaning					
	Paper I	**Paper II**	**Paper III**	**Paper IV**	**Paper V**	**Paper VI**
B	State matrix	Virtual damping matrix	-	State matrix		
C	Coriolis and centripetal forces matrix					
	Output matrix	-	-	-	-	-
D	Feedforward matrix	-	Virtual damping matrix			
F	Auxiliary matrix	Cartesian force vector				
G	-	-	Gravity vector			
	Auxiliary matrix	-	Transfer function	-	-	-
H	Prediction horizon	-	High-pass filter	Lyapunov function	-	Auxiliary matrix
I	-	Virtual inertia matrix	-	Identity matrix		
L	-	-	Learning filter	Cost function		
	-	-	-	Lie derivative		-

Table A.3 Uppercase Latin letters used differently in each of the papers included in this thesis (continuation).

Symbol	Meaning					
	Paper I	**Paper II**	**Paper III**	**Paper IV**	**Paper V**	**Paper VI**
N	Null-space projection matrix	No. of samples	No. of iterations	-	Null-space Jacobian	No. of samples
Q	Weighting matrix	-	Low-pass filter	Quadratic term	-	Weighting matrix
R	Weighting matrix	-	Auxiliary matrix	-	-	Weighting matrix
T	-	-	-	Stored energy variable		Auxiliary matrix
V	Cost function	-	Performance index	Lyapunov function		
W	-	-	-	Stored energy variable	Weighting matrix	Auxiliary matrix
Z	-	-	-	Odd constant	Null-space projection matrix	-

Table A.4 Greek letters used differently in each of the papers included in this thesis.

Symbol	Meaning					
	Paper I	**Paper II**	**Paper III**	**Paper IV**	**Paper V**	**Paper VI**
α	Amplitude of sinusoidal signal	-	-	Auxiliary variable		
β	-	-	Iterative learning gain	-	-	Auxiliary variable
γ	End-effector twist	Threshold coefficient	-	Auxiliary variable		-
Γ	Discrete input matrix	-	Auxiliary matrix			Discrete input matrix
ω	Angular velocity	Frequency		-	-	-
Φ	Discrete state matrix	-	Auxiliary matrix			
σ	Standard deviation	-	Auxiliary variable			-
ζ	Discrete state variable	-	Auxiliary vector	-	-	-

Paper I

Joint Stiction Avoidance with Null-Space Motion in Real-Time Model Predictive Control for Redundant Collaborative Robots

Julian M. Salt Ducaju **Björn Olofsson**
Anders Robertsson **Rolf Johansson**

Abstract

Model Predictive Control (MPC) is an efficient point-to-point trajectory-generation method for robots that can be used in situations that occur under time constraints. The motion plan can be recalculated online to increase the accuracy of the trajectory when getting close to the goal position. We have implemented this strategy in a Franka Emika Panda robot, a redundant collaborative robot, by extending previous research that was performed on a 6-DOFs robot. We have also used null-space motion to ensure a continuous movement of all joints during the entire trajectory execution as an approach to avoid joint stiction and allow accurate kinesthetic teaching. As is conventional for collaborative and industrial robots, the Panda robot is equipped with an internal controller, which allows to send position and velocity references directly to the robot. Therefore, null-space motion can be added directly to the MPC-generated velocity references. The observed trajectory deviation caused by discretization approximations of the Jacobian matrix when implementing null-space motion has been corrected experimentally using sensor feedback for the real-time velocity-reference recalculation and by performing a fast sampling of the null-space vector. Null-space motion has been experimentally seen to contribute to reducing the friction torque dispersion present in static joints.

© 2021 IEEE. Reprinted, with permission, from 2021 IEEE International Conference on Robot and Human Interactive Communication (RO-MAN), August 8-12, Virtual, pp. 307–314.

1. Introduction

Trajectory generation is a well-studied problem in the robotics field. It consists of defining the path and the course of motion as a function of time. An overview of the many ways for doing this task is provided in [Kröger, 2010]. In an industrial setting, it is common to aim for performing a task in the shortest time possible to increase productivity. To this purpose, the robot should perform the given task under time constraints, making it convenient to formulate the problem as an optimal control problem, which provides a performance metric by means of an objective function [LaValle, 2006].

Model Predictive Control (MPC) [Mayne *et al.*, 2000; Maciejowski, 2002] is a well-grounded option for trajectory generation in robotic applications, since its formulation can include a final-state constraint to be satisfied at the end of its prediction horizon while respecting states' and inputs' limits during the motion. MPC uses a model of the robot to predict the future states and outputs based on the solution's choice of the input sequence. In the presence of an internal controller with a short time constant considering the robot dynamics, position or velocity references can be used directly making a complex dynamic model not necessary in the MPC. Therefore, a purely kinematic model can be used.

Moreover, online MPC trajectory recalculation can be performed to increase the resolution of the computed trajectory by setting a fixed final time while keeping the number of discretization points of the MPC prediction horizon constant. Then, the continuous-time prediction horizon of the MPC problem will shrink, successively causing a reduction of the sampling period every time the trajectory is recalculated online [Ghazaei Ardakani *et al.*, 2019].

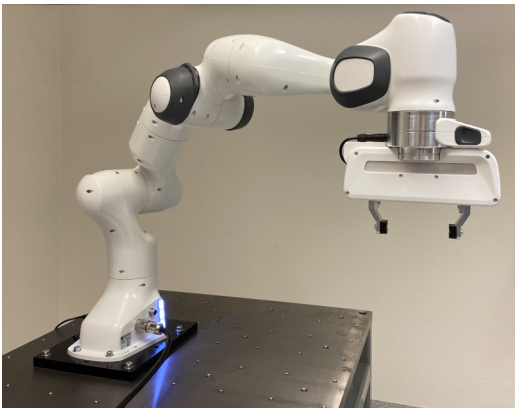

Figure 1. Franka Emika Panda robot used in the experiments.

In the context of robot trajectory reprogramming, it is convenient that a human

operator guides the robot through direct interaction [Capurso *et al.*, 2017], which is known as kinesthetic teaching [Wrede *et al.*, 2013] or lead-through programming (LTP), throughout the entire trajectory or parts of it. For an operator to be able to teach the robot, it is necessary to apply force on the robot end-effector or links. In this situation, the human operator should be comfortable with the physical interaction with the robot. Thus, it is important to be familiar with the force/torque required for leading the robot. Furthermore, the online MPC trajectory recalculation scheme is useful in the presence of human-robot interaction (HRI) since, after the human intervention is over, it can still be possible to reach the robot's goal pose without violating the problem's fixed-time constraint.

Therefore, the necessary force should not vary greatly between different human interventions. In order to ensure that the force that the operator needs to apply is always similar, joint stiction should be avoided. Joint static friction, or stiction, occurs when a joint has zero velocity and it becomes locked and constrained against relative motion [Haug *et al.*, 1986]. This phenomenon is caused by the interactions between the asperities of the surface in contact in a robot joint, such as gears, bearings, and shafts [Bittencourt and Gunnarsson, 2012].

Dithering has been proven as a successful method to reduce these uncertainties [Linderoth *et al.*, 2013]. However, it may cause vibration of the robot if the torque feedforward signal's amplitude is too high. Another option to avoid stiction, only available for robots that have more than 6 degrees of freedom (DOF), is to use null-space motion [Sadeghian *et al.*, 2013]. Null-space motion is a linear combination of joint angular velocities in an over-actuated robot that causes no change in the end-effector's pose ($Jb = 0$ with $b \neq 0$, being J the Jacobian and b the null-space vector) [Siciliano and Khatib, 2016]. It has previously been used in kinesthetic teaching to modify the robot's configuration without altering the end-effector's pose [Wahrburg *et al.*, 2016]. However, it can also be added to the trajectory reference to ensure that no joint remains still during the trajectory execution.

A trajectory generated for a 7 (or more) DOF robot may not necessarily involve varying the angular position of all of its joints, since it is a redundant system and it might be able to reach any end-effector's goal pose by only moving 6 of its joints. However, there could be an unexpected robot response if the operator tries to move a stationary joint since the force/torque required will be difficult to predict because of joint stiction [Haug *et al.*, 1986]. The method that we propose to avoid joint stiction consists of adding null-space motion to an MPC-generated trajectory reference.

The purpose of this paper is to experimentally analyze the effects of adding null-space motion to an MPC-generated point-to-point trajectory reference to evaluate the possible advantages and drawbacks of this method. Moreover, HRI, facilitated by the addition of null-space motion, would allow the operator to locally modify the robot's path, which could be relevant in this context since the trajectory reference is generated considering only an initial and a final point. The implementation has been performed on the Panda robot by Franka Emika [Franka Emika, 2019], a collaborative robot [Colgate *et al.*, 1996], which can be seen in Fig. 1.

Furthermore, in previous research [Ghazaei Ardakani *et al*., 2019], an open-loop strategy was implemented for the online trajectory recalculation where the initial state of the robot used to solve the MPC problem was estimated using the previous MPC solution. However, the addition of null-space motion to the MPC-generated reference may increase the error in the initial state estimation at every trajectory recalculation period, or metaperiod, and this error will accumulate at every online recalculation. For this reason, it is also a goal of this paper to evaluate the influence of joint angular position sensor feedback in the estimation of the initial state of the robot at the beginning of every metaperiod when adding null-space motion to an MPC-generated trajectory reference. The use of sensor feedback is referred to as the closed-loop strategy, as opposed to the previously used open-loop strategy [Ghazaei Ardakani *et al*., 2019].

This paper is outlined as follows: Sec. 2 presents the method for solving the problem that is being considered. Section 3 explains the experimental setup and the experiments performed, and presents the results obtained. Finally, conclusions are drawn in Sec. 4.

2. Methods

In this section, we introduce the MPC formulation used for trajectory generation and explain a strategy to add null-space motion to it. The goal of the trajectory-generation formulation used is that the robot reaches a final configuration under a time constraint. Additionally, we outline a hybrid dual-mode controller that would allow to switch between an MPC-based trajectory-following controller with null-space motion, and an admittance controller for human interaction.

2.1 Trajectory Generation Using MPC

The motion plan generated by MPC consists of a sequence of joint angular velocity references, since the robot's internal controller takes care of applying the necessary torques to each of the joints. Therefore, the optimization problem can be formulated in the joint space of the robot, using the robot's joint configuration $q \in \mathbb{R}^7$ since the robot has 7 joints, instead of formulating the problem in terms of the robot end-effector pose, $\xi \in SE(3)$, which is composed by the end-effector's position and orientation.

The initial and final joint configurations, q_0 and q_F, of the problem are obtained from the initial and desired end-effector poses, ξ_0 and ξ_F, respectively, by means of inverse kinematics [Corke, 2013]:

$$q = \mathscr{K}^{-1}(\xi) \tag{1}$$

Since this problem considers a 7 DOF robot, there will be an infinite number of solutions. Therefore, redundancy can be conveniently exploited to meet additional

constraints on the kinematic control problem in order to obtain greater manipulability in terms of manipulator configurations, interaction with the environment, and null-space motion.

Moreover, since the robot is equipped with an internal controller that allows a velocity-reference control mode and we assume good tracking performance without exceeding the torque limits [Bäuml *et al.*, 2010], the MPC does not need to use a complex nonlinear robot dynamic model where the torque is the input, and a simpler kinematic linear model is considered where the motion is defined in terms of position, velocity, and other higher-order time derivatives of position [Ghazaei, 2016]. Also, the internal controller reduces the effect of dynamic coupling between joints by means of torque feedforward.

Then, as in previous research [Ghazaei Ardakani *et al.*, 2019], the continuous-time model chosen can be constructed by multiple decoupled chains of integrators. Thus, the continuous-time state vector, $x_c \in \mathbb{R}^{21}$, is composed by the angular position, q_i, velocity, $\dot{q}_i$, and acceleration, $\ddot{q}_i$, of each of the robot joints $i = 1, \ldots, 7$:

$$x_c = \begin{bmatrix} q_1 & \dot{q}_1 & \ddot{q}_1 & \cdots & q_7 & \dot{q}_7 & \ddot{q}_7 \end{bmatrix}^{\mathrm{T}} \tag{2}$$

The continuous-time linear model can thus be written as:

$$\dot{x}_c(t) = A_c x_c(t) + B_c u_c(t) \tag{3}$$

$$y_c(t) = C_c x_c(t) \tag{4}$$

with

$$A_c = \mathrm{blkdiag}([\tilde{A}_c, \ldots, \tilde{A}_c]), \quad B_c = \mathrm{blkdiag}([\tilde{B}_c, \ldots, \tilde{B}_c])$$

and $C_c = I_{21}$, where I_{21} is the identity matrix in $\mathbb{R}^{21\mathrm{x}21}$, $\mathrm{blkdiag}(\cdot)$ forms a block diagonal matrix from the given list of matrices, $A_c \in \mathbb{R}^{21\mathrm{x}21}$, $B_c \in \mathbb{R}^{21\mathrm{x}7}$, and

$$\tilde{A}_c = \begin{bmatrix} 0 & 1 & 0 \\ 0 & 0 & 1 \\ 0 & 0 & 0 \end{bmatrix}, \quad \tilde{B}_c = \begin{bmatrix} 0 & 0 & 1 \end{bmatrix}^{\mathrm{T}}$$

The continuous-time input is the angular jerk of the joints, $u_c = \dddot{q} \in \mathbb{R}^7$.

For the choice of sampling period, h, to discretize the continuous-time linear system, a sampling period different from the one of the controlled system was chosen for the discretization of the kinematics in the optimization. Then, a linear interpolation of the calculated input sequence is used to provide references at the sampling rate of the robot [Ghazaei Ardakani *et al.*, 2019]. This justifies the use of a predictive first-order-hold (FOH) sampling method [Åström and Wittenmark, 2013]:

$$x_{k+1} = \Phi x_k + \frac{1}{h}\Gamma_1 u_{k+1} + \left(\Gamma - \frac{1}{h}\Gamma_1\right) u_k \tag{5}$$

$$y_k = C x_k \tag{6}$$

with

$$\Phi = \text{blkdiag}([\tilde{\Phi}, \ldots, \tilde{\Phi}]), \quad \Gamma_1 = \text{blkdiag}([\tilde{\Gamma}_1, \ldots, \tilde{\Gamma}_1]),$$
$$\Gamma = \text{blkdiag}([\tilde{\Gamma}, \ldots, \tilde{\Gamma}])$$

where $\Phi \in \mathbb{R}^{21\text{x}21}$, $\Gamma_1, \Gamma \in \mathbb{R}^{21\text{x}7}$, and:

$$\tilde{\Phi} = \begin{bmatrix} 1 & h & h^2/2 \\ 0 & 1 & h \\ 0 & 0 & 1 \end{bmatrix}$$
$$\tilde{\Gamma} = \begin{bmatrix} h^3/6 & h^2/2 & h \end{bmatrix}^{\text{T}}$$
$$\tilde{\Gamma}_1 = \begin{bmatrix} h^4/24 & h^3/6 & h^2/2 \end{bmatrix}^{\text{T}}$$
$$C = C_c$$

As developed in previous research [Ghazaei Ardakani *et al.*, 2019], the discrete-time model obtained from the FOH sampling method (5), (6) can be rewritten in the standard form by using a new discrete state variable, $\zeta \in \mathbb{R}^{21}$:

$$\zeta_{k+1} = A\zeta_k + Bu_k \tag{7}$$
$$y_k = C\zeta_k + Du_k \tag{8}$$

where

$$A = \Phi, \quad B = \Gamma + \frac{1}{h}(\Phi - I_{21})\Gamma_1, \quad D = \frac{\Gamma_1}{h}$$

Since $y_k = x_k$ because of (6) and $C = I_{21}$, we can from (8) obtain the relation:

$$x_k = C\zeta_k + Du_k \tag{9}$$

It should be mentioned that the input u is the discretized counterpart of u_c, and the discrete controlled variable x is the discretized counterpart of x_c. On the contrary, the discrete-time state ζ is not a discretized version of any variable found in the continuous-time state-space system formulation (3), (4).

Moreover, the quadratic cost function chosen for solving this problem at time step k is:

$$V_k(U_k) = \sum_{j=k+1}^{k+H} x_j^{\text{T}} Q x_j + \sum_{j=k}^{k+H-1} u_j^{\text{T}} R u_j \tag{10}$$

where $U_k = [u_k, \ldots, u_{k+H-1}] \in \mathbb{R}^{7\text{x}H}$ is the input signal sequence over the control horizon of H steps that minimizes the cost function over the MPC prediction horizon of H steps at every metaperiod, and $Q \in \mathbb{R}^{21\text{x}21}$ and $R \in \mathbb{R}^{7\text{x}7}$ are positive semi-definite weight matrices that penalize the controlled variables and inputs, respectively.

This optimization problem is subject to the discrete-time model of the system (7), (9). Additionally, a hard constraint on the value of the discrete-time final controlled variables is used to ensure that the robot reaches the desired configuration at the end of the trajectory:

$$x_{k+H} = x_{\text{goal}} \tag{11}$$

In addition, a set of linear constraints must be included to bound the admissible range of the inputs and controlled variables:

$$F[u_k^{\mathrm{T}}, \ldots, u_{k+H-1}^{\mathrm{T}}]^{\mathrm{T}} \leq f \tag{12}$$

$$G[x_{k+1}^{\mathrm{T}}, \ldots, x_{k+H}^{\mathrm{T}}]^{\mathrm{T}} \leq g \tag{13}$$

The choice of the cost function as convex, as well as a linear model and convex constraint sets, makes the whole problem convex, which is beneficial for the computation of the problem since if a solution exists, it is the globally optimal [Boyd and Vandenberghe, 2004].

Finally, this convex problem is solved at every trajectory recalculation period, or metaperiod. The sampling period, h, used in the discretization is equal to:

$$h = \frac{T_F - t_k}{H} \tag{14}$$

where H is the number of discrete steps in the prediction horizon, T_F is the final time where the goal state must be reached, and t_k is the time when the robot starts using the newly recalculated trajectory reference. As mentioned earlier, the continuous-time prediction horizon of the problem will shrink since, as time goes by, t_k will increase while the final time T_F and H are constant, thus increasing the resolution of the computed trajectory as the goal state, x_{goal}, is approached.

2.2 Null-Space Motion Addition to the Reference Trajectory

The manipulator's Jacobian matrix, $J(q) \in \mathbb{R}^{6\text{x}7}$, maps the joint angular velocities, $\dot{q}$, to the end-effector's twist, $\gamma = [\omega^{\mathrm{T}}, v^{\mathrm{T}}]^{\mathrm{T}} \in \mathbb{R}^6$, with v and ω denoting the linear and angular velocity of the end-effector, respectively:

$$\gamma = J(q)\dot{q} \tag{15}$$

Therefore, null-space motion is constructed by using the null-space vector of this Jacobian matrix:

$$\dot{q} = J^{\dagger}(q)\gamma + N(q)\dot{q}_{\text{a}} \tag{16}$$

where the matrix $N(q) = I_7 - J^{\dagger}(q)J(q) \in \mathbb{R}^{7\text{x}7}$ projects the additional arbitrary joint angular velocity, $\dot{q}_{\text{a}}$, into the null space so that it is independent of the end-effector Cartesian motion [Corke, 2013].

The first term of (16) is the relationship between the joint velocity $\dot{q}$ and the end-effector's twist γ by means of the manipulator Jacobian (15), and superscript †

denotes the Moore-Penrose pseudoinverse matrix given by $J^{\dagger} = (J^{\mathrm{T}}J)^{-1}J^{\mathrm{T}}$ [Ben-Israel and Greville, 2003]. This term is shared for both 6 and 7 DOF robots, although in the case of 6 DOFs, the Jacobian is a square matrix. However, the second term of (16) is the null-space motion, which only appears in redundant manipulators. The null-space motion unitary vector is calculated as:

$$\dot{q}_{\mathrm{nsu}} = \frac{N(q)\dot{q}_{\mathrm{a}}}{\|N(q)\dot{q}_{\mathrm{a}}\|} \tag{17}$$

Also, since the Jacobian matrix is particular for each robot configuration, this vector should be sampled in real-time.

The null-space unitary vector given in (17) has to be scaled before being included with the MPC-generated angular velocity references. A sinusoidal signal has been chosen to smoothly transition between positive and negative scaling values to avoid reaching any joint limit. Its frequency depends on the length of the trajectory execution, to make sure that the first and last velocity references sent are equal to 0. Additionally, $\alpha \in \mathbb{R}$ is a constant used to scale its amplitude:

$$\dot{q}_{\mathrm{NS}} = \dot{q}_{\mathrm{nsu}}\alpha \sin\left(\frac{2\pi t}{T_F}\right) \tag{18}$$

Then, null-space motion is calculated at each robot sampling instant and added to the velocity references calculated by the optimization to avoid joint stiction:

$$\dot{q}_{\mathrm{ref}} = \dot{q}_{\mathrm{MPC}} + \dot{q}_{\mathrm{NS}} \tag{19}$$

where $\dot{q}_{\mathrm{ref}}$ is the velocity references sent to the robot, $\dot{q}_{\mathrm{MPC}}$ is the linearly interpolated velocity reference sequence calculated by the MPC, and $\dot{q}_{\mathrm{NS}}$ is the null-space motion component obtained from (18).

Moreover, the controlled-variable constraint (13) should consider the superposition of the null-space motion on the MPC solution to avoid any possible constraint violation. Therefore, when solving the MPC optimization the joint-velocity range should be reduced for every joint in a proportional way to the maximum possible joint-velocity component corresponding to the added null-space motion. With this approach, it is guaranteed that the joint-velocity limits are fulfilled. Also, the joint-acceleration range should be conservative to never exceed the joints' torque limits [Bäuml *et al.*, 2010].

Finally, joint angular position sensor feedback can be used to reduce the mismatch between the estimation of the initial state used for the online optimization-problem calculation at every metaperiod and its real value caused by the addition of null-space motion to the MPC-generated trajectory. Therefore, a closed-loop form of the problem is proposed to obtain a more accurate estimation of the initial state to be used in the MPC. However, data samples from the robot's sensors cannot be directly used as the initial state, since there is a planned computational delay that

accounts for the time required to solve the optimization problem in the MPC. Therefore, in order to provide a precise initial state estimation it is necessary to use the system's model described by (7) and (9) to estimate the state evolution between the sampling time of the sensor feedback and the time where the new trajectory velocity references are deployed to the system.

2.3 Human-Robot Interaction (HRI)

Even though the main focus of this research is to analyze the effects of a method that facilitates HRI by reducing joint stiction, we also provide an illustrative example of one possible way that a human operator can interact with the robot. Then, we outline a hybrid dual-mode controller where the robot receives commands from the MPC-generated trajectory that includes null-space motion (19), or from human-robot interaction, but never from both sources simultaneously, as summarized in Algorithm 1.

Since human input is, in this scenario, a path correction to the previously generated MPC trajectory reference, admittance control [Wahrburg *et al.*, 2016] is a suitable strategy for the human-interaction control mode. Another common human-robot interaction control strategy such as compliance control [Hogan, 1985] is less appropriate for this application since its virtual spring component would try to bring the robot closer to the MPC reference rather than allowing the human to freely operate the robot.

If a joint-torque interface is available, a simple way to implement admittance control is to supply the robot with joint torque commands. For this, the rigid-body dynamics of the robot is used [Siciliano and Khatib, 2016]:

$$M(q)\ddot{q} + C(q,\dot{q})\dot{q} + g(q) + \tau_{\text{fric}} = \tau_{\text{mot}} \tag{20}$$

where $M(q) \in \mathbb{R}^{7\text{x}7}$ is the generalized inertia matrix, $C(q,\dot{q}) \in \mathbb{R}^{7\text{x}7}$ describes the Coriolis and centripetal forces effects, $g(q) \in \mathbb{R}^{7\text{x}1}$ captures the gravity-induced torques, and $\tau_{\text{fric}} \in \mathbb{R}^{7\text{x}1}$ and $\tau_{\text{mot}} \in \mathbb{R}^{7\text{x}1}$ represent the friction and motor torques, respectively.

Then, if the admittance controller is active (Algorithm 1, Line 2), it will send commanding torques to joint motors that are equal to the sensed external joint torques, $\tau_{\text{ext}} \in \mathbb{R}^{7\text{x}1}$:

$$\tau_{\text{mot}} = \tau_{\text{ext}} \tag{21}$$

where part of the commanded joint torque is used for robot motion, but a fraction of the commanded joint torque is used to overcome joint friction, as seen in Eq. (20).

Friction is present in any element that involves relative motion in robot mechanisms. All friction models have in common a significant change of friction magnitude in the zero-velocity vicinity, as shown in Fig. 2, which is the major concern of friction compensation [Cai and Song, 1993; Karnopp, 1985; Freidovich *et al.*, 2009; Shiriaev *et al.*, 2003]. For this reason, avoiding joint stiction is helpful for

the human operator that interacts with the robot to predict beforehand the necessary force that he/she should apply to the robot to achieve the desired displacement.

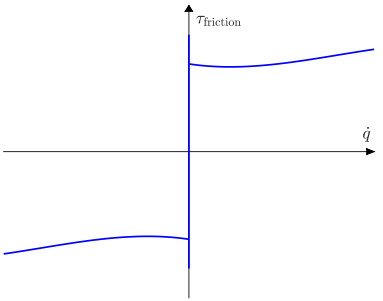

Figure 2. Joint friction as a function of joint angular velocity.

Finally, a switching mechanism between both control modes (Algorithm 1, Line 1), trajectory following with null-space motion addition and admittance control, based on external torque sensor feedback, can be either automatic, following a collision detection and classification method (a summary of different strategies can be found in [Cioffi *et al.*, 2020]), or manually determined by the human operator.

Algorithm 1 Hybrid Dual-Mode Controller

1: **if** human is interacting with robot **then**
2: *HRI mode*: Send τ_{ext} (21) as command to the robot's torque-reference interface.
3: **else**
4: *Trajectory-following mode*: Send $\dot{q}_{\text{ref}}$ (19) as command to the robot's velocity-reference interface.
5: **end if**

3. Experiments and Results

The experiments presented in this section evaluated the performance of the addition of null-space motion onto an MPC-generated trajectory.

3.1 Implementation and Experimental Setup

The robot used in the experiments is the Franka Emika Panda [Franka Emika, 2019], a 7-DOF robotic arm. In addition to the joint velocity interface, the robot's internal controller also allows the operator to send joint position and torque commands. The

Panda robot has a sampling rate of 1 kHz, and therefore, references should be sent to it every 1 ms. A photo of the robot used is shown in Fig. 1.

This collaborative robot, or *cobot* [Colgate *et al.*, 1996], is designed to share its workspace with humans in a safe manner, and it allows the human operator to set different maximum external-torque thresholds for each of the control modes so that if an accidental collision between the robot and the operator happened, the robot would perform a security shutdown.

As for the design choices for trajectory generation, the MPC prediction horizon was chosen to be equal to $H = 25$ as a trade-off between trajectory resolution and real-time computational cost, and the recalculation metaperiod was equal to 0.1 s. Also, the weighting matrix Q penalized the joint velocity and acceleration, but not the joint angular position, since there was no specific desired position between the initial and the final states [Ghazaei Ardakani *et al.*, 2019], and since a hard constraint (11) was imposed on the final joint position, $Q = \text{blkdiag}([\tilde{Q}, \ldots, \tilde{Q}])$ where $\tilde{Q} = \text{diag}(\begin{bmatrix} 0 & 1 & 1 \end{bmatrix})$. Additionally, the input was less penalized than the states, $R = 0.001\, I_7$.

The first experiment presented analyzed the detrimental effects of slowing the sampling rate of the null-space vector of the Jacobian matrix. Then, the second experiment showed the suitability of using sensor feedback when adding null-space motion to MPC-generated trajectory references. Moreover, the third experiment focused on the results obtained for a closed-loop, fast null-space sampling approach where one of the joints would have remained static if null-space motion had not been included. Finally, the last experiment evaluated the dispersion of friction torque as a function of the joint angular velocity.

3.2 Experiment 1: Analysis of the effects of the null-space sampling rate on the trajectory accuracy

This experiment studied the effects of null-space discretization by performing the same trajectory in different runs, the only difference being that each run was performed at a different sampling rate of the null-space vector of the Jacobian matrix (1, 2, 5, and 10 ms). Since the null-space vector depends on the robot's configuration, a slower null-space sampling increases the difference between the null-space vector that is used for the velocity reference and the actual null-space vector.

The robot's initial configuration, randomly chosen, was, in radians:

$$q_0 = \begin{bmatrix} 0 & -0.79 & 0.0 & -2.36 & 0.0 & 1.57 & 0.0 \end{bmatrix} \tag{22}$$

Moreover, the trajectory lasted 10 s, enough time to clearly see the detrimental effects of a slower sampling rate of the null-space vector. Also, the trajectory consisted only of null-space motion, and the unitary null-space vector was scaled by a sinusoidal wave of frequency equal to 1 Hz and an amplitude constant, α, equal to 3 in (18). Therefore, at the end of the trajectory, the end-effector should ideally have the same pose as the initial one. Furthermore, an open-loop strategy was used for

this experiment in an attempt to isolate the effects of having an insufficient sampling frequency of the null-space vector.

The temporal evolution of the robot's pose has been analyzed using Figs. 3 and 4. Figure 3 shows the temporal evolution of the end-effector's Cartesian coordinates and Fig. 4 the temporal evolution of the end-effector's orientation, by means of the Euler rotation angles (ZYX) from the robot base coordinate reference system to the end-effector's coordinate reference system. It can be observed how slowing the sampling rate caused the robot to drift from the desired constant end-effector's Cartesian pose.

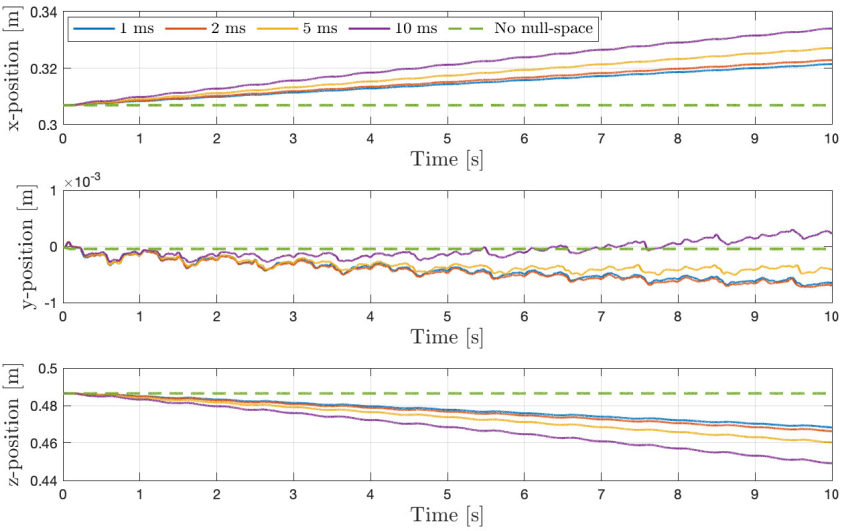

Figure 3. Experiment 1 — End-effector's position with respect to base frame.

Consequently, the null-space vector should be updated at the fastest update rate available, which in this case was the robot's sampling frequency (1 kHz). However, varying the null-space velocity references in intervals of 1 ms still introduced a slight deviation from the planned trajectory, as seen in Figs. 3 and 4. For this reason, the next experiment considered a closed-loop approach to compensate the disturbances introduced by the approximate null-space motion.

3.3 Experiment 2: Comparison of the open-loop and the closed-loop strategies

Sensor feedback from joint position sensors can be used when updating the initial state estimation for online optimization in the MPC to account for the degrading effects of low-rate null-space sampling observed in the previous experiment. To

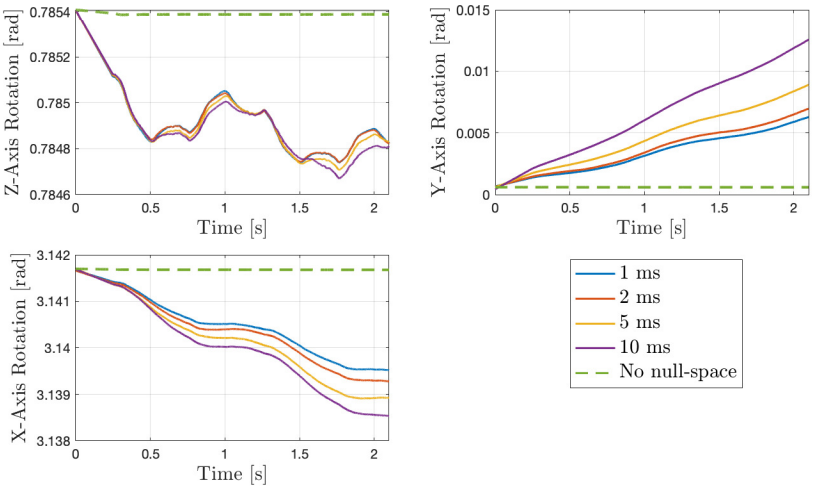

Figure 4. Experiment 1 — End-effector's orientation with respect to base frame.

show the benefits of using sensor feedback, it was necessary to compare the results of the implementation of null-space motion in the closed-loop MPC strategy versus the open-loop MPC strategy.

Several reference trajectories with different initial and goal robot configurations were used for this experiment. Additionally, each of them was executed five times. These trajectories combined null-space motion and MPC-generated trajectory references. Also, the null-space vector was sampled every ms and the sinusoidal scaling function's period was equal to the length of the trajectory.

The results of Experiment 2 are presented in Table 1, which shows the mean and standard deviation of the end-effector's Cartesian position error at the end of the trajectory. The following expression was used for calculating this error:

$$e = \sqrt{(x_G - x_F)^2 + (y_G - y_F)^2 + (z_G - z_F)^2} \tag{23}$$

where the subindex G refers to the goal position and the subindex F refers to the final position end-effector coordinate of the corresponding trial.

Table 1. End-effector's Final Cartesian Position Errors [mm]

	CL - NS	*CL*	*OL - NS*	*OL*
Mean	1.43	0.48	5.97	1.18
Std. Dev.	0.78	0.25	0.39	0.11

In Table 1, *CL* and *OL* refer to the closed-loop and the open-loop implementations, respectively, and *NS* to the runs that included null-space motion. Several assertions can be made based on Table 1. First, when no null-space motion was added, the closed-loop strategy provided a more precise final Cartesian position, since there was a better initial state estimation at each MPC trajectory recalculation. Also, in both open-loop and closed-loop scenarios, including null-space motion was detrimental to the final state precision of the trajectory. Finally, using an open-loop strategy caused a greater total final Cartesian position error and therefore, if possible, a closed-loop scheme should be used to implement null-space motion.

3.4 Experiment 3: Null-space motion integration with closed-loop MPC in a trajectory that would have left one joint static

Once the two previous sets of experiments had shown the suitability of sampling the null-space vector as fast as possible and using a closed-loop control strategy to compensate for the degrading effects of adding null-space motion to an MPC-generated trajectory reference, the results for the closed-loop controller in one of the trajectories of Experiment 2 were analyzed.

Figure 5 shows how the addition of null-space motion modified the total velocity references (19). It can be seen that Joint 3 was not used in the MPC-generated trajectory, but it was desired to have it continuously moving to avoid its stiction, thus justifying the addition of null-space motion to the trajectory.

Figures 6 and 7 show the temporal evolution of the end-effector's position in Cartesian coordinates and the temporal evolution of the end-effector's orientation parameterized in the Euler rotation angles (ZYX) between the robot's base frame and the end-effector's frame, respectively. Even though the velocity references were different, null-space motion was properly implemented in the MPC trajectory generation since the temporal evolution of the end-effector pose was very similar in both trials, and it only showed slight deviations in the y-position in Fig. 6 and in the x-axis rotation in Fig. 7, which were compensated before the motion was finished. Therefore, joint stiction in Joint 3 was addressed by adding null-space motion, while still being able to perform an accurate trajectory under the task time constraints.

3.5 Experiment 4: Friction torque dispersion

The final experiment evaluated the dispersion of the friction torque in a joint as a function of its angular velocity. For this purpose, the torque-based admittance controller in Sec. 2.3 was implemented, so that the commanded torque to each of the joints was equal to their sensed external torque signals. Also, the friction torque for all joints was estimated by rewriting Eq. (20) as:

$$\hat{\tau}_{\text{fric}} = \hat{\tau}_{\text{ext}} - (M(\hat{q})\hat{\ddot{q}} + C(\hat{q},\hat{\dot{q}})\hat{\dot{q}} + g(\hat{q})) \tag{24}$$

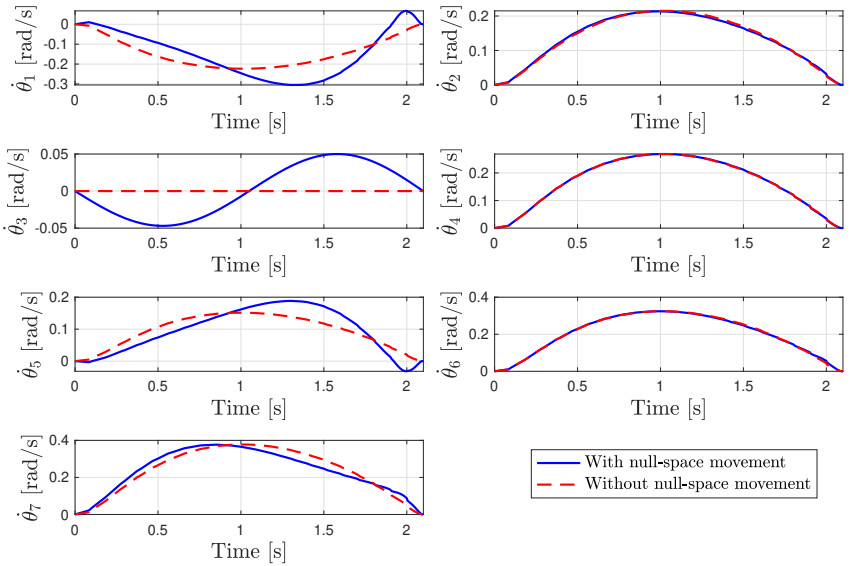

Figure 5. Experiment 3 — Joint angular commanded velocities' evolution.

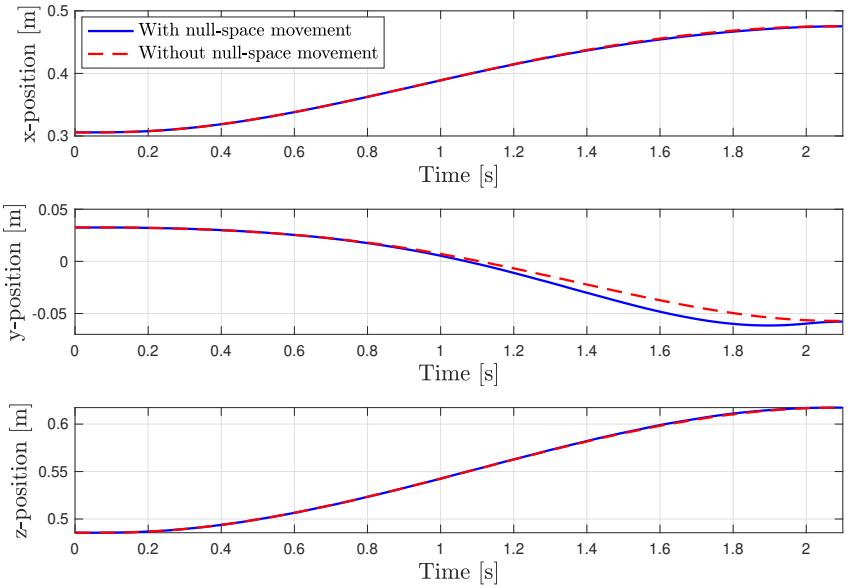

Figure 6. Experiment 3 — End-effector's position with respect to base frame.

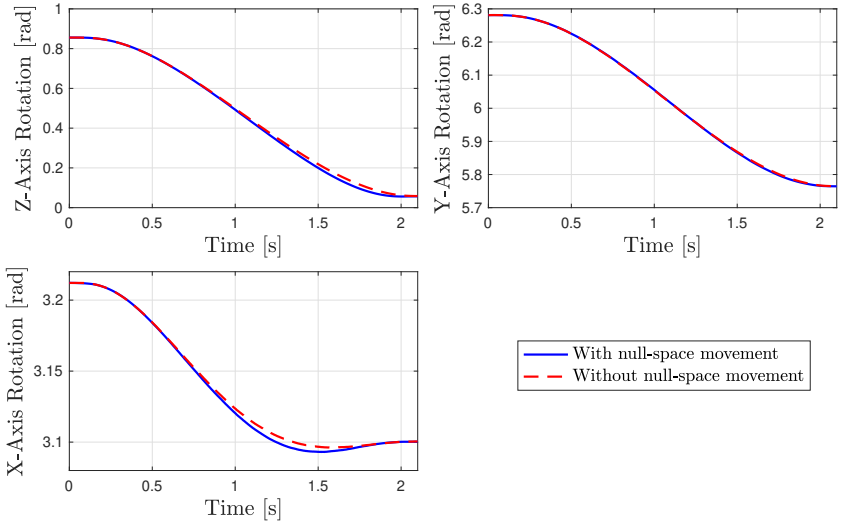

Figure 7. Experiment 3 — End-effector's orientation with respect to base frame.

where the superscript $\hat{}$ denotes a variable that has been estimated using joint position or torque sensor data.

Then, the experiment consisted of a human operator leading-through the robot for 15 s using this torque-based admittance controller. Figure 8 shows the results in terms of the standard deviation, σ, of the estimated friction torque of a joint in Eq. (24) with respect to its angular velocity.

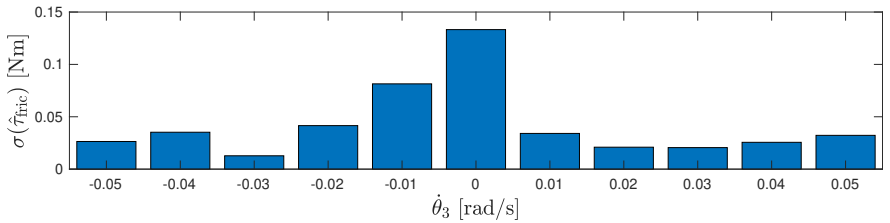

Figure 8. Experiment 4 — Standard deviation of the friction torque as a function of angular velocity of Joint 3.

The choice of joint and its angular-velocity range, shown in Fig. 8, was related to the experiment presented in Sec. 3.4, since the motion of Joint 3 was generated only by null-space motion and had the same angular velocity range, as seen in Fig. 5.

It can be seen that the standard deviation of the friction torque was greater when the angular velocity of the joint was close to zero: $\sigma(\hat{\tau}_{\text{fric}}) = 0.13$ Nm in the vicinity

of zero velocity compared to an average value of $\sigma(\hat{\tau}_{\text{fric}}) = 0.03$ Nm in the rest of the angular velocity range analyzed. Therefore, adding null-space motion to a static joint can contribute to reducing the friction torque dispersion.

4. Conclusion

We have proposed the addition of null-space motion to an MPC fixed-time point-to-point online trajectory generation method in order to facilitate kinesthetic teaching in a redundant robot. This approach allows a continuous motion of all joints throughout the trajectory execution, even if the MPC-generated trajectory does not include them in its planning, so that joint stiction is suppressed and a human operator can predict the force/torque necessary to move the robot. A reduction of the friction-torque dispersion has been experimentally observed as a consequence of adding null-space motion in a static joint.

The discrete-time control of null-space motion has been observed to be sensitive to discretization approximations of the Jacobian matrix. The experiments performed have justified the extension of a previously studied open-loop scheme [Ghazaei Ardakani *et al*., 2019] to a closed-loop scheme and a fast Jacobian matrix sampling to correct these slight degrading effects on the trajectory execution performance, thus allowing the addition of null-space motion to the trajectory without causing a significant loss of final-state accuracy.

An additional benefit of the presented closed-loop strategy is that, if human intervention takes place during the trajectory execution, the trajectory can be recalculated online once human intervention is concluded using an accurate estimation of the initial state in the MPC problem.

References

Åström, K. J. and B. Wittenmark (2013). *Computer-Controlled Systems: Theory and Design*. Courier Corporation, Chelmsford, MA, USA.

Bäuml, B., T. Wimböck, and G. Hirzinger (2010). "Kinematically optimal catching a flying ball with a hand-arm-system". In: *IEEE/RSJ International Conference on Intelligent Robots and Systems (IROS)*. Oct. 18–22. Taipei, Taiwan, pp. 2592–2599.

Ben-Israel, A. and T. N. Greville (2003). *Generalized Inverses: Theory and Applications*. Springer-Verlag, New York, USA.

Bittencourt, A. C. and S. Gunnarsson (2012). "Static friction in a robot joint—Modeling and identification of load and temperature effects". *Journal of Dynamic Systems, Measurement, and Control* **134**:5, pp. 1–10.

Boyd, S. P. and L. Vandenberghe (2004). *Convex Optimization*. Cambridge Univ. Press, Cambridge, UK.

Cai, L. and G. Song (1993). "A smooth robust nonlinear controller for robot manipulators with joint stick-slip friction". In: *IEEE International Conference on Robotics and Automation (ICRA)*. May 2–6. Atlanta, GA, USA, pp. 449–454.

Capurso, M., M. M. G. Ardakani, R. Johansson, A. Robertsson, and P. Rocco (2017). "Sensorless kinesthetic teaching of robotic manipulators assisted by observer-based force control". In: *IEEE International Conference on Robotics and Automation (ICRA)*. May 29–Jun. 2. Singapore, pp. 945–950.

Cioffi, G., S. Klose, and A. Wahrburg (2020). "Data-efficient online classification of human-robot contact situations". In: *European Control Conference (ECC)*. May 12–15. Saint Petersburg, Russia, pp. 608–614.

Colgate, J. E., J. Edward, M. A. Peshkin, and W. Wannasuphoprasit (1996). "Cobots: Robots for collaboration with human operators". In: *Proceedings of the ASME Dynamic Systems and Control Division: ASME International Mechanical Engineering Congress and Exposition*. Nov. 17–22. Atlanta, GA, USA, pp. 433–439.

Corke, P. (2013). *Robotics, Vision and Control: Fundamental Algorithms in MATLAB*. Springer, Berlin, Germany.

Franka Emika (2019). *Franka Emika Panda – Data Sheet*. `https://www.generationrobots.com/media/panda-franka-emika-datasheet.pdf`. (Visited on 2022-09-13).

Freidovich, L., A. Robertsson, A. Shiriaev, and R. Johansson (2009). "LuGre-model-based friction compensation". *IEEE Transactions on Control Systems Technology* **18**:1, pp. 194–200.

Ghazaei, M. (2016). *On Trajectory Generation for Robots*. English. TFRT-1116. PhD thesis. Dept. Automat. Control, Lund Univ., Lund, Sweden. ISBN: 978-91-7753-048-0.

Ghazaei Ardakani, M., B. Olofsson, A. Robertsson, and R. Johansson (2019). "Model predictive control for real-time point-to-point trajectory generation". *IEEE Transactions on Automation Science and Engineering* **16**:2, pp. 972–983.

Haug, E. J., S. C. Wu, and S. M. Yang (1986). "Dynamics of mechanical systems with Coulomb friction, stiction, impact and constraint addition-deletion—I Theory". *Mechanism and Machine Theory* **21**:5, pp. 401–406.

Hogan, N. (1985). "Impedance control: an approach to manipulation: part I". *Journal of Dynamic Systems, Measurement, and Control* **107**:1, pp. 1–7.

Karnopp, D. (1985). "Computer simulation of stick-slip friction in mechanical dynamic systems". *Journal of Dynamic Systems, Measurement, and Control* **107**:1, pp. 100–103.

Kröger, T. (2010). *On-Line Trajectory Generation in Robotic Systems: Basic Concepts for Instantaneous Reactions to Unforeseen (Sensor) Events*. Vol. 58. Springer, Berlin, Germany.

LaValle, S. M. (2006). *Planning Algorithms*. Cambridge Univ. Press, Cambridge, UK.

Linderoth, M., A. Stolt, A. Robertsson, and R. Johansson (2013). "Robotic force estimation using motor torques and modeling of low velocity friction disturbances". In: *IEEE/RSJ International Conference on Intelligent Robots and Systems (IROS)*. Nov. 3–7. Tokyo, Japan, pp. 3550–3556.

Maciejowski, J. M. (2002). *Predictive Control: with Constraints*. Prentice Hall, Harlow, UK.

Mayne, D., J. Rawlings, C. Rao, and P. Scokaert (2000). "Constrained model predictive control: Stability and optimality". *Automatica* **36**:6, pp. 789–814.

Sadeghian, H., L. Villani, M. Keshmiri, and B. Siciliano (2013). "Task-space control of robot manipulators with null-space compliance". *IEEE Transactions on Robotics* **30**:2, pp. 493–506.

Shiriaev, A., A. Robertsson, and R. Johansson (2003). "Friction compensation for passive systems based on the LuGre model". In: *2nd IFAC Workshop on Lagrangian and Hamiltonian Methods for Nonlinear Control*. Apr. 3–5. Seville, Spain, pp. 183–188.

Siciliano, B. and O. Khatib (2016). *Springer Handbook of Robotics*. Springer, Berlin, Germany.

Wahrburg, A., J. Boes, B. Matthias, F. Dai, and H. Ding (2016). "Sensorless null-space admittance control for redundant manipulators". In: *Proceedings of ISR 2016: 47st International Symposium on Robotics*. Jun. 21–22. VDE. Munich, Germany, pp. 1–7.

Wrede, S., C. Emmerich, R. Grünberg, A. Nordmann, A. Swadzba, and J. Steil (2013). "A user study on kinesthetic teaching of redundant robots in task and configuration space". *Journal of Human-Robot Interaction* **2**:1, pp. 56–81.

Paper II

Fast Contact Detection and Classification for Kinesthetic Teaching in Robots using only Embedded Sensors

Julian M. Salt Ducaju **Björn Olofsson**
Anders Robertsson **Rolf Johansson**

Abstract

Collaborative robots have been designed to perform tasks where human cooperation may occur. Additionally, undesired collisions can happen in the robot's environment. A contact classifier may be needed if robot trajectory recalculation is to be activated depending on the source of robot–environment contact. For this reason, we have evaluated a fast contact detection and classification method and we propose necessary modifications and extensions so that it is able to detect a contact in any direction and distinguish if it has been caused by voluntary human cooperation or by accidental collision with a static obstacle for kinesthetic teaching applications. Robot compliance control is used for trajectory following as an active strategy to ensure safety of the robot and its environment. Only sensor data that are conventionally available in commercial collaborative robots, such as joint-torque sensors and joint-position encoders/resolvers, are used in our method. Moreover, fast contact detection is ensured by using the frequency content of the estimated external forces, whereas external force direction and sense relative to the robot's motion is used to classify its source. Our method has been experimentally proven to be successful in a collaborative assembly task for a number of different experimentally recorded trajectories and with the intervention of different operators.

© 2022 IEEE. Reprinted, with permission, from 2022 IEEE International Conference on Robot and Human Interactive Communication (RO-MAN), August 29-September 2, Naples, Italy, pp. 1138–1145.

1. Introduction

Physical Human–Robot Interaction (pHRI) has become a research topic of major interest during the later years in the robotics community [Villani *et al*., 2018]. The reason behind this is allowing robots to safely work in partially unknown environments where humans and robots can cooperate. One way that human operators can cooperate with the robot is through direct interaction, known as kinesthetic teaching [Wrede *et al*., 2013], which is useful for robot trajectory reprogramming [Karlsson *et al*., 2017]. Consequently, collaborative robots have increased in popularity since their lightweight, compliant design is especially convenient when robots share their workspace with humans.

As part of the desire of increasing the flexibility and versatility of robots, it is common to find applications (*e.g.*, collaborative assembly [Sadrfaridpour and Wang, 2018]) where human cooperation is not the only contact that the robots may experience with their environment, and where unexpected collisions with obstacles may also occur. For this reason, it is essential that robots are capable of quickly distinguishing if a contact has occurred, and if so, whether it has been caused by human cooperation (defined as intentional) or by an obstacle collision (defined as accidental). Therefore, contact detection and classification, while the robot behaves in a compliant way with respect to its environment, is a key concern in these applications.

1.1 Previous Research

As summarized in [Cioffi *et al*., 2020], there are two main sets of methods, which are primarily based on external force/torque estimation, being used to detect and classify contacts: using machine-learning approaches [Golz *et al*., 2015; Popov *et al*., 2017; Briquet-Kerestedjian *et al*., 2019; Cioffi *et al*., 2020], or analyzing their frequency content [Geravand *et al*., 2013; Kouris *et al*., 2016; Kouris *et al*., 2018]. In such scenarios, a fast detection and classification is essential since a successful robot trajectory reprogramming should depend on it [Karlsson *et al*., 2017; Wrede *et al*., 2013; Haddadin *et al*., 2008].

Machine-learning approaches have shown to provide promising results for contact detection and classification, but their fast execution may be challenging. In [Golz *et al*., 2015], the authors used the entire contact event to extract features that allow to discriminate between intended and unintended contacts. An extensive classification approach was presented in [Popov *et al*., 2017], but it cannot run in real-time. In [Briquet-Kerestedjian *et al*., 2019], the authors were able to classify a detected contact in a minimum of 160 ms. Finally, an online classification method using machine learning was proposed in [Cioffi *et al*., 2020], but it is operator dependent and needs the joint load-torque signals of a previous, uncollided, execution of the trajectory.

In contrast, frequency-response analysis methods can achieve a faster detection and classification: in [Geravand *et al*., 2013], the authors detected contacts in less

than 50 ms, and the authors of [Kouris *et al*., 2016; Kouris *et al*., 2018] detected and classified contacts in a single force direction in less than 10 ms. However, frequency-based methods come with their own challenges, one of the more significant being the difficulty of tuning their thresholds and cut-off frequencies. In [Geravand *et al*., 2013], six different thresholding parameters per joint were needed to classify the contact situation based on filtered motor-current signals, which, unfortunately, are not available in some robot controller interfaces.

Moreover, these frequency-based contact-detection and classification methods are based on the premise that human voluntary cooperation with the robot presents forces with a lower rate of change than accidental collisions, and therefore, their frequency characteristics can be differentiated: cooperation will present lower frequency components than the accidental collisions. To sustain this assumption, the authors in [Kouris *et al*., 2016] and [Kouris *et al*., 2018] presented experimental data for one force direction recorded from an external force sensor mounted between the robot's flange and a handle.

1.2 Problem Formulation

In this paper, we address the problem of fast contact-detection and classification for kinesthetic teaching applications in collaborative robots relying only on available information provided by its embedded sensors, which in most cases are the joint motor encoders/resolvers that are able to provide joint angular positions (and joint angular velocity and possibly acceleration by differentiation), and the joint-torque sensors that are used to measure the joint applied torques. These variables are then used to estimate the external forces/torques applied to the robot. We refer to [Haddadin *et al*., 2017] for a summary of different methods to obtain these external forces/torques, and especially for the justification of the generalized momentum observer that was used in our experiments. Moreover, robot compliant control is used to ensure safety in a contact-rich environment and to allow human cooperation.

To solve the problem addressed in this paper, while ensuring fast contact detection, we evaluated the use of frequency-response analysis of the estimated external force and the benefits of comparing the robot Cartesian motion and its sensed external force. The method should allow a fast detection and to distinguish between human cooperation and accidental collisions in any contact direction for a collaborative assembly task using data only from robot embedded sensors. To evaluate this method, several experiments were performed, using the Panda robot by Franka Emika [Franka Emika, 2019] with a peg-in-hole setup as seen in Fig. 2.

1.3 Outline

The paper is organized as follows: Sec. 2 presents the method for solving the problem described in Sec. 1. Section 3 explains the experiments performed. Then, Sec. 4 presents the results obtained. Finally, a discussion is included in Sec. 5 and conclusions are drawn in Sec. 6.

2. Method

First, we introduce the robot compliance controller used. Then, we evaluate the use of frequency-based contact detection and classification for our problem. Finally, we propose modifications and extensions to ensure contact detection in any direction and classification between human cooperation and obstacle collision for a collaborative assembly task.

2.1 Torque-Based Cartesian Impedance Control

External forces may be applied to the robot at any moment while executing a desired trajectory. Therefore, the robot must behave in a compliant way toward these forces to avoid any harm of both the robot and the colliding object. Also, a compliant robot behavior allows direct human cooperation without the need of switching to a dedicated admittance controller. The aim of a Cartesian impedance controller [Hogan, 1985] is to establish a mass-damper-spring relationship between the Cartesian pose variation from its reference, $\Delta\xi$, and the Cartesian force, F [Albu-Schäffer and Hirzinger, 2002]:

$$F = I\ddot{\xi} + B\dot{\xi} + K\Delta\xi \tag{1}$$

where I, B, and K are the virtual inertia, damping, and stiffness matrices, respectively. Further, $\Delta\xi = \begin{bmatrix}\Delta p^{\mathrm{T}} & \Delta\varepsilon^{\mathrm{T}}\end{bmatrix}^{\mathrm{T}}$, where the translation variations in the Cartesian pose are calculated with $\Delta p = p_d - \hat{p}$, and the rotation variations are calculated with $\Delta\mathscr{Q} = \hat{\mathscr{Q}}^{-1}\mathscr{Q}_d$, $\Delta\varepsilon$ being the vector part of the unit-quaternion representation of the rotation variation with respect to the base frame, $\Delta\mathscr{Q}$. Here, $\hat{\xi} = \begin{bmatrix}\hat{p}^{\mathrm{T}} & \hat{\mathscr{Q}}^{\mathrm{T}}\end{bmatrix}^{\mathrm{T}}$ is the estimated Cartesian pose of the robot end-effector computed from joint angle measurements, and $\xi_d = \begin{bmatrix}p_d^{\mathrm{T}} & \mathscr{Q}_d^{\mathrm{T}}\end{bmatrix}^{\mathrm{T}}$ is the reference Cartesian pose of the robot end-effector.

With F from Eq. (1), the task torque is calculated as:

$$\tau_{\text{task}} = J^{\mathrm{T}}(q)F \tag{2}$$

where $J(q)$ is the Jacobian relative to the base frame of the robot and q are the sensed joint angular positions. Finally, the contribution from Coriolis and centripetal forces, $C(q,\dot{q})$, is added to the task torque to obtain the reference torque:

$$\tau_{\text{ref}} = \tau_{\text{task}} + C(q,\dot{q})\dot{q} \tag{3}$$

where $\dot{q}$ represents the sensed joint angular velocities. The gravitational-forces term does not appear in Eq. (3) since the robot's internal controller takes care of the gravity compensation.

2.2 Frequency-Based Contact Detection and Classification

Previous research on frequency-based contact detection and classification is based on the idea that the frequency characteristics of motor currents or external force

acting on the robot in an accidental collision situation are different from the ones obtained while a human is cooperating with the robot [Geravand *et al.*, 2013; Kouris *et al.*, 2016; Kouris *et al.*, 2018]. For a sliding time window, if the p–norm of the discrete Fourier transform of the force signal over a given frequency interval is greater than a user-defined force threshold, F_{th}, then it is considered that the contact should be classified an accidental obstacle collision [Kouris *et al.*, 2016; Kouris *et al.*, 2018]. If not, then it is classified as interference from human cooperation.

Figure 1 illustrates the L_∞-norm of the frequency content of the force signal in the frequency range between ω_{min} and ω_{max} using a sliding window of N samples at every time step, as suggested in [Kouris *et al.*, 2016], but using the joint-torque sensors embedded in the robot to estimate the external force. This frequency range has an upper limit determined by the Nyquist frequency ($\omega_{\text{max}} \leq {}^{1}/_{2h}$) and a lower limit determined by the measurement duration ($\omega_{\text{min}} \geq {}^{1}/_{Nh}$), with h being the sample period. Moreover, the Cartesian impedance control parameters used are the same as in Sec. 3.1.

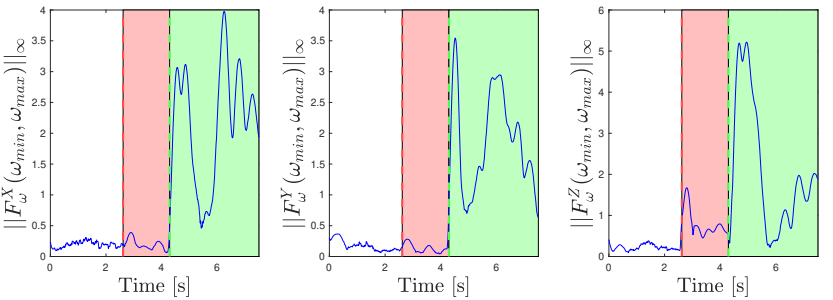

Figure 1. Temporal evolution of the L_∞-norm of the frequency content for all three force directions: F^X, F^Y, and F^Z, in a collaborative assembly task (peg-in-hole). The frequency range used is $\omega \in [10, 100]$ Hz, and the temporal sliding window is $N = 500$ samples long.

In the trajectory used for Fig. 1, the robot transitions from free, undisturbed motion (white background), to obstacle collision (red background), and then to human cooperation (green background). The obstacle collision, which occurs along the Z-direction, can be distinguishable from the free motion when analyzing the frequency content that belongs to F_Z. However, human cooperation also causes an identifiable spike in this same force direction later in the trajectory. Therefore, when the experiments are performed for a robot with compliant behavior using the joint-torque sensors embedded in the robot instead of external force sensors, the distinction of frequency content between accidental collisions and cooperation becomes uncertain, which motivates the proposal of modifications and extensions to the method.

2.3 Contact Detection

From the analysis of Fig. 1, it can be concluded that force-thresholding can be useful for contact detection, but extra variables are needed for classifying the contact if only joint-torque sensors are used. Thus, our proposal consists of a decoupled process between contact detection and classification. For contact detection, the method presented in [Kouris *et al*., 2016; Kouris *et al*., 2018] was extended to all three force directions. Therefore, the proposed detection process consists of evaluating if

$$\hat{F}_{\omega}^{i} > F_{\text{th}} \tag{4}$$

for $i \in \{X, Y, Z\}$, where F_{th} is the selected frequency-based threshold valid for any direction i for each time step, and $\hat{F}_{\omega}^{i}$ is equal to the L_{∞}-norm of the discrete Fourier transform of the external sensed force along direction i in the frequency range between ω_{min} and ω_{max} using a sliding window of N samples.

The contact-detection method, which is called at each time step, has been summarized in Algorithm 1. If the robot is moving in free motion (*STATE = FREE*), the condition (4) is evaluated in all directions (Algorithm 1, Line 2). If this condition is true, a contact is detected, and the classifier takes care of evaluating if the contact is accidental or if a human operator is collaborating with the robot (Algorithm 1, Line 5; detailed in Algorithm 2). The contact classifier uses the system's state at the exact time of the contact, which is obtained (in Algorithm 1, Line 4) by performing a backwards search in the external force signal from the contact-detection time along the contact's direction (determined in Algorithm 1, Line 3).

Algorithm 1 Contact Detection

```
1:  if STATE == FREE then
2:      if Check contact == TRUE then
3:          Get contact direction
4:          Get contact time
5:          STATE ← Contact Classifier (Algorithm 2)
6:      end if
7:  else if STATE == COLL then
8:      Get contact direction
9:      if Check new contact direction == TRUE then
10:         Get contact time
11:         STATE ← Contact Classifier (Algorithm 2)
12:     end if
13:     Update active collision directions
14: else if STATE == COOP then
15:     if Check cooperation stopped == TRUE then
16:         STATE ← FREE
17:     end if
18: end if
```

Moreover, while an accidental collision is occurring (*STATE = COLL*), an additional contact could be detected (whose source can be human cooperation) if the force threshold is violated again along any direction, with the exception of the directions that previously experienced the accidental collision (Algorithm 1, Line 9). The contact-detection algorithm will update the active collision directions if a collision along a new direction is detected or if the value of a previously collided direction has stopped violating the threshold (Algorithm 1, Line 13).

Furthermore, when a contact has been labelled as human cooperation (*STATE = COOP*), the contact-detection algorithm will only determine that the cooperation has stopped if the forces along all three directions are below the force threshold, F_{th} (Algorithm 1, Line 15).

2.4 Contact Classification

In contrast with contact detection, the frequency content of the estimated external force is not enough to classify the contact event when only using embedded sensors (as indicated in Fig. 1). Therefore, to properly categorize the contact in a kinesthetic teaching application, knowledge of the performed robot motion can be used.

Our classifier algorithm is based on two assumptions:

- **Assumption A1**: An accidental collision of the robot end-effector or attached tool with a static obstacle must occur in the direction of the movement and with the opposite sense from the one of the motion.

- **Assumption A2**: Human cooperation should have less dominant external force components in the direction of the robot's motion because of the typical spatial layout and interaction of a human operator and a robotic manipulator in kinesthetic teaching.

These two ideas are used to formulate an algorithm next, along with the explanation of the steps of the classifier algorithm.

The contact classifier will be activated once contact has been detected. The contact-classifying algorithm has been summarized in Algorithm 2. The first step is to analyze if, for any of the external forces sensed that have trespassed their threshold (where inequality (4) holds), the force is being applied in the same sense as the motion at the moment that this force signal started rising (Algorithm 2, Line 1). If this is the case, it is straightforward to affirm that human cooperation is occurring (*A1*):

$$\text{sign}\left(\hat{F}^i_{\text{ext}}\dot{\hat{\xi}}^i\right) > 0 \tag{5}$$

only when $\hat{F}^i_{\omega} > F_{\text{th}}$, $i \in \{X,Y,Z\}$, F_{th} being the selected frequency-based threshold, and $\dot{\hat{\xi}}$ being the time derivative of the estimated Cartesian pose of the robot end-effector. The time derivative of the estimated external force along direction i, $\dot{\hat{F}}^i_{\text{ext}}$,

is preferred compared to the estimated external force along direction i, $\hat{F}^i_{\text{ext}}$, since the time step where this condition is evaluated is when the force signal starts rising.

The second step is, if the inequality (5) is not true for any of the detected contact directions, to perform a new test that evaluates the direction of the external force vector relative to the Cartesian velocity vector (Algorithm 2, Line 4). The reason for this is that compared to intuitive human cooperation for kinesthetic teaching, the largest external force components in accidental collisions must come from directions where the robot's velocity is the highest (*A2*):

$$||\vec{u}_{\hat{F}_{\text{ext}}} \oslash \vec{u}_{\dot{\hat{\xi}}}||_2 < \gamma \tag{6}$$

where $\vec{u}_j$ represents a unitary vector of variable j, γ is the threshold coefficient, and $||\cdot||_2$ is the L_2-norm. Also, $\oslash$ represents the Hadamard division: $C_{jk} = A_{jk}/B_{jk}$ if $C = A \oslash B$. The smaller the threshold coefficient γ is, the closer the external force will be when compared to the Cartesian velocity. If the inequality (6) is evaluated as true, the contact is classified as accidental collision.

Moreover, the inequality (6) is equivalent to evaluating if the unitary external force vector is contained in the ellipsoid defined by the robot's unitary Cartesian velocity vector:

$$\frac{x^2}{a^2} + \frac{y^2}{b^2} + \frac{z^2}{c^2} < 1 \tag{7}$$

where $[x,y,z] = \vec{u}_{\hat{F}_{\text{ext}}}$ and $[a,b,c] = \gamma \vec{u}_{\dot{\hat{\xi}}}$.

Furthermore, unitary vectors have been chosen to avoid having a dependence on the trajectory or on the applied force magnitude, since the classification should be trajectory-independent and also human-operator independent. Therefore, the algorithm only relies on the external force-vector direction with respect to the tangential direction of the motion.

Algorithm 2 Contact Classification

```
1: if A1 == TRUE then
2:     STATE ← COOP
3: else
4:     if A2 == TRUE then
5:         STATE ← COLL
6:     else
7:         STATE ← COOP
8:     end if
9: end if
```

3. Experiments

The goal of the experiments was to obtain realistic data of a collaborative assembly task where human operators were instructed to cooperate intuitively with the robot

to evaluate the contact detection and classification method for kinesthetic teaching applications proposed in Sec. 2.

3.1 Experimental Platform

The experiments were performed using the Panda robot by Franka Emika [Franka Emika, 2019] mounted onto a table; the robot was able to record with a sample frequency of 1 kHz (sample period $h = 1$ ms), using the setup shown in Fig. 2. As mentioned earlier, we only used data from embedded sensors to estimate the variables of interest, $\hat{\xi}$ and $\hat{F}_{\text{ext}}$, which were used for selecting and evaluating the threshold parameters for contact detection, F_{th}, and contact classification, γ. The end-effector Cartesian pose was obtained by applying forward kinematics, $\mathscr{K}$, to the joint angular-position readings provided by the joint encoders [Corke, 2013]:

$$\hat{\xi} = \mathscr{K}(q) \tag{8}$$

Moreover, the estimate of the external forces was obtained from the external joint-torques, which were estimated based on the generalized momentum observer for the Panda robot that was introduced in [Haddadin *et al.*, 2017], by using the Jacobian relative to the base frame of the robot in an inverse way compared to the one presented in Eq. (2):

$$\hat{F}_{\text{ext}} = J^{\dagger}(q)\,\hat{\tau}_{\text{ext}} \tag{9}$$

where the superscript † denotes the Moore-Penrose pseudoinverse.

Furthermore, the Cartesian impedance control parameters (K, B, and I) of Eq. (1) were chosen to be as follows:

- The stiffness K was equal to 150 $[\text{N}/\text{m}]$ for the translational degrees of freedom and equals to 10 $[\text{N}/\text{rad}]$ for the rotational degrees of freedom.
- The damping B was equal to $2\sqrt{K}$.
- The inertia I was equal to 0.

The relationship between the Cartesian position variation and the task force will, with these parameters, behave along all degrees of freedom as a first-order system with a time constant equal to $2/\sqrt{K}$ [Lawrence, 1988]. This way, we ensured stability of the system and proper following of the trajectory reference (overdamped behavior).

3.2 Experimental Procedure

A cylinder insertion, or peg-in-hole, was the collaborative assembly task chosen for the experiments, as shown in Fig. 2. The reason for the selection of this task was that it presents a high amount of interaction with the environment: the hole where the piston must be inserted was narrow in comparison to the piston, and also the piston must make a vertical descent to avoid contacts. Therefore, the probability of

an accidental collision was high if the reference trajectory was not accurate or if the controller introduced uncertainty in the motion. Furthermore, it is an application where the aid of a human operator can be valuable and it did not require a high level of skill for the operator.

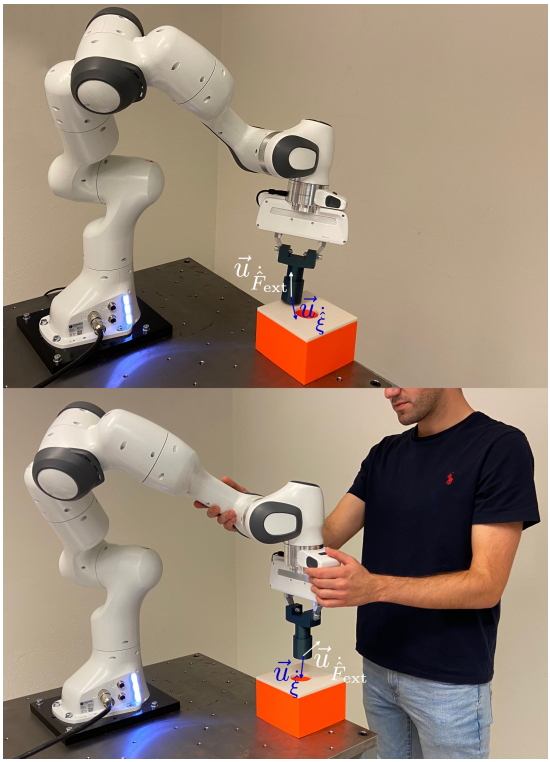

Figure 2. Setup for the collaborative assembly task (peg-in-hole) used for the experiments. Figure 2-A (top) shows an accidental collision scenario, and Fig. 2-B (bottom) shows a human cooperation event. The unitary vector of external forces (white) and the unitary vector of Cartesian velocity (blue) were used in the contact-classification algorithm proposed in Sec. 2.4. A video of the experiments can be found at [*Experiments video* 2022].

The trajectories used range from almost-ideal trajectories, where the robot could complete the insertion task and the only collisions were with the borders of the hole of the box, to failed trajectories where the robot collided with the side of the box and the robot was not able to overcome this collision and insert the piston in the hole without human intervention. Other trajectories used were flawed with manifest collisions with the top of the box, and depending on the nature of the

trajectory, the robot might be able to find its way to the hole with no human input. All trajectories were recorded several times using different initial poses to avoid a trajectory-dependent contact detection and classification.

The desired trajectory of Cartesian poses, $\xi_d(t)$, were recorded before the experiments by leading through the robot and recording the Cartesian pose of the robot end-effector. These trajectories served as the reference for the Cartesian impedance controller of Eq. (1). The reference trajectory was solely time-dependent and did not rely on the robot's current pose, since ideally, the contact-detection and classification algorithm should be implemented in a time-constrained scenario.

Additionally, regarding human cooperation, to test the validity of the assumptions proposed in Sec. 2.4 for a kinesthetic teaching application, the operators were instructed to cooperate in an intuitive manner with the robot to either help the robot with its cylinder insertion task or to push/pull the robot out of its trajectory to avoid colliding with the box. Moreover, since human cooperation in a kinesthetic teaching application may occur at different points of the trajectory in each of the runs, some of the human interventions occurred while the piston was in collision with the box and others while the robot was in free motion. Also, for the sake of data completeness, the operators were also instructed to vary the location of contact with the robot so that the human-cooperation events took place throughout all the links of the robot and not only at a location close to the robot end-effector.

Furthermore, as commented in previous research, human–robot cooperation may be very operator-dependent [Geravand *et al*., 2013; Briquet-Kerestedjian *et al*., 2019; Cioffi *et al*., 2020]. Therefore, a total of four different operators (including three external participants) individually manipulated the robot during the recording of the experiments to test the sensitivity and robustness of the classification. Also, the operators had different experience levels with robot manipulation to analyze the role of this variable for the contact-classification method proposed.

4. Results

The total amount of data that were recorded included 266 contact events. These collision events were divided into 148 accidental obstacle collisions and 118 voluntary human cooperation events. In total, 28 accidental collisions and 28 human cooperation events (from a single human operator) were used for the parameter tuning, and the remaining contact events were used for the method's evaluation.

4.1 Tuning and Evaluation of the Method

First, for contact detection, the force threshold parameter has been assigned a value of $F_{\text{th}} = 0.85$ N, for all Cartesian directions. This value of the force-detection threshold allowed that all contacts recorded in the evaluation experiments were detected, and that no contact-detection false positive was detected. The frequency range used for detection was $\omega \in [10, 100]$ Hz.

Accidental collisions were detected within 71 ms on average, with a standard deviation of 31 ms. On the contrary, voluntary human-cooperation events were detected within 133 ms on average, with a standard deviation of 66 ms. Thus, the capacity of this method to detect contacts fast can be confirmed.

Additionally, the contact-classification threshold parameter was chosen to have a value of $\gamma = 6.2$. This value should be chosen conservatively high, since it is preferred to misclassify human cooperation events than accidental collisions. This idea will be further developed in Sec. 5.

The results for the evaluation of the classification method are shown in Tables 1 and 2. Table 1 displays the confusion matrix for all evaluation experiments performed. It can be seen how 93.3% of the accidental collisions were correctly classified (specificity), whereas for the cooperation events, 88.9% of them were correctly classified (sensitivity).

Table 1. Confusion Matrix for Evaluation Experiments

	Classified as	
	Collision	Cooperation
Collision	112 (93.3%)	8 (6.7%)
Cooperation	10 (11.1%)	80 (88.9%)

Moreover, Table 2 breaks down the recorded cooperation events of Table 1 into the four different operators involved in the evaluation experiments. As commented before, the success rate of the contact classifier varied depending on the human operator. For the method proposed, the sensitivity ranged from 85.2% to 96.2%. Therefore, the sensitivity achieved using this method was still high for the human operator with the lowest classification rate. Furthermore, the sensitivity of the method for experienced operators (Operators 1 and 2 in Table 2) was on average 91% with a standard deviation of 5.3%, which is higher than the sensitivity of the method for inexperienced operators (Operators 3 and 4 in Table 2), which was equal to 86.4% with a standard deviation of 1.2%.

Table 2. Detail of Confusion Matrix for each Human Operator

	Cooperation classified as	
	Collision	Cooperation
Operator 1	1 (3.8%)	25 (96.2%)
Operator 2	3 (14.3%)	18 (85.7%)
Operator 3	4 (14.8%)	23 (85.2%)
Operator 4	2 (12.5%)	14 (87.5%)

4.2 Contact Detection and Classification Example

Figure 1 provides an example of the data extracted for one trajectory execution. The robot was initialized in free motion. It can be seen that at $t = 2.616$ s, a contact was detected along the Z-direction. The contact was detected 87 ms after the external force signal along the Z-direction starts rising. Once contact was detected, the contact-classifying part of the algorithm analyzed the force sense along the Z-direction and compared it to the motion component along this direction using condition (5). Since their signs were opposite, it cannot be determined that the contact was a human-cooperation event. Then, the inequality (6) was used. Since $||\vec{u}_{\hat{F}_{\text{ext}}} \oslash \vec{u}_{\hat{\xi}}||_2 = 2.97 < 6.2 = \gamma$, it can be concluded that the contact was an accidental collision.

Moreover, at $t = 4.290$ s, a new contact was detected along the Y-direction just 85 ms after this new contact occurred. Now, by evaluating condition (5) at the contact time, it was seen that both the force component along the Y-direction and the motion along this direction share the same sign and therefore it is concluded that the contact belongs to the human cooperation category. Furthermore, if the inequality (6) had been evaluated in this situation, the contact would also have been labelled as a human cooperation, since $||\vec{u}_{\hat{F}_{\text{ext}}} \oslash \vec{u}_{\hat{\xi}}||_2 = 41.84 > 6.2 = \gamma$.

Finally, no false positives occurred for contact detection for the entire trajectory shown in Fig. 1, since, for the accidental collision, no force violated the threshold along the X and Y-directions and no force violated the threshold along the Z-direction once the value was lower than this threshold. Also, for the human-cooperation segment, the force was at all times above the force threshold for some of the three Cartesian directions after $t = 4.290$ s.

5. Discussion

In the event that only embedded sensors are available and the external force signal is estimated using the generalized momentum observer [Haddadin *et al.*, 2017], which is currently implemented in commercial collaborative robots such as the Franka Emika Panda [Franka Emika, 2019] and the KUKA LBR product family [Bischoff *et al.*, 2010], the assumption, considered in [Geravand *et al.*, 2013; Kouris *et al.*, 2016; Kouris *et al.*, 2018], that the frequency content of the estimated force is easily distinguishable between voluntary human cooperation and accidental collisions with static obstacles is not certain anymore in a collaborative assembly task. However, we have experimentally demonstrated that the frequency content of the external force signal can still be used for contact detection in this application. Nevertheless, additional sensor information, provided by the embedded joint-position sensors, regarding the robot's motion prior to the detected contact, can be used to classify the contact.

Moreover, several aspects of the implementation of the proposed method allow

freedom to the designer for their selection, and this also has several consequences. First, there is a trade-off between the contact-detection time, defined as the time between the contact occurs and when it is detected, and the force threshold parameter F_{th}: if shorter detection times are desired, more false positives in the contact detection will occur since F_{th} would be smaller. Using only embedded joint-torque sensors causes longer detection times when compared to previous research that included this same force threshold parameter but used external force/torque sensors for a single force-direction detection [Kouris *et al*., 2016], [Kouris *et al*., 2018]. Nevertheless, the force-threshold parameter value used in our experiments has been proven able to provide faster response times for all three force directions than alternative machine-learning methods [Golz *et al*., 2015; Popov *et al*., 2017; Briquet-Kerestedjian *et al*., 2019], while presenting no false positives in contact detection.

Second, the contact classifier's threshold parameter, γ, can be varied depending on the desired ratio between the sensitivity (percentage of human cooperation events correctly classified) and the specificity (percentage of accidental collisions correctly classified), since it is not possible to obtain a threshold parameter that allows no ambiguity in the classifier part. Here, specificity must be prioritized to avoid false positives in human cooperation. This is because the proposed method is aimed to be used in a collaborative assembly task where the presence of accidental collisions is expected, and if human cooperation is detected, the cooperation event can be used for trajectory reprogramming using kinesthetic teaching [Karlsson *et al*., 2017].

Third, the method proposed solely requires tuning of two thresholding parameters (F_{th} and γ) to achieve a proper contact detection and classification along all three force directions, compared to the 6 parameters per joint used for tuning the method in [Geravand *et al*., 2013] and to the single parameter needed in [Kouris *et al*., 2016; Kouris *et al*., 2018] for a single force direction. Also, as discussed in [Kouris *et al*., 2016], the choice of the virtual inertia, damping, and mass of Eq. (1) will have an effect on the sensed external force signal, and therefore, the two thresholding parameters used in our proposed method must be varied if the desired impedance behavior of the robot is different from the one described using the values defined in Sec. 3.1.

The proposed method was not tested to detect transitions between accidental collision to free motion, or from cooperation to accidental collision since we were not interested in these situations in the experimental application used for evaluation. First, the peg-in-hole application would not have the accidental-collision to free-motion situation, since when the piston impacts the cylinder, it would not stop its impact without human intervention. Second, for this application, a human intervention for kinesthetic teaching would not end up in a purposeful direct transition to an obstacle collision. Also, the proposed method can detect human-cooperation events while an accidental collision with an obstacle is occurring, whereas this transition has not been tested by machine-learning methods [Golz *et al*., 2015; Popov *et al*., 2017; Briquet-Kerestedjian *et al*., 2019; Cioffi *et al*., 2020] or by the previously-proposed frequency-based meth-

ods [Geravand *et al*., 2013; Kouris *et al*., 2016; Kouris *et al*., 2018]. This feature is especially relevant for applications that use kinesthetic teaching for corrective trajectory demonstration [Karlsson *et al*., 2017].

In addition, the proposed method's accuracy (percentage of total contacts correctly classified) outperformed other methods previously presented (91.4% for the proposed method, 86.3% for the method in [Cioffi *et al*., 2020], 89.5% for the method in [Popov *et al*., 2017], and 81.9% for the method in [Briquet-Kerestedjian *et al*., 2019]). The method presented in [Golz *et al*., 2015] provides the highest accuracy, 97.8%, but only one human operator was used for gathering experimental data. Also, the proposed method's accuracy (91.4%) was higher than the accuracy obtained when using the same relevant variables ($\vec{u}_{\hat{F}_{\text{ext}}}$ and $\vec{u}_{\hat{\xi}}$) as parameter estimates in Fisher's Linear Discriminant [Fisher, 1938] for contact classification (83.3%).

Moreover, our method is novel compared to the methods in [Cioffi *et al*., 2020; Golz *et al*., 2015; Popov *et al*., 2017; Briquet-Kerestedjian *et al*., 2019] in that it has been designed for kinesthetic teaching applications, where a human operator can lead-through the robot for trajectory reprogramming [Karlsson *et al*., 2017]: the robot's compliant behavior, contrary to the stiffer robot behavior in [Cioffi *et al*., 2020; Golz *et al*., 2015; Popov *et al*., 2017; Briquet-Kerestedjian *et al*., 2019], allows lead-through without controller switching (as well as providing safety for both the robot and its environment), and also the method is able to classify a human-cooperation event happening while an accidental collision is occurring.

Furthermore, the proposed method, although its evaluation involved only four participants, can be considered robust with respect to different operators since the standard deviation between operators of the sensitivity was equal to 4.4 percentage points, which was lower than in other methods (10.1 percentage points in [Cioffi *et al*., 2020], where four operators were involved, and 7.3 percentage points in [Briquet-Kerestedjian *et al*., 2019], where three operators were involved). Also, the difference in accuracy between trained and untrained operators was lower than in [Briquet-Kerestedjian *et al*., 2019], being 4.6 percentage points (91% and 86.4%, respectively) the difference in our method compared to 14.6 percentage points (86.4% and 71.9%, respectively) in [Briquet-Kerestedjian *et al*., 2019], which showed the validity of the assumptions for the intuitive human cooperation in kinesthetic teaching that were included in Sec. 2.4 for both trained and untrained operators in a collaborative assembly task. Thus, the proposed method can be used by different operators for kinesthetic teaching in these tasks without the need for retuning.

6. Conclusion

Fast contact detection and classification based on the frequency-response analysis of the estimated external force signals was evaluated, and necessary modifications and extensions to detect and classify a contact in any direction for kinesthetic teaching applications were proposed. Cartesian impedance control was used to allow safe

human cooperation. The only sensors used for obtaining the external force estimate were sensors that are conventionally embedded in commercial collaborative robots and whose values were easily attainable: joint-torque sensors and joint-position encoders/resolvers.

The proposed modified method was proven to provide accurate results for both accidental collision with stiff and static obstacles and voluntary human cooperation in a collaborative assembly task. In addition, the method is trajectory-independent, and was tested for a meaningful number of different operators, showing interesting results for both trained and untrained operators.

References

Albu-Schäffer, A. and G. Hirzinger (2002). "Cartesian impedance control techniques for torque controlled light-weight robots". In: *IEEE International Conference on Robotics and Automation (ICRA)*. Vol. 1. May 11–15. Washington DC, USA, pp. 657–663.

Bischoff, R., J. Kurth, G. Schreiber, R. Koeppe, A. Albu-Schäffer, A. Beyer, O. Eiberger, S. Haddadin, A. Stemmer, G. Grunwald, and G. Hirzinger (2010). "The KUKA-DLR lightweight robot arm—A new reference platform for robotics research and manufacturing". In: *International Symposium on Robotics (ISR)*. Jun. 7–9. Munich, Germany, pp. 1–8.

Briquet-Kerestedjian, N., A. Wahrburg, M. Grossard, M. Makarov, and P. Rodriguez-Ayerbe (2019). "Using neural networks for classifying human-robot contact situations". In: *18th European Control Conference (ECC)*. Jul. 25–28. Naples, Italy, pp. 3279–3285.

Cioffi, G., S. Klose, and A. Wahrburg (2020). "Data-efficient online classification of human-robot contact situations". In: *European Control Conference (ECC)*. May 12–15. Saint Petersburg, Russia, pp. 608–614.

Corke, P. (2013). *Robotics, Vision and Control: Fundamental Algorithms in MATLAB*. Springer, Berlin, Germany.

Experiments video (2022). `https://youtu.be/5Bq4oB6nDbw`.

Fisher, R. A. (1938). "The statistical utilization of multiple measurements". *Ann. Eugen.* **8**:4, pp. 376–386.

Franka Emika (2019). *Franka Emika Panda – Data Sheet*. `https://www.generationrobots.com/media/panda-franka-emika-datasheet.pdf`. (Visited on 2022-09-13).

Geravand, M., F. Flacco, and A. De Luca (2013). "Human-robot physical interaction and collaboration using an industrial robot with a closed control architecture". In: *IEEE International Conference on Robotics and Automation (ICRA)*. May 6–10. Karlsruhe, Germany, pp. 4000–4007.

Golz, S., C. Osendorfer, and S. Haddadin (2015). "Using tactile sensation for learning contact knowledge: Discriminate collision from physical interaction". In: *IEEE International Conference on Robotics and Automation (ICRA)*. May 26–30. Seattle, USA, pp. 3788–3794.

Haddadin, S., A. Albu-Schäffer, A. De Luca, and G. Hirzinger (2008). "Collision detection and reaction: a contribution to safe physical human-robot interaction". In: *IEEE/RSJ International Conference on Intelligent Robots and Systems (IROS)*. Sep. 22–26. Nice, France, pp. 3356–3363.

Haddadin, S., A. De Luca, and A. Albu-Schäffer (2017). "Robot collisions: a survey on detection, isolation, and identification". *IEEE Transactions on Robotics* **33**:6, pp. 1292–1312.

Hogan, N. (1985). "Impedance control: an approach to manipulation: part I". *Journal of Dynamic Systems, Measurement, and Control* **107**:1, pp. 1–7.

Karlsson, M., A. Robertsson, and R. Johansson (2017). "Autonomous interpretation of demonstrations for modification of dynamical movement primitives". English. In: *IEEE International Conference on Robotics and Automation (ICRA)*. May 29–Jun. 2. Singapore, pp. 316–321.

Kouris, A., F. Dimeas, and N. Aspragathos (2016). "Contact distinction in human-robot cooperation with admittance control". In: *IEEE International Conference on Systems, Man, and Cybernetics (SMC)*. Oct. 9–12. Budapest, Hungary, pp. 1951–1956.

Kouris, A., F. Dimeas, and N. Aspragathos (2018). "A frequency domain approach for contact type distinction in human–robot collaboration". *IEEE Robotics and Automation Letters* **3**:2, pp. 720–727.

Lawrence, D. A. (1988). "Impedance control stability properties in common implementations". In: *IEEE International Conference on Robotics and Automation (ICRA)*. Apr. 24–29. Philadelphia, USA, pp. 1185–1190.

Popov, D., A. Klimchik, and N. Mavridis (2017). "Collision detection, localization & classification for industrial robots with joint torque sensors". In: *26th IEEE International Symposium on Robot and Human Interactive Communication (RO-MAN)*. Aug. 28–31. Lisbon, Portugal, pp. 838–843.

Sadrfaridpour, B. and Y. Wang (2018). "Collaborative assembly in hybrid manufacturing cells: An integrated framework for human–robot interaction". *IEEE Transactions on Automation Science and Engineering* **15**:3, pp. 1178–1192.

Villani, V., F. Pini, F. Leali, and C. Secchi (2018). "Survey on human–robot collaboration in industrial settings: safety, intuitive interfaces and applications". *Mechatronics* **55**, pp. 248–266.

Wrede, S., C. Emmerich, R. Grünberg, A. Nordmann, A. Swadzba, and J. Steil (2013). "A user study on kinesthetic teaching of redundant robots in task and configuration space". *Journal of Human-Robot Interaction* **2**:1, pp. 56–81.

Paper III

Iterative Reference Learning for Cartesian Impedance Control of Robot Manipulators

Julian M. Salt Ducaju **Björn Olofsson** **Rolf Johansson**

Abstract

In this paper, an iterative reference learning strategy was developed to improve trajectory tracking for an impedance-controlled robot manipulator. In this learning strategy, an update law to modify the Cartesian reference of an impedance controller was proposed, and the conditions that ensured its convergence considering the dynamics of the robot were provided. Finally, an experimental evaluation was performed using a Franka Emika Panda robot in two different robot tasks, and its results showed that robot task completion could be achieved in a small number of iterations, while maintaining a smooth physical interaction between the robot and its surroundings.

Submitted to review for presentation at IEEE/RSJ International Conference on Intelligent Robots and Systems (IROS) 2024.

1. Introduction

The recent trends in the manufacturing industry to replace mass production for mass customization could not be addressed by former industrial settings, characterized by a fixed-structure workplace [Schou *et al*., 2013]. To avoid these limitations in modern-day industrial environments, manufacturing processes should be able to adapt with ease to rapidly changing requirements. Kinesthetic teaching, which is a human–robot collaboration (HRC) strategy where a human collaborator manually guides a robot to define or modify a robot trajectory [Argall *et al*., 2009], has been proposed for this purpose in the last years, since it allowed the use of human dexterity and intelligence in robot task adaptation [Cencen *et al*., 2018].

In less-structured industrial environments, indirect force-control strategies, such as impedance control [Hogan, 1985], are widely used, since, compared to other force-control strategies, they rely less on an accurate description of the robot environment [Villani and De Schutter, 2016]. Impedance control regulates the interacting forces between a robot and its environment by modeling the external force applied to the robot as a mass-spring-damper relationship between the robot state variation from a user-defined reference. By regulating the interaction force between a robot and its environment, impedance control allows the physical guidance of a robot by human operators, and provides physical safety to the actors involved. However, the dynamical relationship imposed by impedance-control strategies inherently introduces a deviation in the robot trajectory, which might cause a robot to not complete its designated task, *e.g.*, in an insertion task where the peg–hole tolerance is small.

Several strategies proposed in the past to improve trajectory tracking in a robotic manipulator might cause undesired effects in collaborative environments. First, position-feedback control [Kawamura *et al*., 1988] would modify the interaction forces between the robot and its environment by increasing the robot stiffness, which might damage the manipulated objects and pose a safety threat to robots and/or humans involved. Also, other strategies that consist in trajectory scaling [Dahl, 1992; Dahlin and Karayiannidis, 2021] would inherently slow down the execution of the robot motion and might not be able to complete the robot task if the dynamics of the robot is not fully modeled, *e.g.*, joint elasticity or friction.

Moreover, strategies based on learning the desired robot behavior could be used in this context [Bristow *et al*., 2006]. Among these strategies, Reinforcement Learning (RL) has gained popularity in recent years [Ibarz *et al*., 2021], although it might still be too time-consuming for these robot applications, since this strategy often requires a high number of trials to learn a desired robot behavior [Pierallini *et al*., 2023]. Also, Iterative Learning Control (ILC) [Arimoto *et al*., 1984] has been used extensively in the past to improve robot behavior. Nevertheless, in its linear formulation [Norrlöf, 2000; Cano Marchal *et al*., 2014], ILC might not allow to fully exploit the robot dynamics. Alternatively, adaptive iterative learning techniques (AILC) [Park *et al*., 1996; Lee *et al*., 2019] can deal with robot nonlinearities, while re-

lieving the high-stiffness requirements of previously-proposed strategies [Kuc *et al.*, 1991] (which had the same limitations as position-feedback controllers [Kawamura *et al.*, 1988] for physical interaction). However, the adaptive terms in AILC would online modify the impedance behavior of a robot [Della Santina *et al.*, 2017]. Finally, the use of learning techniques for impedance-controlled robots has been explored in the past [Cheah and Wang, 1998; Arimoto *et al.*, 1999], but it was focused on impedance matching, *i.e.*, matching a desired physical interaction, instead of reducing trajectory tracking error.

In this paper, we address the problem of improving trajectory tracking in robotic applications where impedance control is used by proposing an iterative learning strategy that provides a Cartesian reference update. To validate our proposal, several experiments have been performed using a real robotic manipulator: a peg-in-hole experiment, and the snap-fit assembly of a switch.

The paper is organized as follows: Sec. 2 introduces the dynamics model used for Cartesian impedance control of robot manipulators. Then, Sec. 3 presents an iterative reference learning strategy to improve robot Cartesian reference tracking. The method proposed in Sec. 3 was extensively evaluated in experiments with a real robot, presented in Sec. 4. Finally, a discussion is included in Sec. 5 and conclusions are drawn in Sec. 6.

2. Modeling Background

The dynamic behavior of a robot manipulator controlled by a Cartesian impedance strategy is introduced in this section.

2.1 Robot Dynamics

The dynamics of the robot can be written in the joint space of the robot, $q \in \mathbb{R}^n$, as [Siciliano and Khatib, 2016]

$$M(q)\ddot{q} + C(q,\dot{q})\dot{q} + G(q) = \tau + \tau^{\text{ext}} \tag{1}$$

where $M(q) \in \mathbb{R}^{n\times n}$ is the generalized inertia matrix, $C(q,\dot{q}) \in \mathbb{R}^{n\times n}$ describes the Coriolis and centripetal forces effects, and $G(q) \in \mathbb{R}^n$ captures the gravity-induced torques. Finally, $\tau \in \mathbb{R}^n$ represents the input torques, n being the number of joints of the robot, and $\tau^{\text{ext}} \in \mathbb{R}^n$ are the external torques.

Moreover, the rigid-body equation of the robot can be rewritten in terms of its end-effector pose $\xi \in \mathbb{R}^m$, which is composed by the position and orientation of the end-effector

$$M_\xi(q)\ddot{\xi} + C_\xi(q,\dot{q})\dot{\xi} + G_\xi(q) = F + F^{\text{ext}} \tag{2}$$

where $F \in \mathbb{R}^m$ is the input force, and $F^{\text{ext}} \in \mathbb{R}^m$ the external Cartesian forces. Additionally, for a fully-actuated robot ($n = m$), $M_\xi \in \mathbb{R}^{m\times m}$, $C_\xi \in \mathbb{R}^{m\times m}$, and $G_\xi \in \mathbb{R}^m$

are equal to

$$M_\xi = J^{-\mathrm{T}}(q)M(q)J^{-1}(q) \tag{3}$$
$$C_\xi = J^{-\mathrm{T}}(q)(C(q,\dot{q}) - M(q)J^{-1}(q)\dot{J}(q))J^{-1}(q) \tag{4}$$
$$G_\xi = J^{-\mathrm{T}}(q)G(q) \tag{5}$$

assuming that the Jacobian relative to the base frame of the robot, $J(q) \in \mathbb{R}^{m\times m}$, has full rank [Khatib, 1987].

Furthermore, it is relevant to highlight two properties of a robot manipulator [Ott, 2008, Ch. 3]:

- The robot inertia matrix M_ξ in (2) is a positive definite matrix,

$$x^{\mathrm{T}} M_\xi x > 0, \ \ \forall x \neq 0 \tag{6}$$

- The matrix $\dot{M}_\xi - 2C_\xi$ is skew symmetric,

$$x^{\mathrm{T}}\left(\dot{M}_\xi - 2C_\xi\right)x = 0, \ \ \forall x \neq 0 \tag{7}$$

2.2 Robot Cartesian Impedance Control

An input force F in (2) equal to [Ott, 2008, Ch. 3]

$$F = K\Delta\xi - D\dot{\xi} + G_\xi(q) \tag{8}$$

would achieve a Cartesian impedance control of the robot end-effector, *i.e.*, a mass-spring-damper relationship between the Cartesian pose variation from its reference, $\Delta\xi = \xi_d - \xi$ (ξ_d being the Cartesian reference) and the external Cartesian force F^{ext},

$$F^{\text{ext}} = M_\xi(q)\ddot{\xi} + (C_\xi(q,\dot{q}) + D)\dot{\xi} - K\Delta\xi \tag{9}$$

where $K \in S^m_{++}$ and $D \in S^m_{++}$ (S_{++} denoting symmetric positive-definiteness) are diagonal matrices that represent the control-induced stiffness and damping, respectively.

3. Iterative Reference Learning Control

An iterative learning strategy to improve the Cartesian pose reference tracking for a Cartesian impedance-controlled robot is presented in this section.

3.1 Robot Input Feedforward and Error Dynamics

The input force F in (2) commanded to the robot could include an additional feedforward term F_{ff} [Kuc *et al.*, 1991; Park *et al.*, 1996] computed using iterative learning

$$F = F_{fb} + F_{ff} \tag{10}$$

where $F_{ff} = 0$ at the first learning iteration, and the input force feedback term F_{fb} is given by the desired Cartesian impedance behavior (9). Then, choosing an error variable $e \in \mathbb{R}^6$ with respect to a desired Cartesian pose, $\xi_R \in \mathbb{R}^6$, as

$$e = \xi_R - \xi \tag{11}$$

the error dynamics of the system in the absence of external forces acting on the robot would be equal to

$$M_\xi \ddot{e} + (C_\xi + D)\dot{e} + Ke = -F_{ff} \tag{12}$$

with $\dot{\xi}_R = \ddot{\xi}_R = 0$.

3.2 Learning Update Law

An update law at iteration $\mathrm{i}+1$ for the Cartesian impedance controller reference used in (9),

$${}^{\mathrm{i}+1}\xi_d = {}^{\mathrm{i}}\xi_d + \beta K^{-1} D \left[R(\xi_R - {}^{\mathrm{i}}\xi) - {}^{\mathrm{i}}\dot{\xi} \right] \tag{13}$$

where $\beta > 0$ is the iterative learning gain, ${}^{0}\xi_d = \xi_R$, and

$$R = D^{-1}(K - \Upsilon) > 0 \tag{14}$$

was obtained from the following force input feedforward strategy

$${}^{\mathrm{i}+1}F_{ff} = {}^{\mathrm{i}}F_{ff} + \beta D\, {}^{\mathrm{i}}\zeta \tag{15}$$

with ${}^{\mathrm{i}}\zeta \in \mathbb{R}^6$ that considered the Cartesian pose error (11) and its time derivative,

$${}^{\mathrm{i}}\zeta = {}^{\mathrm{i}}\dot{e} + R\, {}^{\mathrm{i}}e \tag{16}$$

REMARK The impedance-controlled robot behavior resulting from an iterative strategy where ξ_d in (9) is modified at every iteration step so that the error signal e in (11) converges to 0, would be stable by design. See [Salt Ducaju *et al.*, 2022, Lemma III.2] for more details of the stability justification for such impedance-controlled robots. □

The structure for the proposed Iterative Reference Learning Controller (IRLC) was illustrated in Fig. 1. It can be seen that at every iteration, the Cartesian

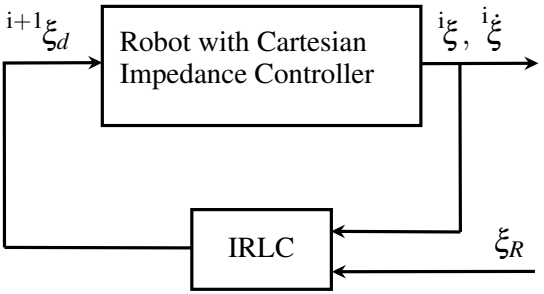

Figure 1. Illustration of the iterative learning controller proposed to reduce the robot trajectory error.

impedance reference sent to the controller is calculated considering the robot motion at the previous iteration, and the desired Cartesian pose.

Moreover, the update law in (13) is equivalent to, after $N > 0$ iterations

$$ {}^{N}\xi_d = \xi_R + \beta K^{-1} D\left[R\left(N\xi_R - \sum_{j=0}^{N-1} {}^{j}\xi\right) - \sum_{j=0}^{N-1} {}^{j}\dot{\xi}\right] \tag{17} $$

3.3 Convergence Analysis

A convergence analysis of the update law provided in Sec. 3.2 is presented in this section.

THEOREM 3.1
The proposed update law (13) would allow ξ to converge to ξ_R provided that the learning gain $\beta > 0$ of the iterative scheme is chosen so that the following conditions are fulfilled

$$ g_{\dot{e}} = (2-\beta)\lambda_{\mathrm{m}}(D) - 2R\lambda_{\mathrm{M}}(M_\xi) > 0 \tag{18} $$

$$ g_e = (2-\beta)\lambda_{\mathrm{m}}(D) - 2\lambda_{\mathrm{M}}(C_\xi) + 2\lambda_{\mathrm{m}}(R^{-1}\Upsilon) > 0 \tag{19} $$

$$ \sqrt{g_{\dot{e}} g_e} > \lambda_{\mathrm{M}}(\|R^{-1}\Upsilon - RM_\xi - C_\xi\|) \tag{20} $$

where λ_{m} and λ_{M} refer to the minimum and maximum eigenvalues, for all $t \in [0, t_{\mathrm{F}}]$, respectively, with t_{F} being the final time of the robot task execution. □

Proof. Using the performance index

$$ {}^{\mathrm{i}}V = \beta \int_0^t \left({}^{\mathrm{i}}\zeta\right)^{\mathrm{T}} D\left({}^{\mathrm{i}}\zeta\right) dt > 0 \tag{21} $$

and (15), it can be shown that

$$\begin{aligned} {}^{\mathrm{i}+1}V &= \beta \int_0^t \left({}^{\mathrm{i}+1}\zeta\right)^{\mathrm{T}} D\left({}^{\mathrm{i}+1}\zeta\right) dt \\ &= \beta \int_0^t \left[\left({}^{\mathrm{i}}\zeta\right)^{\mathrm{T}} D\left({}^{\mathrm{i}}\zeta\right) + \left({}^{\mathrm{i}}\Delta\zeta\right)^{\mathrm{T}} D\left({}^{\mathrm{i}}\Delta\zeta\right) + 2\left({}^{\mathrm{i}}\Delta\zeta\right)^{\mathrm{T}} D\,{}^{\mathrm{i}}\zeta\right] dt \end{aligned} \tag{22}$$

where ${}^{\mathrm{i}+1}\zeta = {}^{\mathrm{i}}\zeta + {}^{\mathrm{i}}\Delta\zeta$. Then, the error dynamics of the system (12) expressed in terms of the variable $\Delta\zeta$ (and assuming that M_ξ and C_ξ do not vary between the same sample time of consecutive iterations) is equal to

$$M_\xi\, {}^{\mathrm{i}}\Delta\dot{\zeta} + (C_\xi + D - RM_\xi)\, {}^{\mathrm{i}}\Delta\zeta + (-RC_\xi + R^2 M_\xi + \Upsilon)\, {}^{\mathrm{i}}\Delta e = -\beta D\, {}^{\mathrm{i}}\zeta \tag{23}$$

and it can be obtained that

$$\begin{aligned} {}^{\mathrm{i}}\Delta V = {}^{\mathrm{i}+1}V - {}^{\mathrm{i}}V = \int_0^t \Big[&\beta\left({}^{\mathrm{i}}\Delta\zeta\right)^{\mathrm{T}} D\left({}^{\mathrm{i}}\Delta\zeta\right) - 2\left({}^{\mathrm{i}}\Delta\zeta\right)^{\mathrm{T}} M_\xi\, {}^{\mathrm{i}}\Delta\dot{\zeta} \\ &- 2\left({}^{\mathrm{i}}\Delta\zeta\right)^{\mathrm{T}} (C_\xi - D - RM_\xi)\, {}^{\mathrm{i}}\Delta\zeta - 2\left({}^{\mathrm{i}}\Delta\zeta\right)^{\mathrm{T}} (R^2 M_\xi - RC_\xi + \Upsilon)\, {}^{\mathrm{i}}\Delta e\Big] dt \end{aligned} \tag{24}$$

Moreover,

$$\frac{d}{dt}\left(\left({}^{\mathrm{i}}\Delta\zeta\right)^{\mathrm{T}} M_\xi\, {}^{\mathrm{i}}\Delta\zeta\right) = \left({}^{\mathrm{i}}\Delta\zeta\right)^{\mathrm{T}} \dot{M}_\xi\, {}^{\mathrm{i}}\Delta\zeta + 2\left({}^{\mathrm{i}}\Delta\dot{\zeta}\right)^{\mathrm{T}} M_\xi\, {}^{\mathrm{i}}\Delta\zeta \tag{25}$$

so (24) can be rewritten as

$$\begin{aligned} {}^{\mathrm{i}}\Delta V = &-\left({}^{\mathrm{i}}\Delta\zeta\right)^{\mathrm{T}} M_\xi \left({}^{\mathrm{i}}\Delta\zeta\right) + \int_0^t \Big[\left({}^{\mathrm{i}}\Delta\zeta\right)^{\mathrm{T}} M_\xi \left({}^{\mathrm{i}}\Delta\zeta\right) + \beta\left({}^{\mathrm{i}}\Delta\zeta\right)^{\mathrm{T}} D\left({}^{\mathrm{i}}\Delta\zeta\right) \\ &- 2\left({}^{\mathrm{i}}\Delta\zeta\right)^{\mathrm{T}} (C_\xi + D - RM_\xi)\left({}^{\mathrm{i}}\Delta\zeta\right) - 2\left({}^{\mathrm{i}}\Delta\zeta\right)^{\mathrm{T}} (R^2 M_\xi - RC_\xi + \Upsilon)\left({}^{\mathrm{i}}\Delta e\right)\Big] dt \end{aligned} \tag{26}$$

Since M_ξ is positive definite, (6), and $\dot{M}_\xi - 2C_\xi$ is a skew-symmetric matrix, (7),

$$\begin{aligned} {}^{\mathrm{i}}\Delta V \leq \int_0^t \Big[&\beta\left({}^{\mathrm{i}}\Delta\zeta\right)^{\mathrm{T}} D\left({}^{\mathrm{i}}\Delta\zeta\right) - 2\left({}^{\mathrm{i}}\Delta\zeta\right)^{\mathrm{T}} (D - RM_\xi)\left({}^{\mathrm{i}}\Delta\zeta\right) \\ &- 2\left({}^{\mathrm{i}}\Delta\zeta\right)^{\mathrm{T}} (R^2 M_\xi - RC_\xi + \Upsilon)\left({}^{\mathrm{i}}\Delta e\right)\Big] dt \end{aligned} \tag{27}$$

which is equivalent to

$$\begin{aligned} {}^{\mathrm{i}}\Delta V \leq \int_0^t \Big[&\left({}^{\mathrm{i}}\Delta\zeta\right)^{\mathrm{T}} ((\beta - 2)D + 2RM_\xi)\left({}^{\mathrm{i}}\Delta\zeta\right) \\ &- 2\left({}^{\mathrm{i}}\Delta\zeta\right)^{\mathrm{T}} (R^2 M_\xi - RC_\xi + \Upsilon)\left({}^{\mathrm{i}}\Delta e\right)\Big] dt \end{aligned} \tag{28}$$

Using (16) to substitute ${}^{\mathrm{i}}\Delta\zeta$,

$$\begin{aligned}
&\int_0^t \left({}^{\mathrm{i}}\Delta\zeta\right)^{\mathrm{T}}((\beta-2)D+2RM_\xi)\left({}^{\mathrm{i}}\Delta\zeta\right)dt = \\
&\int_0^t \left({}^{\mathrm{i}}\Delta\dot{e}\right)^{\mathrm{T}}((\beta-2)D+2RM_\xi)\left({}^{\mathrm{i}}\Delta\dot{e}\right)dt \\
&+\int_0^t \left(R\,{}^{\mathrm{i}}\Delta e\right)^{\mathrm{T}}((\beta-2)D+2RM_\xi)\left(R\,{}^{\mathrm{i}}\Delta e\right)dt \\
&+2\int_0^t \left(R\,{}^{\mathrm{i}}\Delta e\right)^{\mathrm{T}}((\beta-2)D+2RM_\xi)\left({}^{\mathrm{i}}\Delta\dot{e}\right)dt
\end{aligned} \tag{29}$$

and,

$$\begin{aligned}
&\int_0^t -2\beta\left({}^{\mathrm{i}}\Delta\zeta\right)^{\mathrm{T}}(R^2M_\xi - RC_\xi + \Upsilon)\left({}^{\mathrm{i}}\Delta e\right)dt = \\
&-2R\int_0^t \beta\left({}^{\mathrm{i}}\Delta e\right)^{\mathrm{T}}(RM_\xi - C_\xi + R^{-1}\Upsilon)\left(R\,{}^{\mathrm{i}}\Delta e\right)dt \\
&-2\int_0^t \beta\left({}^{\mathrm{i}}\Delta\dot{e}\right)^{\mathrm{T}}(RM_\xi - C_\xi + R^{-1}\Upsilon)\left(R\,{}^{\mathrm{i}}\Delta e\right)dt
\end{aligned} \tag{30}$$

Therefore,

$$\begin{aligned}
{}^{\mathrm{i}}\Delta V \leq &\int_0^t \left({}^{\mathrm{i}}\Delta\dot{e}\right)^{\mathrm{T}}((\beta-2)D+2RM_\xi)\left({}^{\mathrm{i}}\Delta\dot{e}\right)dt \\
&+2\int_0^t \left({}^{\mathrm{i}}\Delta\dot{e}\right)^{\mathrm{T}}((\beta-2)D+RM_\xi+C_\xi-R^{-1}\Upsilon)\left(R\,{}^{\mathrm{i}}\Delta e\right)dt \\
&+\int_0^t \left(R\,{}^{\mathrm{i}}\Delta e\right)^{\mathrm{T}}((\beta-2)D+2C_\xi-2R^{-1}\Upsilon)\left(R\,{}^{\mathrm{i}}\Delta e\right)dt
\end{aligned} \tag{31}$$

Then, applying integration by parts,

$$\begin{aligned}
{}^{\mathrm{i}}\Delta V \leq &\int_0^t \left({}^{\mathrm{i}}\Delta\dot{e}\right)^{\mathrm{T}}((\beta-2)D+2RM_\xi)\left({}^{\mathrm{i}}\Delta\dot{e}\right)dt \\
&+2\int_0^t \left({}^{\mathrm{i}}\Delta\dot{e}\right)^{\mathrm{T}}(RM_\xi+C_\xi-R^{-1}\Upsilon)\left(R\,{}^{\mathrm{i}}\Delta e\right)dt \\
&+\int_0^t \left(R\,{}^{\mathrm{i}}\Delta e\right)^{\mathrm{T}}((\beta-2)-2R^{-1}\Upsilon+2C_\xi)\left(R\,{}^{\mathrm{i}}\Delta e\right)dt \\
&+\left({}^{\mathrm{i}}\Delta e\right)^{\mathrm{T}}D((\beta-2)D)\left(R\,{}^{\mathrm{i}}\Delta e\right)
\end{aligned} \tag{32}$$

where $\left({}^{\mathrm{i}}\Delta e\right)^{\mathrm{T}}((\beta-2)D)\left(R\,{}^{\mathrm{i}}\Delta e\right) \leq 0$ for $\beta < 2$. This expression can be rewritten as

$${}^{\mathrm{i}}\Delta V \leq -\int_0^t \begin{bmatrix} {}^{\mathrm{i}}\Delta\dot{e} \\ R\,{}^{\mathrm{i}}\Delta e \end{bmatrix}^{\mathrm{T}} \Omega \begin{bmatrix} {}^{\mathrm{i}}\Delta\dot{e} \\ R\,{}^{\mathrm{i}}\Delta e \end{bmatrix} dt \tag{33}$$

for

$$\Omega = \begin{bmatrix} g_{\dot{e}} I_6 & R^{-1}\Upsilon - RM_\xi - C_\xi \\ R^{-1}\Upsilon - RM_\xi - C_\xi & g_e I_6 \end{bmatrix} \tag{34}$$

where $I_6 \in \mathbb{R}^{6\times 6}$ represents an identity matrix. If conditions (18), (19), (20) are fulfilled, $\Omega \geq 0$, *i.e.*, all the eigenvalues of Ω would be nonnegative. Therefore, ${}^{\mathrm{i}}\Delta V \leq 0$, where ${}^{\mathrm{i}}\Delta V = 0$ would only hold for ${}^{\mathrm{i}}\Delta e = {}^{\mathrm{i}}\Delta \dot{e} = 0$. As discussed in [Kuc *et al.*, 1991], where a performance index similar to (21) was used, this would imply that $\lim_{\mathrm{i}\to\infty} {}^{\mathrm{i}}e = 0$ for all $t \in [0, t_{\mathrm{F}}]$. □

4. Experiments

The IRLC strategy proposed in Sec. 3 was evaluated for several robot tasks.

4.1 Application Scenario

Kinesthetic teaching [Wrede *et al.*, 2013] allows a human operator to manually guide a robot manipulator to define or to correct a robot trajectory, which corresponds to a certain robot task (see Fig. 2). However, a robot controlled with an impedance controller, such as the Cartesian impedance controller in (8), that uses these operator-defined Cartesian poses as references might not be able to complete its task because of the trajectory-tracking deviation introduced by these controllers (to the advantage of allowing physical interaction between the robot and its surroundings).

Therefore, the goal of the experiments presented in this section is to evaluate if the iterative learning strategy proposed in Sec. 3 would allow a robot to complete its desired task by updating a manually-defined Cartesian reference used in a Cartesian impedance-controlled robot.

The experiments presented in this section were performed using a Franka Emika Panda [*Panda – Data Sheet* 2019] robot mounted on a table, as shown in Fig. 2. Since robot joint redundancy is out of the scope of this paper, the seventh joint of the robot was locked at $\theta_7 = \pi/2$ rad, and only the first six joints of the robot were controlled. The robot was controlled at a sampling rate equal to 1 kHz.

4.2 Peg-in-Hole Task

In a peg-in-hole robot task, a robot manipulator should insert a peg (in this experiment, with cylindrical shape) attached to its end-effector in a hole whose dimensions are slightly larger than the ones of the peg.

For this experiment, the Cartesian impedance values selected were:

- The virtual stiffness K was chosen as 150 [N/m] for the translational degrees of freedom and as 15 [N/rad] for the rotational degrees of freedom.
- The virtual damping D was chosen as 50 [Ns/m] for the translational degrees of freedom and as 10 [Ns/rad] for the rotational degrees of freedom.

Figure 2. A human operator manually guiding a Franka Emika Panda [*Panda – Data Sheet* 2019] robot mounted on a table to define the desired robot Cartesian poses, ξ_R in (11), for a peg-in-hole task.

Moreover, for the learning update law (presented in Sec. 3.2), the Cartesian impedance parameters selected (K and D), together with the iterative convergence conditions (18)–(20) of Theorem 3.1, allowed to choose $\beta = 0.5$, and $R = 2.5$ for the translational degrees of freedom and $R = 0.92$ for the rotational degrees of freedom.

The results for this experiment are shown in Figs. 3, 4, and 5. Figure 3 shows the temporal evolution of the end-effector position of the robot. It can be seen in Fig. 3 that before using the iterative learning strategy proposed (labeled *No IRLC*), the Cartesian impedance controller deviated from the desired trajectory (labeled ξ_R), which prevented the robot to complete its task, *i.e.*, to insert the peg in the hole. This is also shown in the left image of Fig. 4, which displays the position of the peg once the robot trajectory is executed for two different scenarios: before learning (left) and after learning (right). Finally, Fig. 3 shows that the deviation with respect to the desired trajectory decreased at every learning iteration, with the robot being able to complete its task after only two learning iterations. Consistent with the tracking-error reduction at each learning iteration, the performance index ${}^{\mathrm{i}}V$ of Eq. (21) decreased at each iteration, *i.e.*, the performance index variation, ${}^{\mathrm{i}}\Delta V$ of Eq. (24), is negative for all learning iterations, as shown in Fig. 5, which matches

the convergence analysis of this method presented in Theorem 3.1.

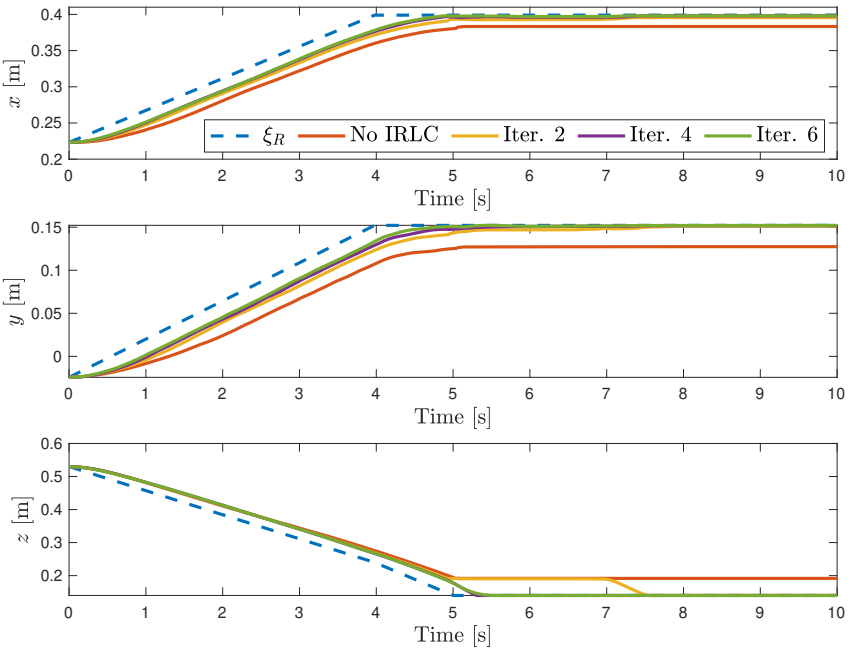

Figure 3. Temporal evolution of the position of the robot end-effector along each Cartesian direction x, y, z with respect to its desired values for a peg-in-hole task.

Comparison with an Alternative ILC Method The benefits of the iterative reference learning proposal presented in Sec. 3 is highlighted by comparing its performance to one of the methods that have been used extensively in literature, namely ILC [Arimoto *et al.*, 1984; Norrlöf, 2000]. An ILC strategy could be defined using an input update law

$$^{i+1}U(z) = Q(z)(^{i}U(z) + L(z)\,^{i}E(z)) \tag{35}$$

with $^{i}E(z) = Y_R(z) - {}^{i}Y(z)$ being the output error signal, $L(z)$ representing a learning filter, $Q(z)$ being a low-pass filter used to improve the robustness of the ILC method, and z representing the discrete-time operator. Then, the Cartesian impedance behavior (9) of the robot was used to obtain m transfer functions where each output, $y_m \in \mathbb{R}$, of the system would be equal to the corresponding component of ξ and each input, $u_m \in \mathbb{R}$, of the system would be equal to the corresponding component of ξ_R, by considering the behavior of the robot during the initial execution of the

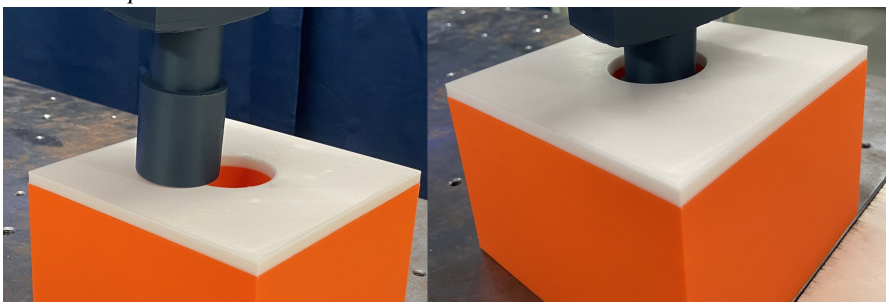

Figure 4. Comparison between the final position of the peg before the proposed iterative learning strategy was used (left) and after six iterations of the proposed learning controller (right) for a peg-in-hole task.

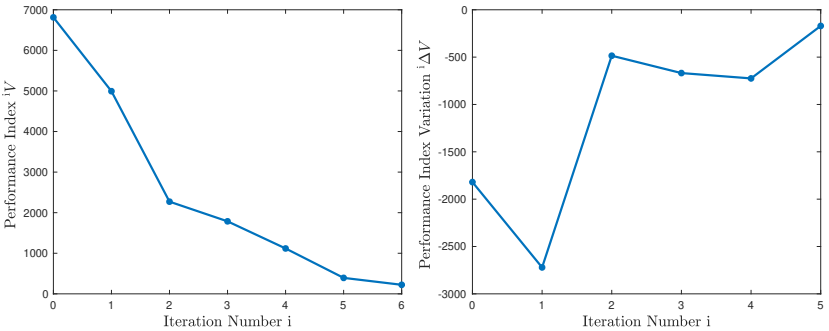

Figure 5. Performance index (left), ${}^{i}V$ of Eq. (21), and performance index variation (right), ${}^{i}\Delta V$ of Eq. (24), for each learning iteration i for a peg-in-hole task.

peg-insertion task to formulate each of these transfer functions. The transfer functions obtained, in the Laplace domain, are

$$G_c(s) = \frac{\omega_n^2}{s^2 + 2\delta\omega_n s + \omega_n^2} \tag{36}$$

with $\omega_n = 3.78$ rad/s and $\delta = 0.64$ for the position DOFs, and $\omega_n = 2.58$ rad/s and $\delta = 1.44$ for the orientation DOFs, which are then discretized using a zero-order hold (ZOH) method at the sampling period of the robot, *i.e.*, $h = 0.001$ s, to obtain each $G(z)$. The learning gain $L(z)$ in (35) was chosen as

$$L(z) = \widetilde{G}^{-1}(z)(1 - H(z)) \tag{37}$$

with $\widetilde{G}^{-1}(z)$ being an approximation to the inverse of $G(z)$, where the inverted zeros of $G(z)$ that have a negative real part were mirrored to the unit circle to avoid

obtaining a ringing behavior [Cano Marchal *et al.*, 2014], and $H(z)$ is a first-order high-pass filter used to determine the convergence rate [Norrlöf, 2000]. The selection of the learning gain $L(z)$ as in (37), together with choosing $Q(z)$ as a first-order low-pass filter with cut-off frequency $\omega_c = 50$ Hz for robustness, fulfills the convergence criterion for this formulation [Norrlöf, 2000]:

$$\sup_{\omega \in [-\pi,\pi]} \left|\left|1 - G(e^{i\omega h})L(e^{i\omega h})\right|\right| < Q(e^{i\omega h})^{-1} \tag{38}$$

for all DOFs.

Moreover, Figs. 6 and 7 show a comparison between the proposed IRLC solution presented in Sec. 3 and the alternative ILC method. The differences in the temporal evolution of the Euclidean norm of the position error between these two methods are observed in Fig. 6: the ILC method (right) commanded more aggressive position corrections, yet fourteen iterations were necessary for robot task completion. On the contrary, the IRLC solution proposed (left) provided a smoother convergence for all iterations that allowed a faster robot task completion (since its second iteration). Furthermore, Fig. 7 shows a comparison of the absolute input force (8) variation $||\Delta F||$ between our proposal and the alternative ILC at their final iteration, *i.e.*, the iteration where the peg insertion task was completed (without the peg impacting the box containing the hole before its insertion) for each formulation. It can be observed in Fig. 7 that the aggressive corrections performed by the alternative ILC method translated into much greater impedance force variation requirements (21.2 N on average) compared to the IRLC proposal (4.4 N on average).

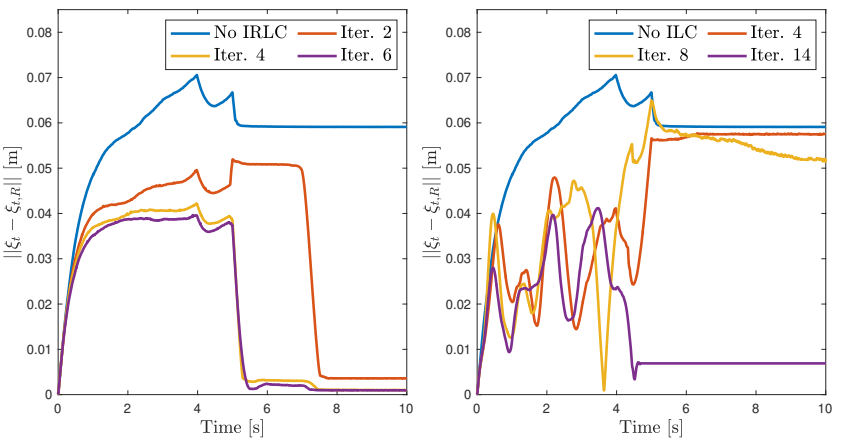

Figure 6. Temporal evolution of the Euclidean norm of the position error of the robot end-effector for a peg-in-hole task. Comparison between the proposed IRLC solution (left) and an ILC alternative (right).

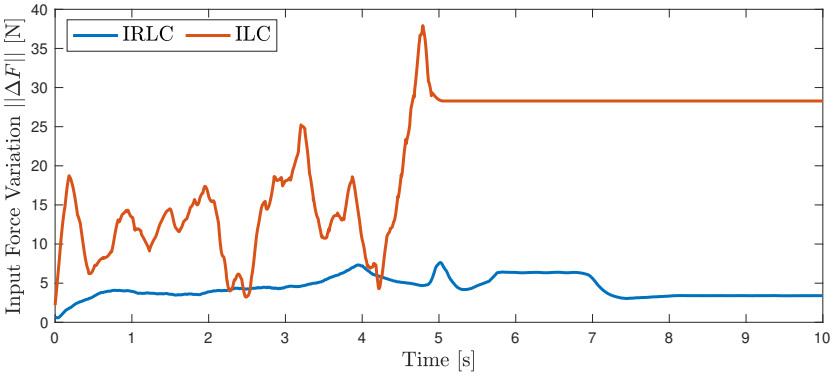

Figure 7. Comparison of the input force variation $||\Delta F||$ between the proposed IRLC solution (blue) and an ILC alternative (red).

Choosing Different Cartesian Impedance Parameters The impedance requirements of a robot task might change over time, which would imply the selection of a different set of robot impedance parameters, *i.e.*, its virtual stiffness K and damping D. As a result, the trajectory tracking behavior of the robot would be modified in this scenario, thus leading to the possibility that a, previously-successful, robot task might not be completed when the robot impedance parameter values are updated.

In this experiment, the translational Cartesian impedance parameters of the previous experiment were changed from 150 to 200 [N/m] for the virtual stiffness K, and from 50 to 70 [Ns/m] for the virtual damping D. The initial Cartesian reference for this experiment was chosen as the one used at the last iteration (*i.e.*, Iteration 6) of the previous experiment.

Figure 8 shows the temporal evolution of the position of the robot end-effector when varying the Cartesian impedance values in this peg-in-hole task, zoomed at the proximity of the inserted-peg position, see Fig. 4 (right). It is observed in Fig. 8 how the trajectory-tracking variation that occurred when selecting different robot impedance parameters caused the robot to not complete its task (labeled *Iter. 0*). However, using the iterative reference learning strategy proposed in Sec. 3, peg-in-hole task completion was achieved after only three additional iterations.

4.3 Snap-Fit Assembly of a Switch

The use of the IRLC strategy proposed in Sec. 3 to improve robot trajectory tracking was also evaluated for the snap-fit assembly of a switch, where the same values for impedance (K and D) and learning parameters (β and R) as in the previous experiments were selected. The workpieces involved in this assembly, which were components of an emergency stop button [Stolt *et al.*, 2011], can be seen in Fig. 9, *i.e.*, the switch, in a dark grey color and gripped by the robot, and a light gray piece with slots where the two lateral tabs of the switch should be inserted.

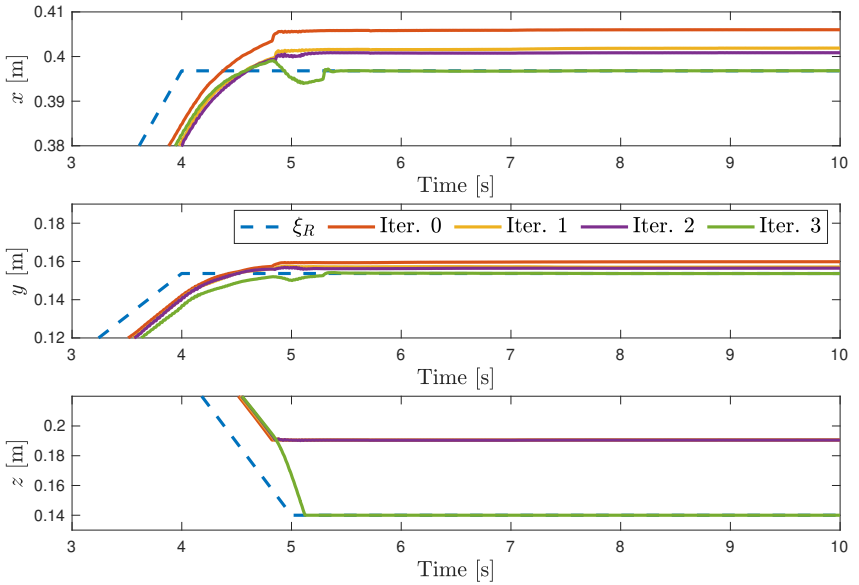

Figure 8. Temporal evolution of the position of the robot end-effector along each Cartesian direction x, y, z with respect to its desired values for a peg-in-hole task with different Cartesian impedance values (zoom at the proximity of peg insertion).

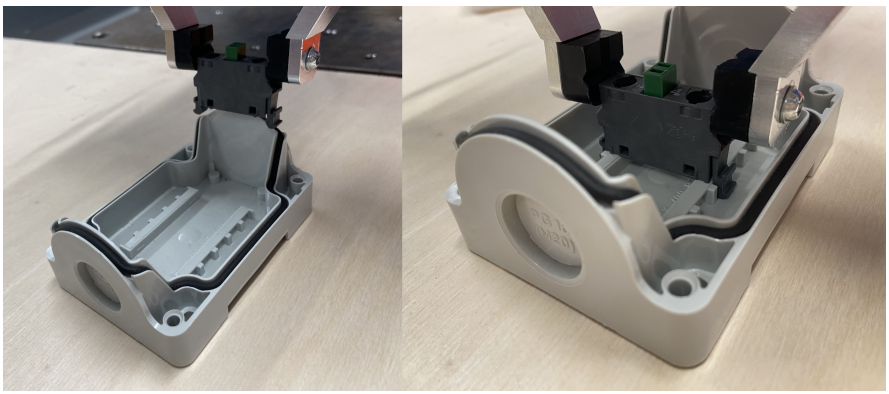

Figure 9. Comparison between the final position of the switch before iterative learning was used (left) and after eight iterations of the proposed learning controller (right) for the snap-fit assembly of a switch.

Figure 10 shows the robot end-effector position throughout the switch snap-fit assembly experiments for different iterations. It can be seen in Fig. 10 that trajectory tracking improved at each iteration, which, as in the peg-in-hole experiment, is consistent with the monotonous decrease of the performance index ${}^{\mathrm{i}}V$ of Eq. (21), and the negative performance index variation, ${}^{\mathrm{i}}\Delta V$ of Eq. (24), shown in Fig. 11 for all learning iterations. Also, the robot was able to complete its task after only eight iterations.

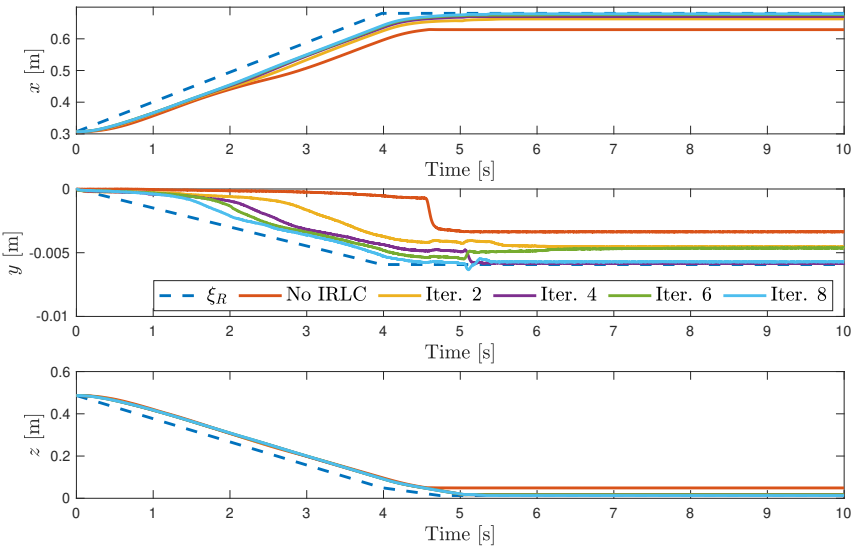

Figure 10. Temporal evolution of the position of the robot end-effector along each Cartesian direction x, y, z with respect to its desired values for the snap-fit assembly of a switch.

The trajectory-tracking requirements of this switch snap-fit assembly task were more demanding than in the previous peg-in-hole scenario in terms of the assembly tolerance and in the greater possibility of the two pieces involved in the robot task getting stuck, see, *e.g.*, Fig. 9 (left). Also, compared to the previously-presented peg-in-hole experiment, these assembly experiments would require to compensate for the external force needed to snap-fit the switch. For these reasons, slightly more iterations (eight) than in the peg-in-hole scenario were needed to obtain an updated Cartesian reference that allowed robot task completion.

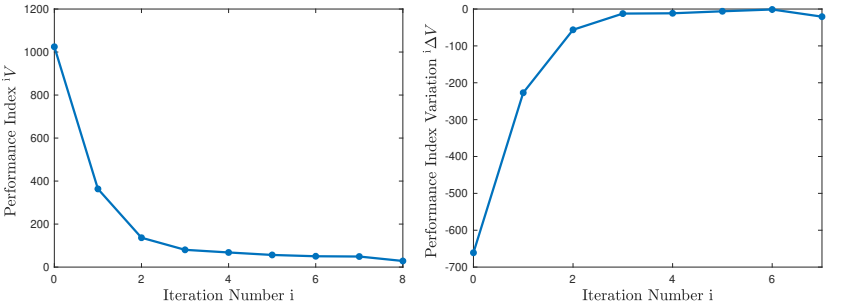

Figure 11. Performance index (left), ^{i}V of Eq. (21), and performance index variation (right), $^{i}\Delta V$ of Eq. (24), for each iterative learning iteration i for the snap-fit assembly of a switch.

5. Discussion

In this paper, we have proposed an iterative reference learning strategy that modifies the Cartesian reference of a robot impedance controller to achieve robot task completion. The proposed strategy has shown to improve the tracking of a robot Cartesian trajectory defined by human guidance in the context of kinesthetic teaching.

Moreover, the proposed strategy is compatible with a selection of robot impedance parameters (virtual stiffness K and damping D) that allowed a non-damaging interaction with the environment of the robot. This would have been a limitation of previously-proposed high-stiffness learning techniques [Kuc *et al*., 1991], where a performance index similar to the one in Eq. (21) was used. Also, contrary to adaptive learning techniques [Park *et al*., 1996; Lee *et al*., 2019], the selection of impedance parameters needed not be modified online in our proposal. These previous adaptive learning techniques [Park *et al*., 1996; Lee *et al*., 2019] formulated update laws for the force input feedforward signal similar to our proposal in Eq. (15). However, in comparison, the update law in our proposal allowed to choose difference position gain values, R in Eq. (16), for each DOF.

Furthermore, the extensive evaluation experiments performed with a real collaborative robot manipulator showed that our proposal was able to achieve task completion for several robot tasks in a few iterations, which contrasted with the high number of iterations often required in other learning techniques, such as in Reinforcement Learning [Pierallini *et al*., 2023]. Additionally, as seen in the experimental comparison performed between the proposed method and an alternative ILC method [Arimoto *et al*., 1984], the linearity assumptions in the alternative ILC method [Norrlöf, 2000; Cano Marchal *et al*., 2014] allowed convergence guarantees for aggressive compensations that turned inferior in the experimental task performed, resulting in slower robot task completion and larger impedance force vari-

ation. In comparison, our proposal considered the nonlinearities of robot dynamics in its convergence analysis, which translated into a more conservative trajectory reference update that lead to a faster (*i.e.*, in less iterations) convergence to robot task completion.

6. Conclusion

Iterative learning can improve trajectory tracking for robot applications where impedance control is used by providing a Cartesian reference update. The proposed IRLC strategy was evaluated in several experiments using a real collaborative robot. These experiments showed a smooth convergence toward robot task completion in a small number of learning iterations, also compared to an alternative ILC method, which highlighted the suitability of the proposed method for collaborative human–robot applications.

References

Argall, B. D., S. Chernova, M. Veloso, and B. Browning (2009). "A survey of robot learning from demonstration". *Robotics and Autonomous Systems* **57**:5, pp. 469–483.

Arimoto, S., S. Kawamura, and F. Miyazaki (1984). "Bettering operation of robots by learning". *Journal of Robotic systems* **1**:2, pp. 123–140.

Arimoto, S., P. Nguyen, and T. Naniwa (1999). "Learning of robot tasks via impedance matching". In: *IEEE International Conference on Robotics and Automation (ICRA)*. Vol. 4. May 10–15. Detroit, MI, USA, pp. 2786–2792.

Bristow, D. A., M. Tharayil, and A. G. Alleyne (2006). "A survey of iterative learning control". *IEEE Control Systems Magazine* **26**:3, pp. 96–114.

Cano Marchal, P., O. Sörnmo, B. Olofsson, A. Robertsson, J. Gómez Ortega, and R. Johansson (2014). "Iterative learning control for machining with industrial robots". *IFAC Proceedings Volumes* **47**:3, pp. 9327–9333.

Cencen, A., J. C. Verlinden, and J. Geraedts (2018). "Design methodology to improve human-robot coproduction in small-and-medium-sized enterprises". *IEEE/ASME Transactions on Mechatronics* **23**:3, pp. 1092–1102.

Cheah, C.-C. and D. Wang (1998). "Learning impedance control for robotic manipulators". *IEEE Transactions on Robotics and Automation (T-RO)* **14**:3, pp. 452–465.

Dahl, O. (1992). *Path Constrained Robot Control*. Thesis No. TFRT-1038. Doctoral Thesis. Department of Automatic Control, Faculty of Engineering LTH, Lund University, Lund, Sweden.

Dahlin, A. and Y. Karayiannidis (2021). "Temporal coupling of dynamical movement primitives for constrained velocities and accelerations". *IEEE Robotics and Automation Letters* **6**:2, pp. 2233–2239.

Della Santina, C., M. Bianchi, G. Grioli, F. Angelini, M. Catalano, M. Garabini, and A. Bicchi (2017). "Controlling soft robots: balancing feedback and feedforward elements". *IEEE Robotics and Automation Magazine* **24**:3, pp. 75–83.

Hogan, N. (1985). "Impedance control: An approach to manipulation: Parts I–III". *Journal of Dynamic Systems, Measurement, and Control* **107**:1, pp. 1–24.

Ibarz, J., J. Tan, C. Finn, M. Kalakrishnan, P. Pastor, and S. Levine (2021). "How to train your robot with deep reinforcement learning: Lessons we have learned". *The International Journal of Robotics Research* **40**:4-5, pp. 698–721.

Kawamura, S., F. Miyazaki, and S. Arimoto (1988). "Is a local linear PD feedback control law effective for trajectory tracking of robot motion?" In: *IEEE International Conference on Robotics and Automation (ICRA)*. Apr. 24–29. Philadelphia, PA, USA, pp. 1335–1340.

Khatib, O. (1987). "A unified approach for motion and force control of robot manipulators: The operational space formulation". *IEEE Journal on Robotics and Automation* **3**:1, pp. 43–53.

Kuc, T.-Y., K. Nam, and J. S. Lee (1991). "An iterative learning control of robot manipulators". *IEEE Transactions on Robotics and Automation (T-RO)* **7**:6, p. 835.

Lee, R., L. Sun, Z. Wang, and M. Tomizuka (2019). "Adaptive iterative learning control of robot manipulators for friction compensation". *IFAC-PapersOnLine* **52**:15, pp. 175–180.

Norrlöf, M. (2000). *Iterative Learning Control : Analysis, Design, and Experiments*. PhD thesis 653. Div. Automatic Control, Linköping University, Linköping, Sweden. ISBN: 91-7219-837-0.

Ott, C. (2008). *Cartesian impedance control of redundant and flexible-joint robots*. Springer, Berlin, Germany.

Panda – Data Sheet (2019). Franka Emika.

Park, B., T.-Y. Kuc, and J. S. Lee (1996). "Adaptive learning control of uncertain robotic systems". *International Journal of Control* **65**:5, pp. 725–744.

Pierallini, M., F. Angelini, R. Mengacci, A. Palleschi, A. Bicchi, and M. Garabini (2023). "Iterative learning control for compliant underactuated arms". *IEEE Transactions on Systems, Man, and Cybernetics: Systems (T-SMCA)* **53**:6, pp. 3810–3822.

Salt Ducaju, J. M., B. Olofsson, A. Robertsson, and R. Johansson (2022). "Robot Cartesian compliance variation for safe kinesthetic teaching using safety control barrier functions". In: *IEEE International Conference on Automation Science and Engineering (CASE)*. Aug. 20–24. Mexico City, pp. 2259–2266.

Schou, C., J. Damgaard, S. Bøgh, and O. Madsen (2013). "Human-robot interface for instructing industrial tasks using kinesthetic teaching". In: *44th IEEE International Symposium on Robotics (ISR)*. Oct. 19–27. Seoul, Korea, pp. 1–6.

Siciliano, B. and O. Khatib (2016). *Springer Handbook of Robotics*. Springer, Berlin, Germany.

Stolt, A., M. Linderoth, A. Robertsson, and R. Johansson (2011). "Force controlled assembly of emergency stop button". In: *IEEE International Conference on Robotics and Automation (ICRA)*. May 9–13. Shanghai, China, pp. 3751–3756.

Villani, L. and J. De Schutter (2016). "Force control". In: Siciliano, B. *et al*. (Eds.). *Springer Handbook of Robotics*. Springer, Berlin. Chap. 9, pp. 195–217.

Wrede, S., C. Emmerich, R. Grünberg, A. Nordmann, A. Swadzba, and J. Steil (2013). "A user study on kinesthetic teaching of redundant robots in task and configuration space". *Journal of Human-Robot Interaction* **2**:1, pp. 56–81.

Paper IV

Robot Cartesian Compliance Variation for Safe Kinesthetic Teaching using Safety Control Barrier Functions

Julian M. Salt Ducaju **Björn Olofsson**
Anders Robertsson **Rolf Johansson**

Abstract

Kinesthetic teaching allows human operators to reprogram part of a robot's trajectory by manually guiding the robot. To allow kinesthetic teaching, and also to avoid any harm to both the robot and its environment, Cartesian impedance control is here used for trajectory following. In this paper, we present an online method to modify the compliant behavior of a robot toward its environment, so that undesired parts of the robot's workspace are avoided during kinesthetic teaching. The stability of the method is guaranteed by a well-known passivity-based energy-storage formulation that has been modified to include a strict Lyapunov function, *i.e.*, its time derivative is a globally negative-definite function. Safety Control Barrier Functions (SCBFs) that consider the rigid-body dynamics of the robot are formulated as inequality constraints of a quadratic optimization (QP) problem to ensure forward invariance of the robot's states in a safe set. An experimental evaluation using a Franka Emika Panda robot is provided.

© 2022 IEEE. Reprinted, with permission, from 2022 IEEE International Conference on Automation Science and Engineering (CASE), August 20-24, Mexico City, Mexico, pp. 2259–2266.

1. Introduction

Physical Human–Robot Interaction (pHRI) has become a popular topic in the robotics community, since it addresses the recent trend in the manufacturing industry to replace mass production for mass customization [Schou *et al*., 2013]. As part of this change of paradigm, human operators have become direct collaborators in robotic tasks, and robots that are compliant toward their environment have gained relevance.

An interesting application of human collaboration in robotics is to reprogram part of the robot's trajectory [Karlsson *et al*., 2017] by manually guiding the robot, which is known as kinesthetic teaching [Schou *et al*., 2013]. However, the workspace that humans and robots share may not be entirely available, *e.g.*, if another robot arm is occupying part of the workspace, or if there is sensitive equipment in the workspace. Then, the robot's compliant behavior toward its environment should be modified so that the human operator cannot guide the robot to unsafe situations. In addition, the compliance variations must be done in such a way that the stability of the robot's controller is ensured. Passivity-based energy storage has been used previously to provide a stable variation of the impedance parameters of a robot [Ferraguti *et al*., 2013; Landi *et al*., 2018].

Moreover, Safety Control Barrier Functions (SCBFs) have gained attention in recent years [Ames *et al*., 2019; Wang *et al*., 2017; Landi *et al*., 2019; Ferraguti *et al*., 2020; Rauscher *et al*., 2016; Singletary *et al*., 2021], because they provide more formal guarantees for obstacle avoidance than the artificial potential-field methods used in the past for this purpose [Khatib, 1985]. Safety control barrier functions provide safety by enforcing forward invariance of a set, *i.e.*, SCBFs ensure that a system does not leave a safe set [Ames *et al*., 2019]. They can be formulated as inequality constraints of a quadratic optimization (QP) problem to modify the input to the system [Ames *et al*., 2019; Wang *et al*., 2017]. Additionally, SCBFs have been used to perform a minimally-invasive modification of the robot's behavior to avoid safety threats, such as obstacle collisions [Landi *et al*., 2019; Ferraguti *et al*., 2020; Rauscher *et al*., 2016; Singletary *et al*., 2021].

In this paper, we address the problem of safe kinesthetic teaching by modifying the Cartesian compliant behavior of a robot with respect to its environment in a strictly stable manner, such that we can ensure that the robot's end-effector avoids undesired parts of its workspace. Safety control barrier functions that consider the rigid-body dynamics of the robot are used as inequality constraints of a quadratic optimization problem to online modify the robot's compliance behavior in a minimally-invasive way, so that the human operator can still manipulate the robot while avoiding any safety threat.

The paper is organized as follows: Sec. 2 introduces relevant mathematical concepts that are used in our method. Then, Sec. 3 presents the method for solving the described problem. Section 4 explains the experiments performed, and Sec. 5 presents the results obtained. Finally, a discussion is included in Sec. 6 and conclu-

sions are drawn in Sec. 7.

2. Mathematical Background

In this section, we discuss two relevant mathematical concepts. First, SCBFs for safe set forward invariance. Second, passivity-based energy storage for stable variation of the robot compliant behavior with respect to its environment.

2.1 Safety Control Barrier Functions (SCBFs)

Consider a nonlinear control-affine system:

$$\dot{x} = f(x) + g(x)u \tag{1}$$

that has closed-loop system dynamics with a state-feedback controller k according to

$$\dot{x} = f_{cl}(x,t) = f(x) + g(x)k(x,t) \tag{2}$$

Moreover, define a safe set $\mathscr{C}$, with boundary $\partial\mathscr{C}$ and interior $\text{Int}(\mathscr{C})$, as [Ames *et al.*, 2019]

$$\mathscr{C} = \{x \in \mathbb{R}^n \mid h(x) \geq 0\} \tag{3}$$
$$\partial\mathscr{C} = \{x \in \mathbb{R}^n \mid h(x) = 0\} \tag{4}$$
$$\text{Int}(\mathscr{C}) = \{x \in \mathbb{R}^n \mid h(x) > 0\} \tag{5}$$

For $\mathscr{C}$ to be forward invariant [Ames *et al.*, 2019],

$$\sup_{u \in \mathscr{U}} [L_f h(x) + L_g h(x) u] \geq -\kappa(h(x)) \tag{6}$$

for all $x \in \mathscr{D}$, being h the SCBF, $h : \mathscr{D} \to \mathbb{R}$ with $\mathscr{C} \subseteq \mathscr{D} \subset \mathbb{R}^n$, κ an extended class-$\mathscr{K}_\infty$ function (strictly monotonically increasing), $L_f h(x) = (\partial h/\partial x) f(x)$, and $L_g h(x) = (\partial h/\partial x) g(x)$. Also, the authors in [Wang *et al.*, 2017] highlight the possibility of choosing $\kappa(h) = \gamma h^Z$ ($\gamma > 0$) for any positive odd integer Z.

Furthermore, a quadratic optimization (QP) problem can be formulated to minimize the difference between the input to the system, u, and the nominal state-feedback controller in (2), k^d, while using SCBFs to formulate an inequality constraint that allows obstacle avoidance [Ames *et al.*, 2019]:

$$\begin{aligned} k(x,t) = &\arg\min_{u \in \mathbb{R}^m} \frac{1}{2} \left|\left| u - k^d(x,t) \right|\right|_2^2 \\ &\text{s.t. } \dot{h}(x,t,u) \geq -\kappa(h(x,t)) \end{aligned} \tag{7}$$

2.2 Passivity-Based Energy Storage

Energy storage has previously been used to handle stiffness variations in robots [Ferraguti *et al.*, 2013; Landi *et al.*, 2018]. This formulation is based on the idea of keeping the energy introduced to the system lower that the energy dissipated by the system. The energy dissipated by the system's damping is stored in an energy reservoir with state $z(t) \in \mathbb{R}$ and dynamics

$$\dot{z} = \frac{\varphi}{z} P_D - \frac{\sigma}{z} P_K \tag{8}$$

where P_D and P_K represent the dissipated power due to damping and the power caused by the stiffness variation, respectively. Also, the parameter $\varphi \in \{0,1\}$ controls the storage of dissipated energy and disables the storage if the energy stored is higher than an upper bound $\bar{T}$, and the parameter $\sigma \in \{\varphi,1\}$ controls the injection or extraction of energy from the storage. The energy stored is

$$T(z) = \frac{1}{2} z^2 \tag{9}$$

and its time derivative is

$$\dot{T}(z) = z\dot{z} = \varphi P_D - \sigma P_K \tag{10}$$

A lower bound δ is used for the minimum amount of energy stored. In addition, to avoid singularities, $z(t=0) > 0$ with $T(z(0)) \geq \delta$. Then, the authors in [Ferraguti *et al.*, 2013; Landi *et al.*, 2018] showed that the system is passive with respect to the pair $(F^{\text{ext}}, \dot{\xi})$ if $T(t) \geq \delta$, where $F^{\text{ext}} \in \mathbb{R}^6$ is the external force and $\xi \in SE(3)$ is the end-effector pose of the robot.

3. Method

We aim to formulate a state-feedback controller (2) that allows safe kinesthetic teaching. Here, the nominal state-feedback controller, k^d, represents the robot's desired Cartesian compliant behavior. Then, the robot's compliant behavior is modified by a quadratic optimization problem (7) to ensure that the robot's states stay in a safe set.

3.1 Robot System

The rigid-body dynamics of the robot can be written in the joint space of the robot, $q \in \mathbb{R}^n$, as [Siciliano and Khatib, 2016]

$$M(q)\ddot{q} + C(q,\dot{q})\dot{q} + G(q) = \tau + \tau^{\text{ext}} \tag{11}$$

where $M(q) \in \mathbb{R}^{n\times n}$ is the generalized inertia matrix, $C(q,\dot{q}) \in \mathbb{R}^{n\times n}$ describes the Coriolis and centripetal forces effects, $G(q) \in \mathbb{R}^n$ captures the gravity-induced

torques, and $\tau \in \mathbb{R}^n$ represents the input torques, n being the number of joints of the robot. Finally, $\tau^{\text{ext}} \in \mathbb{R}^n$ represents the external torques.

The rigid-body equation of the robot can be written in terms of its end-effector pose, ξ, which is composed by the end-effector's position and orientation:

$$M_\xi(q)\ddot{\xi} + C_\xi(q,\dot{q})\dot{\xi} + G_\xi(q) = F + F^{\text{ext}} \tag{12}$$

where $F \in \mathbb{R}^6$ is the input force, and, for a fully-actuated robot ($n = 6$), $M_\xi \in \mathbb{R}^{6\times6}$, $C_\xi \in \mathbb{R}^{6\times6}$, and $G_\xi \in \mathbb{R}^6$ are equal to

$$M_\xi = J^{-\mathrm{T}}(q)M(q)J^{-1}(q) \tag{13}$$

$$C_\xi = J^{-\mathrm{T}}(q)(C(q,\dot{q}) - M(q)J^{-1}(q)\dot{J}(q))J^{-1}(q) \tag{14}$$

$$G_\xi = J^{-\mathrm{T}}(q)G(q) \tag{15}$$

assuming that the Jacobian relative to the base frame of the robot, $J(q) \in \mathbb{R}^{6\times6}$, has full rank [Khatib, 1987].

By applying partial feedback linearization [Khalil, 2014, Ch. 9], we can write the input, $u \in \mathbb{R}^6$, to the system as the gravity-compensated force:

$$u = F + F^{\text{ext}} - G_\xi(q) \tag{16}$$

Then, by choosing the state vector as $x = [\xi^{\mathrm{T}}, \dot{\xi}^{\mathrm{T}}]^{\mathrm{T}} \in \mathbb{R}^{12}$, the linearized system is

$$\dot{x} = A(q,\dot{q})x + B(q)u \tag{17}$$

where

$$A = \begin{bmatrix} 0_6 & I_6 \\ 0_6 & -M_\xi^{-1}(q)C_\xi(q,\dot{q}) \end{bmatrix},\ B = \begin{bmatrix} 0_6 \\ M_\xi^{-1}(q) \end{bmatrix} \tag{18}$$

LEMMA 3.1
$M_\xi(q)$ is invertible since $J(q)$ is also invertible. □

Proof. We know that $M(q)$ is invertible because $M(q)$ is a symmetric positive-definite matrix ($M(q) \in S^n_{++}$) [Siciliano and Khatib, 2016]. Then, it can be obtained from (13) that

$$M_\xi^{-1}(q) = (J^{-\mathrm{T}}(q)M(q)J^{-1}(q))^{-1} = J(q)M^{-1}(q)J^{\mathrm{T}}(q) \tag{19}$$

which holds since we have assumed that $J(q)$ has full rank to formulate the rigid-body equation (12). □

3.2 Cost Function

The nominal state-feedback controller (2), $k^d \in \mathbb{R}^6$, should achieve the robot's desired Cartesian compliant behavior. A Cartesian impedance controller [Hogan, 1985] is used to establish a mass-spring-damper relationship between the Cartesian pose variation from its reference, $\Delta\xi = \xi_d - \xi$, ξ_d being the Cartesian reference, and the external Cartesian force, F^{ext}:

$$F^{\text{ext}} = M_\xi(q)\ddot{\xi} + (D + C_\xi(q,\dot{q}))\dot{\xi} - K\Delta\xi \tag{20}$$

where D and K are the virtual damping and stiffness matrices, respectively. The virtual inertia is chosen equal to the robot inertia, $M_\xi(q)$, to avoid inertia shaping [Ott, 2008, Ch. 3.2], so that the input force F does not require feedback from the external forces and is equal to

$$F = K\Delta\xi - D\dot{\xi} + G_\xi(q) \tag{21}$$

Therefore, the gravity-compensated nominal state-feedback controller is

$$k^d = K\Delta\xi - D\dot{\xi} + F^{\text{ext}} \tag{22}$$

and we can formulate a new cost function analogous to the cost function in (7),

$$L(\xi,\dot{\xi},u,F^{\text{ext}}) = \frac{1}{2}\left|\left|u - K\Delta\xi + D\dot{\xi} - F^{\text{ext}}\right|\right|_2^2 \tag{23}$$

Then, the cost function (23) can be expressed in terms of the states and inputs of the system, assuming that $\dot{\xi}_d = 0$, $(x - x_d) = \left[-\Delta\xi^{\mathrm{T}}, \quad \dot{\xi}^{\mathrm{T}}\right]^{\mathrm{T}}$:

$$L(x,u,F^{\text{ext}}) = \frac{1}{2}\left|\left|u + \begin{bmatrix}K, & D\end{bmatrix}(x - x_d) - F^{\text{ext}}\right|\right|_2^2 \tag{24}$$

3.3 Inequality Constraint

A safety function can be formulated to ensure that the safety distance is always greater or equal than the current distance to the obstacles subtracted by the distance needed to brake the system into a full stop with constant and instantaneous acceleration [Wang *et al.*, 2017; Ferraguti *et al.*, 2020]. For our problem, each of these three elements can be formulated as:

- The safety distance D_s is a constant parameter that can be formulated as

$$D_s = r_{rb} + r_o \tag{25}$$

  where r_{rb} and r_o are the radii of two protective spheres around the robot end-effector and an obstacle that represents the undesired part of the workspace, respectively.

- The current distance $||\Delta\rho||$ is defined using the difference between the robot end-effector position and the obstacle's position,

$$\Delta\rho = \rho - \rho_o \tag{26}$$

where $\rho = \begin{bmatrix}\xi_x, & \xi_y, & \xi_z\end{bmatrix}^{\mathrm{T}}$ is the robot's position vector and $\rho_o = \begin{bmatrix}\xi_{o,x}, & \xi_{o,y}, & \xi_{o,z}\end{bmatrix}^{\mathrm{T}}$ is the position of the obstacle. The parameters in ρ_o are constant parameters, since we are considering a static (or semi-static) obstacle.

- The distance needed to brake the robot to full stop is slightly more elaborated. For a constant acceleration, $a_{\mathrm{br}} > 0$, the total distance between a final position ρ_{F} and an initial position ρ_0 after an elapsed time t of an object that starts at ρ_0 with relative velocity $v_{\mathrm{rel}} < 0$ is

$$||\rho_{\mathrm{F}} - \rho_0|| = -v_{\mathrm{rel}}t - \frac{1}{2}a_{\mathrm{br}}t^2 \tag{27}$$

and since the time to brake to full stop is $t = -v_{\mathrm{rel}}/a_{\mathrm{br}}$, the braking distance is equal to

$$||\rho_{\mathrm{F}} - \rho_0|| = \frac{v_{\mathrm{rel}}^2}{2a_{\mathrm{br}}} \tag{28}$$

v_{rel} being the velocity prior to braking in the direction of the obstacle,

$$v_{\mathrm{rel}} = \frac{\Delta\rho^{\mathrm{T}}}{||\Delta\rho||}v \tag{29}$$

where $v = \begin{bmatrix}\dot{\xi}_x, & \dot{\xi}_y, & \dot{\xi}_z\end{bmatrix}^{\mathrm{T}}$. Also, a_{br} is a parameter defined by the user that other authors commonly define as the maximum braking ability of the robot [Wang *et al.*, 2017; Ferraguti *et al.*, 2020]. However, one could decide to choose a smaller value to have even larger margins.

Finally, the safety function is formulated as

$$D_s \geq ||\Delta\rho|| - \frac{v_{\mathrm{rel}}^2}{2a_{\mathrm{br}}} \tag{30}$$

so the SCBF candidate $h : \mathbb{R}^n \to \mathbb{R}$ is

$$h(x) = \sqrt{2a_{\mathrm{br}}(||\Delta\rho|| - D_s)} + \frac{\Delta\rho^{\mathrm{T}}}{||\Delta\rho||}v \tag{31}$$

In addition, we know that

$$\frac{d(||\Delta\rho||)}{dt} = v_{\mathrm{rel}} = \frac{\Delta\rho^{\mathrm{T}}}{||\Delta\rho||}v \tag{32}$$

and from the system's model (17), (18),

$$\frac{d(\Delta\rho)}{dt} = v \tag{33}$$

$$\frac{dv}{dt} = -\Phi v + \Gamma \begin{bmatrix} I_3, & 0_3 \end{bmatrix} u \tag{34}$$

where

$$\Phi = \left(M_\xi^{-1}(q) C_\xi(q,\dot{q}) \right)_{[1:3,1:3]} \in \mathbb{R}^{3\times 3} \tag{35}$$

$$\Gamma = \left(M_\xi^{-1}(q) \right)_{[1:3,1:3]} \in \mathbb{R}^{3\times 3} \tag{36}$$

are submatrices composed by the first three rows and columns of their original matrices (Matlab notation). Then, considering that

$$\frac{d\left(\sqrt{2a_{\text{br}}(||\Delta\rho|| - D_s)}\right)}{dt} = \frac{a_{\text{br}}}{\sqrt{2a_{\text{br}}(||\Delta\rho|| - D_s)}} \frac{d(||\Delta\rho||)}{dt} \tag{37}$$

and

$$\frac{d\left(\frac{\Delta\rho^{\text{T}}}{||\Delta\rho||} v\right)}{dt} = \frac{d\left(\frac{\Delta\rho^{\text{T}}}{||\Delta\rho||}\right)}{dt} v + \frac{\Delta\rho^{\text{T}}}{||\Delta\rho||} \frac{dv}{dt} \tag{38}$$

with

$$\frac{d\left(\frac{\Delta\rho^{\text{T}}}{||\Delta\rho||}\right)}{dt} v = \left(\frac{v^{\text{T}}}{||\Delta\rho||} - \frac{\Delta\rho^{\text{T}} v \Delta\rho^{\text{T}}}{||\Delta\rho||^3} \right) v \tag{39}$$

the time derivative of $h(x)$ in (31) is equal to

$$\begin{aligned} \frac{dh(x)}{dt} = & \frac{a_{\text{br}} \Delta\rho^{\text{T}} v}{||\Delta\rho|| \sqrt{2a_{\text{br}}(||\Delta\rho|| - D_s)}} + \frac{\Delta\rho^{\text{T}} \Gamma \begin{bmatrix} I_3, & 0_3 \end{bmatrix} u}{||\Delta\rho||} \\ & - \frac{\Delta\rho^{\text{T}} \Phi v}{||\Delta\rho||} + \frac{||v||^2}{||\Delta\rho||} - \frac{(\Delta\rho^{\text{T}} v)^2}{||\Delta\rho||^3} \end{aligned} \tag{40}$$

Therefore, to fulfill the condition (6) that ensures that the safe set is forward invariant, we must satisfy the inequality constraint

$$\begin{aligned} & \frac{a_{\text{br}} \Delta\rho^{\text{T}} v}{||\Delta\rho|| \sqrt{2a_{\text{br}}(||\Delta\rho|| - D_s)}} + \frac{\Delta\rho^{\text{T}} \Gamma \begin{bmatrix} I_3, & 0_3 \end{bmatrix} u}{||\Delta\rho||} \\ & - \frac{\Delta\rho^{\text{T}} \Phi v}{||\Delta\rho||} + \frac{||v||^2}{||\Delta\rho||} - \frac{(\Delta\rho^{\text{T}} v)^2}{||\Delta\rho||^3} + \gamma h^Z \geq 0 \end{aligned} \tag{41}$$

which can be rewritten as

$$A_{\text{CBF}} u \leq b_{\text{CBF}} \tag{42}$$

where

$$A_{\text{CBF}} = -\Delta\rho^{\text{T}}\Gamma\begin{bmatrix} I_3, & 0_3 \end{bmatrix} \tag{43}$$

$$b_{\text{CBF}} = \frac{a_{\text{br}}\Delta\rho^{\text{T}}v}{\sqrt{2a_{\text{br}}(||\Delta\rho|| - D_s)}} + ||v||^2 - \frac{(\Delta\rho^{\text{T}}v)^2}{||\Delta\rho||^2} + ||\Delta\rho||\gamma h^Z - \Delta\rho^{\text{T}}\Phi v \tag{44}$$

3.4 Discrete-Time QP Problem Implementation

The discrete-time implementation of the nominal state-feedback controller in (22) allows to obtain the input at time-step i by using the robot state (x_i) and the estimated external force ($\hat{F}_i^{\text{ext}}$) at the same time-step. Therefore, the only free variable of the cost function in (24) is u_i,

$$L(u_i) = \frac{1}{2}\left|\left|u_i + \begin{bmatrix} K, & D \end{bmatrix}(x_i - x_{d,i}) - \hat{F}_i^{\text{ext}}\right|\right|_2^2 \tag{45}$$

The cost function in (45) can be reduced (by eliminating its constant terms) to a standard Quadratic Program (QP) problem:

$$L_r(u_i) = \frac{1}{2}u_i^{\text{T}}Qu_i + c^{\text{T}}u_i \tag{46}$$

where $Q = I_6$ and $c^{\text{T}} = \begin{bmatrix} K, & D \end{bmatrix}(x_i - x_{d,i}) - \hat{F}_i^{\text{ext}}$. It is trivial to see that the quadratic term of the cost function in (46) is positive definite, $Q \in S_{++}^n$.

Moreover, similar to the cost function (46), A_{CBF} and b_{CBF} of the SCBF-based inequality constraint (42) only depend on x_i and therefore they can be treated as constants at each time-step for this problem. Therefore, analogous to (7), the QP problem to online modify the robot's compliant behavior at each time-step i is

$$\begin{aligned} k_i = &\arg\min_{u_i \in \mathbb{R}^6} L_r(u_i) \\ &\text{s.t. } A_{\text{CBF}}u_i \leq b_{\text{CBF}} \end{aligned} \tag{47}$$

3.5 Varying the Compliant Behavior of the System

If the inequality constraint (42) of the QP problem is active, the cost function (46) will not be equal to zero ($L_r(u) > 0$). In this case, since $u \neq k^d - G_\xi(q)$, the relationship between the Cartesian pose variation from its reference and the external Cartesian force (20) is modified,

$$F^{\text{ext}} = M_\xi(q)\ddot{\xi} + (D + C_\xi(q,\dot{q}))\dot{\xi} - K\Delta\xi - \Delta u \tag{48}$$

Then, the additional force Δu can used to vary the stiffness and damping parameters,

$$K'(t) = K + \Delta K(t) \tag{49}$$

$$D'(t) = D + \Delta D(t) \tag{50}$$

where $K', D' \in S^n_{++}$, and

$$\Delta u = \Delta K \Delta\xi - \Delta D \dot{\xi} \tag{51}$$

To vary the Cartesian compliance parameters in a stable manner, we first show that, using an approach based on [Santibáñez and Kelly, 1997], the nominal state-feedback controller (22) is stable.

LEMMA 3.2
The time-varying Lyapunov function

$$V(x,t) = \frac{1}{2}\dot{\xi}^{\mathrm{T}} M_\xi(q)\dot{\xi} + \frac{1}{2}\Delta\xi^{\mathrm{T}} K \Delta\xi - \alpha \Delta\xi^{\mathrm{T}} M_\xi(q)\dot{\xi} \tag{52}$$

where $x = \begin{bmatrix}\Delta\xi^{\mathrm{T}}, & \dot{\xi}^{\mathrm{T}}\end{bmatrix}^{\mathrm{T}}$, shows the global asymptotic stability of the nominal state-feedback controller k^d in (22) for $\alpha > 0$ satisfying

$$\min\left(\sqrt{\frac{\lambda_{m,K}}{\lambda_{M,M_\xi}}},\ \frac{2\lambda_{m,K}}{\lambda_{M,D}},\ \frac{\lambda_{m,D}}{2(\lambda_{M,M_\xi} + k_C||\Delta\xi||)}\right) > \alpha \tag{53}$$

where $\lambda_{m,\Pi}$ and $\lambda_{M,\Pi}$ are the smallest and largest eigenvalues of a matrix Π, respectively, and k_C is a positive constant such that for all $x, y, z \in \mathbb{R}^n$ [Santibáñez and Kelly, 1997]

$$||C_\xi(x,y)z|| \leq k_C||y||||z|| \tag{54}$$

□

Proof. See Appendix A. □

Then, since $M_\xi(q), K, D \in S^n_{++}$, a passive map from the external force F^{ext} to the velocity $\dot{\xi}$ is guaranteed,

$$\dot{V} < \dot{\xi}^{\mathrm{T}} F^{\mathrm{ext}} - \frac{1}{2}\left[\dot{\xi} - \alpha\Delta\xi\right]^{\mathrm{T}} D \left[\dot{\xi} - \alpha\Delta\xi\right] < \dot{\xi}^{\mathrm{T}} F^{\mathrm{ext}} \tag{55}$$

where the passivity condition valid for passive environments is

$$V(t) - V(0) < \int_0^t \dot{\xi}^{\mathrm{T}}(\tau) F^{\mathrm{ext}}(\tau) d\tau \tag{56}$$

However, the additional force Δu (51) produces extra energy, which can break the passivity of the system if the additional energy that is injected into the system causes a positive variation of the stiffness, $\dot{K}'(t) > 0$. Defining H as a Lyapunov function that is equivalent to considering (52) with time-varying $K'(t)$ and $D'(t)$, its time derivative is

$$\dot{H} < \dot{\xi}^{\mathrm{T}} F^{\mathrm{ext}} - P_D + P_K \tag{57}$$

where

$$P_D = \frac{1}{2}\left[\dot{\xi} - \alpha\Delta\xi\right]^{\mathrm{T}} D' \left[\dot{\xi} - \alpha\Delta\xi\right] \tag{58}$$

$$P_K = \frac{1}{2}\Delta\xi^{\mathrm{T}}\dot{K}'\Delta\xi \tag{59}$$

Then, a storage function for the system can be defined as

$$W = H + T \tag{60}$$

where T is the energy stored in a reservoir (9), as in [Ferraguti *et al.*, 2013; Landi *et al.*, 2018]. The time derivative of W is equal to

$$\dot{W} = \dot{H} + \dot{T} < \dot{\xi}^{\mathrm{T}} F^{\mathrm{ext}} - (1-\varphi)P_D + (1-\sigma)P_K \tag{61}$$

Choosing, as in [Landi *et al.*, 2018], that $\sigma = 1$ when $\dot{K}'(t) > 0$,

$$\dot{W} < \dot{\xi}^{\mathrm{T}} F^{\mathrm{ext}} \tag{62}$$

Therefore, analogous to (56), the passivity condition valid for passive environments is

$$W(t) - W(0) < \int_0^t \dot{\xi}^{\mathrm{T}}(\tau) F^{\mathrm{ext}}(\tau) d\tau \tag{63}$$

Moreover, enough stored energy in the reservoir is needed to ensure passivity. We can use the following metric for an arbitrary time interval $\left[t_s, \quad t_f\right]$ to ensure that the storage does not get empty [Ferraguti *et al.*, 2013; Landi *et al.*, 2018],

$$T(t_f) = T(t_s) + \int_{t_s}^{t_f} P_D d\tau - \int_{t_s}^{t_f} P_K d\tau \geq \delta \tag{64}$$

which gives

$$T(t_s) - \delta \geq -\int_{t_s}^{t_f} P_D d\tau + \int_{t_s}^{t_f} P_K d\tau \tag{65}$$

The energy needed to increase the stiffness is equal to

$$\int_{t_s}^{t_f} P_K d\tau = \frac{1}{2}\Delta\xi^{\mathrm{T}}\Delta K\Delta\xi \tag{66}$$

whereas the energy that we can inject into the reservoir in the time interval $[t_s, t_f]$ is

$$\int_{t_s}^{t_f} P_D d\tau = \frac{\eta}{2}\left[\dot{\xi} - \alpha\Delta\xi\right]^{\mathrm{T}} D' \left[\dot{\xi} - \alpha\Delta\xi\right] \tag{67}$$

with $\eta = t_f - t_s$ being the duration of the time interval $[t_s, t_f]$. Therefore, as long as $K'(t), D'(t) \in S^n_{++}$ and (51) is satisfied, the virtual damping coefficient, $D' = D + \Delta D(t)$, can be increased with $\Delta D(t) \geq 0$ to ensure that the energy storage does not get empty, (65), if the stiffness variation is too high.

4. Experiments

In this section, we present the experiments performed to evaluate the proposed method for a kinesthetic teaching application.

4.1 Application Scenario

The application scenario that motivated the experiments regards automatic quality-assurance processes in the food-packaging industry using images recorded from a camera mounted onto the end-effector of a robot [Kakani *et al.*, 2020; Zhu *et al.*, 2021]. Since the distance needed between the camera mounted on the robot and the food item for a correct food-quality analysis is unknown, and varies for different types of food, the trajectory of the robot has to be varied. Then, for each type of food, a human operator can be used to manually guide the robot arbitrarily close to the food item for robot trajectory reprogramming, while ensuring that a collision between the end-effector and the food item does not occur, so that neither of the two is damaged.

4.2 Experimental Setup

The performed experiments consisted of a robot motion in which, during the robot's trajectory execution, a human operator manually guided the robot to bring it arbitrarily close to the object of interest, here, an egg. The experiment was performed using the Panda robot by Franka Emika [Franka Emika, 2019] mounted on a table (see Fig. 1). This robot had seven rotational joints, but since the formulation for the proposed method was focused on fully-actuated non-redundant robots, we locked the last joint ($\theta_7 = -\pi/2$ rad), and then the robot used six degrees of freedom, $n = 6$.

Moreover, the initial impedance parameters used were:

- The initial virtual stiffness K was equal to 250 $[\mathrm{N/m}]$ for the translational degrees of freedom and equaled to 10 $[\mathrm{N/rad}]$ for the rotational degrees of freedom.

- The initial virtual damping D was equal to $2\sqrt{K}$ for all degrees of freedom.

Furthermore, the choice of additional parameters used for the inequality constraint of the quadratic optimization problem (47) were: $\gamma = 1$, $Z = 3$, $D_s = 0.05$ m, and $a_{\mathrm{br}} = 10\ \mathrm{m/s^2}$ (a_{br} was chosen conservatively, since its maximum value was configuration-dependent). Note that γ must be a positive number and Z must be a positive odd integer to guarantee safety [Wang *et al.*, 2017]. Also, a new quadratic optimization problem was solved every 1 ms, since the sampling rate of the robot was 1 kHz.

Figure 1. Setup for the kinesthetic teaching task described in Sec. 4.2. A Franka Emika Panda robot is mounted on a table. The blue piece allows to attach a camera to the robot's end effector. The human operator is manually guiding the robot and displacing it away from its original trajectory and arbitrarily close to the object of interest, here, an egg.

5. Results

In this section, we evaluate the results obtained from the experiments described in Sec. 4. First, Fig. 2 shows a 3D representation of the path $\rho(t)$ traversed by the robot. It can be seen how the external force generated by the human operator displaced the robot from its unperturbed path $\rho_{\text{un}}(t)$, where no external force acted on the robot. The robot was able to avoid the undesired parts of its workspace even when the operator was manually guiding the robot, which was ensured by solving the quadratic optimization problem in (47) at each time-step.

Moreover, Fig. 3 shows the temporal evolution of the safety control barrier function h. It can be seen how the robot end-effector stayed inside the forward-invariant safe set (3), $h(x) \geq 0$, throughout the entire trajectory, thus confirming that undesired parts of the robot's workspace were avoided using the proposed method.

Furthermore, as mentioned in Sec. 3.5, the solution of the quadratic optimization problem (47) was used to online modify the impedance parameters of the Cartesian compliance controller to avoid undesired parts of the robot's workspace. Figure 4 shows the temporal variation of the external force, as well as the stable temporal variation of the virtual stiffness during the trajectory segment where the inequality constraint of the QP optimization problem (47) was active ($t = 2.658$ s

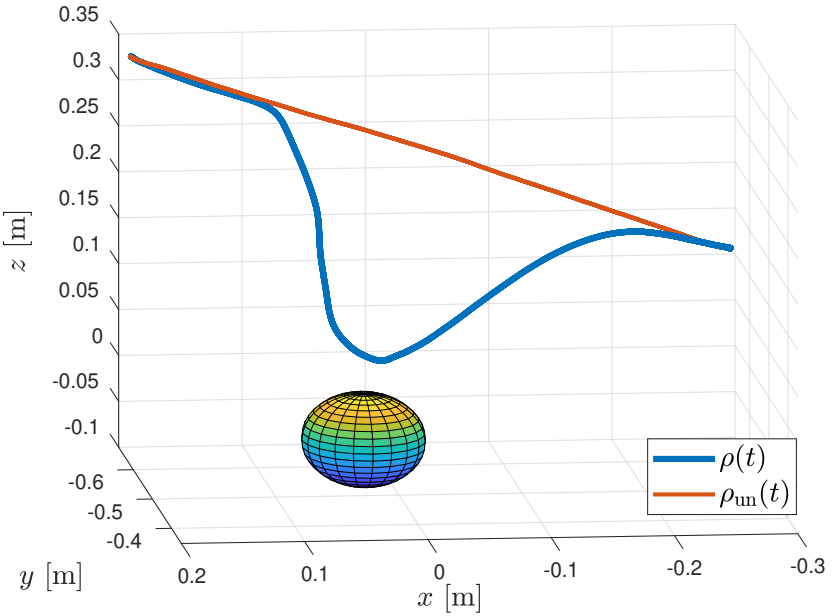

Figure 2. 3D plot of the path $\rho(t)$ traversed by the robot's end-effector. The operator displaced the robot from its unperturbed path $\rho_{\text{un}}(t)$. The plotted sphere is centered at the obstacle (egg) at ρ_o, and its radius is equal to D_s.

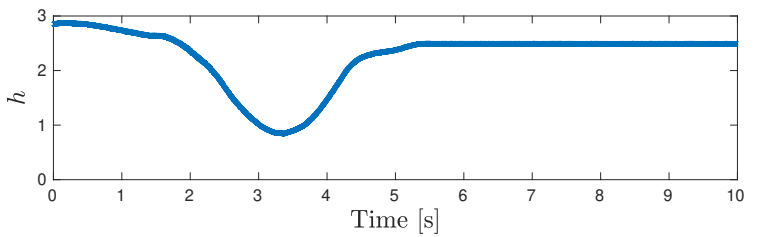

Figure 3. Temporal variation of the SCBF, $h(x)$ in (31), throughout the experiment.

to $t = 3.575$ s). Then, Fig. 5 shows the temporal variation of the joint input torques τ, which were commanded to the robot to achieve the virtual stiffness variation seen in Fig. 4. Figure 5 also shows the unmodified input torques τ_{un} that would be commanded for a constant virtual stiffness, $K' = K$ in (49). It can be seen, in both Figs. 4 and 5, how the nominal controller of the robot was only modified when needed in a minimally-invasive fashion. Therefore, when the SCBF-based inequality constraint (47) was not active, *i.e.*, before $t = 2.658$ s and after $t = 3.575$ s, the desired compliant behavior of the robot, $K' = K$ and $D' = D$, was achieved. Additionally, in this experiment, the virtual stiffness K' in (49) was modified while leaving the virtual damping constant $D' = D$ in (50).

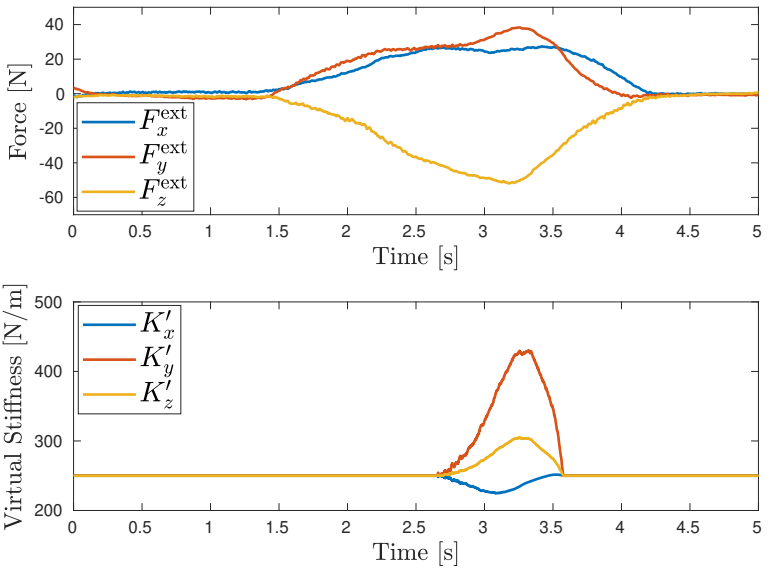

Figure 4. Temporal variation of the external force and the virtual stiffness throughout the experiment.

6. Discussion

In this paper, we have proposed a method to modify the Cartesian compliance parameters of a robot to avoid that human operators manually guide a robot to undesired parts of its workspace in the context of safe kinesthetic teaching. The proposed method modifies a nominal controller, whose goal is to achieve the desired compli-

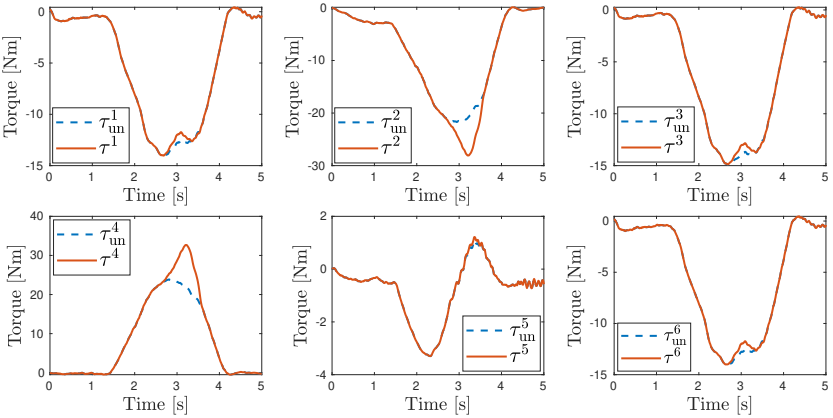

Figure 5. Temporal variation of the input torques τ^j, compared to the unmodified (*i.e.*, without SCBF-based compliance variation) input torques τ^j_{un} for each joint $j \in \{1, \ldots, 6\}$, throughout the experiment.

ant behavior of the robot, using an SCBF as an inequality constraint of a QP problem to ensure forward invariance of the safe set of robot states.

Prior to the formulation of SCBF-based methods, artificial potential fields have been used for robot obstacle avoidance [Khatib, 1985]. However, SCBFs have recently gained popularity, since they ensure formal guarantees for obstacle avoidance. Also, while potential fields do not emphasize optimality [Liu and Tomizuka, 2016], SCBFs are minimally invasive and only modify the nominal controller behavior if needed [Ames *et al.*, 2019], as illustrated in Sec. 5. In addition, the main appeal of artificial potential fields is the low computational loads needed, but fast problem-solving is also guaranteed for our method, since the proposed QP problem (47) is a convex problem with positive definite quadratic term, $Q \in S^n_{++}$: using a convex optimization solver such as CVXGEN [Mattingley and Boyd, 2012] with C++ to solve (47) took on average 5.2 μs with an standard deviation of 3.1 μs using a single PC (Intel Xeon CPU E3-1245, 3.7 GHz, 4 cores, 64-bit).

Moreover, several authors have formulated SCBFs as inequality constraints of a QP problem for obstacle avoidance in robot manipulators [Landi *et al.*, 2019; Ferraguti *et al.*, 2020; Rauscher *et al.*, 2016; Singletary *et al.*, 2021]. However, it is a novelty of our proposed method to explicitly take the rigid-body dynamics of the robot into consideration: [Landi *et al.*, 2019] and [Ferraguti *et al.*, 2020] considered the robot kinematics, [Rauscher *et al.*, 2016] included a simplified version of the dynamics that neglects the Coriolis and centripetal forces, and [Singletary *et al.*, 2021] performed a purely kinematic implementation of a SCBF but guarantees safety at the level of dynamics by incorporating kinetic energy to the SCBF. The benefit of considering the robot dynamics when formulating our SCBF is that adherence to the

constraints can be guaranteed [Rauscher *et al.*, 2016], as illustrated by the experiments performed (see Fig. 3). In contrast, SCBF-based constraint violations may occur for a kinematic formulation depending on the choice of the optimization parameters, as illustrated in [Singletary *et al.*, 2021]. Also, slight constraint violations were observed in [Rauscher *et al.*, 2016] for a simplified-dynamics formulation.

Furthermore, an additional benefit of using an explicit formulation of the dynamic model of the robot is that it allows to quantify the additional Cartesian force, Δu in (48), required to modify the nominal state-feedback controller k^d to ensure safety. It is a novelty of the proposed method to calculate the required variation of the Cartesian compliant behavior of the system (as shown in Fig. 4) that is necessary to achieve this additional force (49)–(51), so that SCBF-based constraints are satisfied. This is relevant for kinesthetic teaching applications, *e.g.*, in the scenario shown in Sec. 4, since it indicates the changes in the robot's compliant behavior toward external force that human operators would feel when manually guiding the robot. Another example of a kinesthetic teaching scenario where our method may be relevant is for avoiding potential collisions occurring when an operator guides a robot with a sensitive object grasped in its end-effector.

Finally, previous works [Landi *et al.*, 2019; Ferraguti *et al.*, 2020; Rauscher *et al.*, 2016; Singletary *et al.*, 2021] where a robot nominal controller was modified using SCBFs focused on the stability guarantees of the nominal controller. In addition, we provided global asymptotic stability guarantees of convergence to the robot's desired state for the modified controller obtained from the QP problem. We used a passivity-based energy-storage formulation to ensure that the variation of the Cartesian compliance parameters determined by the proposed method is stable. This formulation has previously been used for a robot puncturing task through a three-layers box that simulated the varying stiffness of a human body [Ferraguti *et al.*, 2013], and also to allow stable robot controller-switching between position control and compliance control [Landi *et al.*, 2018]. Therefore, its use in showing stability for SCBF-based modifications of a nominal controller is novel. In addition, our contribution to this energy-storage formulation, as presented in Lemma 3.2 (Sec. 3.5) and its proof (Appendix A), is to replace the nonstrict Lyapunov function used in [Ferraguti *et al.*, 2013; Landi *et al.*, 2018] by a Lyapunov function with strictly negative time-derivative to ensure the strict stability of our method. As a trade-off, the power available to fill the energy storage, P_D in (58), is smaller for our method.

7. Conclusion

Safety control barrier functions have been used to online modify the Cartesian compliant behavior of a robot in a strictly stable manner (global asymptotic stability), so as to avoid that human operators manually guide a robot's end-effector to undesired parts of its workspace in the context of safe kinesthetic teaching. The rigid-body dynamics of the robot is considered in our method to guarantee adherence to the

safety constraints. The proposed method has been successfully evaluated through experiments using a Franka Emika Panda robot for a kinesthetic teaching application.

References

Ames, A. D., S. Coogan, M. Egerstedt, G. Notomista, K. Sreenath, and P. Tabuada (2019). "Control barrier functions: Theory and applications". In: *European Control Conference (ECC)*. Jun. 25–28. Naples, Italy, pp. 3420–3431.

Ferraguti, F., M. Bertuletti, C. T. Landi, M. Bonfè, C. Fantuzzi, and C. Secchi (2020). "A control barrier function approach for maximizing performance while fulfilling to ISO/TS 15066 regulations". *IEEE Robotics and Automation Letters* **5**:4, pp. 5921–5928.

Ferraguti, F., C. Secchi, and C. Fantuzzi (2013). "A tank-based approach to impedance control with variable stiffness". In: *IEEE International Conference on Robotics and Automation (ICRA)*. May 6–10. Karlsruhe, Germany, pp. 4948–4953.

Franka Emika (2019). *Franka Emika Panda – Data Sheet*. `https://www.generationrobots.com/media/panda-franka-emika-datasheet.pdf`. (Visited on 2022-09-13).

Hogan, N. (1985). "Impedance control: An approach to manipulation: Parts I–III". *Journal of Dynamic Systems, Measurement, and Control* **107**:1, pp. 1–24.

Kakani, V., V. H. Nguyen, B. P. Kumar, H. Kim, and V. R. Pasupuleti (2020). "A critical review on computer vision and artificial intelligence in food industry". *Journal of Agriculture and Food Research* **2**, p. 100033.

Karlsson, M., A. Robertsson, and R. Johansson (2017). "Autonomous interpretation of demonstrations for modification of dynamical movement primitives". English. In: *IEEE International Conference on Robotics and Automation (ICRA)*. May 29–Jun. 2. Singapore, pp. 316–321.

Khalil, H. K. (2014). *Nonlinear control*. Pearson Higher Ed., New York.

Khatib, O. (1985). "Real-time obstacle avoidance for manipulators and mobile robots". In: *IEEE International Conference on Robotics and Automation (ICRA)*. Vol. 2. Mar. 25–28. St. Louis, MO, USA, pp. 500–505.

Khatib, O. (1987). "A unified approach for motion and force control of robot manipulators: The operational space formulation". *IEEE Journal on Robotics and Automation* **3**:1, pp. 43–53.

Landi, C. T., F. Ferraguti, S. Costi, M. Bonfè, and C. Secchi (2019). "Safety barrier functions for human-robot interaction with industrial manipulators". In: *European Control Conference (ECC)*. Jun. 25–28. Naples, Italy, pp. 2565–2570.

Landi, C. T., F. Ferraguti, C. Fantuzzi, and C. Secchi (2018). "A passivity-based strategy for coaching in human-robot interaction". In: *IEEE International Conference on Robotics and Automation (ICRA)*. May 21–25. Brisbane, Australia, pp. 3279–3284.

Liu, C. and M. Tomizuka (2016). "Algorithmic safety measures for intelligent industrial co-robots". In: *IEEE International Conference on Robotics and Automation (ICRA)*. May 16–21. Stockholm, Sweden, pp. 3095–3102.

Mattingley, J. and S. Boyd (2012). "CVXGEN: A code generator for embedded convex optimization". *Optimization and Engineering* **12**:1, pp. 1–27.

Ott, C. (2008). *Cartesian impedance control of redundant and flexible-joint robots*. Springer, Berlin, Germany.

Rauscher, M., M. Kimmel, and S. Hirche (2016). "Constrained robot control using control barrier functions". In: *IEEE/RSJ International Conference on Intelligent Robots and Systems (IROS)*. Oct. 9–14. Daejeon, Korea, pp. 279–285.

Santibáñez, V. and R. Kelly (1997). "Strict Lyapunov functions for control of robot manipulators". *Automatica* **33**:4, pp. 675–682.

Schou, C., J. Damgaard, S. Bøgh, and O. Madsen (2013). "Human-robot interface for instructing industrial tasks using kinesthetic teaching". In: *44th IEEE International Symposium on Robotics (ISR)*. Oct. 19–27. Seoul, Korea, pp. 1–6.

Siciliano, B. and O. Khatib (2016). *Springer Handbook of Robotics*. Springer, Berlin, Germany.

Singletary, A., S. Kolathaya, and A. D. Ames (2021). "Safety-critical kinematic control of robotic systems". *IEEE Control Systems Letters* **6**, pp. 139–144.

Wang, L., A. D. Ames, and M. Egerstedt (2017). "Safety barrier certificates for collisions-free multirobot systems". *IEEE Transactions on Robotics* **33**:3, pp. 661–674.

Zhu, L., P. Spachos, E. Pensini, and K. N. Plataniotis (2021). "Deep learning and machine vision for food processing: A survey". *Current Research in Food Science* **4**, pp. 233–249.

A. Proof of Lemma 3.2

It is noted in [Santibáñez and Kelly, 1997] that the time-varying Lyapunov function

$$V_1(\xi, \Delta\xi, t) = \frac{1}{2}\dot{\xi}^{\mathrm{T}} M_\xi(q)\dot{\xi} + \frac{1}{2}\Delta\xi^{\mathrm{T}} K \Delta\xi \tag{68}$$

that is often used to show the stability of a Cartesian impedance controller [Ott, 2008, Ch. 3], such as the nominal state-feedback controller k^d (22), is a nonstrict Lyapunov function, *i.e.*, its time derivative is a globally negative-semidefinite function. Then, the authors in [Santibáñez and Kelly, 1997] have proposed the following

alternative Lyapunov candidate to obtain a globally negative-definite time derivative [Santibáñez and Kelly, 1997]:

$$V_2(x,t) = \frac{1}{2}\dot{\xi}^{\mathrm{T}} M_\xi(q)\dot{\xi} + \frac{1}{2}\Delta\xi^{\mathrm{T}} K \Delta\xi - \alpha f(\Delta\xi)^{\mathrm{T}} M_\xi(q)\dot{\xi} \tag{69}$$

where

$$f(\Delta\xi) = \frac{1}{1+||\Delta\xi||}\Delta\xi \tag{70}$$

and $\alpha > 0$ must satisfy

$$\min\left(\sqrt{\frac{\lambda_{m,K}}{\lambda_{M,M_\xi}}},\ \frac{2\lambda_{m,K}}{\lambda_{M,D}},\ \frac{\lambda_{m,D}}{2(k_C + 2\lambda_{M,M_\xi})}\right) > \alpha \tag{71}$$

However, using a scaling factor $f(\Delta\xi)$ in the cross-term of the Lyapunov candidate function can cause slow convergence to the equilibrium point, $\left[\Delta\xi^{\mathrm{T}},\quad \dot{\xi}^{\mathrm{T}}\right] = 0 \in \mathbb{R}^{2n}$. Therefore, we present a solution based on the work by [Santibáñez and Kelly, 1997], but removing the scaling factor $f(\Delta\xi)$:

$$V(x,t) = \frac{1}{2}\dot{\xi}^{\mathrm{T}} M_\xi(q)\dot{\xi} + \frac{1}{2}\Delta\xi^{\mathrm{T}} K \Delta\xi - \alpha\Delta\xi^{\mathrm{T}} M_\xi(q)\dot{\xi} \tag{72}$$

The Lyapunov candidate (72) is equivalent to

$$V(x) = \frac{1}{2}\left[\dot{\xi} - \alpha\Delta\xi\right]^{\mathrm{T}} M_\xi(q)\left[\dot{\xi} - \alpha\Delta\xi\right] + \frac{1}{2}\Delta\xi^{\mathrm{T}}\left[K - \alpha^2 M_\xi(q)\right]\Delta\xi \tag{73}$$

Therefore, the Lyapunov candidate is strictly positive ($V(x \neq 0) > 0$ and $V(x=0) = 0$) for

$$\alpha < \sqrt{\frac{\lambda_{m,K}}{\lambda_{M,M_\xi}}} \tag{74}$$

which ensures $K - \alpha^2 M_\xi(q) > 0$.

Moreover, the time-derivative of the Lyapunov candidate (72) is equal to

$$\begin{aligned}\dot{V}(x) = &-\alpha\Delta\xi^{\mathrm{T}}\left[\dot{M}_\xi(q) - C_\xi(q,\dot{q})\right]\dot{\xi} + \alpha\dot{\xi}^{\mathrm{T}} M_\xi(q)\dot{\xi} \\ &- \dot{\xi}^{\mathrm{T}} D\dot{\xi} - \alpha\Delta\xi^{\mathrm{T}} K\Delta\xi + \alpha\Delta\xi^{\mathrm{T}} D\dot{\xi}\end{aligned} \tag{75}$$

Considering that the matrix $\dot{M}_\xi(q) - 2C_\xi(q,\dot{q})$ is skew symmetric [Ott, 2008, Ch. 2]:

$$\dot{V}(x) = -\alpha\Delta\xi^{\mathrm{T}} C_\xi(q,\dot{q})\dot{\xi} + \alpha\dot{\xi}^{\mathrm{T}} M_\xi(q)\dot{\xi} - \dot{\xi}^{\mathrm{T}} D\dot{\xi} - \alpha\Delta\xi^{\mathrm{T}} K\Delta\xi + \alpha\Delta\xi^{\mathrm{T}} D\dot{\xi} \tag{76}$$

Then, defining the upper bound on certain terms:

$$-\dot{\xi}^{\mathrm{T}} D\dot{\xi} \leq -\frac{1}{2}\dot{\xi}^{\mathrm{T}} D\dot{\xi} - \frac{1}{2}\lambda_{m,D}\left|\left|\dot{\xi}\right|\right|^2 \tag{77}$$

$$\alpha\dot{\xi}^{\mathrm{T}} M_\xi(q)\dot{\xi} \leq \alpha\lambda_{M,M_\xi}\left|\left|\dot{\xi}\right|\right|^2 \tag{78}$$

$$-\alpha\Delta\xi^{\mathrm{T}} C_\xi(q,\dot{q})\dot{\xi} \leq \alpha k_C\left|\left|\Delta\xi\right|\right|\left|\left|\dot{\xi}\right|\right|^2 \tag{79}$$

it follows that

$$\begin{aligned}\dot{V}(x) \leq & -\frac{1}{2}\left[\dot{\xi}-\alpha\Delta\xi\right]^{\mathrm{T}} D\left[\dot{\xi}-\alpha\Delta\xi\right]+\frac{1}{2}\alpha^2\Delta\xi^{\mathrm{T}} D\Delta\xi-\frac{1}{2}\lambda_{m,D}\left|\left|\dot{\xi}\right|\right|^2 \\ & -\alpha\Delta\xi^{\mathrm{T}} K\Delta\xi+\alpha k_C\left|\left|\Delta\xi\right|\right|\left|\left|\dot{\xi}\right|\right|^2+\alpha\lambda_{M,M_\xi}\left|\left|\dot{\xi}\right|\right|^2 \end{aligned} \tag{80}$$

which can be rewritten as

$$\begin{aligned}\dot{V}(x) \leq & -\frac{1}{2}\left[\dot{\xi}-\alpha\Delta\xi\right]^{\mathrm{T}} D\left[\dot{\xi}-\alpha\Delta\xi\right]+\alpha\Delta\xi^{\mathrm{T}}\left[\tfrac{\alpha}{2}D-K\right]\Delta\xi \\ & -\frac{1}{2}\lambda_{m,D}\left|\left|\dot{\xi}\right|\right|^2+\alpha k_C\left|\left|\Delta\xi\right|\right|\left|\left|\dot{\xi}\right|\right|^2+\alpha\lambda_{M,M_\xi}\left|\left|\dot{\xi}\right|\right|^2 \end{aligned} \tag{81}$$

It can be ensured that the term

$$\alpha\Delta\xi^{\mathrm{T}}\left[\tfrac{\alpha}{2}D-K\right]\Delta\xi \tag{82}$$

is strictly negative for

$$\alpha<\frac{2\lambda_{m,K}}{\lambda_{M,D}} \tag{83}$$

and that the term

$$-\frac{1}{2}\lambda_{m,D}\left|\left|\dot{\xi}\right|\right|^2+\alpha k_C\left|\left|\Delta\xi\right|\right|\left|\left|\dot{\xi}\right|\right|^2+\alpha\lambda_{M,M_\xi}\left|\left|\dot{\xi}\right|\right|^2 \tag{84}$$

is strictly negative for

$$\alpha<\frac{\lambda_{m,D}}{2(\lambda_{M,M_\xi}+k_C||\Delta\xi||)} \tag{85}$$

Therefore, if $\alpha>0$ satisfies (53)

$$\min\left(\sqrt{\frac{\lambda_{m,K}}{\lambda_{M,M_\xi}}},\ \frac{2\lambda_{m,K}}{\lambda_{M,D}},\ \frac{\lambda_{m,D}}{2(\lambda_{M,M_\xi}+k_C||\Delta\xi||)}\right)>\alpha \tag{86}$$

the Lyapunov candidate function $V(x)$ is strictly positive ($V(x\neq 0)>0$ and $V(x=0)=0$) and its time-derivative is strictly negative ($\dot{V}(x)<0$).

Paper V

Null-Space Compliance Variation for Safe Human–Robot Collaboration in Redundant Manipulators using Safety Control Barrier Functions

Julian M. Salt Ducaju **Björn Olofsson**
Anders Robertsson **Rolf Johansson**

Abstract

In this paper, Safety Control Barrier Functions (SCBFs) were used to adjust the null-space compliant behavior of a redundant robot to improve safety in Human–Robot Collaboration (HRC) without modifying the robot behavior with respect to its main Cartesian task. A Lyapunov function was included in an energy storage formulation compatible with strict passivity to provide global asymptotic stability guarantees for the null-space compliance variation, and the necessary conditions for stability were formulated as inequality constraints of the optimization problem used for the null-space compliance variation. Experimental validation was performed using a Franka Emika Panda robot for a collaborative assembly application and its results showed that safety can be improved by using SCBFs simultaneously to the optimization of the robot configuration, while employing a single degree of freedom.

© 2023 IEEE. Reprinted, with permission, from 2023 IEEE/RSJ International Conference on Intelligent Robots and Systems (IROS), October 1-5, Detroit, MI, USA, pp. 5903–5909.

1. Introduction

The recent interest in the manufacturing industry to replace mass production for mass customization has caused an increase in the relevance of Human–Robot Collaboration (HRC) in the robotics community [Schou *et al*., 2013]. Human operators can use their intelligence and dexterity to increase flexibility in robotic manufacturing and to decrease the complexity of the robot tools, while robots can reduce the operator fatigue, *e.g.*, in industries, such as aeronautics, where assembly applications are still mainly manual as a result of their complexity [Kousi *et al*., 2018].

Human safety is a requirement of collaborative applications. A control strategy often used for human collaboration is impedance control [Hogan, 1985], which establishes a compliant robot behavior with respect to external forces acting on it, and has the additional benefit in human–robot collaborative applications of allowing physical human guidance of the robot. Even though robot compliance effectively reduces the transferred energy from the robot to the operator during an accidental collision, additional safety features can be included to further protect the operators and to avoid contacts with their most sensitive surfaces. In the context of robot obstacle avoidance, Safety Control Barrier Functions (SCBFs)[Forsgren *et al*., 2002] have been gaining popularity in recent years [Salt Ducaju *et al*., 2022; Ferraguti *et al*., 2020; Landi *et al*., 2019; Rauscher *et al*., 2016; Singletary *et al*., 2021; Benzi and Secchi, 2021], since they emphasize optimality and are minimally-invasive [Ames *et al*., 2019]. Recently, SCBFs have been used to adjust the Cartesian compliant behavior of a robot for obstacle avoidance with respect to its end-effector [Salt Ducaju *et al*., 2022].

Moreover, when obstacle avoidance does not involve the Cartesian motion of the robot end-effector, but rather its link configuration, the main robot task needs not be modified. In this context, kinematic redundancy allows robotic manipulators to perform additional subtasks, such as obstacle avoidance, without modifying the robot behavior with respect to its main task by projecting the additional tasks in the null-space of the robot main task [Salt Ducaju *et al*., 2021]. For this, a dynamic formulation that augments the Cartesian coordinates of the main robotic task by null-space velocities [Park, 2000] is often used, since it allows decoupling of kinetic energies for each task. A compliant controller in the null-space of the robot main task based on the dynamic formulation in [Park, 2000] was proposed in [Ott *et al*., 2008]. By avoiding inertia shaping, the controller in [Ott *et al*., 2008] avoided using feedback from the external forces and provided robustness with respect to model inaccuracies in the controller, while achieving a decoupling of the Cartesian and the null-space motion. Semi-definite Lyapunov functions were used in [Ott *et al*., 2008] to provide asymptotic stability guarantees for the null-space compliant motion. Nevertheless, stability guarantees for the variation of the stiffness and damping parameters for null-space compliant behavior have not been provided in this context so far.

Furthermore, obstacle avoidance is not the only beneficial subtask for HRC,

and optimizing the robot joint configuration is also desirable, since it can maximize the robot manipulability, *e.g.*, by controlling that the angular positions of the robot joints are far from their limits [Nakamura, 1990]. An extension of [Ott *et al*., 2008] was presented in [Dietrich *et al*., 2013] for a hierarchical control structure with an arbitrary number of subtasks, where each additional subtask is projected on the null-space of the higher-priority tasks. However, the robots designed to perform collaborative tasks with humans (cobots) are usually built with 7 rotational joints, *e.g.*, the KUKA LBR iiwa robot or the Franka Emika Panda robot, and therefore, in robotic applications where the main task involves controlling the position and orientation of its end-effector, only one degree of freedom (DOF) would be available for additional subtasks. Then, it is not guaranteed that more than one subtask can be performed using the additional DOF with a hierarchical structure as in [Dietrich *et al*., 2013].

In this paper, we address the problem of improving safety in HRC for redundant robots by extending our previous work in [Salt Ducaju *et al*., 2022] to contact-risk situations that do not involve the robot end-effector, but rather its link configuration. A joint impedance controller is projected in the null-space of the Cartesian robot motion to achieve a compliant motion toward a desired joint configuration, while keeping the main robotic task unperturbed. The novelty of our proposal consists in using SCBFs to adjust the null-space compliant behavior of the robot for obstacle avoidance with respect to the body of the robot. In addition to improved safety, our proposed method should not affect the Cartesian robot end-effector motion nor require additional DOFs to be performed, since the SCBF-based obstacle avoidance shares the null-space DOF with the joint optimization subtask. A Lyapunov function is proposed to provide global asymptotic stability guarantees for varying the null-space compliant motion. Laboratory experiments have been performed for a collaborative assembly application to validate our method on a 7-DOFs manipulator.

The paper is organized as follows: Sec. 2 presents the kinematic and dynamic models used for redundant robotic manipulators. Then, Sec. 3 presents the nominal state-feedback controller, which is modified by a Quadratic Optimization (QP) problem presented in Sec. 4, where SCBFs are used as inequality constraints for obstacle avoidance. Section 5 explains the experiments performed for a collaborative assembly application and presents the results obtained. Finally, a discussion is included in Sec. 6 and conclusions are drawn in Sec. 7.

2. Modeling for Redundant Robots

First, we review relevant kinematics and dynamics for redundant manipulators that show that the dynamics for the robot main task and for its null-space can be decoupled.

2.1 Kinematics for Redundant Robots

The kinematic relation between a robotic manipulator with n degrees of freedom (DOFs) and its main task in the m-dimensional task space is:

$$\xi = \mathscr{K}(q) \tag{1}$$

where $\xi \in \mathbb{R}^m$ represents the coordinates of the main robotic task and $q \in \mathbb{R}^n$ represents the coordinates of the joint space of the robot. Then, the manipulator Jacobian, $J(q) \in \mathbb{R}^{m\times n}$ is used to relate the main task velocity, $\dot{\xi}$, with respect to the joint velocity, $\dot{q}$:

$$\dot{\xi} = J(q)\dot{q} \tag{2}$$

where $J(q)$ is assumed to be of full rank throughout the presented work as in [Khatib, 1987]. A robotic manipulator is considered to be kinematically redundant when $n > m$, and $r = n - m$ is called the degrees of redundancy.

A possible solution to the inverse kinematics for (2) is

$$\dot{q} = J_W^{\dagger}(q)\dot{\xi} + (I_n - J^{\mathrm{T}}(q)J_W^{\dagger\mathrm{T}}(q))\dot{q}_0 \tag{3}$$

where $\dot{q}_0 \in \mathbb{R}^n$ is an arbitrary vector in the robot joint space, $I_n \in \mathbb{R}^{n\times n}$ represents an identity matrix, and $J_W^{\dagger}(q)$ is the weighted generalized inverse

$$J_W^{\dagger}(q) = W^{-1}(q)J^{\mathrm{T}}(q)(J(q)W^{-1}(q)J^{\mathrm{T}}(q))^{-1} \tag{4}$$

with $W \in \mathbb{R}^{n\times n}$ being a symmetric positive definite matrix, $W \in S_{++}^n$. The second term of the right-hand side of (3) projects the arbitrary joint space vector $\dot{q}_0$ into the null-space of the main task, $\mathscr{N}(J)$, and it is necessary for a full decomposition of the joint motion in redundant manipulators.

Moreover, the velocity in the null-space of the main task can be rewritten by defining velocities $v_N \in \mathbb{R}^r$ [Park, 2000], so

$$\dot{q}_{\mathrm{NS}} = (I_n - J^{\mathrm{T}}(q)J_W^{\dagger\mathrm{T}}(q))\dot{q}_0 = Z^{\mathrm{T}}(q)v_N \tag{5}$$

where $Z(q) \in \mathbb{R}^{r\times n}$ is composed by linearly independent vectors in $\mathscr{N}(J)$, $J(q)Z^{\mathrm{T}}(q) = 0$. Analogous to (2), the null-space velocities, v_N, can be related to the robot joint velocity by a Jacobian, $N(q) = (ZWZ^{\mathrm{T}})^{-1}ZW \in \mathbb{R}^{r\times n}$:

$$v_N = N(q)\dot{q} \tag{6}$$

REMARK There might not exist compatible null-space coordinates, $s(q)$, such that $N(q) = \partial s(q)/\partial q$, so the null-space velocities, v_N, are, in general, not integrable [Ott *et al.*, 2008]. □

2.2 Dynamics for Redundant Robots

The rigid-body dynamics of the robot can be written in the joint space of the robot as [Siciliano and Khatib, 2016]:

$$M(q)\ddot{q} + C(q,\dot{q})\dot{q} + G(q) = \tau + \tau^{\text{ext}} \tag{7}$$

where $M(q) \in \mathbb{R}^{n\times n}$ is the generalized inertia matrix, $C(q,\dot{q}) \in \mathbb{R}^{n\times n}$ is the Coriolis matrix, $G(q) \in \mathbb{R}^n$ captures the gravity-induced torques, and $\tau \in \mathbb{R}^n$ represents the input torques. Finally, $\tau^{\text{ext}} \in \mathbb{R}^n$ represents the external torques. For a kinematically redundant robot, the input torques can be decoupled as

$$\tau = \tau_\xi + \tau_{\text{ns}} = J^{\text{T}}(q)F_\xi + N^{\text{T}}(q)F_N \tag{8}$$

where τ_ξ corresponds to the torques that are involved in the robot's main task, and τ_{ns} are torques acting in the null-space of the main task.

Moreover, if the weighting matrix W of the generalized inverse is chosen to be the generalized inertia matrix, M, $W = M$ in (4), the null-space torque, τ_{ns} in (8), does not cause an acceleration in the main task coordinates ξ [Khatib, 1995]. Then, the task space is inertially decoupled from the minimal null-space motions, and the dynamics of each space can be considered separately:

$$M_\xi(q)\ddot{\xi} + C_\xi(q,\dot{q})\dot{\xi} + G_\xi(q) = F_\xi + F_\xi^{\text{ext}} \tag{9}$$

$$M_N(q)\dot{v}_N + C_N(q,\dot{q})v_N + G_N(q) = F_N + F_N^{\text{ext}} \tag{10}$$

However, to obtain fully-decoupled dynamics as in (9) and (10), a power-conserving feedback compensation on the centrifugal and Coriolis cross-terms should be included [Ott *et al*., 2008].

3. Nominal State-Feedback Controller

Consider a control-affine system:

$$\dot{x} = f(x) + g(x)u \tag{11}$$

that has closed-loop system dynamics with a state-feedback controller k according to:

$$\dot{x} = f_{cl}(x,t) = f(x) + g(x)k(x,t) \tag{12}$$

Then, the nominal state-feedback controller, $k = k^d$ in (12), should achieve the robot's desired behavior for human–robot collaboration: a Cartesian compliant behavior of the robot end-effector for safety, and possibly, human guidance, and a joint compliance behavior in the null-space of the main Cartesian task that increases the robot manipulability.

3.1 Main Task: Cartesian Impedance Control

A Cartesian impedance controller [Hogan, 1985] is used to establish a mass-spring-damper relationship between the Cartesian pose variation of the robot end-effector from its reference, $\Delta\xi = \xi_D - \xi$ (ξ_D being the Cartesian reference), and the external Cartesian force, F_ξ^{ext}:

$$F_\xi^{\text{ext}} = M_\xi(q)\ddot{\xi} + (D + C_\xi(q,\dot{q}))\dot{\xi} - K\Delta\xi \tag{13}$$

where D and K are the virtual damping and stiffness matrices, respectively. The virtual inertia is chosen equal to the robot inertia, $M_\xi(q)$, to avoid inertia shaping [Ott *et al.*, 2008]. The input force F_ξ, when the Cartesian external force is defined as in (13), should be equal to

$$F_\xi = K\Delta\xi - D\dot{\xi} + G_\xi(q) \tag{14}$$

3.2 Redundancy and Null-Space Motion

To obtain a compliant behavior in the null-space of the main task, the null-space component of the input torque, τ_{ns} in (8), can be chosen as a projection of a torque that contains a spring stiffness term, k_n, with respect to the joint position variation from its reference, $\Delta q = q_D - q$, and a damping term, d_n, for the null-space velocities, v_N [Ott *et al.*, 2008]:

$$\tau_{\text{ns}} = N^{\text{T}}(q)k_n Z(q)\Delta q - N^{\text{T}}(q)d_n v_N \tag{15}$$

The desired joint configuration, q_D, is chosen as the closest configuration to the mid of the range of the joints, q_{mid}, where $\xi_D = p(q_D)$ to increase the robot manipulability. An optimization problem can be formulated to obtain q_D:

$$\begin{aligned} q_D = &\arg\min_{q_D \in \mathbb{R}^n} \frac{1}{2}\left|\left|q_D - q_{\text{mid}}\right|\right|_2^2 \\ &\text{s.t. } \xi_D = p(q_D) \end{aligned} \tag{16}$$

Then, the gravity-compensated closed-loop dynamics of the system obtained from (10) and using the decoupled torque input defined in (8) with (15) is

$$F_N^{\text{ext}} = M_N(q)\dot{v}_N + (d_n + C_N(q,\dot{q}))v_N - k_n Z(q)\Delta q \tag{17}$$

3.3 Controller Stability

The stability properties of the closed-loop system (13) and (17) have been studied in [Ott *et al.*, 2008] using conditional stability and proposing a semi-definite Lyapunov function to show the asymptotic stability of the equilibrium point ($q = q_D$, $\dot{q} = 0$) for free-space motion. However, based on recent research that proved the global asymptotic stability for the main task (13) in a non-redundant robotic manipulator [Salt Ducaju *et al.*, 2022], we consider a strictly definite Lyapunov candidate function to provide a stronger proof of stability for the null-space motion:

LEMMA 3.1
The Lyapunov function candidate

$$V_{\text{ns}}(\Delta q, v_N) = \frac{1}{2} v_N^{\text{T}} M_N v_N + \frac{k_n}{2} \Delta q^{\text{T}} \Delta q - \alpha \Delta q^{\text{T}} Z^{\text{T}} M_N v_N \tag{18}$$

shows the global asymptotic stability of the null-space motion with input torque τ_{ns} in (15) for $\alpha > 0$ satisfying:

$$\min \left(\sqrt{\frac{k_n}{\lambda_{M,M_Z}}}, \frac{2k_n}{d_n}, \frac{d_n}{2(\lambda_{M,M_Z} + k_C ||Z\Delta q||)} \right) > \alpha \tag{19}$$

where λ_{M,M_Z} is the largest eigenvalue of the matrix $Z^{\text{T}} M_N Z$, and k_C is a positive constant such that for all $w_1, w_2, w_3 \in \mathbb{R}^r$ [Santibáñez and Kelly, 1997]

$$||C_N(w_1, w_2) w_3|| \leq k_C ||w_2|| ||w_3|| \tag{20}$$

□

Proof. The detailed proof for the global asymptotic stability of the null-space motion has been omitted for conciseness since it is analogous to the proof of the stability of the Cartesian impedance controller in [Salt Ducaju *et al.*, 2022] but replacing $\Delta\xi$, $\dot{\xi}$, M_ξ, C_ξ, K, and D for Δq, v_N, M_N, C_N, k_n, and d_n, respectively. □

4. Quadratic Optimization

In this section, we modify the robot's null-space compliant behavior (17) of the nominal state-feedback controller k^d using a quadratic optimization problem that ensures that the robot states stay in a safe set to improve safety in HRC.

4.1 System Linearization

By applying partial feedback linearization [Khalil, 2014, Ch. 9], the input, $u \in \mathbb{R}^n$, to the system in joint-space coordinates (7) can be written as the gravity-compensated joint torque:

$$u = \tau + \tau^{\text{ext}} - G(q) \tag{21}$$

Then, by choosing the state vector as $x = [q^{\text{T}}, \dot{q}^{\text{T}}]^{\text{T}} \in \mathbb{R}^{2n}$, the linearized system is

$$\dot{x} = A(q, \dot{q}) x + B(q) u \tag{22}$$

where

$$A = \begin{bmatrix} 0_n & I_n \\ 0_n & -M^{-1}(q) C(q, \dot{q}) \end{bmatrix}, \; B = \begin{bmatrix} 0_n \\ M^{-1}(q) \end{bmatrix} \tag{23}$$

4.2 Cost Function

Obstacle avoidance with respect to the body of the robot can be achieved without perturbing the robot main task if the additional torque required to avoid obstacles is applied in the null-space of the main task:

$$\Delta u = \Delta\tau_{\text{ns}} \tag{24}$$

Then, the compliance parameters of the joint torque (15) in the null-space projection of the main task can be varied to fulfill (24) so that the desired joint configuration q_D is not modified, thus achieving obstacle avoidance while allowing the optimization of the robot joint configuration:

$$\Delta\tau_{\text{ns}} = N^{\text{T}}(q)(-\Delta d_n v_N + \Delta k_n Z(q)\Delta q) \tag{25}$$

Therefore, a cost function that minimizes the value of the null-space stiffness and damping variation,

$$z = \begin{bmatrix}\Delta k_n & \Delta d_n\end{bmatrix}^{\text{T}} \tag{26}$$

can be formulated:

$$L(z) = \frac{1}{2}\left|\left|W_z z\right|\right|_2^2 \tag{27}$$

where a weighting matrix, $W_z \in \mathbb{R}^{2\times 2}$, is used to select the desired ratio between the null-space stiffness and damping variations. Since $W_z \in S_{++}^2$ yields $Q \in S_{++}^2$, Q being the quadratic term of the cost function (27), W_z may be chosen as:

$$W_z = \begin{bmatrix}1 & 0\\ 0 & \beta\end{bmatrix} \tag{28}$$

for $\beta \in \mathbb{R}_{>0}$. Then, if $\beta > 1$ the variation of the stiffness is prioritized and if $\beta < 1$ the damping variation is prioritized. In addition, selecting (27) as the cost function to be solved in the QP problem yields a minimal variation of the input torque to the robot, $\Delta\tau_{\text{ns}}$ of Eq. (25), thus minimizing the difference between the system input u and the nominal state-feedback k^d.

4.3 Inequality Constraint for Obstacle Avoidance

An inequality constraint for the input of the linearized system (22)

$$A_{\text{BF}} u \leq b_{\text{BF}} \tag{29}$$

can be used to ensure that the body of the robot stays within a safety distance of an obstacle by guaranteeing the forward invariance of a safe (*i.e.*, uncollided) set of robot states [Ames *et al.*, 2019]:

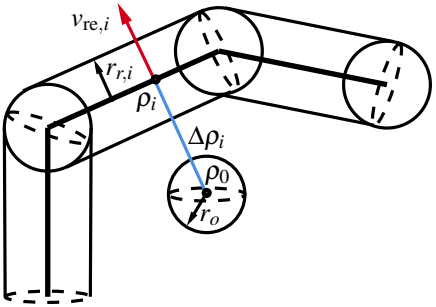

Figure 1. Illustration of the capsules model [Lin *et al.*, 2017; Landi *et al.*, 2019] (for a 3-link robot) used to determine the safety distance. The blue line represents the distance, $\Delta\rho_i$, between the obstacle's position, ρ_0, and its closest point within the i-th link of the robot, ρ_i. The red arrow represents the relative velocity, $v_{\text{re},i}$, of ρ_i with respect to the obstacle ρ_0 and $r_{r,i}$, r_o are the safety distances around the robot's i-th link and the obstacle, respectively.

THEOREM 4.1
A safe set $\mathscr{C} = \{x \in \mathbb{R}^{2n} \mid h(x) \geq 0\}$ is forward invariant if

$$\sup_{u \in \mathscr{U}} [L_f h(x) + L_g h(x) u] \geq -\kappa(h(x)) \tag{30}$$

for all $x \in \mathscr{D}$, h being the Safety Control Barrier Function (SCBF), $h : \mathscr{D} \to \mathbb{R}$ with $\mathscr{C} \subseteq \mathscr{D} \subset \mathbb{R}^{2n}$, κ an extended class-$\mathscr{K}_\infty$ function (strictly monotonically increasing), $L_f h(x) = {}^{\partial h}/_{\partial x} f(x)$, and $L_g h(x) = {}^{\partial h}/_{\partial x} g(x)$ [Ames *et al.*, 2019]. □

Therefore, a safety function has been formulated so that the safety distance is always greater than or equal to the current distance from the robot to the obstacle subtracted by the distance needed to brake the system into a full stop with constant and instantaneous acceleration [Salt Ducaju *et al.*, 2022; Wang *et al.*, 2017; Ferraguti *et al.*, 2020]. Moreover, to avoid having a computationally-expensive calculation of the distance between the robot and the obstacle, each link of the robot geometry is simplified using basic geometric models, such as capsules, which have recently gained popularity [Lin *et al.*, 2017; Landi *et al.*, 2019] for fitting well to the shape of a robotic manipulator (see Fig. 1).

Then, for each link $i \in \{1, \ldots, n\}$, the SCBF, $h_i : \mathscr{D} \to \mathbb{R}$, that enforces obstacle avoidance is, as in [Salt Ducaju *et al.*, 2022; Wang *et al.*, 2017; Ferraguti *et al.*, 2020]:

$$h_i(x) = \sqrt{2a_{\text{br}}(||\Delta\rho_i|| - D_{s,i})} + \frac{\Delta\rho_i^{\mathrm{T}}}{||\Delta\rho_i||} J_i \dot{q} \tag{31}$$

with $\Delta\rho_i = \rho_i - \rho_o$ being the distance between the closest point to the obstacle in the i-th link, ρ_i, and the obstacle's position ρ_o, and $J_i \in \mathbb{R}^{3\times n}$ being a Jacobian that relates the linear velocity of the selected point in the i-th link, ρ_i, with the angular

velocity of the joints $\dot{q}$. Also, the safety distance, $D_{s,i} = r_{r,i} + r_o$, uses $r_{r,i}$ and r_o as protective distances around the link i and the obstacle, respectively, and $a_{\text{br}} > 0$ denotes the robot braking acceleration. Moreover, the second term of the right-hand side of (31) is equivalent to the relative velocity, $v_{\text{re},i}$ of ρ_i with respect to ρ_o, as shown in Fig. 1.

Considering the system model (22), (23) and choosing the inequality constraint that must be satisfied to ensure that the safe set is forward invariant (30) as $\dot{h}(x) + \gamma h^{\omega} \geq 0$ [Wang *et al.*, 2017], the elements in (29) are for each link i equal to

$$A_{\text{BF,i}} = -\Delta\rho_i^{\text{T}} J_i M^{-1} \tag{32}$$

$$b_{\text{BF,i}} = \frac{a_{\text{br}} \Delta\rho_i^{\text{T}} \begin{bmatrix} 0_{3\times n}, & J_i \end{bmatrix} x}{\sqrt{2a_{\text{br}}(||\Delta\rho_i|| - D_{s,i})}} + \left|\left| \begin{bmatrix} 0_{3\times n}, & J_i \end{bmatrix} x \right|\right|^2 + ||\Delta\rho_i|| \gamma h_i^{\omega} - \frac{\left(\Delta\rho_i^{\text{T}} \begin{bmatrix} 0_{3\times n}, & J_i \end{bmatrix} x\right)^2}{||\Delta\rho_i||^2} + \Delta\rho_i^{\text{T}} \begin{bmatrix} 0_{3\times n}, & \dot{J}_i - J_i M^{-1} C \end{bmatrix} x \tag{33}$$

Therefore, the inequality constraint (29) in z (26) is equivalent to

$$A'_{\text{BF}} z \leq b'_{\text{BF}} \tag{34}$$

for $A'_{\text{BF}} = A_{\text{BF}} N^{\text{T}} \begin{bmatrix} Z\Delta q, & -v_N \end{bmatrix}$ and $b'_{\text{BF}} = b_{\text{BF}} - A_{\text{BF}} k^d$.

4.4 Stable Variation of the Null-Space Compliant Behavior

The strict stability of the null-space motion has previously been shown in Lemma 3.1 for constant null-space stiffness and damping parameters. Also, analogous to the passivity condition shown for a Cartesian impedance controller in [Salt Ducaju *et al.*, 2022], since $M_N, k_n, d_n \in S_{++}$, a passive map from the null-space external force, F_N^{ext}, to the null-space velocity, v_N, was guaranteed:

$$\dot{V}_{\text{ns}} < v_N^{\text{T}} F_N^{\text{ext}} \tag{35}$$

with $\dot{V}_{\text{ns}}$ being the time-derivative of the Lyapunov function (18) with constant null-space stiffness and damping terms.

However, if these compliance parameters vary with time, additional terms $\Delta\dot{V}_{\text{ns}}(t)$, which may break the passivity of the system, appear in the time-derivative of the Lyapunov function used for the stability proof of the null-space motion:

$$\dot{V}'_{\text{ns}}(t) = \dot{V}_{\text{ns}} + \Delta\dot{V}_{\text{ns}}(t) \tag{36}$$

with $\dot{V}'_{\text{ns}}(t)$ being the time-derivative of the Lyapunov function with time-varying terms. The additional terms are equal to

$$\Delta\dot{V}_{\text{ns}}(t) = -\frac{\Delta d_n}{2} \left[v_N - \alpha Z \Delta q\right]^{\text{T}} \left[v_N - \alpha Z \Delta q\right] + \frac{\dot{k}_n}{2} \Delta q^{\text{T}} \Delta q \tag{37}$$

Moreover, energy-based virtual storage methods can be used to guarantee the passivity of the system by controlling that the amount of energy introduced to the robotic manipulator for varying the stiffness of the robot is lower than the energy dissipated by itself [Ferraguti *et al.*, 2013; Landi *et al.*, 2018]. Being T the energy stored in a virtual reservoir, the total energy of the system composed by the robot and the virtual storage is equal to $W_{\text{ns}} = T + V'_{\text{ns}} > 0$, with $\dot{W}_{\text{ns}} < 0$. Then, the only additional condition needed to ensure the passivity of the system is that there is enough energy in the storage. For a time interval $\begin{bmatrix} t_s, & t_f \end{bmatrix}$, this condition is [Landi *et al.*, 2018]:

$$T(t_f) = T(t_s) + \int_{t_s}^{t_f} P_D d\tau - \int_{t_s}^{t_f} P_K d\tau \geq \delta \tag{38}$$

with δ being the minimum amount of energy allowed in the storage. Also, P_D and P_K represent the dissipated power due to damping and the power caused by stiffness variation, respectively,

$$P_D = \frac{d_n + \Delta d_n}{2} \begin{bmatrix} v_N - \alpha Z \Delta q \end{bmatrix}^{\text{T}} \begin{bmatrix} v_N - \alpha Z \Delta q \end{bmatrix} \tag{39}$$

$$P_K = \frac{\dot{k}_n}{2} \Delta q^{\text{T}} \Delta q \tag{40}$$

Then, the condition to ensure that the energy storage used to guarantee the passivity of the system does not get empty (38) can be rewritten as an inequality constraint:

$$A_{\text{T}} z \leq b_{\text{T}} \tag{41}$$

with

$$A_{\text{T}} = \begin{bmatrix} \frac{1}{2} \Delta q^{\text{T}} \Delta q \\ -\frac{t_f - t_s}{2} \begin{bmatrix} v_N - \alpha Z \Delta q \end{bmatrix}^{\text{T}} \begin{bmatrix} v_N - \alpha Z \Delta q \end{bmatrix} \end{bmatrix}^{\text{T}} \tag{42}$$

$$b_{\text{T}} = d_n \frac{t_f - t_s}{2} \begin{bmatrix} v_N - \alpha Z \Delta q \end{bmatrix}^{\text{T}} \begin{bmatrix} v_N - \alpha Z \Delta q \end{bmatrix} + \frac{\Delta k_n(t_s)}{2} \Delta q^{\text{T}} \Delta q + T(t_s) - \delta \tag{43}$$

Additionally, the positive-definiteness of the null-space stiffness and damping, *i.e.*, $k_n + \Delta k_n(t) \in S_{++}$ and $d_n + \Delta d_n(t) \in S_{++}$, are necessary conditions to show the stability of the null-space motion using Lemma 3.1. These conditions can be enforced by rewriting them as:

$$A_{\text{kd}} z < b_{\text{kd}} \tag{44}$$

with $A_{\text{kd}} = -I_2$ and $b_{\text{kd}} = \begin{bmatrix} k_n & d_n \end{bmatrix}^{\text{T}}$.

4.5 Quadratic Optimization Problem Summary

Finally, the resulting optimization problem to modify the nominal state-feedback controller for obstacle avoidance is:

$$\begin{aligned} z = \arg\min\nolimits_{z\in\mathbb{R}^2} & L(z) \\ \text{s.t. } & A'_{\mathrm{BF}} z \leq b'_{\mathrm{BF}} \\ & A_{\mathrm{kd}} z < b_{\mathrm{kd}} \\ & A_{\mathrm{T}} z \leq b_{\mathrm{T}} \end{aligned} \tag{45}$$

5. Experiments

In this section, we provide an experimental evaluation of the proposed method for an assembly application.

5.1 Experimental Setup

The experimental validation consisted in a collaborative assembly of an emergency button using a redundant robotic manipulator, Franka Emika Panda [Franka Emika, 2019], as seen in Fig. 2. This assembly process consisted of three events. First, while the robot snapped the switch into the bottom box [Stolt *et al.*, 2011], the human operator secured the pusher to the top box with a small plastic nut. Finally, the robot joined the top and bottom boxes.

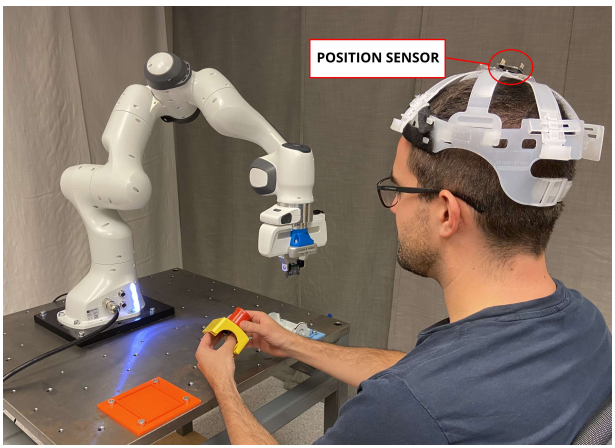

Figure 2. Experimental setup for the collaborative assembly of an emergency button.

A Cartesian compliance controller was implemented to allow the operators to interact with the position and orientation of the robot arm to correct any robot mal-

function, and also to allow a careful handling of the assembly pieces, while a null-space compliance controller optimized the robot joint configuration. However, to increase safety in the most sensitive parts of the operator's body, *i.e.*, its head, the operator wore a helmet, which was equipped with a position sensor (see Fig. 2). Then, the null-space compliance parameters were varied based on the optimization problem in (45) to avoid any collision between the body of the robot and the operator's head.

5.2 Results

The results for a situation where a potential collision was avoided during the assembly event in which the robot joined the top and the bottom of the box are shown in Figs. 3 and 4 and in Table 1. First, it is seen in Fig. 3 how the safety control barrier function $h_{\min} = \min(h_i)\ \forall\ i \in \{1,\ldots,n\}$ had a positive value throughout this motion, thus the states of the robot stayed inside the safe set $\mathscr{C}$. Also, the inequality constraint (34) of the QP problem (45) was active between $t = 1.18$ s and $t = 3.91$ s, which caused the variation of the null-space stiffness $k_n + \Delta k_n$ and damping $d_n + \Delta d_n$, so that the forward invariance condition of the safe set $\mathscr{C}$ (30) was fulfilled.

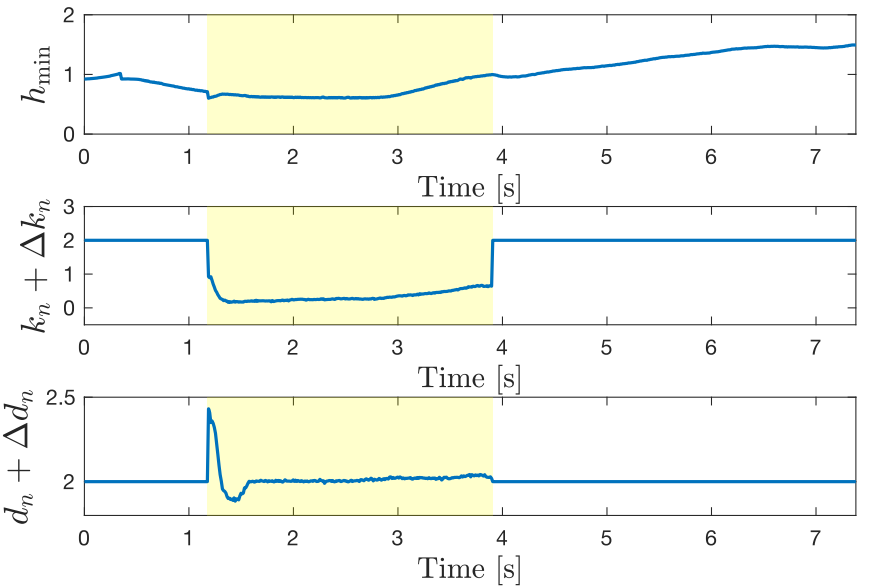

Figure 3. Temporal evolution of the barrier function $h_{\min}$, the null-space stiffness $k_n + \Delta k_n$, and the null-space damping $d_n + \Delta d_n$. The yellow background indicated the time interval when the inequality constraint (34) of the QP problem (45) was active.

Moreover, Table 1 shows relevant performance metrics for the highest-risk situation, defined as the time instant where the safety control barrier function $h_{\min}$ was the closest to zero. As seen in Table 1, the highest-risk situation occurred at $t = 1.19$ s, where the minimum distance between the operator's head and the body of the robot, $D_{\min}$, was equal to 0.25 m. It is also shown in Table 1 that the time-to-collision, TTC, defined as the time that would elapse until a collision occurred for a constant relative velocity between the operator's head and the robot's body, was equal to 0.37 s, which highlights the minimally-invasive features of the proposed method.

Table 1. Performance metrics for the highest-risk situation

Time (t)	Minimum Distance ($D_{\min}$)	Time-to-Collision (TTC)
1.19 s	0.25 m	0.37 s

Furthermore, Fig. 4 shows the temporal evolution of the L_2-norm of the difference between the joint configuration q and the midpoint configuration q_{mid} for the developed controller (*NS+QP*) compared to the cases where no null-space motion was implemented (*No NS*) and where no null-space compliance variation was used (*No QP*). The implementation of null-space motion could effectively be used to decrease the difference between the robot configuration and the midpoints of the robot joints' ranges to increase the robot manipulability. Also, since there was only one DOF available in the null-space of the main (Cartesian) task, the controller was able to increase the robot manipulability as long as it did not conflict with the safety condition in (34).

6. Discussion

Several authors have used SCBFs for obstacle avoidance in robotic manipulators [Landi *et al*., 2019; Ferraguti *et al*., 2020; Rauscher *et al*., 2016; Singletary *et al*., 2021; Salt Ducaju *et al*., 2022; Benzi and Secchi, 2021]. However, these previous works focused on non-redundant robots, and therefore, obstacle avoidance would modify the main robotic task. The novelty of the method presented here is that we consider redundant robots and use their additional DOFs to apply the necessary joint torque variation in the null-space of the robot's main task in a dynamically consistent way such that this main robotic task is not altered unnecessarily. Further, it is straightforward to combine the proposed method with previous proposals that achieved obstacle avoidance with respect to the robot end-effector, such as [Salt Ducaju *et al*., 2022], thus achieving a safe robot behavior in any contact-risk situation.

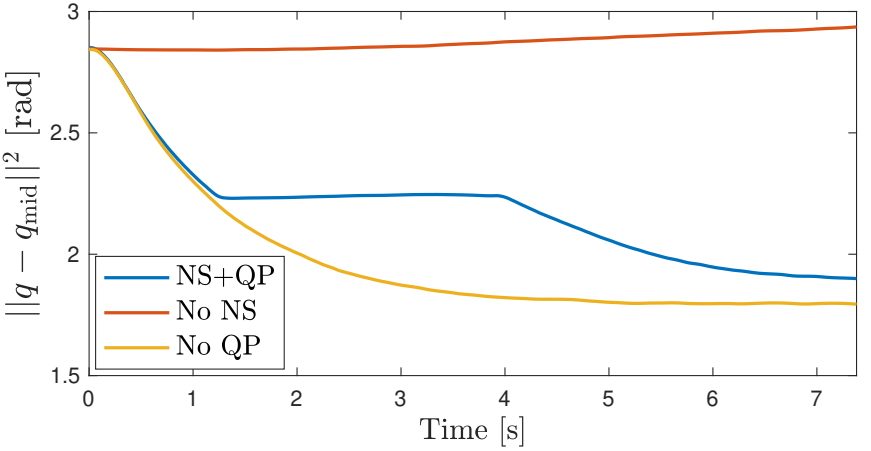

Figure 4. Temporal evolution of the L_2-norm of the difference between the joint configuration q and the midpoint configuration q_{mid}.

Moreover, the use of the null-space projection of the main robotic task for obstacle avoidance has been studied in the past [Lin *et al.*, 2016]. However, artificial potential field methods [Khatib, 1985] were used in these works. The main benefits of using SCBFs instead of artificial potential fields were discussed in [Salt Ducaju *et al.*, 2022], *i.e.*, SCBFs only modify the nominal behavior of the system when necessary. Additionally, the use of SCBFs in our formulation allows to explicitly take the dynamics of the robot into consideration when formulating the SCBF to guarantee adherence to the constraints [Rauscher *et al.*, 2016; Salt Ducaju *et al.*, 2022], thus avoiding potential constraint violations that may occur when only considering the robot kinematics in the formulation of SCBFs [Landi *et al.*, 2019; Ferraguti *et al.*, 2020; Benzi and Secchi, 2021], as illustrated by [Singletary *et al.*, 2021].

Furthermore, the proposed null-space compliance-varying controller achieved shared use of the only DOF available in the null-space of the main robot task, simultaneously, for obstacle avoidance and for the increase of the robot manipulability, thus benefiting human–robot collaborative applications. Also, the desired joint configuration in the proposed null-space controller was chosen as the closest configuration to the midpoints of the joints being $\xi_D = p(q_D)$. An alternative choice of desired joint configuration could be one where a performance index, such as the manipulability index [Khatib, 1987; Oh *et al.*, 1998], is maximized. However, depending on the task being executed, the manipulability index in [Khatib, 1987; Oh *et al.*, 1998] could be locally maximized close to a joint limit, leaving little or no margin for human guidance. In addition, the condition $\xi_D = p(q_D)$ used to set the null-space compliant behavior of the robot ensures the global asymptotic stability of the null-space motion based on Lemma 3.1 [Ott *et al.*, 2008].

Additionally, showing stability proofs for the null-space compliant motion of a robotic manipulator is challenging. In [Ott *et al*., 2008], the authors used the concept of conditional stability to propose a semi-definite Lyapunov function to prove the asymptotic stability of null-space motion. Our contribution consisted in adding a cross-term to the Lyapunov function candidate, in the same fashion as it was done in [Santibáñez and Kelly, 1997; Salt Ducaju *et al*., 2022] for non-redundant manipulators, to provide a stronger stability proof, *i.e.*, global asymptotic stability of the null-space motion. In addition, the stability of the variation of the null-space stiffness and damping coefficients has been shown by using a passive-energy storage method [Ferraguti *et al*., 2013], as was done in [Salt Ducaju *et al*., 2022] for Cartesian impedance control.

Finally, an interesting novelty of the here presented work with respect to [Salt Ducaju *et al*., 2022] is that the optimization problem is formulated with the variation of the compliance parameters as the optimization variables, which allowed us to express the necessary conditions for stability as inequality constraints (41), (44) of the QP problem, as well as ensured that the quadratic term of the QP problem is positive definite. Also, even though it has not been observed for the experiments described in Sec. 5, a hypothetical infeasibility of the QP problem would indicate the conditions for which a safety shutdown of the null-space motion was required, *e.g.*, if stability could not be ensured.

7. Conclusion

Safety in human–robot collaborative applications can be improved in a stable manner while keeping the main robotic Cartesian task unperturbed. For this, we proposed to modify the joint compliant behavior of a redundant robot projected in the null-space of the Cartesian task using SCBFs. In experiments with a 7-DOFs robot for a collaborative assembly application, we demonstrated that safety can be improved simultaneously to the optimization of the robot joint configuration in a single DOF.

References

Ames, A. D., S. Coogan, M. Egerstedt, G. Notomista, K. Sreenath, and P. Tabuada (2019). "Control barrier functions: Theory and applications". In: *European Control Conference (ECC)*. Jun. 25–28. Naples, Italy, pp. 3420–3431.

Benzi, F. and C. Secchi (2021). "An optimization approach for a robust and flexible control in collaborative applications". In: *IEEE International Conference on Robotics and Automation (ICRA)*. May 31–Jun. 4. Xi'an, China, pp. 3575–3581.

Dietrich, A., C. Ott, and A. Albu-Schäffer (2013). "Multi-objective compliance control of redundant manipulators: hierarchy, control, and stability". In: *IEEE/RSJ International Conference on Intelligent Robots and Systems (IROS)*. Nov. 3–7. Tokyo, Japan, pp. 3043–3050.

Ferraguti, F., M. Bertuletti, C. T. Landi, M. Bonfè, C. Fantuzzi, and C. Secchi (2020). "A control barrier function approach for maximizing performance while fulfilling to ISO/TS 15066 regulations". *IEEE Robotics and Automation Letters* **5**:4, pp. 5921–5928.

Ferraguti, F., C. Secchi, and C. Fantuzzi (2013). "A tank-based approach to impedance control with variable stiffness". In: *IEEE International Conference on Robotics and Automation (ICRA)*. May 6–10. Karlsruhe, Germany, pp. 4948–4953.

Forsgren, A., P. E. Gill, and M. H. Wright (2002). "Interior methods for nonlinear optimization". *SIAM Review* **44**:4, pp. 525–597.

Franka Emika (2019). *Franka Emika Panda – Data Sheet*. `https://www.generationrobots.com/media/panda-franka-emika-datasheet.pdf`. (Visited on 2022-09-13).

Hogan, N. (1985). "Impedance control: An approach to manipulation: Parts I–III". *Journal of Dynamic Systems, Measurement, and Control* **107**:1, pp. 1–24.

Khalil, H. K. (2014). *Nonlinear control*. Pearson Higher Ed., New York.

Khatib, O. (1985). "Real-time obstacle avoidance for manipulators and mobile robots". In: *IEEE International Conference on Robotics and Automation (ICRA)*. Vol. 2. Mar. 25–28. St. Louis, MO, USA, pp. 500–505.

Khatib, O. (1987). "A unified approach for motion and force control of robot manipulators: The operational space formulation". *IEEE Journal on Robotics and Automation* **3**:1, pp. 43–53.

Khatib, O. (1995). "Inertial properties in robotic manipulation: An object-level framework". *The International Journal of Robotics Research* **14**:1, pp. 19–36.

Kousi, N., G. Michalos, S. Aivaliotis, and S. Makris (2018). "An outlook on future assembly systems introducing robotic mobile dual arm workers". *Procedia CIRP* **72**, pp. 33–38.

Landi, C. T., F. Ferraguti, S. Costi, M. Bonfè, and C. Secchi (2019). "Safety barrier functions for human-robot interaction with industrial manipulators". In: *European Control Conference (ECC)*. Jun. 25–28. Naples, Italy, pp. 2565–2570.

Landi, C. T., F. Ferraguti, C. Fantuzzi, and C. Secchi (2018). "A passivity-based strategy for coaching in human-robot interaction". In: *IEEE International Conference on Robotics and Automation (ICRA)*. May 21–25. Brisbane, Australia, pp. 3279–3284.

Lin, H.-C., Y. Fan, T. Tang, and M. Tomizuka (2016). "Human guidance programming on a 6-DOF robot with collision avoidance". In: *IEEE/RSJ International Conference on Intelligent Robots and Systems (IROS)*. Oct. 9–14. Daejeon, Korea, pp. 2676–2681.

Lin, H.-C., C. Liu, Y. Fan, and M. Tomizuka (2017). "Real-time collision avoidance algorithm on industrial manipulators". In: *Conference on Control Technology and Applications (CCTA)*. Aug. 27–30. Kohala Coast, HI, USA, pp. 1294–1299.

Nakamura, Y. (1990). *Advanced robotics: redundancy and optimization*. Addison-Wesley, Reading, MA, USA.

Oh, Y., W. Chung, and Y. Youm (1998). "Extended impedance control of redundant manipulators based on weighted decomposition of joint space". *Journal of Robotic Systems* **15**:5, pp. 231–258.

Ott, C., A. Kugi, and Y. Nakamura (2008). "Resolving the problem of non-integrability of nullspace velocities for compliance control of redundant manipulators by using semi-definite Lyapunov functions". In: *IEEE International Conference on Robotics and Automation (ICRA)*. May 19–23. Pasadena, CA, USA, pp. 1999–2004.

Park, J. (2000). *Analysis and control of kinematically redundant manipulators: An approach based on kinematically decoupled joint space decomposition*. Doc. No. 991000372949703286. PhD thesis. Dept. Mech. Eng., Pohang University of Science and Technology, Pohang, South Korea.

Rauscher, M., M. Kimmel, and S. Hirche (2016). "Constrained robot control using control barrier functions". In: *IEEE/RSJ International Conference on Intelligent Robots and Systems (IROS)*. Oct. 9–14. Daejeon, Korea, pp. 279–285.

Salt Ducaju, J. M., B. Olofsson, A. Robertsson, and R. Johansson (2021). "Joint stiction avoidance with null-space motion in real-time model predictive control for redundant collaborative robots". In: *IEEE International Conference on Robot and Human Interactive Communication (RO-MAN)*. Aug. 8–12. Vancouver, Canada (Virtual), pp. 307–314.

Salt Ducaju, J. M., B. Olofsson, A. Robertsson, and R. Johansson (2022). "Robot Cartesian compliance variation for safe kinesthetic teaching using safety control barrier functions". In: *IEEE International Conference on Automation Science and Engineering (CASE)*. Aug. 20–24. Mexico City, pp. 2259–2266.

Santibáñez, V. and R. Kelly (1997). "Strict Lyapunov functions for control of robot manipulators". *Automatica* **33**:4, pp. 675–682.

Schou, C., J. Damgaard, S. Bøgh, and O. Madsen (2013). "Human-robot interface for instructing industrial tasks using kinesthetic teaching". In: *44th IEEE International Symposium on Robotics (ISR)*. Oct. 19–27. Seoul, Korea, pp. 1–6.

Siciliano, B. and O. Khatib (2016). *Springer Handbook of Robotics*. Springer, Berlin, Germany.

Singletary, A., S. Kolathaya, and A. D. Ames (2021). "Safety-critical kinematic control of robotic systems". *IEEE Control Systems Letters* **6**, pp. 139–144.

Stolt, A., M. Linderoth, A. Robertsson, and R. Johansson (2011). "Force controlled assembly of emergency stop button". In: *IEEE International Conference on Robotics and Automation (ICRA)*. May 9–13. Shanghai, China, pp. 3751–3756.

Wang, L., A. D. Ames, and M. Egerstedt (2017). "Safety barrier certificates for collisions-free multirobot systems". *IEEE Transactions on Robotics* **33**:3, pp. 661–674.

Paper VI

Model-Based Predictive Impedance Variation for Robot Obstacle Avoidance in Safe Human–Robot Collaboration

Julian M. Salt Ducaju Björn Olofsson Rolf Johansson

Abstract

Human–robot collaboration (HRC) in manufacturing environments requires that physical safety can be guaranteed. Control methods that implicitly regulate the interaction forces between a controlled robot and its environment, such as impedance control, are often used for safety in HRC. However, these methods could be complemented by restricting the robot operational space for additional safety guarantees. In this context, obstacle avoidance might benefit from considering a prediction of the controlled-robot motion and/or the behavior of the human collaborator. To this end, we proposed to include linearized Safety Control Barrier Functions (SCBFs) in a linear Model Predictive Control (MPC) strategy for robot impedance variation online. The convex optimization problem that was obtained from our proposal presented two advantages compared to nonlinear MPC alternatives. First, optimality was ensured in our method under linearity assumptions on human guidance and linearized robot dynamics, whereas a controller synthesized by nonlinear MPC strategies would depend on the fundamental characteristics of the problem. Second, our method enabled implementation at a faster control frequency, thus allowing a rapid adaptation to changes occurring in the robot environment. Finally, experimental validation was performed using a Franka Emika Panda robot in a human–robot collaborative scenario, and the stability of the method was shown using Lyapunov theory.

Submitted to review for publication in IEEE Transactions on Automation Science and Engineering.

Note to Practitioners

Modern-day industrial manufacturing environments are characterized by collaboration between human operators and robot manipulators. In this scenario, where humans and robots share workspace, physical safety is required. This research aims to improve safety in human–robot collaboration by proposing a novel robot control strategy. In our approach, the interaction forces between the controlled robot and its environment were regulated implicitly using impedance control, to allow, among other interactions, that an operator could manually guide the robot. Then, obstacle avoidance was included to modify the robot impedance behavior for restricting undesired collisions with, for example, the operator head, while ensuring stability of the method. Our main contribution is that the proposed formulation allows to consider a prediction of the robot motion and/or the operator behavior for robot obstacle avoidance. It was shown in experiments with a real robot that adding prediction capabilities reduced the risk of undesired collisions, while also decreasing the robot trajectory error. Moreover, the method could be implemented at a fast rate so that the robot could react rapidly to changes in its environment. Also, this implementation allowed to achieve a minimal variation with respect to the nominal impedance behavior of the robot. To conclude, this method is intended for scenarios where a robot is required to interact with its, possible restricted, environment: for example, a robot with a drill attached to its end-effector that is being guided to modify its trajectory, but where the operator should not be allowed to accidentally be harmed; or a robot performing a polishing task where a section of the polished object should remain unpolished. Therefore, a possible extension of this research would be, using the proposed robot control strategy, to provide an improved prediction of the human operator intention depending on the desired robotic task and the role of the operator.

1. Introduction

Former industrial settings, characterized by a fixed-structure workspace, present limitations when addressing current manufacturing trends, in which mass production has been replaced for mass customization, *i.e.*, smaller volumes of products are manufactured during shorter time frames [Schou *et al*., 2013]. As an attempt to improve human contribution, in terms of intelligence, dexterity, and responsiveness, in this rapidly changing industrial environment, human–robot collaboration (HRC) has increased its relevance in recent years [Cencen *et al*., 2018]. Several methods for HRC involve a physical interaction between humans and robots (pHRI), such as kinesthetic teaching [Wrede *et al*., 2013], where human guidance is used to modify a robot trajectory; or human–robot cooperation [Liu *et al*., 2021], where a robot provides proactive assistance to a human operator.

The most important requirement of any collaborative manufacturing scenario is that physical safety can be guaranteed for all humans, robots, and any other ac-

tor present in the shared workspace. To achieve this, indirect force control methods, such as impedance control [Hogan, 1985], are often used. Impedance control improves physical safety in HRC by implicitly regulating the interaction forces between the controlled robot and its environment, which also allows physical guidance of the robot. However, the interaction-force regulation achieved by an impedance-control strategy might not be sufficient to ensure safety in HRC applications, *e.g.*, if fragile equipment was located in the shared workspace, or if further protection was desired for the most sensitive body parts of human operators, such as their heads. In these scenarios, it is necessary to constrain the available operational space of the robot by creating restricted zones that the robot should avoid.

Safety Control Barrier Functions (SCBFs) [Ames *et al*., 2019] have been extensively used in recent years to bound the operational space of robot manipulators [Landi *et al*., 2019; Singletary *et al*., 2021; Ferraguti *et al*., 2020; Rauscher *et al*., 2016; Salt Ducaju *et al*., 2022] since they provide formal forward-invariance conditions to ensure that a robot does not leave a safe set of states, *i.e.*, a robot that started its motion in its allowed operational space would not invade a restricted zone. To achieve a minimally-invasive modification of the nominal behavior of the robot, SCBFs have been included as inequality constraints in a quadratic optimization (QP) problem whose goal was to minimize the difference between a nominal control signal and a control signal that would satisfy the safety requirements imposed by the SCBFs [Ames *et al*., 2019]. Convexity guarantees in this formulation ensured optimality, and allowed a fast execution of this safety strategy at the sampling frequency of the controlled robot, which can be as fast as 1 kHz. Moreover, in the context of HRC, SCBFs have been considered to adapt the acceleration of a robot depending on a human–robot separation distance [Ferraguti *et al*., 2020], resulting in a safety improvement for human–robot contacts. Then, regarding safety in pHRI, SCBFs have been considered to modify an impedance control structure for robot obstacle avoidance [Rauscher *et al*., 2016; Salt Ducaju *et al*., 2022].

Furthermore, so far, SCBF-based proposals to constrain the operational space of robot manipulators [Landi *et al*., 2019; Singletary *et al*., 2021; Ferraguti *et al*., 2020; Rauscher *et al*., 2016; Salt Ducaju *et al*., 2022] have been formulated as 1-step QP problem, thus not containing prediction capabilities regarding robot motion and/or the behavior of the operator. The advantages of prediction for collision avoidance have been studied for other types of robotic systems, such as legged robots [Grandia *et al*., 2021] and mobile robots [Zeng *et al*., 2021], where SCBFs were combined with Model Predictive Control (MPC) strategies to include longer temporal-horizon predictions for safety improvement. However, nonlinear MPC strategies were proposed in [Grandia *et al*., 2021; Zeng *et al*., 2021], which caused their optimization problem to depend on the fundamental characteristics of the problem, thus no guarantees for global optimality could be provided from the obtained solution. Additionally, the longer computational times of the nonlinear MPC strategies prevented their implementation at a fast rate, hence reducing the robots capacity to react to changes in their environment, which is especially relevant in safety-related robotic

scenarios.

In this paper, we address the problem of improving safety in HRC by considering a longer temporal-horizon prediction of the behavior of both the controlled robot and the human operator involved. To this end, we propose to vary the impedance behavior of a robot manipulator using a linear MPC strategy that includes the forward-invariance condition of a SCBF that is linearized at each time-step. The MPC formulation presented results in a convex QP problem that could be solved at the control rate of a real robot (1 kHz), while ensuring optimality in the proposed method under linearity assumptions on human guidance and linearized robot dynamics. Additionally, a Lyapunov function is used to provide global asymptotic stability guarantees and real experiments were performed to evaluate the method on a robot manipulator.

The paper is organized as follows: Sec. 2 introduces the dynamics model used for impedance control of the robot manipulator. Then, Sec. 3 presents a linearized barrier function for robot obstacle avoidance, which is used as a linear inequality constraint in the optimization problem developed in Sec. 4 for safe human–robot collaboration. The method proposed in Sec. 4 was evaluated in simulations, included in Section 5, and experiments with a real robot, presented in Section 6. Finally, a discussion is included in Sec. 7 and conclusions are drawn in Sec. 8.

2. Modeling

First, we show how a Cartesian impedance controller acting on the rigid-body dynamics of a robot can be written as a Linear Parameter-Varying (LPV) model.

2.1 Robot Rigid-Body Dynamics

The rigid-body dynamics of the robot can be written in the joint space of the robot, $q \in \mathbb{R}^n$, as [Siciliano and Khatib, 2016]

$$M(q)\ddot{q} + C(q,\dot{q})\dot{q} + G(q) = \tau + \tau^{\text{ext}} \tag{1}$$

where $M(q) \in \mathbb{R}^{n\times n}$ is the generalized inertia matrix, $C(q,\dot{q}) \in \mathbb{R}^{n\times n}$ describes the Coriolis and centripetal forces effects, $G(q) \in \mathbb{R}^n$ captures the gravity-induced torques, and $\tau \in \mathbb{R}^n$ represents the input torques, n being the number of joints of the robot. Finally, $\tau^{\text{ext}} \in \mathbb{R}^n$ represents the external torques.

Moreover, the rigid-body equation of the robot can be rewritten in terms of its end-effector pose $\xi \in \mathbb{R}^m$ which is composed by the end-effector's position and orientation:

$$M_\xi(q)\ddot{\xi} + C_\xi(q,\dot{q})\dot{\xi} + G_\xi(q) = F + F^{\text{ext}} \tag{2}$$

where $F \in \mathbb{R}^m$ is the input force, and, for a fully-actuated nonredundant robot

($n = m$), $M_\xi \in \mathbb{R}^{m\times m}$, $C_\xi \in \mathbb{R}^{m\times m}$, and $G_\xi \in \mathbb{R}^m$ are equal to

$$M_\xi = J^{-\mathrm{T}}(q)M(q)J^{-1}(q) \tag{3}$$

$$C_\xi = J^{-\mathrm{T}}(q)(C(q,\dot{q}) - M(q)J^{-1}(q)\dot{J}(q))J^{-1}(q) \tag{4}$$

$$G_\xi = J^{-\mathrm{T}}(q)G(q) \tag{5}$$

assuming that the Jacobian relative to the base frame of the robot, $J(q) \in \mathbb{R}^{m\times m}$, has full rank [Khatib, 1987].

2.2 Robot Impedance Control

To achieve a Cartesian impedance control of the robot end-effector [Hogan, 1985], *i.e.*, a mass-spring-damper relationship between the Cartesian pose variation from its reference, $\Delta\xi = \xi_d - \xi$ (ξ_d being the Cartesian pose reference) and the external Cartesian force F^{ext},

$$F^{\text{ext}} = M_\xi(q)\ddot{\xi} + (C_\xi(q,\dot{q}) + D)\dot{\xi} - K\Delta\xi \tag{6}$$

the input force F in Eq. (2) should be equal to

$$F = K\Delta\xi - D\dot{\xi} + G_\xi(q) \tag{7}$$

where $K \in S^m_{++}$ and $D \in S^m_{++}$ (S_{++} denoting symmetric positive-definiteness) are diagonal matrices that represent the control-induced stiffness and damping, respectively.

REMARK The control-induced inertia was chosen equal to the robot inertia $M_\xi(q)$ to avoid inertia shaping [Ott, 2008, Ch. 3.2], so that the input force F would not require feedback from the external forces. □

Moreover, by choosing the state vector as $x = [\Delta\xi^{\mathrm{T}}, \Delta\dot{\xi}^{\mathrm{T}}]^{\mathrm{T}} \in \mathbb{R}^{2m}$, the linearized system is

$$\dot{x} = A(q,\dot{q})x + B(q)u \tag{8}$$

where the input $u \in \mathbb{R}^m$ is equal to

$$u = F^{\text{ext}} \tag{9}$$

and the matrices that define the system are equal to

$$A = \begin{bmatrix} 0_m & I_m \\ -M_\xi^{-1}(q)K & -M_\xi^{-1}(q)(C_\xi(q,\dot{q}) + D) \end{bmatrix} \tag{10}$$

$$B = \begin{bmatrix} 0_m \\ -M_\xi^{-1}(q) \end{bmatrix} \tag{11}$$

where $I_m \in \mathbb{R}^{m\times m}$ represents an identity matrix, and $M_\xi(q)$ is invertible since $J(q)$ is also invertible [Salt Ducaju *et al*., 2022, Lemma III.1].

Furthermore, the impedance control resulting in Eq. (8) can be shown to be globally asymptotically stable [Salt Ducaju *et al*., 2022]. For completeness, a short version of the proof is provided here, see [Salt Ducaju *et al*., 2022, Lemma III.2] for an extended version of this proof.

PROPOSITION 1
The time-varying Lyapunov function

$$V(x,t) = \frac{1}{2}\Delta\dot{\xi}^{\mathrm{T}} M_\xi(q)\Delta\dot{\xi} + \frac{1}{2}\Delta\xi^{\mathrm{T}} K\Delta\xi + \alpha\Delta\xi^{\mathrm{T}} M_\xi(q)\Delta\dot{\xi} \tag{12}$$

where $x = \left[\Delta\xi^{\mathrm{T}}, \quad \Delta\dot{\xi}^{\mathrm{T}}\right]^{\mathrm{T}}$ shows the global asymptotic stability of the impedance robot behavior in Eq. (6) for $\alpha > 0$ satisfying

$$\min\left(\sqrt{\frac{\lambda_{m,K}}{\lambda_{M,M_\xi}}},\ \frac{2\lambda_{m,K}}{\lambda_{M,D}},\ \frac{\lambda_{m,D}}{2(\lambda_{M,M_\xi} + k_C||\Delta\xi||)}\right) > \alpha \tag{13}$$

where $\lambda_{m,\Pi}$ and $\lambda_{M,\Pi}$ are the smallest and largest eigenvalues of a matrix Π, respectively, and k_C is a positive constant such that for all $x, y, z \in \mathbb{R}^n$ [Santibáñez and Kelly, 1997]

$$||C_\xi(x,y)z|| \leq k_C||y||||z|| \tag{14}$$

□

Proof. The Lyapunov candidate (12) is strictly positive for

$$\alpha < \sqrt{\frac{\lambda_{m,K}}{\lambda_{M,M_\xi}}} \tag{15}$$

Moreover, considering that the matrix $\dot{M}_\xi(q) - 2C_\xi(q,\dot{q})$ is skew symmetric [Ott, 2008, Ch. 2], the time-derivative of the Lyapunov candidate (12) is equal to

$$\begin{aligned}\dot{V}(x) = &-\alpha\Delta\xi^{\mathrm{T}} C_\xi(q,\dot{q})\Delta\dot{\xi} + \alpha\Delta\dot{\xi}^{\mathrm{T}} M_\xi(q)\Delta\dot{\xi} \\ &- \Delta\dot{\xi}^{\mathrm{T}} D\Delta\dot{\xi} - \alpha\Delta\xi^{\mathrm{T}} K\Delta\xi + \alpha\Delta\xi^{\mathrm{T}} D\Delta\dot{\xi}\end{aligned} \tag{16}$$

Then, defining the upper bound on certain terms:

$$-\Delta\dot{\xi}^{\mathrm{T}} D\Delta\dot{\xi} \leq -\frac{1}{2}\Delta\dot{\xi}^{\mathrm{T}} D\Delta\dot{\xi} - \frac{1}{2}\lambda_{m,D}\left|\left|\Delta\dot{\xi}\right|\right|^2 \tag{17}$$

$$\alpha\Delta\dot{\xi}^{\mathrm{T}} M_\xi(q)\Delta\dot{\xi} \leq \alpha\lambda_{M,M_\xi}\left|\left|\Delta\dot{\xi}\right|\right|^2 \tag{18}$$

$$-\alpha\Delta\xi^{\mathrm{T}} C_\xi(q,\dot{q})\Delta\dot{\xi} \leq \alpha k_C\left|\left|\Delta\xi\right|\right|\left|\left|\Delta\dot{\xi}\right|\right|^2 \tag{19}$$

it follows that

$$\begin{aligned}\dot{V}(x) \leq & -\frac{1}{2}\left[\Delta\dot{\xi} - \alpha\Delta\xi\right]^{\mathrm{T}} D\left[\Delta\dot{\xi} - \alpha\Delta\xi\right] \\ & + \alpha\Delta\xi^{\mathrm{T}}\left[\tfrac{\alpha}{2}D - K\right]\Delta\xi - \frac{1}{2}\lambda_{m,D}\left|\left|\Delta\dot{\xi}\right|\right|^2 \\ & + \alpha k_C\left|\left|\Delta\xi\right|\right|\left|\left|\Delta\dot{\xi}\right|\right|^2 + \alpha\lambda_{M,M_\xi}\left|\left|\Delta\dot{\xi}\right|\right|^2 \end{aligned} \tag{20}$$

which is equivalent to

$$\dot{V}(x) \leq -\frac{1}{2}\left[\Delta\dot{\xi} - \alpha\Delta\xi\right]^{\mathrm{T}} D\left[\Delta\dot{\xi} - \alpha\Delta\xi\right] \tag{21}$$

for

$$\min\left(\frac{2\lambda_{m,K}}{\lambda_{M,D}},\ \frac{\lambda_{m,D}}{2(\lambda_{M,M_\xi} + k_C||\Delta\xi||)}\right) > \alpha \tag{22}$$

Therefore, if $\alpha > 0$ satisfies (13), the Lyapunov candidate function $V(x)$ is strictly positive and its time-derivative $\dot{V}(x)$ is strictly negative. □

Additionally, since $M_\xi(q), K, D \in S^m_{++}$, a passive map from the external force F^{ext} to $\Delta\dot{\xi}$ is guaranteed,

$$\begin{aligned}\dot{V} &< \Delta\dot{\xi}^{\mathrm{T}} F^{\text{ext}} - \frac{1}{2}\left[\Delta\dot{\xi} - \alpha\Delta\xi\right]^{\mathrm{T}} D\left[\Delta\dot{\xi} - \alpha\Delta\xi\right] \\ &< \Delta\dot{\xi}^{\mathrm{T}} F^{\text{ext}} \end{aligned} \tag{23}$$

where the passivity condition valid for passive environments is

$$V(x,t) - V(x,0) < \int_0^t \Delta\dot{\xi}^{\mathrm{T}}(\tau) F^{\text{ext}}(\tau)\mathrm{d}\tau \tag{24}$$

3. Robot Obstacle Avoidance

Robot obstacle avoidance can be achieved by defining a safe set of robot states and ensuring that the robot would stay inside this set. For this, a barrier function $h : \mathscr{D} \to \mathbb{R}$ was defined for all $x \in \mathscr{D} \subset \mathbb{R}^{2m}$ based on the condition that the distance from the robot position, $\rho(x) \in \mathbb{R}^3$, to an obstacle located at position $\rho_{\text{obs}} \in \mathbb{R}^3$ would always be greater than or equal to a safety distance $D_s \in \mathbb{R}$ as

$$h(x) = ||\rho(x) - \rho_{\text{obs}}|| - D_s \geq 0 \tag{25}$$

which is equivalent to

$$h(x) = (\rho(x) - \rho_{\text{obs}})^2 - D_s^2 \geq 0 \tag{26}$$

The forward-invariance of the safe set $\mathscr{C} \subseteq \mathscr{D}$ defined by the barrier function in (26),

$$\mathscr{C} = \{x \in \mathbb{R}^{2m} \mid h(x) \geq 0\} \tag{27}$$

can be ensured if the following inequality constraint is satisfied [Ames *et al.*, 2019]

$$\dot{h}(x) + \gamma h(x) \geq 0 \tag{28}$$

where $\gamma > 0$.

Moreover, the forward-invariance condition (28) of the safe set $\mathscr{C}$ can be rewritten for a variable $z = [\rho^{\mathrm{T}}, \dot{\rho}^{\mathrm{T}}]^{\mathrm{T}}$ as a quadratic constraint

$$z^{\mathrm{T}} A_z z + B_z z + C_z \geq 0 \tag{29}$$

where

$$A_z = \begin{bmatrix} \gamma I_3 & I_3 \\ I_3 & 0_3 \end{bmatrix} \tag{30}$$

$$B_z = -2\rho_{\mathrm{obs}}^{\mathrm{T}} \begin{bmatrix} \gamma I_3, & I_3 \end{bmatrix} \tag{31}$$

$$C_z = \gamma(\rho_{\mathrm{obs}}^{\mathrm{T}} \rho_{\mathrm{obs}} - D_s^2) \tag{32}$$

which is equivalent to a quadratic inequality constraint in x

$$x^{\mathrm{T}} A_x x + B_x x + C_x \geq 0 \tag{33}$$

since

$$z = \begin{bmatrix} \rho_d \\ 0_{3\times 1} \end{bmatrix} - T_x x \tag{34}$$

where

$$T_x = \begin{bmatrix} I_3 & 0_3 & 0_3 & 0_3 \\ 0_3 & 0_3 & I_3 & 0_3 \end{bmatrix} \tag{35}$$

and ρ_d is the Cartesian position reference. Also, $0_m \in \mathbb{R}^{m\times m}$ represents a zero matrix.

Furthermore, since including a quadratic constraint would cause an optimization problem to be a Quadratically Constrained Quadratic Program (QCQP), which is NP-hard in its general case, the quadratic inequality constraint (29) was linearized around $z_{\mathrm{int}} = [\rho_{\mathrm{int}}^{\mathrm{T}}, 0]^{\mathrm{T}}$, ρ_{int} being the intersection between the vector $\overrightarrow{\rho_{\mathrm{obs}}\rho}$ and a sphere with center at ρ_{obs} and radius equal to the safety distance D_s. Since this sphere-vector pair would intersect at two points, ρ_{int} would be chosen as the closest of these two points to the position of the robot, ρ. The linearized inequality constraint is equal to

$$(\rho_{\mathrm{int}} - \rho_{\mathrm{obs}})^{\mathrm{T}} \left(\begin{bmatrix} I_3, & \frac{1}{\gamma} I_3 \end{bmatrix} z - \rho_{\mathrm{int}} \right) \geq 0 \tag{36}$$

which is equivalent to a linear inequality constraint in x (34)

$$A_{\mathrm{BF}} x \leq b_{\mathrm{BF}} \tag{37}$$

with

$$A_{\mathrm{BF}} = (\rho_{\mathrm{int}} - \rho_{\mathrm{obs}})^{\mathrm{T}} \left[I_3, \quad \tfrac{1}{\gamma} I_3 \right] T_x \tag{38}$$

$$b_{\mathrm{BF}} = (\rho_{\mathrm{int}} - \rho_{\mathrm{obs}})^{\mathrm{T}} (\rho_d - \rho_{\mathrm{int}}) \tag{39}$$

REMARK The linear inequality constraint (37) satisfies the forward-invariance condition in Eq. (28) of the safe set $\mathscr{C}$, and is equivalent to linearizing a protective surface that was defined using an impedance variable equal to $\left[I_3, \quad \tfrac{1}{\gamma} I_3 \right] z$ around the obstacle. □

4. Model Predictive Variable Impedance (MPVI) Controller

A linear model predictive controller was designed to vary the impedance behavior of a robot using the safety condition of Eq. (37) defined in Sec. 3 to allow robot obstacle avoidance for safe HRC.

4.1 Optimization Problem

The proposed model predictive controller solves, at every sampling step k, an optimization problem that minimizes the difference between the behavior of the robot and a reference impedance behavior defined by reference states x^r and inputs u^r throughout a prediction horizon h_p. This is equivalent to the minimization of the cost function

$$L(U_{k,p}) = \sum_{i=k+1}^{k+h_p} \Big[(x_i^r - x_i)^{\mathrm{T}} Q (x_i^r - x_i) + (u_{i-1}^r - u_{i-1})^{\mathrm{T}} R (u_{i-1}^r - u_{i-1}) \Big] \tag{40}$$

with $Q \in S_{++}^{2m}$ and $R \in S_{++}^{m}$ being symmetric positive-definite matrices that penalize, respectively, the system states and inputs variation from their impedance reference at every time step. Also, $U_{k,p} = [u_k^{\mathrm{T}}, \ldots, u_{k+h_p-1}^{\mathrm{T}}]^{\mathrm{T}} \in \mathbb{R}^{mh_p}$ is the sequence of computed inputs to the system throughout the control horizon (which was chosen to have the same length as the prediction horizon, $h_c = h_p$).

The minimization of the cost function in Eq. (40) was subject to two types of constraints. First, the robot should exhibit impedance properties. To this purpose, the continuous-time impedance model of the robot of Eq. (8) was discretized using a zero-order hold (ZOH) [Åström and Wittenmark, 2013] sampling method

$$x_{k+j} = \Phi x_{k+j-1} + \Gamma u_{k+j-1} \tag{41}$$

with

$$\Phi = e^{AT_s}, \ \Gamma = \int_0^{T_s} e^{As} \mathrm{d}s B \tag{42}$$

and T_s being the sampling period of the system, which affects the duration of the prediction horizon.

Second, obstacle avoidance was implemented in the optimization problem as an inequality constraint to ensure that the states of the system fulfilled the linearized condition for forward-invariance of Eq. (37) of the safe set $\mathscr{C}$ at every time-step over the prediction horizon

$$A_{\mathrm{BF}} x_{k+j} \leq {}^{j}b_{\mathrm{BF}} \tag{43}$$

REMARK The inequality constraint (43) might take different values for each time-step $k+j$ of the prediction horizon since ${}^{j}b_{\mathrm{BF}}$ would depend on the, possibly time-varying, position reference ρ_d, as seen in Eq. (39). □

As a summary, the optimization problem solved at every time-step k in the proposed Model Predictive Variable Impedance (MPVI) formulation is

$$\begin{aligned} U^*_{k,p} = \min_{U_{k,p}} \ & L(U_{k,p}) \\ \text{s.t. } & x_{k+j} = \Phi x_{k+j-1} + \Gamma u_{k+j-1}, \\ & A_{\mathrm{BF}} x_{k+j} \leq {}^{j}b_{\mathrm{BF}} \ \forall \ j \in [1, \ldots, h_p] \end{aligned} \tag{44}$$

4.2 Human-Guidance Force Estimation

In addition to the estimation of the robot motion provided by the equality constraint in Eq. (41), a prediction of human behavior can be included in the optimization problem. To this end, a linear model was chosen to describe the temporal variation of the external force throughout the prediction horizon of the MPC. In discrete time, the external force was modeled by

$$F^{\mathrm{ext}}_{k+j} = F^{\mathrm{ext}}_{k} + r_k (t_{k+j} - t_k) \tag{45}$$

where r_k is related to the estimated rate of change of this signal over the prediction horizon at every sampling step k.

Moreover, the prediction of $F^{\mathrm{ext}}_{k+j} \ \forall \ j \in [1, \ldots, h_p]$ determined, using Eq. (9), the reference input sequence,

$$U^r_{k,p} = \left[(u^r_k)^{\mathrm{T}}, \ldots, (u^r_{k+h_p-1})^{\mathrm{T}} \right]^{\mathrm{T}} \in \mathbb{R}^{m h_p} \tag{46}$$

used in the cost function of Eq. (40), as shown in the continuous-time input (9) of the impedance-controlled system. Additionally, the reference state sequence,

$$X^r_{k,p} = \left[(x^r_{k+1})^{\mathrm{T}}, \ldots, (x^r_{k+h_p})^{\mathrm{T}} \right]^{\mathrm{T}} \in \mathbb{R}^{2 m h_p} \tag{47}$$

determined by the desired impedance properties of Eq. (41) and the reference input sequence $U^r_{k,p}$.

4.3 Optimality

PROPOSITION 2

An analytic expression for the optimal solution to the optimization problem presented in Eq. (44) can be derived. □

Proof. The optimization problem of Eq. (44) could be expressed as a function of the entire sequence of states over the prediction horizon,

$$X_{k,p} = [x_{k+1}^{\mathrm{T}}, \ldots, x_{k+h_p}^{\mathrm{T}}]^{\mathrm{T}} \in \mathbb{R}^{2mh_p} \tag{48}$$

Then, the equality constraint (41) is equivalent to

$$X_{k,p} = M_p U_{k,p} + N_p x_k \tag{49}$$

with $M_p \in \mathbb{R}^{2mh_p \times mh_p}$ and $N_p \in \mathbb{R}^{2mh_p \times 2m}$ being

$$M_p = \begin{bmatrix} \Gamma & 0 & \ldots & 0 \\ \Phi\Gamma & \Gamma & & 0 \\ \vdots & \vdots & \ddots & \vdots \\ \Phi^{h_p-1}\Gamma & \Phi^{h_p-2}\Gamma & \ldots & \Gamma \end{bmatrix}, \; N_p = \begin{bmatrix} \Phi \\ \vdots \\ \Phi^{h_p} \end{bmatrix} \tag{50}$$

Moreover, the safety condition in Eq. (43) is equivalent to

$${}^{p}A_{\mathrm{BF}} X_{k,p} \leq {}^{p}b_{\mathrm{BF}} \tag{51}$$

with ${}^{p}A_{\mathrm{BF}} \in \mathbb{R}^{h_p \times h_p}$ and ${}^{p}b_{\mathrm{BF}} \in \mathbb{R}^{h_p}$ being

$${}^{p}A_{\mathrm{BF}} = \mathrm{diag}\left([A_{\mathrm{BF}}, \ldots, A_{\mathrm{BF}}]\right) \tag{52}$$

$${}^{p}b_{\mathrm{BF}} = [{}^{1}b_{\mathrm{BF}}, \ldots, {}^{h_p}b_{\mathrm{BF}}]^{\mathrm{T}} \tag{53}$$

where $\mathrm{diag}(\cdot)$ forms a block diagonal matrix from a given list of matrices. Also, Eq. (51) is equivalent, in terms of the sequence $U_{k,p}$ of inputs over the prediction horizon, to

$$T U_{k,p} \leq W_1 + W_2 x_k \tag{54}$$

where

$$T = {}^{p}A_{\mathrm{BF}} M_p, \; W_1 = {}^{p}b_{\mathrm{BF}}, \; W_2 = -{}^{p}A_{\mathrm{BF}} N_p \tag{55}$$

Additionally, if these expressions are rewritten in terms of the error dynamics

$$\tilde{U}_{k,p} = U_{k,p}^{r} - U_{k,p}, \; \tilde{X}_{k,p} = X_{k,p}^{r} - X_{k,p} \tag{56}$$

the cost function of Eq. (40) is equivalent to

$$L(\tilde{U}_{k,p}) = \tilde{X}_{k,p}^{\mathrm{T}} Q_p \tilde{X}_{k,p} + \tilde{U}_{k,p}^{\mathrm{T}} R_p \tilde{U}_{k,p} \tag{57}$$

where $Q_p = \text{diag}\left(\left[Q,\ldots,Q\right]\right) \in \mathbb{R}^{2mh_p \times 2mh_p}$ and $R_p = \text{diag}\left(\left[R,\ldots,R\right]\right) \in \mathbb{R}^{mh_p \times mh_p}$ and the inequality constraint (54) could be rewritten as:

$$T_{\text{e}}\tilde{U}_{k,p} \leq W_{1,\text{e}} + W_{2,\text{e}}\tilde{x}_k \tag{58}$$

where

$$T_{\text{e}} = -T,\ W_{1,\text{e}} = W_1 - U^r_{k,p} + W_2 x^r_k,\ W_{2,\text{e}} = -W_2 \tag{59}$$

Finally, since the system reference ($X^r_{k,p}$ and $U^r_{k,p}$) followed the same desired impedance behavior that was imposed as an equality constraint of Eq. (41) of the optimization problem, the equality constraint in terms of the error dynamics is equivalent to

$$\tilde{X}_{k,p} = M_p\tilde{U}_{k,p} + N_p\tilde{x}_k \tag{60}$$

for M_p and N_p defined in (50).

Once the optimization problem (44) has been expressed in terms of its error dynamics sequence, it is straightforward to see that the cost function of Eq. (57), when considering the equality constraint (60), is equal to

$$L_u(\tilde{U}_{k,p}) = \tilde{U}^{\text{T}}_{k,p}F\tilde{U}_{k,p} + 2\tilde{U}^{\text{T}}_{k,p}G\tilde{x}_k + \tilde{x}^{\text{T}}_k H\tilde{x}_k \tag{61}$$

for

$$F = M^{\text{T}}_p Q_p M_p + R_p,\ G = M^{\text{T}}_p Q_p N_p,\ H = N^{\text{T}}_p Q_p N_p \tag{62}$$

Then, Lagrange multipliers λ_k could be used to form the Lagrangian [Johansson, 2020]

$$L(\tilde{U}_{k,p}) = \tilde{U}^{\text{T}}_{k,p}F\tilde{U}_{k,p} + 2\tilde{U}^{\text{T}}_{k,p}G\tilde{x}_k + \tilde{x}^{\text{T}}_k H\tilde{x}_k + 2\lambda^{\text{T}}_k\left(T_{\text{e}}\tilde{U}_{k,p} - W_{1,\text{e}} - W_{2,\text{e}}\tilde{x}_k\right) \tag{63}$$

By completion of squares, this expression is equal to

$$\begin{aligned} L(\tilde{U}_{k,p}) = &\left(\tilde{U}_{k,p} + F^{-1}\begin{bmatrix}G, & T^{\text{T}}_{\text{e}}\end{bmatrix}\begin{bmatrix}\tilde{x}_x \\ \lambda_k\end{bmatrix}\right)^{\text{T}} F\left(\tilde{U}_{k,p} + F^{-1}\begin{bmatrix}G, & T^{\text{T}}_{\text{e}}\end{bmatrix}\begin{bmatrix}\tilde{x}_x \\ \lambda_k\end{bmatrix}\right) \\ &- \begin{bmatrix}\tilde{x}_k \\ \lambda_k\end{bmatrix}^{\text{T}}\left(\begin{bmatrix}G, & T^{\text{T}}_{\text{e}}\end{bmatrix}^{\text{T}} F^{-1}\begin{bmatrix}G, & T^{\text{T}}_{\text{e}}\end{bmatrix}\right)\begin{bmatrix}\tilde{x}_k \\ \lambda_k\end{bmatrix} + \tilde{x}^{\text{T}}_k H\tilde{x}_k \\ &- 2\lambda^{\text{T}}_k\left(W_{1,\text{e}} + W_{2,\text{e}}\tilde{x}_k\right) \end{aligned} \tag{64}$$

Therefore, the optimal control sequence is equal to

$$\tilde{U}^*_{k,p} = -F^{-1}\begin{bmatrix}G, & T^{\text{T}}_{\text{e},k}\end{bmatrix}\begin{bmatrix}\tilde{x}_k \\ \lambda^*_k\end{bmatrix} \tag{65}$$

where only the inequality constraints that were active at time-step k were considered ($T_{\text{e},k}$ and λ^*_k). The minimal cost function

$$\min L(\tilde{U}_{k,p}) = L(\tilde{U}^*_{k,p}) = \tilde{x}^{\text{T}}_k\left(H - G^{\text{T}}F^{-1}G\right)\tilde{x}_k + \left(\lambda^*_k\right)^{\text{T}} T_{\text{e},k}F^{-1}T^{\text{T}}_{\text{e},k}\lambda^*_k \tag{66}$$

was obtained from the optimal control sequence of Eq. (65). □

4.4 Stability in Error Dynamics

PROPOSITION 3
Asymptotic stability guarantees for the error dynamics of the proposed method can be provided. □

Proof. Since the equality constraint of the optimization problem in Eq. (41) ensures that both the obtained solution and the reference behavior of the system (defined by the state and input references, x^r and u^r), followed the desired robot impedance behavior, the error dynamics could be described with:

$$\dot{\tilde{x}} = A(q,\dot{q})\tilde{x} + B(q)(u^r - u) \tag{67}$$

where

$$\tilde{x} = x^r - x = \left[\widetilde{\Delta\xi}^{\mathrm{T}}, \dot{\widetilde{\Delta\xi}}^{\mathrm{T}}\right]^{\mathrm{T}} \tag{68}$$

Moreover, the Lyapunov function that was used to show the global asymptotic stability for the system dynamics in Eq. (8) can also be used to show the global asymptotic stability for the system error dynamics by replacing x for $\tilde{x}$ in Eq. (12):

$$V(\tilde{x},t) = \frac{1}{2}\dot{\widetilde{\Delta\xi}}^{\mathrm{T}} M_\xi(q)\dot{\widetilde{\Delta\xi}} + \frac{1}{2}\widetilde{\Delta\xi}^{\mathrm{T}} K\widetilde{\Delta\xi} + \alpha\Delta\xi^{\mathrm{T}} M_\xi(q)\dot{\widetilde{\Delta\xi}} \tag{69}$$

for analogous conditions on $\alpha > 0$ as the ones in Eq. (13). □

5. Simulations

We started the empirical evaluation of the MPVI method by performing simulations with a two-dimensional double integrator system, which might be used for robot manipulators if their maximally-allowed accelerations are conservatively chosen [Bäuml *et al*., 2010; Ghazaei Ardakani *et al*., 2019]. The input $u \in \mathbb{R}^2$ to this system was equal to the acceleration of the system

$$u = \ddot{\rho} \in \mathbb{R}^2 \tag{70}$$

with the system's position being $\rho = [\rho_x, \rho_y]^{\mathrm{T}} \in \mathbb{R}^2$. Additionally, analogous to the impedance controller for the robot dynamics in Eq. (7), an impedance behavior could be achieved for the double-integrator model with

$$u = u_0 + \Delta u,\ \ u_0 = K\Delta\rho - D\dot{\rho},\ \ \Delta\rho = \rho_d - \rho \tag{71}$$

such that the continuous-time impedance behavior of the system, with state vector $x = [\Delta\rho^{\mathrm{T}}, \Delta\dot{\rho}^{\mathrm{T}}]^{\mathrm{T}} \in \mathbb{R}^4$ was modeled by

$$\dot{x} = \begin{bmatrix} 0_2 & I_2 \\ -K & -D \end{bmatrix} x + \begin{bmatrix} 0_2 \\ -I_2 \end{bmatrix} \Delta u \tag{72}$$

where $K = kI_2$ and $D = dI_2$, with $k, d > 0$.

Moreover, for the simulations performed, it was desired that a system with initial position $\rho_0 = [0,0]^{\mathrm{T}}$ followed a trajectory determined by a constant speed of 0.4 m/s along each direction, which yielded a position reference at each discrete time-step k equal to:

$$\rho_{d,k} = \rho_{d,k-1} + 0.4 \begin{bmatrix} 1 \\ 1 \end{bmatrix} T_s \tag{73}$$

with T_s being the discrete-sampling period of the system, which was chosen as 0.1 s for this simulation. The MPVI controller of Eq. (44) was used to achieve robot obstacle avoidance, and the resulting optimization problem was solved using the convex optimization solver CVXGEN [Mattingley and Boyd, 2012]. For this simulation, the obstacle was located at $\rho_{\mathrm{obs}} = \left[2, 1.5\right]^{\mathrm{T}}$ m, with a safety distance of $D_s = 0.5$ m.

Furthermore, the control-induced stiffness and damping were chosen as $k = 1$ and $d = 1/\gamma$ for $\gamma = 1.5$ and the total simulation time was 10 s. Also, regarding the parameters of the MPC optimization problem, the control and prediction horizons were chosen as $h_p = h_c = 10$, and the states and input penalization with respect to their reference in the cost function of Eq. (40) were $Q = I_4$ and $R = 0.1I_2$, respectively.

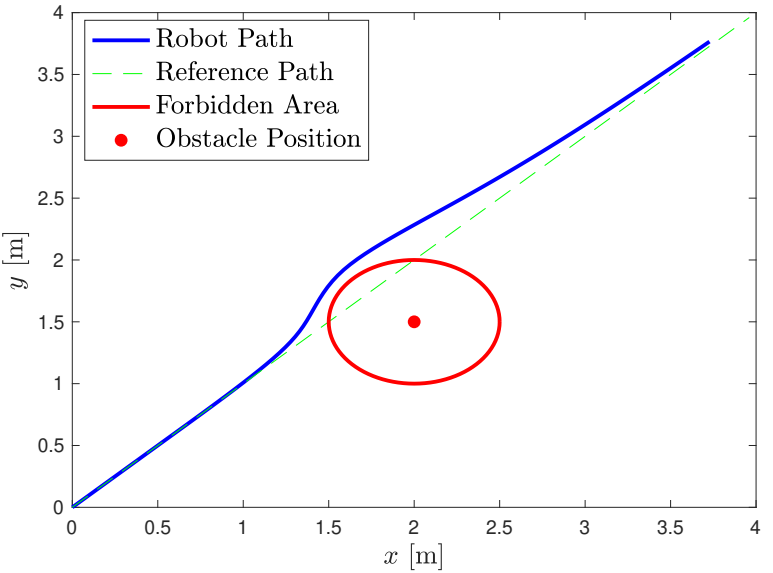

Figure 1. Simulated path traversed by the robot compared to its reference path.

Figures 1 and 2 show the simulation results of modifying the impedance behavior of a two-dimensional double integrator for robot obstacle avoidance using MPVI. Determined by the MPVI controller, the system closely followed the reference until a detour was commanded to avoid the forbidden area that surrounded the obstacle (Fig. 1). Once the commanded detour was not needed anymore for obstacle avoidance, the system was able to converge to its nominal path. Additionally, the input commanded to the system is shown in Fig. 2. The conservative acceleration values seen in this figure justified the use of a double integrator model for this simulation.

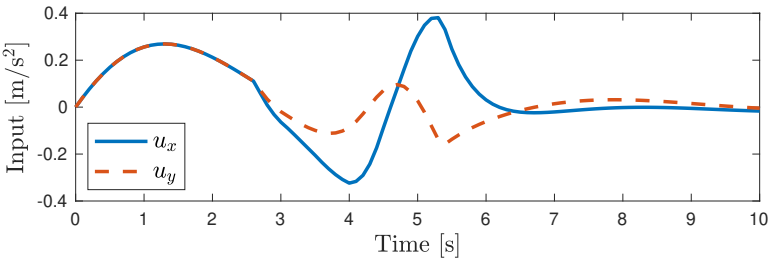

Figure 2. Temporal evolution of the input signal throughout the simulation.

6. Experiments

We extended the empirical evaluation of the proposed method with a series of experiments performed with a real robot in an experimental setup that allowed human–robot collaboration. The MPVI solution was compared to a previous formulation [Salt Ducaju *et al.*, 2022] where prediction was not considered, to highlight the benefits of using a model-predictive scheme in these collaborative applications.

6.1 Experimental Setup

The experimental setup that was used to evaluate the method on a real robot consisted of a Franka Emika Panda robot [*Panda – Data Sheet* 2019] mounted on a table (as seen in Fig. 3). This robot has seven rotational joints, $n = 7 > 6 = m$, so, the last joint was locked at $\theta_7 = \pi/2$ rad, and only the first six joints of the robot were controlled. In addition, the controller was running at the sampling rate of the Panda robot, equal to 1 kHz, using a single PC (Intel Xeon CPU E3-1245, 3.7 GHz, 4 cores, 64-bit), and CVXGEN [Mattingley and Boyd, 2012] was used to obtain the optimal control of Eq. (65).

Moreover, the nominal robot impedance that enabled HRC by allowing an operator to guide the robot was defined by a control-induced stiffness, K in Eq. (7),

Figure 3. A human–robot collaborative scenario where an operator was guiding a Franka Emika Panda robot mounted on a table.

equal to 150 N/m for the translational degrees of freedom and equal to 10 N/rad for the rotational degrees of freedom, and a control-induced damping, D in Eq. (7), equal to $2\sqrt{K}$ for all degrees of freedom [Karlsson *et al.*, 2018].

Furthermore, regarding the parameters of the MPC optimization problem for the experiments, both the control and the prediction horizons lasted 1 s, divided into ten discrete-time steps ($h_p = h_c = 10$) that were equally spaced at 0.1 s. Also, the penalization of the states and inputs with respect to their reference in the cost function of Eq. (40) was chosen as $Q = I_6$ and $R = 0.1I_3$, respectively, and all the experiments presented lasted 10 s, $t \in [0, t_{\max} = 10]$ s.

6.2 Robot Obstacle Avoidance in Free Motion and Influence of the Selection of γ

The behavior of the robot was evaluated for a scenario where, in the absence of external guidance force, the nominal impedance behavior of the robot would have resulted in an unmodified robot path, ρ_{un}, that collided with an obstacle, as shown in Fig. 4. Figure 4 also shows the 3D plot of the path ρ, traversed by the MPVI-controlled robot. The initial position of the robot relative to its base frame was equal to $\rho_0 = [0.358, -0.2, 0.395]$ m, and the final position of the robot was equal to $\rho_{\text{F}} = \rho_0 + \Delta\rho$ for $\Delta\rho = [0.1, 0.5, 0.1]$ m. The position reference of Eq. (6) of the robot was defined to increase linearly with time

$$\rho_d(t) = \rho_0 + \frac{\Delta\rho}{t_{\max}} t \tag{74}$$

Also, the obstacle was placed at $\rho_{\text{obs}} = [0.4, 0.0, 0.45]$ m and the safety distance was equal to $D_s = 0.05$ m.

As seen in Fig. 4, the MPVI-based strategy was able to avoid any collision between the robot and the obstacle. Additionally, this controller allowed that the path followed by the robot converged toward the unmodified path, ρ_{un}, once the robot passed the obstacle. Moreover, it is also observed in Fig. 4 that the selection of γ in the forward-invariance condition in Eq. (28) of the safe set $\mathscr{C}$ had a significant influence on the behavior of the MPVI-controlled robot, *i.e.*, a higher value of γ yielded a less conservative solution, where the robot got closer to the obstacle during the trajectory execution. Indeed, this observation was supported when the temporal evolution of the barrier function h of Eq. (26) was analyzed, as depicted in Fig. 5. Even though the MPVI-solution avoided the obstacle for all the analyzed values of γ, it can be seen in Fig. 5 that the robot motion was less conservative for higher values of γ.

Furthermore, Fig. 6 shows the difference in the commanded forces to the robot, F in Eq. (2), along each Cartesian direction depending on the choice of γ compared to the unperturbed impedance solution with no robot obstacle avoidance. Selecting a higher value of γ allowed the robot to achieve a less conservative solution where a smaller deviation with respect to the nominal impedance behavior, both in terms of the amount of time deviating from the nominal impedance behavior, and in terms of the magnitude of the deviation, was observed.

6.3 Comparison with a 1-step Solution in Free Motion

The collision-avoidance situation in free motion described in Sec. 6.2 was used for comparing the MPVI solution with respect to a 1-step formulation [Salt Ducaju *et al.*, 2022], which was also executed at the sampling frequency of the robot, *i.e.*, 1 kHz. The same value of $\gamma = 5$ in Eq. (28) was used for both formulations. The advantages of considering a prediction of the robot motion for robot obstacle avoidance were apparent in this situation.

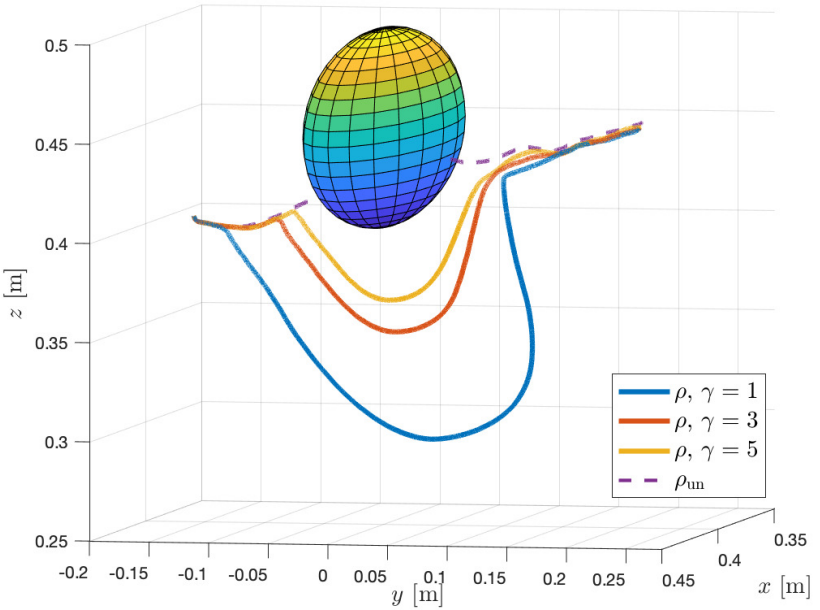

Figure 4. 3D rendering of the path ρ traversed by the end-effector of the MPC-controlled robot for different values of γ (28). The unmodified path, ρ_{un}, showed the path that the robot would follow with its nominal impedance behavior. The plotted sphere was centered at the obstacle position ρ_{obs} and its radius was equal to the safety distance D_s.

First, the MPVI-controlled robot was able to stay less time at risk by acting earlier to modify the nominal impedance behavior, as shown in Fig. 7, where the temporal evolution of the velocity of the robot end-effector is depicted. It can be seen in Fig. 7 that before $t = 4$ s, the MPVI-controlled robot had started to move away from the obstacle, while the 1-step controller commanded the robot to keep a velocity close to zero in all its components until after $t = 6$ s.

Moreover, the robot-motion prediction, combined with the utilization of the temporal evolution of the desired impedance behavior of the robot throughout the prediction horizon, allowed the MPVI controller to reduce the trajectory error. This is seen in Fig. 8, which showed a comparison of the trajectory of the MPVI formulation and the 1-step formulation with respect to the unperturbed, *i.e.*, without collision avoidance, impedance behavior of the robot. The MPVI controller was able to provide a closer tracking of the reference impedance trajectory, which was quantified using the Mean Absolute Error (MAE) between the nominal (unperturbed) and

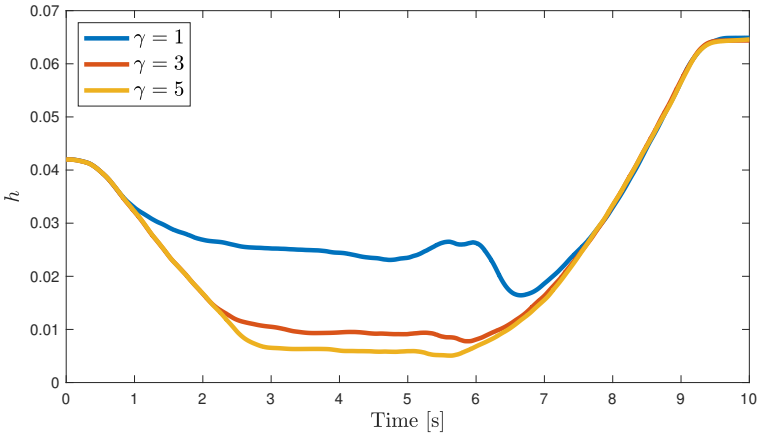

Figure 5. Temporal evolution of the barrier function h in Eq. (26) throughout the experiment for different values of γ in Eq. (28).

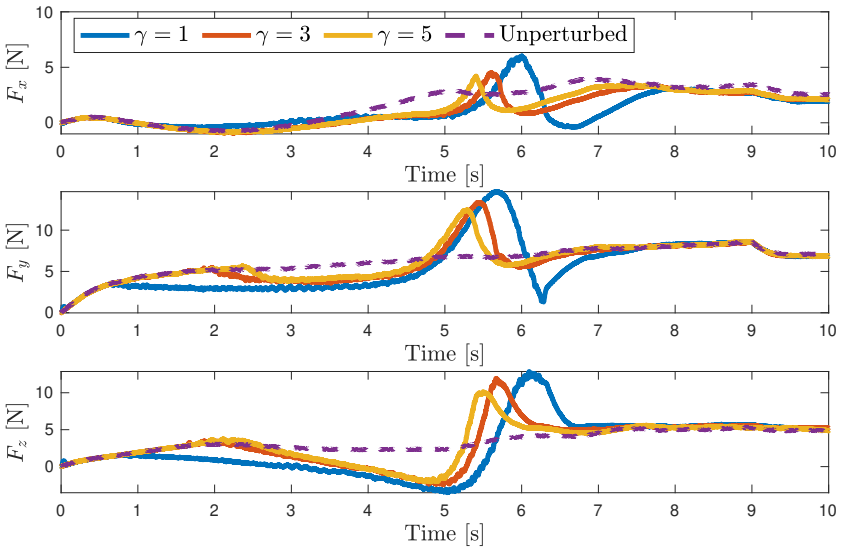

Figure 6. Commanded force F in Eq. (2) to the robot along each Cartesian direction x, y, z throughout the experiment for different values of γ in Eq. (28).

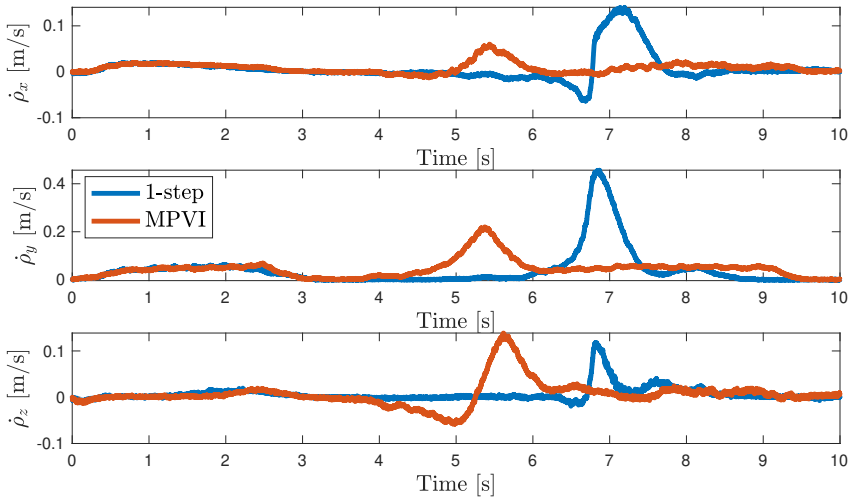

Figure 7. Temporal evolution of the velocity of the robot end-effector along each Cartesian direction x, y, z for the MPVI-controlled robot compared to a 1-step controller formulation [Salt Ducaju *et al.*, 2022].

the actual position of the robot end-effector

$$\text{MAE}(\rho) = \frac{\sum_{k=0}^{N} |\rho_{\text{un},k} - \rho_k|}{N} \tag{75}$$

where $N = f \cdot t_{\max}$ and $f = 1000$ Hz since experimental data were recorded in these experiments at the sampling rate of the Panda robot (1 kHz). For the trajectory described in Fig. 8, the position MAE of the 1-step controller was 0.0553 m, whereas the position MAE of the MPVI controller was 0.0185 m, which implied a reduction of 66.5% of the position MAE.

Additionally, it should be highlighted that not only did the MPVI controller execute a collision-avoidance strategy earlier than the 1-step alternative, but also, since it was able to consider a prediction of the robot motion and the desired robot behavior throughout its prediction horizon, the MPVI controller could pursue a different, and better, path for obstacle avoidance than its 1-step counterpart.

6.4 External Force Prediction

An additional advantage of the MPVI strategy is that it could include a prediction model of the external force applied to the robot by a human operator guiding it throughout its prediction horizon, which could be used to improve the performance of the system. The low-complexity linear model for external force prediction introduced in Sec. 4.2 was evaluated and compared to a model that considered a con-

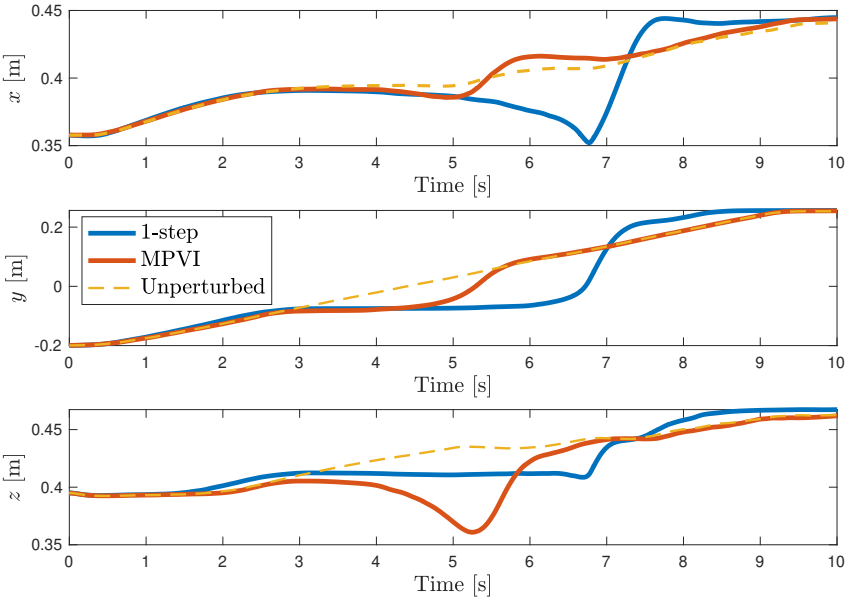

Figure 8. Trajectory followed by the robot end-effector along Cartesian direction x, y, z for both the predictive controller (MPVI) and a 1-step controller [Salt Ducaju *et al.*, 2022], with respect to the unperturbed, nominal, impedance behavior.

stant external force throughout the entire prediction horizon. For this constant-force model, both the value of the external force at the current time and a zero value of the external force were considered as its constant value.

Additionally, the linear model could be estimated using available sensor data prior to the estimation time:

$$\hat{F}^{\text{ext}}_{t|t_k} = F^{\text{ext}}_{t_k} + r_k(t - t_k) \tag{76}$$

where $\hat{F}^{\text{ext}}_{t|t_k}$ is the prediction made at time t_k of the value of the external force at time t. The slope r_k of the linear model was chosen proportional to the Cartesian acceleration of the robot at time t_k, which was recalculated at the sampling rate of the robot using a least-squares method that considered the previous $N_r = 10$ values of the Cartesian acceleration as a moving average to avoid the detrimental effects of measurement noise,

$$r_k \propto \frac{\sum_{i=1}^{N_r}(t_{k-i} - \bar{t}_{N_r})(\ddot{\rho}_{k-i} - \overline{\ddot{\rho}}_{N_r})}{\sum_{i=1}^{N_r}(t_{k-i} - \bar{t}_{N_r})^2} \tag{77}$$

where $\bar{t}_{N_r}$ and $\overline{\ddot{\rho}}_{N_r}$ are, respectively, the averages of t_{k-i} and $\ddot{\rho}_{k-i}$ for $i \in [1, \ldots, N_r]$.

Moreover, the accuracy of the different models proposed to estimate the guidance force was studied for a situation where an operator was trying to move the robot away from its nominal trajectory. Because of the impedance behavior of the robot with respect to its reference, the operator would be required to apply a greater force to move the robot away from its nominal trajectory, the further away the robot was positioned with respect to this trajectory. Therefore, the external force would be expected to increase linearly in this scenario. To evaluate the accuracy of these models used to predict the external force, the MAE between the predicted and the actual external force was computed for each time step j of the prediction horizon h_p as

$$\mathrm{MAE}\left(\hat{F}_j^{\mathrm{ext}}\right) = \frac{\sum_{k=0}^{N} \left|\hat{F}_{k+0.1f\cdot j|k}^{\mathrm{ext}} - F_{k+0.1f\cdot j}^{\mathrm{ext}}\right|}{N} \tag{78}$$

where $j = [1, \ldots, h_p]$, $N = f \cdot t_{\max}$, and $f = 1000$ Hz because of the sampling rate of the robot, as in Eq. (75). The external-force MAE for the different estimation models is shown in Fig. 9 for an experiment where the guidance force was exerted along the negative z-direction.

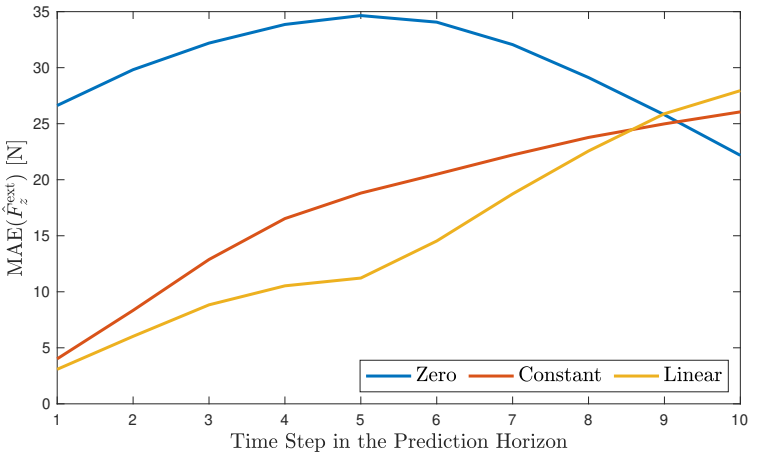

Figure 9. Mean Absolute Error (MAE) of the predicted external force along the negative z-direction throughout the MPVI prediction horizon for different models.

As seen in Fig. 9, the linear model slightly outperformed the constant model that used the initial external force measurement as its constant value. Also, both of these models clearly outperformed the constant zero model, except for the last time-steps of the prediction horizon, where the current state of the robot was not useful for predicting the external force. Moreover, the advantage of using the linear model with respect to the constant model became more evident when analyzing the temporal

evolution of the predicted external force in each of these two models compared to the measured force, as seen in Fig. 10, where the results of the prediction of the human guidance situation for a prediction time of 0.5 s ($j = 5$) are shown.

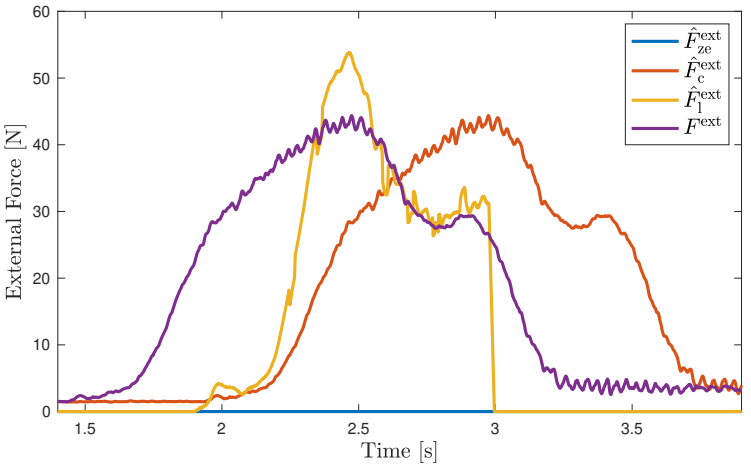

Figure 10. Predicted external force for a human-guidance situation along the negative z-direction. F^{ext} denotes the measured external force and $\hat{F}^{\text{ext}}_{\text{ze}}$, $\hat{F}^{\text{ext}}_{\text{c}}$, and $\hat{F}^{\text{ext}}_{\text{l}}$ denote the zero, constant, and linear predictions of the external force, respectively, for a prediction time of 0.5 s.

As expected, the constant model appeared as a delayed version of the measured external force signal, with a delay equal to the prediction time, which was equal to 0.5 s in Fig. 10. On the other hand, the linear model was able to achieve a faster response to the changes in the measured external force, which might be useful for safety-critical scenarios.

6.5 Comparison with a 1-step Solution during Human Guidance

To obtain a fair comparison between the proposed MPVI controller and a 1-step controller in a human-guidance situation, the same external force should be applied to the robot for each of these two controllers. To this end, a simulated guidance force $f_s(t)$ was used. The simulated force $f_s(t)$ consisted of a sinusoidal signal with an amplitude of 30 N and a period of 3 s (to resemble the external force originated from human guidance seen in Fig. 10), and was applied to the robot along the negative z-direction

$$f_s(t) = -30\sin\Big(\frac{2\pi}{3}(t-2)\Big),\ t \in [2, 3.5]s \tag{79}$$

Moreover, the trajectory used to compare the MPVI solution to a 1-step controller in this human-guidance situation considered that the initial position of the robot was $\rho_0 = [0.357, -0.2, 0.395]$ m, and that the desired position of the robot varied linearly (Eq. (74)) during 10 s until reaching the final reference position $\rho_F = [0.357, -0.2, 0.1]$ m. Additionally, the obstacle was positioned to intersect with the nominal trajectory: $\rho_{obs} = [0.357, -0.2, 0.2]$ m with radius equal to $D_s = 0.05$ m.

Figure 11 shows the 3D plot of the path ρ_{MPVI} traversed by the robot controlled using the MPVI formulation, compared with the path obtained when using a 1-step controller alternative without predictive capabilities, ρ_{ONE}. It can be seen that, for the human-guidance scenario illustrated in Fig. 11, the longer-time prediction of the robot motion and the guidance force allowed the MPVI-controlled robot to circuit the obstacle, whereas when the robot was controlled using a 1-step formulation it got stuck in the surroundings of the obstacle.

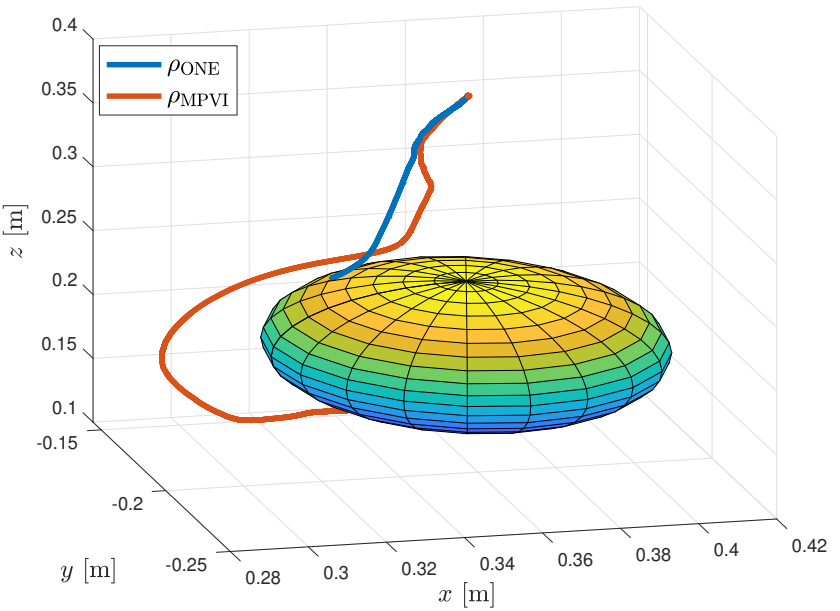

Figure 11. 3D rendering of the path traversed by the robot end-effector controlled using MPVI, ρ_{MPVI}, compared to the path traversed by the robot end-effector controlled using a 1-step controller, ρ_{ONE}, when a simulated guidance force f_s in (79) was applied to the robot along the negative z-direction. The plotted sphere was centered at the obstacle position ρ_{obs} and its radius was equal to the safety distance D_s.

6.6 Human Guidance for an Assembly Task in the Presence of an Obstacle

The proposed MPVI controller was evaluated in a collaborative scenario that involved human guidance with an obstacle present in the shared workspace. Manual guidance of a robot could be used to correct the Cartesian reference, ξ_d in Eq. (6), for a robot assembly task after the requirements of this task had changed, *e.g.*, a peg-in-hole task where the position of the hole had changed. Additionally, a camera mounted on the same table as the robot was present in the shared workspace to be used for visual quality inspection of the workpieces involved in the assembly [Zhou *et al.*, 2022]. From the human-guidance perspective, an accidental collision between the camera and the guided robot should be avoided to refrain from any damage to the camera or the other workpieces and to obtain a valid manual correction for the robot trajectory. An overview of the experimental scenario is shown in Fig. 12.

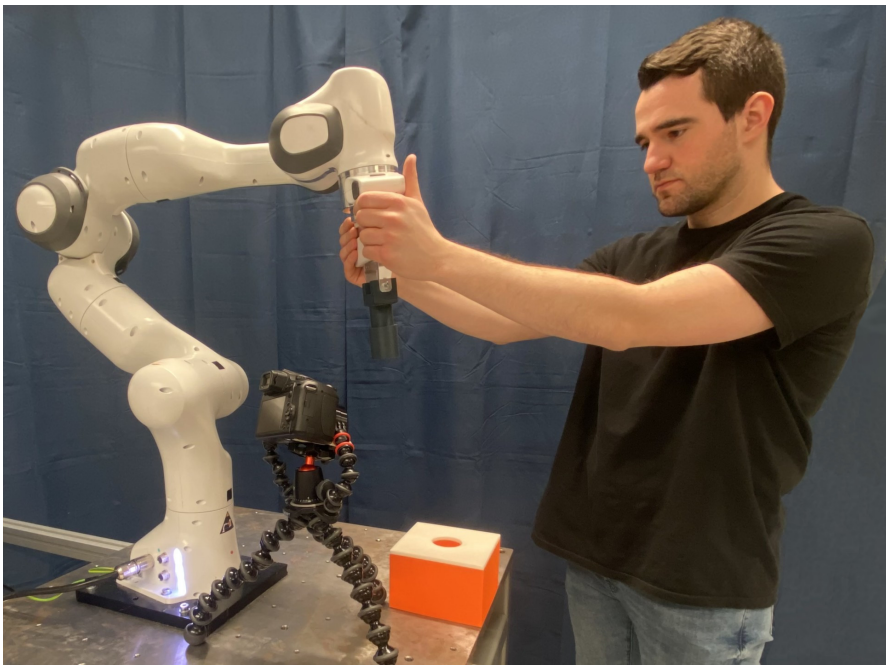

Figure 12. A human–robot collaborative scenario where the operator was guiding the robot to teach a peg-in-hole task in the presence of an obstacle (a camera).

In this experimental scenario, the human operator was instructed to manually guide the robot to achieve its task completion, *i.e.*, the insertion of the peg in the hole, in the shortest time and path possible. However, the presence of the camera in the shared workspace would condition the manual tra-

jectory correction. The initial position of the robot relative to its base frame was equal to $\rho_0 = [0.3, -0.19, 0.683]$ m, and the position reference of the robot varied linearly (Eq. (74)) during 10 s until reaching the final reference position $\rho_F = [0.087, 0.34, -0.55]$ m. Also, the camera was placed at $\rho_{obs} = [0.38, 0.0, 0.33]$ m and the safety distance was equal to $D_s = 0.2$ m.

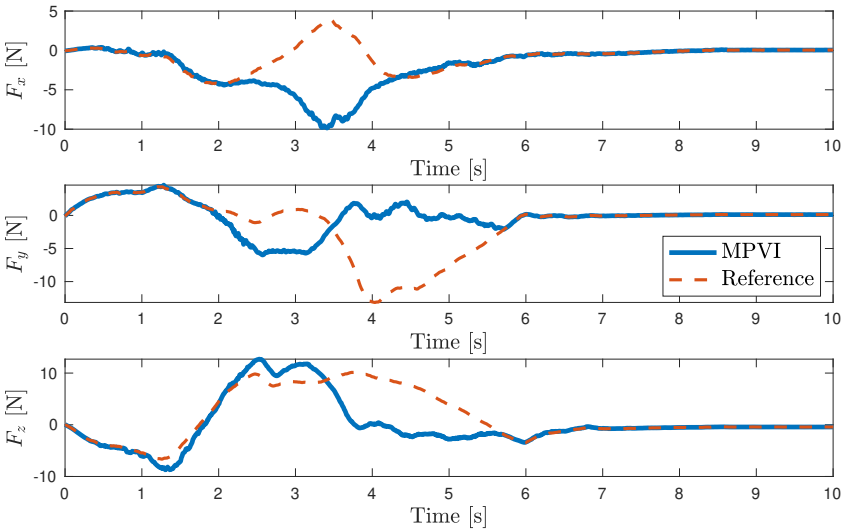

Figure 13. Input force, F in Eq. (2), commanded to the robot by the MPVI controller of Eq. (44) compared to the reference robot impedance behavior Eq. (7) for an assembly task in the presence of an obstacle.

A comparison between the input force, F in Eq. (2), commanded to the robot when using the proposed MPVI controller, and the reference robot impedance behavior for this collaborative scenario was shown in Fig. 13. It can be seen in Fig. 13 that the MPVI controller allowed the robot to behave in an equal manner to the reference robot impedance behavior, until a force input variation was necessary to avoid that the peg would invade the safety distance with respect to the camera. Then, it is also shown in Fig. 13 that after the manually-guided robot stopped being at a risk-of-collision situation, the MPVI controller allowed the robot to resume the reference robot impedance behavior.

Moreover, the external force recorded from human manual guidance for this collaborative scenario is shown in Fig. 14. It can be seen in Fig. 14 the response of the human operator to the robot impedance variation commanded by the MPVI controller. Additionally, the prediction of the external force obtained using the linear model in Eqs. (76) and (77) is shown in Fig. 14 for a time ($t = 1.5$ s) when the MPVI

controller started to command a robot impedance that differed from its reference to achieve obstacle avoidance. It can be observed in Fig. 14 that the linear model accurately predicted (with a MAE at $t = 1.5$ s equal to 1.4 N for the entire prediction horizon) the guidance force applied by the human operator at this time.

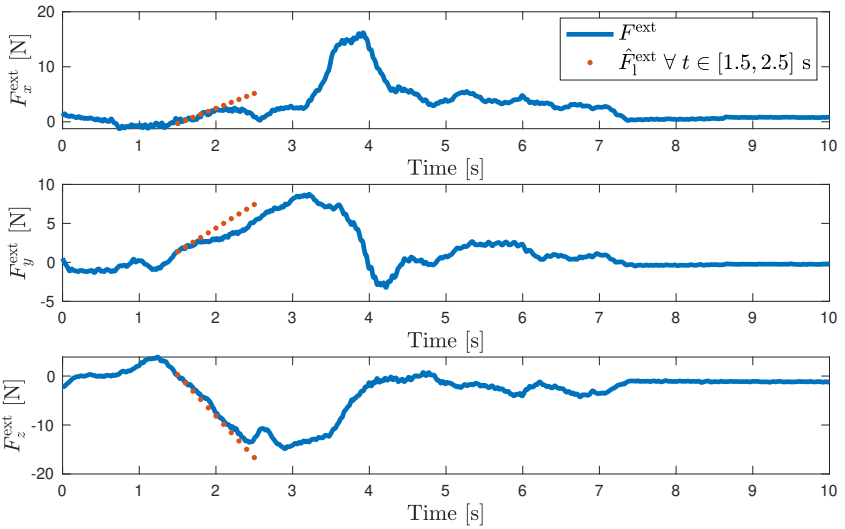

Figure 14. External force recorded from the manual correction for an assembly task in the presence of an obstacle, and prediction at time $t = 1.5$ for the external force between $t = 1.5$ s and $t = 2.5$ s using the linear model in Eqs. (76) and (77).

Furthermore, the optimization problem formulated in Eq. (44) for the proposed MPVI controller took on average 95.8 μs to solve for this experiment, with a standard deviation of 20.6 μs, using a single PC with the hardware specifications described in Sec. 6.1.

7. Discussion

In this paper, we have proposed an approach to include SCBFs in a linear MPC strategy so that a longer-time horizon prediction could be considered for safety in HRC. The advantages in terms of safety obtained by considering a prediction of both the motion of the controlled robot manipulator and the human collaborator, compared to 1-step formulations [Salt Ducaju *et al.*, 2022], were shown in the experimental evaluation presented in Sec. 6. First, this prediction allowed a reduction of the trajectory error and decreased the time where a risk of obstacle-collision was present. Additionally, the prediction capabilities of the proposed method prevented

that the controlled robot would get stuck near an obstacle and allowed the robot to converge to its nominal trajectory.

Moreover, the linear MPC considered in our method satisfied the forward-invariance condition of Eq. (28) for the set of robot states that guaranteed safety during HRC, and resulted in a convex QP problem that was solved within the control frequency of a real robot, *i.e.*, in less than 1 ms, which is significantly faster than the computational time of previously proposed nonlinear, nonconvex, MPC formulations, *i.e.*, around 40 Hz [Grandia *et al.*, 2021] and 35 Hz [Zeng *et al.*, 2021]. Also, multi-layer strategies where a slow nonlinear MPC solution was combined with a faster 1-step QP problem solved at the control frequency of a robot (400 Hz in [Grandia *et al.*, 2021]), would not allow the use of a longer-time prediction at a fast rate to rapidly adapt to changes in the robot environment.

Additionally, the control signal obtained from a nonlinear MPC would depend on the characteristics of the problem, whereas, as shown in Sec. 4.3, optimality was guaranteed in our proposal under linearity assumptions on human guidance and linearized robot dynamics, to achieve convexity in the optimization problem formulated in Eq. (44). It becomes apparent that inaccuracies occurring when modeling the dynamic behavior of the robot and the manual robot guidance might compromise the performance of the proposal. However, in Sec. 6, the proposed formulation that includes such linearity assumptions was experimentally evaluated in robot obstacle avoidance scenarios, and suitable results were obtained both in the presence of manual robot guidance and in its absence.

Furthermore, it should be mentioned that the guidance force that would be exerted by a human operator cannot always be predicted. The experimental validation provided in Sec. 6 showed how a non-complex linear model could be used to predict the temporal variation of the external force signal based on sensor data recorded at previous time-steps. However, previous sensor data might not always provide an accurate prediction, *e.g.*, it can be seen in Fig. 10, how the external-force data recorded before human interaction had started could not be used to predict the increase in external force shown in this figure. Additionally, an accurate prediction of early instances of human guidance force was achieved using this linear model for a collaborative scenario in the presence of an obstacle, as shown in Fig. 14. Accurately predicting such increases in guidance force would allow anticipatory action for safety-critical scenarios. However, the prediction for other instances of human guidance might not be as accurate, as shown in Fig. 9, which provided the external force MAE for an entire human guidance event. Nevertheless, more complex strategies that incorporate further information regarding the intention of the human operator [Wong *et al.*, 2023; Liu *et al.*, 2021], and/or consider biomechanical models of the human operator and measure its muscle activity [Peternel and Ajoudani, 2023], could be integrated with our method to improve the prediction of physical human–robot interaction.

8. Conclusion

Safety in HRC can be improved by considering a longer temporal-horizon prediction of the motion of the controlled robot and the human-collaborator guidance. To this purpose, the impedance behavior of a robot manipulator was varied, in a stable manner, by including linearized SCBFs for robot obstacle avoidance in a linear MPC strategy that ensured optimality. Our MPC-based proposal was evaluated in experiments using a real robot manipulator that was controlled at a fast rate (1 kHz) to allow a fast reaction to changes occurring in the robot environment. These experiments showed that adding prediction capabilities to a robot controller led to a reduced time at risk of collision, improved obstacle bypassing, and decreased the trajectory error caused by obstacle avoidance.

References

Ames, A. D., S. Coogan, M. Egerstedt, G. Notomista, K. Sreenath, and P. Tabuada (2019). "Control barrier functions: Theory and applications". In: *European Control Conference (ECC)*. Jun. 25–28. Naples, Italy, pp. 3420–3431.

Åström, K. J. and B. Wittenmark (2013). *Computer-Controlled Systems: Theory and Design*. Courier Corporation, Chelmsford, MA, USA.

Bäuml, B., T. Wimböck, and G. Hirzinger (2010). "Kinematically optimal catching a flying ball with a hand-arm-system". In: *IEEE/RSJ International Conference on Intelligent Robots and Systems (IROS)*. Oct. 18–22. Taipei, Taiwan, pp. 2592–2599.

Cencen, A., J. C. Verlinden, and J. Geraedts (2018). "Design methodology to improve human-robot coproduction in small-and-medium-sized enterprises". *IEEE/ASME Transactions on Mechatronics* **23**:3, pp. 1092–1102.

Ferraguti, F., M. Bertuletti, C. T. Landi, M. Bonfè, C. Fantuzzi, and C. Secchi (2020). "A control barrier function approach for maximizing performance while fulfilling to ISO/TS 15066 regulations". *IEEE Robotics and Automation Letters* **5**:4, pp. 5921–5928.

Ghazaei Ardakani, M., B. Olofsson, A. Robertsson, and R. Johansson (2019). "Model predictive control for real-time point-to-point trajectory generation". *IEEE Transactions on Automation Science and Engineering* **16**:2, pp. 972–983.

Grandia, R., A. J. Taylor, A. D. Ames, and M. Hutter (2021). "Multi-layered safety for legged robots via control barrier functions and model predictive control". In: *IEEE International Conference on Robotics and Automation (ICRA)*. May 31–Jun. 4. Xi'an, China, pp. 8352–8358.

Hogan, N. (1985). "Impedance control: An approach to manipulation: Parts I–III". *Journal of Dynamic Systems, Measurement, and Control* **107**:1, pp. 1–24.

Johansson, R. (2020). *Model-Based Predictive and Adaptive Control*. KFS Studentbokhandel, Lund, Sweden.

Karlsson, M., A. Robertsson, and R. Johansson (2018). "Convergence of dynamical movement primitives with temporal coupling". In: *European Control Conference (ECC)*. Jun. 12–15. Limassol, Cyprus, pp. 32–39.

Khatib, O. (1987). "A unified approach for motion and force control of robot manipulators: The operational space formulation". *IEEE Journal on Robotics and Automation* **3**:1, pp. 43–53.

Landi, C. T., F. Ferraguti, S. Costi, M. Bonfè, and C. Secchi (2019). "Safety barrier functions for human-robot interaction with industrial manipulators". In: *European Control Conference (ECC)*. Jun. 25–28. Naples, Italy, pp. 2565–2570.

Liu, T., E. Lyu, J. Wang, and M. Q.-H. Meng (2021). "Unified intention inference and learning for human–robot cooperative assembly". *IEEE Transactions on Automation Science and Engineering* **19**:3, pp. 2256–2266.

Mattingley, J. and S. Boyd (2012). "CVXGEN: A code generator for embedded convex optimization". *Optimization and Engineering* **12**:1, pp. 1–27.

Ott, C. (2008). *Cartesian impedance control of redundant and flexible-joint robots*. Springer, Berlin, Germany.

Panda – Data Sheet (2019). Franka Emika.

Peternel, L. and A. Ajoudani (2023). "After a decade of teleimpedance: a survey". *IEEE Transactions on Human-Machine Systems* **53**:2, pp. 401–416.

Rauscher, M., M. Kimmel, and S. Hirche (2016). "Constrained robot control using control barrier functions". In: *IEEE/RSJ International Conference on Intelligent Robots and Systems (IROS)*. Oct. 9–14. Daejeon, Korea, pp. 279–285.

Salt Ducaju, J. M., B. Olofsson, A. Robertsson, and R. Johansson (2022). "Robot Cartesian compliance variation for safe kinesthetic teaching using safety control barrier functions". In: *IEEE International Conference on Automation Science and Engineering (CASE)*. Aug. 20–24. Mexico City, pp. 2259–2266.

Santibáñez, V. and R. Kelly (1997). "Strict Lyapunov functions for control of robot manipulators". *Automatica* **33**:4, pp. 675–682.

Schou, C., J. Damgaard, S. Bøgh, and O. Madsen (2013). "Human-robot interface for instructing industrial tasks using kinesthetic teaching". In: *44th IEEE International Symposium on Robotics (ISR)*. Oct. 19–27. Seoul, Korea, pp. 1–6.

Siciliano, B. and O. Khatib (2016). *Springer Handbook of Robotics*. Springer, Berlin, Germany.

Singletary, A., S. Kolathaya, and A. D. Ames (2021). "Safety-critical kinematic control of robotic systems". *IEEE Control Systems Letters* **6**, pp. 139–144.

Wong, C. Y., L. Vergez, and W. Suleiman (2023). "Vision-and tactile-based continuous multimodal intention and attention recognition for safer physical human–robot interaction". *IEEE Transactions on Automation Science and Engineering*.

Wrede, S., C. Emmerich, R. Grünberg, A. Nordmann, A. Swadzba, and J. Steil (2013). "A user study on kinesthetic teaching of redundant robots in task and configuration space". *Journal of Human-Robot Interaction* **2**:1, pp. 56–81.

Zeng, J., B. Zhang, and K. Sreenath (2021). "Safety-critical model predictive control with discrete-time control barrier function". In: *American Control Conference (ACC)*. May 25–28. New Orleans, LA, USA, pp. 3882–3889.

Zhou, L., L. Zhang, and N. Konz (2022). "Computer vision techniques in manufacturing". *IEEE Transactions on Systems, Man, and Cybernetics: Systems* **53**:1, pp. 105–117.

How to control robots to collaborate with humans?

Julian M. Salt Ducaju
Department of Automatic Control

Popular science summary of the doctoral dissertation *Control Strategies for Physical Human–Robot Collaboration*, June 2024. The thesis can be downloaded from
http://www.control.lth.se/publications

During the First Industrial Revolution, craftsmen were replaced with machines. Later, throughout the second half of the twentieth century, robots were adopted to replace factory workers and automate industry. Over all these years, productivity in manufacturing increased by capitalizing technological development, at the expense of human workers, who saw their relevance in manufacturing environments decrease. Nevertheless, this trend might be disrupted in the upcoming years.

Industrial settings have become very structured environments to allow robots, and other machinery, to perform the same task repeatedly in a very efficiently manner to maximize production. This has resulted in the manufacturing industry being able to produce large amounts of identical products. However, structured industrial settings have the disadvantage of having difficulty adapting to changes, which is especially relevant considering the current industrial trends that focus on product customization.

Human–Robot Collaboration (HRC) has been proposed to improve how industrial environments adapt robot tasks to changes in production processes. The logical argument is the following: humans are intelligent, and robots are very good doing repetitive tasks and do not get tired in the process; then, why not combining their skills and get the best from each? This collaboration would ideally be as simple as having a human operator manually guiding the robot to teach a correction to the motion of the robot. However, the challenge of having a versatile industrial environment where humans are present is that unexpected events can occur. The goal of this thesis is to develop robot control methods to deal with these uncertainties to improve physical collaboration between humans and robots.

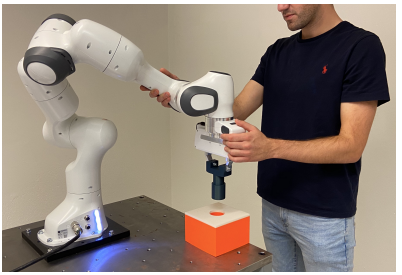

A human operator manually guiding a robot to teach a peg-in-hole task.

The robot control methods presented in this thesis have been focused on improving different aspects of physical HRC. First, robot guidance was facilitated from a human operator perspective by reducing uncertainties present in the amount of force

that the operator should apply to the robot for its guidance. The proposed method could avoid possible structural vibrations and wear of robot components that might occur using an alternative state-of-the-art strategy. Second, a method was developed to distinguish human guidance from an accidental contact between the robot and an obstacle, without the need for additional equipment. This method could be used for an effective modification of a robot task once the operator has finished demonstrating a correction, but also to modify the robot behavior while human guidance is occurring. Third, a strategy was developed for how a robot would learn from a human correction by making the robot execute its task several times, and each of these times using the difference between the robot motion and the human correction to modify the behavior of the robot.

Additionally, safety is mandatory in industrial scenarios, especially when humans are involved. For this reason, this thesis includes methods that allow human guidance of robots only in situations where robots, human operators, and any other object involved in the robot task would not be at risk of collision. With the proposed methods, the human operator guiding the robot would be able to feel how the robot stiffens if there was a risk of collision, making it impossible to cause an accidental collision. A prediction of how the human will guide the robot and how the robot will move in the near future was used to provide anticipation capabilities when evaluating this risk. Moreover, a robot control method to guarantee safety without having to modify how a robot executes its task was also proposed.

Finally, since the robot control methods presented in this thesis were intended to be applied in practical scenarios, experimental evaluations for all these methods were performed on a real collaborative robot.

¿Cómo controlar robots que colaboran con humanos?

Julián M. Salt Ducaju
Departamento de Control Automático

Resumen de Divulgación Científica para la Tesis Doctoral *Estrategias de Control para la Colaboración Física Humano–Robot*, Junio 2024. Esta tesis puede descargarse desde http://www.control.lth.se/publications

---

Durante la Primera Revolución Industrial, se sustituyó a los artesanos por máquinas. Después, durante la segunda mitad del siglo XX, los robots se emplearon para reemplazar a los trabajadores de las fábricas y para automatizar la industria. A lo largo de estos años, la productividad de las actividades de manufactura aumentó gracias a que se capitalizó el desarrollo tecnológico, a costa de los trabajadores humanos, cuya relevancia disminuyó en entornos de manufactura. No obstante, esta tendencia puede verse interrumpida en años venideros.

Las instalaciones industriales se han convertido en espacios muy estructurados para permitir a los robots, así como a otra maquinaria, realizar la misma tarea repetidamente de una manera muy eficiente para maximizar la producción. Como consecuencia, la industria manufacturera es capaz de producir grandes cantidades de productos idénticos. No obstante, una desventaja de estas instalaciones industriales tan estructuradas es la difícil adaptación a cualquier cambio en los procesos productivos, lo cual es especialmente relevante considerando las tendencias industriales actuales de personalización de los productos.

Se ha propuesto usar la Colaboración Humano–Robot para mejorar cómo los entornos industriales adaptan las tareas robotizadas a los cambios que puedan ocurrir en los procesos de producción. El argumento es el siguiente: si los humanos somos inteligentes, y los robots son muy hábiles realizando tareas repetitivas y además no se cansan realizándolas, ¿por qué no combinar las cualidades de ambos y aprovechar lo mejor de cada uno? Esta colaboración debería ser tan simple como permitir que un operador humano guíe manualmente a un robot para enseñarle una corrección del movimiento del robot. No obstante, el desafío de tener entornos industriales versátiles donde trabajadores humanos estén presentes es que pueden ocurrir eventos inesperados. El objetivo de esta tesis es desarrollar métodos para controlar robots que sean capaces de tratar con esta incer-

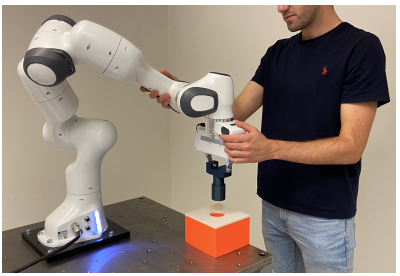

Un operador humano guiando manualmente a un robot para enseñarle una tarea de inserción.

tidumbre y así mejorar la colaboración física entre humanos y robots.

Los métodos de control de robots presentados en esta tesis se han centrado en mejorar distintos aspectos de la colaboración física entre humanos y robots. En primer lugar, se facilitó el guiado manual del robot desde la perspectiva del operador humano al reducir las incertidumbres presentes en la cantidad de fuerza que el operador debería ejercer sobre el robot para guiarlo. El método propuesto evitaría las posibles vibraciones estructurales y el desgaste de los componentes del robot que pueden ocurrir utilizando una estrategia alternativa que forma parte del estado del arte actual. En segundo lugar, se desarrolló un método para distinguir entre el guiado humano y un contacto accidental entre el robot y un obstáculo, sin necesidad de componentes adicionales. Este método podría usarse para modificar de manera efectiva una tarea del robot una vez que el operador haya terminado de demostrar una corrección, pero también para modificar el comportamiento del robot mientras se produce el guiado humano. En tercer lugar, se desarrolló una estrategia sobre el aprendizaje de una corrección humana por parte de un robot, haciendo que el robot ejecutara su tarea varias veces, y usando la diferencia entre el movimiento del robot y la corrección humana de cada ejecución para modificar el comportamiento del robot.

Además, la seguridad es fundamental en entornos industriales, especialmente cuando hay seres humanos involucrados. Por esta razón, esta tesis incluye métodos que permiten el guiado humano de los robots sólo en situaciones en las que los robots, los operadores humanos y cualquier otro objeto involucrado en la tarea del robot no estuvieran en riesgo de colisión. Los métodos propuestos permiten que el operador humano que guíe el robot pueda sentir cómo el robot se rigidiza si hubiera riesgo de colisión, haciendo imposible provocar una colisión accidental. A la hora de evaluar el riesgo de colisión, se utilizó una predicción de cómo el humano guiará al robot y cómo se moverá el robot en un futuro próximo. Asimismo, también se propuso un método de control del robot para garantizar la seguridad sin tener que modificar la ejecución de la tarea principal del robot.

Finalmente, ya que los métodos de control de robots presentados en esta tesis están destinados a ser implementados en escenarios prácticos, todos estos métodos han sido evaluados experimentalmente con un robot colaborativo real.

Printed by Media-Tryck, Lund 2024 NORDIC SWAN ECOLABEL 3041 0903

Department of Automatic Control
P.O. Box 118, 221 00 Lund, Sweden
www.control.lth.se

PhD Thesis TFRT-1144
ISBN 978-91-8104-024-1
ISSN 0280–5316